

**MULTISTABILITY AND
PROBABILISTIC PROPERTIES OF
DIFFERENTIAL DELAY EQUATIONS**

by

JÉRÔME LOSSON

**Department of Physics
McGill University
Montréal, Québec, Canada**

June 1991

**A Thesis submitted to the
Faculty of Graduate Studies and Research
in partial fulfillment
of the requirements for the degree of
Master of Science.**

©Jérôme Losson, 1991

à mes parents, Michèle et Jean-Pierre Losson et à Jacques Michalczak

ABSTRACT

The dynamics of a class of nonlinear delay differential equations (D.D.E's) is studied. We focus attention on D.D.E's with a discrete delay used as models for production/destruction processes. The design of an electronic analog computer simulating an integrable D.D.E is presented. This computer is used to illustrate the presence of bistable solutions in the system. The multistability is investigated numerically with an analytic integration algorithm. Higher order multistability is reported, and the structure of basin boundaries in the space of initial functions is investigated. Pathological dependence of solution behavior on the initial function is shown to be present in large regions of parameter space. A D.D.E obtained as the singular perturbation of the one dimensional "hat map" is studied numerically. Several schemes to undertake a statistical analysis of the equation are presented. We first focus attention on the construction of densities along trajectories, and then on the construction of densities for ensembles of trajectories generated by ensembles of initial functions. A cycling of densities is observed in both cases, and compared to the asymptotic periodicity of the Frobenius-Perron operator for the hat map. Functional analytic techniques used for the analysis of stochastic wave propagation in continuous media and in quantum field theory are extended to the statistical study of D.D.E's, and provide a theoretical framework within which to study D.D.E dynamics in the spirit of ergodic theory and statistical mechanics.

RÉSUMÉ

Cette thèse porte sur l'étude du comportement dynamique d'une classe d'équations différentielles avec mémoire (équations dites à délai, ou E.D.D.) pouvant générer le chaos. Ces équations sont utilisées pour modéliser les processus de contrôle avec rétroaction retardée. Un ordinateur électronique analogue destiné à simuler une E.D.D. intégrable en temps réel est décrit. L'ordinateur est utilisé pour illustrer la présence de cycles limites bistables. Cette bistabilité est par la suite étudiée numériquement grâce à un algorithme d'intégration analytique. La présence de solutions multistables (tristables, quadristables, etc.) est mise en évidence et la structure des frontières de bassins d'attractions dans l'espace des fonctions initiales est analysée. On observe une dépendance pathologique du comportement asymptotique sur les variations de fonctions initiales dans de vastes régions de l'espace des paramètres de contrôle. Une E.D.D. obtenue par perturbation singulière de l'application unidimensionnelle dite "application chapeau" (*hat map*) est simulée numériquement. Plusieurs approches destinées à faciliter une étude numérique statistique de ce système dynamique sont présentées. Tout d'abord, des densités définies le long d'une simple trajectoire sont obtenues. En un second temps, on considère l'évolution de densités définies sur des ensembles de trajectoires générées par des ensembles de fonctions initiales. Dans les deux cas, l'évolution temporelle est cyclique, et donc, à rapprocher de la périodicité asymptotique de l'opérateur de Frobenius-Perron pour l'application chapeau. En dernier lieu, les techniques utilisées pour l'étude de flots stochastiques dans les milieux continus, et les outils de la théorie des champs quantiques sont utilisés pour l'élaboration d'un formalisme théorique formant la base d'une approche nouvelle des systèmes dynamiques avec mémoire, inspirée de la théorie ergodique et de la mécanique statistique.

ACKNOWLEDGEMENTS

I take this opportunity to express my deep gratitude to professor Michael Mackey, my thesis supervisor. The trust and complicity he shares with his graduate students go far beyond the confines of scientific research. His love of the Unsolved Problem, his scientific versatility and his friendly advice have inspired me tremendously.

I also want to thank André Longtin for his continuing support. André originally suggested the analog simulation of delay equations and showed stimulating interest in the rest of the work presented here.

I am indebted to professor John Outerbridge who wrote the software package used to produce most of the figures in the thesis. His limitless patience with my (many) computer blunders and his constructive criticism were greatly appreciated.

I would like to thank my fellow physics student Nick Provatas with whom I have shared countless hours of stimulating conversations on issues of common interest. Further thanks to Chris Cortis with whom I have spent many a week-end in the McIntyre Building trying to get the circuit described in Chapter 2 to oscillate. I have very fond memories of the months of collaboration with Chris on the project and his motivating input to this work is greatly appreciated. The ideas presented in Chapter 5 came as my friend Guy Jonkmans was feverishly cramming for his field theory courses, and I want to thank him for his good humoured support as I was struggling to make sense out of his class notes.

Last but not least, I owe my sanity to the two very special tenants of 3555 Linton, and to Peter Ray for helping me laugh off my thesis hysteria.

TABLE OF CONTENTS

ABSTRACT	i
RÉSUMÉ	ii
ACKNOWLEDGMENTS	iii
TABLE OF CONTENTS	iv
1. INTRODUCTION	1
1.1 History dependent models	3
1.2 Nonlinear dynamics and D.D.E's	6
1.2.1 Introductory remarks	7
1.2.2 D.D.E's	8
1.3 Initial-boundary value problems for hyperbolic P.D.E's: The link with D.D.E's	8
1.4 Distributed delays: Approximating D.D.E's	13
1.5 Discrete delays: Production-destruction models	17
1.5.1 Singular perturbation of a difference equation	18
1.5.2 The paradigm equation: Piecewise constant nonlinearities (PCNL)	21
1.5.2.a The paradigm equation	23
1.5.2.b PCNL: reducing the D.D.E to a shift operator	23
1.6 Summary	27
2. ANALOG SIMULATION OF A D.D.E	28
2.1 Design of the analog computer	29
2.1.1 Stage by stage description of the circuit	30
2.1.1.a Op-amp based components	30
2.1.1.b The delay circuit	34
2.1.1.c The feedback function	38
2.1.2 Noise level in the circuit	41
2.2 Derivation of the circuit equation	41
2.2.1 Stability of the closed loop	43
2.2.2 Qualitative observations	43
2.2.3 Quantitative interpretation of the data	45
2.3 Comparing electronic and numerical solutions	48
2.3.1 Variation of a single parameter	48
2.3.1.a Variations of θ_1 and θ_2	49
2.3.1.b Variations of α	50
2.3.1.c Power spectra	50
2.4 Multistability in the oscillator	52
2.4.1 Hysteresis in the bifurcation diagram	52
2.4.2 Controlling non-constant I.F's	64
2.4.3 Discussion	66
2.5 Summary	68

3.	MULTISTABILITY IN DELAY DIFFERENTIAL EQUATIONS	69
3.1	Multistability and nonlinear dynamics	70
3.1.1	Introductory definitions	71
3.1.2	Bistability in electrophysiological cardiac models	72
3.2	Multistability in physics	75
3.2.1	Optical bistability	75
3.2.1.a	Experimental observations	76
3.2.1.b	Analytic and numerical results	77
3.3	Multistable behavior of an integrable delay differential equation	81
3.3.1	Higher order multistability	82
3.3.1.a	Parametrizing the initial functions	82
3.3.1.b	Digital simulations	83
3.3.2	Basin boundaries in the space of initial functions	86
3.3.2.a	Digital simulations	88
3.4	Summary	93
4.	DYNAMICS OF ENSEMBLES OF D.D.E's	94
4.1	Densities and dynamical systems	95
4.1.1	Densities <i>versus</i> single trajectories	95
4.1.2	Temporal evolution of phase space densities	96
4.1.2.a	Discrete time systems	97
4.1.2.b	Continuous time systems	99
4.1.3	Asymptotically periodic Markov operators	100
4.2	Ensembles of D.D.E's: numerical insight	103
4.2.1	The hat map	104
4.2.2	Densities and D.D.E's	105
4.2.2.a	Densities along trajectories	105
4.2.2.b	Densities for a "sliding" segment of solution	109
4.2.2.c	Average of an ensemble of buffers	109
4.2.2.d	Sampling ensembles of D.D.E's	110
4.3	Analytic expression of the density for an integrable D.D.E	116
4.3.1	Application to a neural network	120
4.4	Summary	122
5.	PROBABILISTIC DESCRIPTION OF DELAYED FEEDBACK SYSTEMS	124
5.1	Introductory definitions	125
5.1.1	σ -algebras measures and measure spaces	125
5.1.2	Generating functions and the functional \mathcal{Z}	16
5.2	Characteristic functionals and D.D.E's	129
5.2.1	A functional differential equation for \mathcal{Z}	131
5.2.2	Moment functions of μ_t	133
5.3	Perturbation theory and the diagram technique	139
5.3.1	Diagrams in stochastic wave analysis	140

5.3.2 Feynman graphs and the moment equations	142
5.4 Connection with the quantum theory of fields.....	144
5.4.1 Path integral formulation of quantum mechanics.....	145
5.4.2 Generating functionals for scalar fields	148
6. Summary	150
CONCLUSION	152
APPENDICES	154
Appendix A: Regrouping the parameters in equation (2.3).....	154
Appendix B: Error analysis	156
B.1 Error on measured quantities.....	156
B.2 Error on effective parameters.....	157
Appendix C: Functional derivatives.....	159
Appendix D: Program listings	161
BIBLIOGRAPHY	176

Chapter 1

Introduction

The use of non-linear equations to obtain insight into the evolution of complex systems is the essence of non-linear dynamics, a field of activity which has greatly expanded in the last thirty years. At this point it appears that the tools of non-linear dynamics potentially hold as much promise for the development of theoretical physics as the use of probability theory did in the first part of this century [66].

This thesis focuses on a small subset of nonlinear dynamics, namely the study the dynamics of a class of non-linear delay differential equations (D.D.E's) which model delayed feedback control loops. Delay differential equations have been used to study problems of laser physics and nuclear engineering, control theory and economic modeling. They also appear frequently in mathematical biology and studies of population dynamics. The appeal of nonlinear dynamics lies in the fact that it is possible to simulate complex (sometimes even *chaotic*) behavior using relatively simple non-linear mathematical models.

In this introductory chapter the origin and formulation of history-dependent models is first described. In Section 1.2, we present some of the basic concepts of non-linear dynamics. The connection between delay-dependent models and a formulation in terms of partial differential equations (P.D.E's) is given in Sections 1.3 and 1.4. Finally singular perturbation limits and some other techniques used to study D.D.E's are explained in Section 1.5.

Chapter 2 describes the design and performance of an analog computer constructed to simulate the solution of a class of delay differential equations with piecewise constant forcing terms. The use of this computer highlighted the sensitivity of delayed dynamics on initial

conditions.

Chapter 3 explores the dynamics of a piecewise integrable delay differential equation using an algorithm which integrates the equation *analytically* (but not *symbolically*) allowing a far greater accuracy than that obtained with traditional numerical integration schemes, and significant reductions in computation times. We focus attention on exploring the presence of multistability in the D.D.E discussed in Chapter 2. In particular, we illustrate the complexity of the basin boundaries in the space of initial functions. The multistability displayed by the D.D.E is studied in detail with a specific set of non constant initial functions.

In Chapter 4, we examine numerically the behavior of large collections of delay differential equations. In Section 4.1 we review some of the techniques used to study deterministic systems from a statistical point of view, and discuss an interesting property of smoothing Markov operators known as *asymptotic periodicity*. In Section 4.2, we numerically investigate the statistical properties of large collections of D.D.E's using several methods (see 4.2.2a,b,c,d) designed to facilitate the numerical study of flows of functions. In Section 4.3, an analytic expression for the density along the trajectory of a piecewise integrable dynamical system is derived, and applied to a delay differential equation and a simple neural network.

In Chapter 5 we present a formalism with which to investigate the dynamics of densities of initial functions (*density functionals*) evolving under the action of delay differential equations. In Section 5.1, some introductory definitions from measure theory and probability theory are given. In Section 5.2 we derive a functional differential equation for the evolution of the density functional and then derive partial differential equations specifying the time evolution of the moments of the distribution of functions. In Section 5.3, we apply the Feynman diagram technique to the statistical study of delay differential equations. We show how the diagrams can be used to derive the partial differential equations mentioned above. Since the Fourier transform of the density functional can be interpreted as a path integral, we explain in Section 5.3 the close connection between the statistical study of delay differential equations and quantum field theories.

1.1 History dependent models.

In the absence of non-local effects, the instantaneous transmission of information between two systems is impossible without a violation of the assumption of causality. The delays involved necessarily impose a fundamental constraint on any theory describing physical interactions. If the time scale of the delays is comparable to that of the processes under consideration, a sound model must explicitly take the delays into account.

The idea that the evolution of a system can only be predicted given some knowledge of its past history is not novel. A review of the relevance of time-delays in control theory can be found in [3]. In biological systems, delays arise because of the finite speed at which biochemical and electrochemical signals propagate. Hormones are carried by the blood flow to their targets; action potentials propagate down axons and neuro-transmitters must diffuse across the synaptic cleft between neurons. In the study of population dynamics, delay-dependent models reflect the time lags that always exist between environmental stimuli and adaptive responses.

The use of delay-dependent models is in no way exclusive to theoretical biology and biomathematics. A number of physical systems require their use to understand their behavior: the stability of nuclear reactors [15, 19, 41], neutron shielding [6, 61] and bistable optical devices [21, 32, 34] to name just a few. As early as the 1930's Kalecki [36] proposed delay-differential equations as models of cyclic economic commodity market activity. In recent work delay dependent models have been used to investigate the dynamics of commodity price fluctuations [2, 50]. Mathematically, the framework within which to investigate such apparently diverse behavior is the theory of functional differential equations.

When a model is formulated in terms of coupled first-order ordinary differential equations for the vector variable $\mathbf{x}(t) = (x_1(t), \dots, x_n(t))$:

$$\frac{d\mathbf{x}(t)}{dt} = \mathbf{F}(x_1(t), \dots, x_n(t)), \quad \mathbf{F} \equiv (F_1, \dots, F_n), \quad (1.1)$$

the initial values $x_i(0)$ suffice to predict the evolution of $x_i(t)$ for any future time. However as the examples cited above illustrate, it is sometimes necessary to use knowledge of the past history of at least one of the variables to allow prediction.

If the evolution of the variable $x_k(t)$ depends on some cumulative effect of *all* its earlier values, it should be replaced by some function f , weighted by a suitable factor g , and integrated over all previous times. Then the evolution equation is an integro-differential equation:

$$\frac{dx(t)}{dt} = F \left(\dots, \int_{-\infty}^t g(t-t')f(x_k(t'))dt', \dots \right). \quad (1.2)$$

The function g (the *kernel* of the equation) specifies the weight to be attached to the function f of x_k at each point of time in the past. This is an example of a D.D.E with distributed delays.

If there is a discrete time lag in the action of x_k on some other variable, we speak of a *discrete* delay in the system (1.1) and in that case at least one of the set of O.D.E's is amended by replacing, for example, $F(\dots, x_k(t), \dots)$ by $F(\dots, x_k(t-\tau), \dots)$. Then the equation of evolution

$$\frac{dx(t)}{dt} = F(x_1(t), \dots, x_k(t-\tau), \dots) \quad (1.3)$$

is a D.D.E with discrete delay. For illustrative purposes, we examine two specific areas of investigation in which the use of delay dependent models has been particularly fruitful. The first one is the study of nuclear reactors, and in which the goal is to write down the conditions on control parameters which guarantee the stability of the system. The second one is the modeling of physiological control loops. In both of these areas, models are often naturally framed as non-linear D.D.E's.

Example 1.1: A NUCLEAR REACTOR DYNAMICS MODEL.

In nuclear engineering, delay differential equations with distributed delays have been used to describe the dynamics (and, in particular, to determine the stability conditions) of circulating-fuel nuclear reactors. Ergen [15] assumed that all the particles of the fuel spent the same time Υ in the reactor and that power extraction was proportional to the integral of power $P(t)$ over past residence times. This led to the following equation for the rate of change of temperature $T(t)$,

$$\frac{dT(t)}{dt} = \epsilon \left[P(t) - \frac{1}{\Upsilon} \int_0^{\Upsilon} P(t-s)ds \right]. \quad (1.4)$$

The relative increase in the power P from one generation of neutrons to the next is

assumed to be proportional to T ,

$$\frac{d \log P(t)}{dt} \propto \left(\frac{-\alpha}{\bar{\tau}} T(t) \right), \quad (1.5)$$

where $-\alpha$ is the temperature coefficient of reactivity and $\bar{\tau}$ is the average life time of one neutron generation. Since neutrons enter the reaction only some time after the occurrence of the fission which produced them, the reactor power at time t depends on the history of the reaction. Thus equation (1.4) is modified to

$$\frac{dP(t)}{dt} = \frac{-\alpha}{\bar{\tau}} T(t)P(t) - \frac{\beta}{\bar{\tau}} P(t) + \frac{\beta}{\bar{\tau}} \int_0^\infty P(t-s)g(s)ds \quad (1.6)$$

where the delay kernel $g(s)$ indicates which fraction of the neutrons produced by a fission at time $t-s$ is available for power production at a time s . The presence of the third term in (1.6), the so-called *delayed term*, is crucial in the reactor stability problem [56].

Example 1.2: PHYSIOLOGICAL CONTROL PROCESSES.

Historically, delay dependent models have been instrumental in the development of control theory. The classical situation that a control theorist faces is to model and understand the dynamics of a remotely controlled variable. Often the interaction between the controlling unit and the controlled process is such that time lags are significant. [For a list of such systems and a control theoretical approach to the treatment of delay dependent models, see [57]]. This paradigm is also applicable to many of the problems facing those investigating the dynamics of physiological control processes.

To clarify the discussion, introduce a variable $x(t)$. Generically, in biological systems $x(t)$ will vary to accommodate a changing internal and/or external environment. In many situations, $x(t)$ is controlled remotely and an accurate model must take the delays into account. For example, the equation

$$\frac{dx}{dt} = -\alpha x(t) + F(x(t-\tau)) \quad (1.7)$$

with different nonlinearities F has been used to describe the oscillations of the pupil area and the pupil eye reflex [47], as a model for the human respiratory system [53, 54], and to describe the regulation of several processes in blood cell production [55]. In these different applications, the function F reflects the type of feedback present in the control loop and the

variable $x(t)$ represents, respectively, the area of the pupil, the concentration of CO_2 in the blood stream, or the number of circulating blood cells.

The use of delay equations is important to understand some clinically observed pathologies which can be thought of as resulting from *deregulations* of these control mechanisms arising from shifts in the parameter space of the process. For example an abnormal variability of the number of red blood cells in the body (one of the symptoms of periodic autoimmune hemolytic anemia) can be understood as arising from a change in system location in parameter space for equation (1.7), resulting in a bifurcation in its dynamics [54]. Periodic autoimmune hemolytic anemia is an example of what has been called a dynamical disease: a malfunction which is not necessarily the result of infection by a pathogen, but the result of a qualitative change in the dynamics of a physiological control loop [54]. The causes of this dynamic change are then interpreted as changes in the parameters of the model under consideration. This relatively new approach to physiological dynamics has proven to be useful for the investigation of several diseases, but the development of the theory and a more systematic use are still hampered by a lack of understanding of the behavior of delay differential equations.

The difficulties inherent in the study of D.D.E dynamics partially stem from the fact that D.D.E's are infinite dimensional dynamical systems. Their phase-space is a normed function space because the initial condition is a function defined everywhere on an initial interval $[-\tau, 0]$ in the case of discrete delay situation, or on $(-\infty, 0]$ in the distributed delay case. The main motivation for this thesis is the paucity of insight and analytic results concerning the influence of initial functions on eventual D.D.E solution dynamics, and the absence of analytic tools with which to investigate D.D.E's statistically.

1.2 Non-linear dynamics and D.D.E's.

Systems of O.D.E's and maps (with either continuous or discrete time) have been studied extensively: the behavior of flows in finite dimensional spaces has been the subject of intense scrutiny [4, 11, 18, 20, 40, 46].

For investigators using D.D.E's as models for physical systems it is necessary to have some

information concerning the generic solution properties of these equations. Thus existence and stability of solutions, the effects of changing initial conditions and the potential existence of chaotic dynamics are all important points to address. They remain largely unanswered but are crucial for the researcher dealing with delay dependent models. Before proceeding, we introduce some of the concepts of non-linear dynamics which will be used throughout the thesis.

1.2.1 Introductory remarks.

An important feature of nonlinear deterministic systems is that they can display very complicated behavior. The essence of this complexity is twofold.

1) It is frequently observed that the topology of the attracting manifold of a given non-linear deterministic system changes as some control parameters are varied [20]. Changes in the topology can be viewed as qualitative changes in solution behavior. For example, a steady-state solution can suddenly become oscillatory, or a hitherto bounded solution can diverge to infinity. These qualitative changes in solution behavior are called bifurcations. Mathematically, the equations of motion are non-linear differential equations and the bifurcations correspond to certain changes in the eigenvalues of the differential operators near fixed points (or points in phase space at which all time derivatives are zero).

2) Simple non-linear deterministic systems can generate turbulent-like behavior (or deterministic chaos) which never repeats itself in the phase space. Deterministic chaos is observed in certain regions of parameter space and may not be ubiquitous for a given system, i.e. many nonlinear systems can display a wide array of dynamic behavior ranging from steady state behavior to oscillations of varying complexity to turbulent like behavior as a control parameter is changed. In fact there are well known routes to chaos [72]. These routes usually consist of a sequence of bifurcations which lead the system from simple motion to chaotic behavior. For example the period doubling route to chaos (Feigenbaum's scenario) is a sequence of doublings of the solution period leading to chaos as a parameter is changed [72].

1.2.2 D.D.E's

In studying D.D.E's concepts familiar to the non-linear dynamicist like fixed points, flows, basins of attraction must be adapted to the framework of functional analysis. This is because delay differential equations are in fact functional operators acting on the elements of a normed function space. For example, a D.D.E with discrete delays *transforms* a function defined on an interval $[j\tau, (j+1)\tau]$ into another function defined on $[(j+1)\tau, (j+2)\tau]$, $j = 0, 1, \dots$, where τ is the largest of the delays present. The fixed points of the D.D.E are invariant functions for the functional operator and the flows are flows of functions. These concepts have been introduced [22] but the formalism makes the results available difficult to access for many investigators likely to encounter D.D.E's in their research. In addition, the presence of basins of attraction in function spaces and the structure of these basin boundaries have apparently never been investigated.

One way of dealing with these difficulties is to reduce the D.D.E's to systems easier to study, O.D.E's or maps for example. Before illustrating some of these techniques, let us highlight the connection between some P.D.E models and a formulation in terms of delay differential equations.

1.3 Initial-Boundary Value problems for hyperbolic P.D.E's: The link with D.D.E's.

To now the focus has been on models for which the dependence on past history is *built in*. That is to say, when the equations are written down, the way in which the system depends on its history is explicit. In some cases, it is possible to obtain a D.D.E from a reinterpretation of *a priori* non history-dependent models. General well-posed non-linear boundary value problems for hyperbolic equations are reducible to functional differential equations, some of which are D.D.E's. This procedure was first noted by A. A. Vitt in 1936 [80], and apparently independently by Miranker [58] and Cooke *et al.* [12] while studying the dynamics of transmission lines terminated by general circuit elements. The method is based on the observation that a hyperbolic P.D.E can be written as set of first order P.D.E's, which can in turn be written as a set of O.D.E's *via* the introduction of the directional (or

total) derivative. Before proceeding further we review the concept of a hyperbolic equation, and the associated *characteristic* curves.

The *normal form* for a hyperbolic P.D.E as defined by Morse and Feshbach [60] is

$$\frac{\partial^2 \psi}{\partial \lambda \partial \mu} = P \frac{\partial \psi}{\partial \lambda} + Q \frac{\partial \psi}{\partial \mu} + R \psi \quad (1.8)$$

where P, Q, R are functions of λ and μ . It is easily shown [60] that the wave equation

$$\frac{\partial^2 \psi}{\partial x^2} - \frac{1}{c^2} \frac{\partial^2 \psi}{\partial t^2} = 0 \quad (1.9)$$

is a hyperbolic equation. If $\psi(x, t)$ is a scalar, it can also be shown that any hyperbolic equation can be written in the matrix form

$$\mathbf{A} \frac{\partial \mathbf{U}}{\partial t} + \mathbf{B} \frac{\partial \mathbf{U}}{\partial x} + \mathbf{C} \mathbf{U} = 0 \quad (1.10)$$

where $\mathbf{A}, \mathbf{B}, \mathbf{C}$, are 2×2 matrices whose entries are functions of x and t , and $\mathbf{U} = \mathbf{U}(x, t)$. In addition there exists a vector $\mathbf{V} = \mathbf{V}(x, t)$ such that

$$\nu(x, t) \mathbf{V}^T \mathbf{A} = \rho(x, t) \mathbf{V}^T \mathbf{B}. \quad (1.11)$$

ν and ρ are not both zero and \mathbf{V}^T is the transpose of \mathbf{V} . Equation (1.10) can therefore be written

$$\mathbf{V}^T \mathbf{A} \left(\rho \frac{\partial}{\partial t} + \nu \frac{\partial}{\partial x} \right) \mathbf{U} + \rho \mathbf{V}^T \mathbf{C} \mathbf{U} = 0. \quad (1.12)$$

The curve \mathcal{L} , parametrized by s and defined by

$$\mathcal{L} : \begin{cases} \dot{x} = \nu \\ \dot{t} = \rho \end{cases} \quad \text{where } (\dot{}) = \frac{d()}{ds}, \quad (1.13)$$

is called a *characteristic curve*, or *characteristic* for equation (1.10). Defining $D_{\mathcal{L}}$ to be the directional derivative along \mathcal{L}

$$D_{\mathcal{L}} = \rho \frac{\partial}{\partial t} + \nu \frac{\partial}{\partial x}, \quad (1.14)$$

we can write (1.12)

$$\mathbf{V}^T \mathbf{A} D_{\mathcal{L}}(\mathbf{U}) + \rho \mathbf{V}^T \mathbf{C} \mathbf{U} = 0, \quad (1.15)$$

and the equation *looks* like a set of O.D.E's. For a given hyperbolic P.D.E the information about the solutions flows along the families of characteristic curves. Note that since \mathbf{U} is

2×2 in our case, there are two families of characteristic curves, but the situation is exactly the same if U is $l \times l$ [67].

Now consider the following initial-boundary value problem:

$$u_t + M(x, t)u_x = \phi(x, t), \quad \text{where } x \in [0, 1] \quad \text{and } t > 0, \quad (1.16)$$

along with

$$M(x, t) = \begin{pmatrix} f_1(x, t) & 0 \\ 0 & f_2(x, t) \end{pmatrix}, \quad u(x, t) = \begin{pmatrix} u_1(x, t) \\ u_2(x, t) \end{pmatrix} \quad \text{and} \quad \phi(x, t) = \begin{pmatrix} \phi_1(x, t) \\ \phi_2(x, t) \end{pmatrix}.$$

The initial conditions are given by

$$u(x, 0) = u_0(x), \quad (1.17)$$

and the boundary conditions are general integro-differential conditions which can be formally written

$$\mathcal{B}_i(u_j^{(k)}(a, t)) = 0 \quad (1.18)$$

where $i = 1, 2$, $j = 1, 2$, $k = 1, 0, -1$ and $a = 0, 1$ so that the argument of the boundary conditions \mathcal{B}_1 and \mathcal{B}_2 in (1.18) is a contraction of 12 terms (for each j , 3 possible k 's, for each (j, k) , 2 possible a 's). We define

$$u_j^{(0)}(a, t) = u_j(a, t), \quad (1.19)$$

the differential term in the boundary condition,

$$u_j^{(1)}(a, t) = \frac{\partial u_j(a, t)}{\partial t}, \quad (1.20)$$

and the integral term,

$$u_j^{(-1)} = \int_0^t u_j(a, t') dt'. \quad (1.21)$$

The functions \mathcal{B}_1 and \mathcal{B}_2 are given, as is the vector function $u_0(x)$. The requirement that ϕ be independent of u is essential at this point. Once the method is developed it is easy to see how more general situations can be treated, and we shall come back to this point at the end of the section.

The characteristics for (1.16) form two families of curves (see Figure 1.1)

$$\mathcal{L}_1 : \frac{dx}{dt} = \frac{1}{f_1} \quad \text{and} \quad \mathcal{L}_2 : \frac{dx}{dt} = \frac{1}{f_2}. \quad (1.22)$$

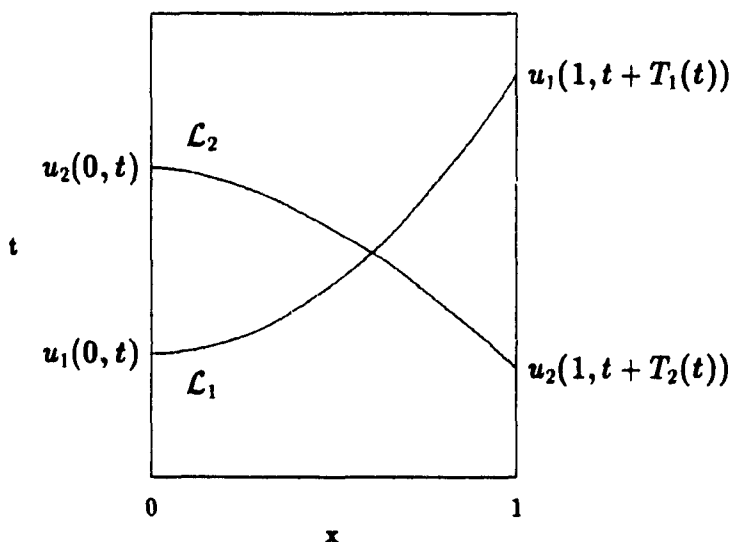


Figure 1.1: Two possible shapes for the characteristic curves of system (1.16).

We assume that through each point $(x, t) \in [0, 1] \times \mathbb{R}^+$ there are two characteristics: \mathcal{L}_1 with positive slope and \mathcal{L}_2 with negative slope. Now introduce the directional derivative

$$D_i = \frac{\partial}{\partial t} + f_i(x, t) \frac{\partial}{\partial x} \quad (i = 1, 2) \quad (1.23)$$

along the characteristic \mathcal{L}_i . Equation (1.16) therefore takes the form

$$D_i u_i = \phi_i \quad (i = 1, 2). \quad (1.24)$$

A characteristic through a point $(0, t)$ will intersect the boundary $x = 1$ at a point $(1, t + T_1(t))$ where $T_1(t)$ can be found by integrating the relation $dx/dt = f_1^{-1}$. Similarly a characteristic through the point $(1, \hat{t})$ will intersect the boundary $x = 0$ at a point $(0, \hat{t} + T_2(\hat{t}))$ where now $T_2(\hat{t})$ depends only on f_2 defined in (1.22)

Integration of $D_1 u_1 = \phi_1$ along the characteristic \mathcal{L}_1 from a point $(0, t)$ to a point $(1, T_1(t))$ yields

$$u_1(1, t + T_1(t)) = u_1(0, t) + \int_t^{t+T_1(t)} \phi(\bar{x}, \bar{t}) d\bar{t}, \quad (1.25)$$

where the integral is a line integral along \mathcal{L}_1 .

Similarly, integration of $D_2 u_2 = \phi_2$ along \mathcal{L}_2 , gives obtain,

$$u_2(1, t) = u_2(0, t + T_2(t)) + \int_{t+T_2(t)}^t \phi_2(\bar{x}, \bar{t}) d\bar{t}. \quad (1.26)$$

(Remember that \mathcal{L}_2 has a negative slope so that $T_2 < 0$.) We have equations linking $u_i^{(0)}(0, t)$ and $u_i^{(0)}(1, t)$ and we can now obtain similar equalities for $u_i^{(\pm 1)}(0, t)$ and $u_i^{(\pm 1)}(1, t)$ by differentiating (or integrating) equations (1.25) and (1.26). To simplify, define

$$\Omega_1(t) = \int_t^{t+T_1(t)} \phi_1(\bar{x}, \bar{t}) d\bar{t}, \quad (1.27)$$

and

$$\Omega_2(t) = \int_{t+T_2(t)}^t \phi_2(\bar{x}, \bar{t}) d\bar{t}. \quad (1.28)$$

Furthermore if

$$y_1(t) = u_1(1, t), \quad y_2(t) = u_2(0, t), \quad (1.29)$$

straightforward differentiation and integration of equation (1.25) yields,

$$u_1(0, t) = y_1(t + T_1(t)) - \Omega_1(t),$$

$$u_1^{(1)}(0, t) = [1 + T_1'(t)]y_1'(t + T_1(t)) - \Omega_1'(t), \quad (1.30)$$

$$u_1^{(-1)}(0, t) = \int_0^t y_1(s + T_1(s)) ds - \int_0^t \Omega_1(s) ds$$

for the first equation, and

$$u_2(0, t) = y_2(t + T_2(t)) + \Omega_2(t),$$

$$u_2^{(1)}(0, t) = [1 + T_2'(t)]y_2'(t + T_2(t)) - \Omega_2'(t), \quad (1.31)$$

$$u_2^{(-1)}(0, t) = \int_0^t y_2(s + T_2(s)) ds - \int_0^t \Omega_2(s) ds$$

for the second equation of system (1.24).

If we substitute these expressions in relation (1.18) for the boundary conditions, we obtain the following system of D.D.E's:

$$\mathcal{B}_i \left(y_1(t), y_1(t + T_1(t)), y_1'(t), y_1'(t + T_1(t)), \int_0^t y_1(s) ds, \int_0^t y_1(s + T_1(s)) ds, \right.$$

$$y_2(t), y_2(t + T_2(t)), y_2'(t), y_2'(t + T_2(t)), \int_0^t y_2(s) ds, \int_0^t y_2(s + T_2(s)) ds, t) = 0 \quad (1.32)$$

where $(t \geq 0)$, $(i = 1, 2)$. Therefore, a solution of (1.16), (1.17) and (1.18) yields a solution of (1.32).

We now show the converse (a solution of (1.32) is a solution of (1.16), (1.17) and (1.18)) to demonstrate the complete equivalence between the original initial-boundary value problem for the P.D.E and the initial value problem for the D.D.E.

Suppose that $y_1(t)$ and $y_2(t)$ satisfy (1.32). Define $u_1(1, t)$ and $u_2(0, t)$ by (1.29) for $t > 0$. To define, $u_1(x, t)$ for $0 \leq x \leq 1$, integrate (1.24) along the characteristic \mathcal{L}_1 , and proceed similarly for the definition of $u_2(x, t)$ using both cases the known values of $u_1(1, t)$ and $u_2(0, t)$. Clearly, (1.25) and (1.26) are then satisfied and so are (1.30) and (1.31). Hence (1.32) leads at once to (1.18) and (1.16) is satisfied because (1.24) is valid. Thus every solution of (1.32) generates in a unique way a solution of (1.16) with boundary conditions (1.18)! In addition, the initial condition (1.17) yields, via the integration along characteristics, two values $y_1'(t)$ and $y_2'(t)$ which are, in general, appropriate initial values for the D.D.E [12].

The original equation (1.16) is linear but general non-linear boundary conditions will make the system of D.D.E's (1.32) non-linear. Because the dynamics of the two systems are exactly the same, one should not be surprised to observe sensitive dependence on the initial conditions (or other types of behaviors typically displayed by non-linear systems) arise in equation (1.16) which is linear.

In conclusion there is a general method for linking mixed problems formulated as hyperbolic P.D.E's and initial value problems for history dependent models. Known theory and techniques for either kind of problem can be applied to the other.

1.4 Distributed delays: Approximating D.D.E's.

The results of the preceding section give us an explicit connection between hyperbolic P.D.E's and delay differential equations. We now consider the transformation of a D.D.E with distributed delays into ordinary or partial differential equations. It is worth emphasizing this possibility because models are often framed as partial differential equations, and the possibilities of (occasionally simpler) alternate formulations are frequently ignored.

Conditions for the reducibility of a D.D.E to a system of ordinary differential equations will first be examined. We shall then give a general statement concerning the equivalence between D.D.E's and P.D.E's.

Consider an integro-differential system of the form,

$$\frac{dx}{dt} = A(x, t) + \int_{-\infty}^t K(x(u), t, u) du \quad (1.33)$$

with the initial conditions

$$\begin{aligned} x(t) &= \varphi(t) \text{ for } t < 0 \\ A(x, t) &= A_0(\varphi, t) \text{ for } t < 0 \\ \int_{-\infty}^0 K(\varphi(u), 0, u) du &= I_0 \end{aligned}$$

Theorem 1.4.1 (Vogel [81]): In equation (1.33), let $K(x(u), t, u)$ be a given kernel differentiable in x and t . If there are functions $f_0(t), f_1(t), \dots, f_{p-1}(t)$ and $W(t, u)$ such that

$$\frac{\partial^p K}{\partial t^p}(x, t, u) = f_0 K(x, t, u) + f_1 \frac{\partial K}{\partial t}(x, t, u) + \dots + f_{p-1} \frac{\partial^{p-1} K}{\partial t^{p-1}}(x, t, u) + W(t, u), \quad (1.34)$$

then the solution $x(t)$ of (1.33) satisfies a $p + 1$ -dimensional system of O.D.E's.

This result is applicable to systems of the form:

$$\frac{dx}{dt} = A(x, t) + \int_{-\infty}^t H(x(u))g(t-u)du, \quad (1.35)$$

with initial conditions

$$\begin{aligned} x(t) &= \varphi(t) \text{ for } t < 0 \\ A(x, t) &= A_0(\varphi, t) \text{ for } t < 0 \\ \int_{-\infty}^0 H(\varphi(u))g(-u) du &= I_0 \end{aligned}$$

which are examples of *Volterra systems* [49, 82]. (Note that equation (1.6) for the power available from a circulating-fuel nuclear reactor belongs to this class of equation, as does the population dynamics model considered in Example 1.3). For equation (1.35), the condition for the reducibility of the integro-differential equation to a system of O.D.E's is that the delay kernel g satisfies,

$$\frac{d^p g}{dt^p} = a_0 g + a_1 \frac{dg}{dt} + \dots + a_{p-1} \frac{d^{p-1} g}{dt^{p-1}}, \quad (1.36)$$

where the a 's are constants. In other words, the condition on the kernel is that it be a sum of exponentials multiplied by polynomials of order at most p .

There are even more fundamental results relating D.D.E's to partial differential equations. Theorem 1.4.2 (Fargue [16]): *If the kernel $K(x(u), t, u)$ is such that (1.33) possesses piecewise differentiable (C^1) solutions, asymptotically bounded above by $b \exp(n | t |^k)$ with $b, n, k, \in R$, then (1.33) is equivalent to the system,*

$$\begin{aligned} \frac{dx}{dt} &= F(x, t) + \int_0^\infty K(p(a, t), t, t - a) da, \\ \frac{\partial p}{\partial t} + \frac{\partial p}{\partial a} &= \delta(a)x(t), \end{aligned}$$

δ being the usual Dirac delta function, and $p(a, t)$ a piecewise C^1 function.

The proof of the theorem is based on the fact that it is possible to replace the trajectory of the system up to time t by a field (or function) p which is defined for scalar systems as the solution of a P.D.E in one dimension. If no memory is present (the relevant information is the state of the system at time t), the field can be chosen to be

$$p(a, t) = H(a)x(t - a),$$

where $H(a)$ is the Heaviside function. Other fields can be introduced depending on the properties of the desired final system. The procedure is not *physical* in the sense that the field p has no direct (physical) meaning since (1.33) can represent quite varied physical situations. However, it allows a new perspective on hereditary systems:

Systems with memory can be interpreted as being non-local (or extended). This allows the introduction of a field which is now intrinsic to the system, and the variable (or property) which satisfies the D.D.E is a functional of this field depending on its value at each point in the system.

These ideas are rather general, and their effectiveness can be illustrated with a simple example taken from the study of population dynamics.

Example 1.3: REDUCTION OF A VOLTERRA TYPE D.D.E TO A SET OF O.D.E'S

Let us suppose the D.D.E is of the form

$$\frac{dx}{dt} = F(x(t), y(t)) \quad \text{where} \quad y(t) = \int_{-\infty}^t g(t - u)x(u)du. \quad (1.37)$$

with initial conditions

$$x(t) = \varphi(t) \text{ for } t < 0$$

$$\int_{-\infty}^0 \varphi(u)g(-u) du = I_0$$

where, again, g is the delay kernel.

Data on insect maturation times can be interpreted in terms of a delay kernel. This kernel can then be used in a distributed delay differential equation, itself obtained from an age-structured model formulated as a P.D.E [5]. For certain species of flies the kernel can be determined with sufficient precision and fitted to a shifted gamma distribution.

Suppose that g is the gamma distribution

$$g = G_a^m(q) = \frac{a^{m+1}}{m!} q^m e^{-aq}, \quad a, m \geq 0 \quad (1.38)$$

where m is an integer. This kernel has a maximum at $q = \frac{m}{a}$ so the average delay is given by

$$\bar{\tau} = \frac{\int_0^\infty q G_a^m(q) dq}{\int_0^\infty G_a^m(q) dp} = \frac{m+1}{a}. \quad (1.39)$$

Note that

$$\lim_{\substack{m, a \rightarrow \infty \\ \bar{\tau} \text{ const}}} G_a^m(q) = \delta(q - \bar{\tau}) \quad (1.40)$$

so that in this limit

$$y(t) = x(t - \bar{\tau}). \quad (1.41)$$

Similarly, we have the recursion relation,

$$\frac{dG_a^m(q-u)}{dq} = a \{ G_a^{m-1}(q-u) - G_a^m(q-u) \}. \quad (1.42)$$

We now introduce

$$z_0(t) \equiv x(t)$$

$$z_i(t) \equiv \int_{-\infty}^t x(u) G_a^{i-1}(t-u) du \quad i = 1, \dots, m+1. \quad (1.43)$$

The equations satisfied by the z_i 's are obtained by computing $\frac{dz_i}{dt}$ (using Leibniz's rule) and the recursion relation (1.42). The result is

$$\frac{dz_0}{dt} = F(z_0, z_{m+1})$$

$$\frac{dz_i}{dt} = a(z_{i-1} - z_i) \quad i = 1, 2, \dots, m+1, \quad (1.44)$$

where the first equation follows from $z_{m+1}(t) = y(t)$. Therefore the original integro-differential equation is strictly equivalent to the system (1.44) of $(m + 2)$ O.D.E's, all of which are linear except for the first one (because it contains F).

If the limit (1.40) is taken, the original equation becomes a D.D.E with discrete delay by virtue of equation (1.41), and it is equivalent to an infinite set of linear O.D.E's plus one non-linear O.D.E.

The initial condition of (1.37) is infinite-dimensional. The initial condition of the equivalent system of O.D.E's is finite dimensional (in the case of distributed delays). The equivalence between the two systems holds, although there is an apparent dimension difference since the initial condition for the integro-differential equation is infinite dimensional but the solution only depends on $m + 2$ integrals:

$$y_i(0) = \int_{-\infty}^0 \varphi(u) G^{i-1}(-u) du \quad (1.45)$$

i.e. the initial conditions for the set of O.D.E's. Here $\varphi(t)$, $t \in (-\infty, 0]$ is the initial function for (1.37).

This is an example of the redundancy of the information contained in an initial condition. Using this redundancy whenever possible is the basis of a technique of reduction of the study of the dynamics of some D.D.E's to the study of so called *shift operators* which will be presented in the next section (cf. Section 1.5.2).

1.5 Discrete delays: Production-Destruction models.

When the kernel g is a Dirac delta function, the dependence on past history is focused around a single instant in time and the dynamics are described by a D.D.E with discrete delays. Suppose the rate of change of a quantity $x(t)$ is equal to the difference between a production rate P and a destruction rate D ,

$$\frac{dx}{dt} = P - D. \quad (1.46)$$

Also assume that the destruction rate D is proportional to $x(t)$ while the production rate P , denoted by F from now on depends on the delayed variable $x(t - \tau)$:

$$\frac{dx}{dt} = -\alpha x(t) + F(x(t - \tau)) \quad \alpha, \tau > 0 \quad (1.47)$$

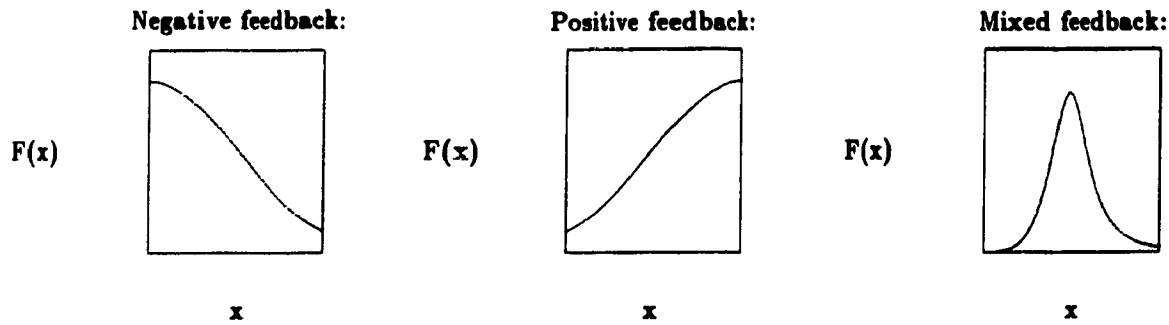


Figure 1.2: Example of three possible types of feedback.

or

$$\nu \frac{dx}{dt} + x(t) = F(x(t - \tau)) \quad \text{where } \nu = \alpha^{-1} \quad \text{and } F = \frac{P}{\alpha} \quad (1.48)$$

This equation has been used to investigate the dynamics of linear arrays of tunnel diodes, electro-optical bistable devices, high frequency generators [10, 13, 14, 23, 34]. It has been applied in mathematical biology to study the regulation of red blood cell populations [55], respiratory control circuits [55], and neural control loops [47].

The function F in (1.48) is the *feedback function*. Its characteristics determine the type of feedback present and the dynamics of (1.48).

- When F is monotone decreasing, the equation models a **negative feedback loop**.
- When F is monotone increasing, the equation models a **positive feedback loop**.
- In general F is not monotone and the maximal production rate occurs at some intermediate values of the variable. In such cases, the equation models a **mixed feedback loop**.

In spite of its simple form, equation (1.48) can display a wide array of behaviors. Its solutions can either be stationary, periodic with arbitrary complexity, or chaotic [14] and we are far from a complete understanding of its dynamics.

1.5.1 Singular perturbation of a difference equation.

A natural approach to equation (1.48) is to consider it as a singular perturbation of the difference equation with continuous argument

$$x(t) = F(x(t - \tau)), \quad t \in R^+ \quad (1.49)$$

along with the consistency condition

$$\lim_{t \rightarrow 0^-} \varphi(t) = F(\varphi(-1)) = x(0), \quad (1.50)$$

where $\varphi(t)$, the initial condition, is a function defined on $[-1, 0]$. From now on, the delay is taken to be 1. This can be done without loss of generality by scaling the time t (or replacing t by $t' = t/\tau$ in the above D.D.E).

A series of papers by Ivanov and Sharkovkiĭ [35] examines the connections between the dynamics of (1.48), those of (1.49) and those of the one-dimensional map

$$F: x \mapsto F(x). \quad (1.51)$$

The asymptotic behavior of solutions of (1.49) is linked to the dynamics of the map (1.51). To study the solutions of (1.49), one follows the continuum of trajectories of the discrete map $\{x_i \mid x_i = F(x_{i-1})\}$ with $x_0 \in \{x = \varphi(t) \mid t \in [-1, 0]\}$. The nature of the solutions (constant, periodic or chaotic) is related to the complexity of the iteration sequence $\{x_i \mid x_i = F(x_{i-1})\}$, $x_0 \in R$. For example a stable fixed point of the map corresponds to an attractive steady state solution for the difference equation. There is a formal correspondence between periodic iteration sequences and limit cycles in the continuous time system [35].

The next question to address is: "to what extent the results obtained by studying the difference equation (1.49) hold for the D.D.E?" The exact influences of the singular perturbation on a difference equation are not fully understood but the following results are a first step towards a complete understanding of equation (1.48). They are valid if the map F has an invariant interval $I = [a, b] \subseteq [0, 1]$ and if the non-linearity F in (1.48) is piecewise continuous.

Definition 1.1 The map F is said to possess an invariant interval $I = [a, b]$ if and only if

$$\forall x \in I, F(x) \in I. \bullet$$

Notation: $C(A, B) = \{f: f(x) \text{ is continuous and bounded above and below by the maximum and the minimum of } B, \text{ for all } x \text{ in } A\}$ with the norm, $\|f\| = \sup\{|f(x)| : x \text{ in } A\}$. The vector x stands for a point (x_1, \dots, x_n) in the n -dimensional space A . $C(A, B)$ is therefore a **Banach space.** •

Definition 1.2 $x_\varphi^\nu(t)$ denotes the solution of (1.48) with the initial condition $\varphi \in \mathcal{X}_I = \mathcal{C}([-1, 0], I)$. Similarly, $x_\varphi(t)$ denotes the solution of (1.49) with initial function $\varphi \in \mathcal{X}_I$.

Definition 1.3 x^* is an attracting fixed point of the map F with a basin of attraction J_0 if

$$\lim_{n \rightarrow \infty} F^n(x_0) = x^*, \forall x_0 \in J_0. \quad (1.52)$$

Further, let $\mathcal{X}_{J_0} = \mathcal{C}([-1, 0], J_0)$. •

Theorem 1.5.1 (Ivanov and Sharkovskii [35]):

For any $\nu > 0$ and $\varphi \in \mathcal{X}_{J_0}$, $\lim_{t \rightarrow \infty} x_\varphi^\nu(t) = x^*$. •

In other words asymptotically constant solutions persist under singular perturbations of (1.49). Theorem 1.5.1 can be extended to the case of an attracting set, an *attractor* of the map F .

Definition 1.4 I_0 is an invariant, attracting set for the map F with basin of attraction J_0 if

$$\lim_{n \rightarrow \infty} \text{dist}(F^n, I_0) \rightarrow 0 \text{ for all } x \in J_0.$$

where $\text{dist}(x, I_0)$ denotes the distance between a point $x \in R$ and a given, but arbitrary point belonging to the interval I_0 . •

Therefore, the basin of attraction is that region of phase space such that any trajectory initially belonging to it will eventually reach the invariant set. In other words, a given attracting invariant set will attract all trajectories originating in a region of phase space. This region is the basin of attraction. It should be noted that the structure of basins of attraction is in general quite complicated. In particular the boundary separating two neighbouring basins of attractions can possess a self-similar structure (see [8] and Section 3.3.2).

Theorem 1.5.2 (Ivanov and Sharkovskii [35]): For any $\nu > 0$ and $\varphi \in \mathcal{C}([-1, 0], J_0)$,

$$\inf\{I_0\} \leq \liminf_{t \rightarrow \infty} x_\varphi^\nu(t) \leq \limsup_{t \rightarrow \infty} x_\varphi^\nu(t) \leq \sup\{I_0\}. \bullet$$

This theorem tells us that when the structure of the attracting set I_0 of the map F is *complicated* [i.e. it is not simply a point, but perhaps a set of points of measure zero (e.g. a Cantor set), or a full interval], then this set also attracts solutions $x_\varphi^\nu(t)$ of the original D.D.E. This is a generalization of Theorem 1.5.1 which states the persistence of an attractive

fixed point under the singular perturbation. Theorem 1.5.2 says that attracting sets for the map are also attracting sets for the D.D.E.

In addition, it is possible to show that closeness between solutions of (1.48) and (1.49) holds uniformly on finite intervals $[0, \bar{t}]$ with $\bar{t} > 0$, for initial conditions φ satisfying the consistency requirement (1.51) [35]. This is in agreement with the intuition that close initial data φ and ψ generate solutions x_φ and x_ψ^ν which are close within at least a finite time interval, provided ν is small enough.

To make this precise, introduce the subset of initial functions $\mathcal{X}_I^0 = \{\varphi \in \mathcal{X}_I^0 \mid \varphi(0) = F(\varphi(-1))\}$. Then we have

Theorem 1.5.3 (Ivanov and Sharkovskii [35]) *For any $\varphi \in \mathcal{X}_I^0$ and positive \bar{t} and ε there exist positive δ and ν_0 depending on \bar{t}, ε and φ such that*

$$\|x_\varphi - x_\psi^\nu\|_{[0, \bar{t}]} \leq \varepsilon \quad \text{for all } 0 \leq \nu \leq \nu_0$$

provided $\|\varphi - \psi\|_{[-1, 0]} \leq \delta$ and $\psi \in \mathcal{X}_I$. •

These results (and others concerning, for example, the persistency of repelling sets) show the usefulness of reducing the D.D.E to a lower dimensional dynamical system when possible. Important qualitative information about the solutions of the functional differential equation can then be obtained with relatively little effort. However, care should be taken when trying to interpret them. In some simple cases the singular term $\nu(dx/dt)$ may yield either a simplification or a complexification of the behavior of the difference equation: the attractor of the difference equation consists of periodic functions, while that of the D.D.E represents chaotic solutions or *vice-versa*.

1.5.2 The paradigm equation: Piecewise constant non-linearities (PCNL).

Another set of techniques developed to study the dynamics of equation (1.48) is the *idealization* of the feedback function to make the equation analytically solvable. To understand the procedure, consider the following D.D.E:

$$\frac{dx}{dt} = -\alpha x(t) + F(x_\tau) \quad \text{where } x_\tau = x(t - \tau), \quad (1.53)$$

with

$$F = \frac{\beta x_\tau^m}{1 + x_\tau^n}, \quad (1.54)$$

a smooth humped function with a unique maximum located at

$$x_{max} = \left(\frac{m}{n - m} \right)^{(1/n)} \quad n > m > 1. \quad (1.55)$$

When the appropriate limit $n, m \rightarrow \infty$ is taken, F becomes piecewise constant:

$$\lim_{n \rightarrow \infty} F(x) = \begin{cases} 0 & \text{if } x \notin [a, b] \\ \xi & \text{if } x \in [a, b] \end{cases} \quad b(m, n) > a(m, n) > 0. \quad (1.56)$$

Equation (1.53), in conjunction to (1.56) is analytically solvable. Its solutions are piecewise exponential. Earlier work [1] shows that studying the equation with PCNL sometimes yields results applicable to the continuous feedback case.

In fact let us state an important theorem by Babai [1] linking the dynamics of an equation like (1.53) with a discontinuous non-linearity (1.56) to those of the equation

$$\frac{dx}{dt} = -\alpha x(t) + F_n(x(t - \tau)), \quad (1.57)$$

with the continuous non-linearity

$$F_n(\xi) = \begin{cases} 0 & \text{if } \xi < a - \frac{1}{n} \text{ or } \xi > b + \frac{1}{n} \\ 1 & \text{if } a + \frac{1}{n} < \xi < b - \frac{1}{n} \\ p_n(\xi) & \text{if } a - \frac{1}{n} < \xi < a + \frac{1}{n} \\ g_n(\xi) & \text{if } b - \frac{1}{n} < \xi < b + \frac{1}{n}. \end{cases} \quad (1.58)$$

In equation (1.58), $\lim_{n \rightarrow \infty} F_n = F$. The solution of (1.53) with (1.56) is $x(t)$ and that of (1.57) with (1.58) is $x_n(t)$.

Theorem 1.5.4 (Babai [1]): *Let $\varphi(t)$ be a continuous, positive function. Further let*

$$x_n(t - \tau) = x(t - \tau) = \varphi(t) \quad \forall t \in [0, \tau],$$

where $x(t)$ and $x_n(t)$ satisfy (1.53)–(1.56) and (1.57)–(1.58) respectively. Then as $n \rightarrow \infty$, x_n converges uniformly onto x in the time interval $[0, \bar{t}]$, $\forall \bar{t} \in R^+$. •

This general result draws the connection between *idealized* systems and real ones and is an important motivation for the work performed on integrable systems.

a) The paradigm equation:

The core of this thesis is the investigation of the dynamics of a D.D.E with a piecewise constant non-linearity emulating a mixed feedback situation

$$\frac{dx}{dt} = -\alpha x(t) + F(x(t-1)) \text{ with } F(\eta) = \begin{cases} c & \text{if } \eta \in [\theta_1, \theta_2] \\ 0 & \text{if } \eta \notin [\theta_1, \theta_2] \end{cases} \quad (1.59)$$

and $c > 0, \theta_2 > \theta_1 > 0$. This "box" shaped nonlinearity is the *idealization* of a smooth hump, characteristic of mixed feedback control functions. In general, with a smooth function (1.53) is not analytically integrable. The PCNL makes analytic integration straightforward, and the solutions are piecewise exponential increasing or decreasing depending on whether the delayed variable is contained in the interval $[\theta_1, \theta_2]$:

$$x(i) = \begin{cases} \gamma + (x(t_0) - \gamma) \exp[-\alpha(t - t_0)] & \text{if } x(s-1) \in [\theta_1, \theta_2] \forall s \in [t_0, t] \\ x(t_0) \exp[-\alpha(t - t_0)] & \text{if } x(s-1) \notin [\theta_1, \theta_2] \forall s \in [t_0, t] \end{cases} \quad (1.60)$$

where $\gamma = c/\alpha$ is the asymptote for the rising exponential.

b) PCNL: reducing the D.D.E to a shift operator.

When the D.D.E's are integrable, if the information contained in the initial function is redundant in certain parameter ranges then it is possible to reduce the equations to discrete time maps whose dynamics are closely tied to those of the D.D.E's.

One way to understand this is to see that the complete solution of equation (1.59) can be obtained by manipulating the extrema and the times at which the solution crosses either θ_1 or θ_2 . (This property is used in Chapter 3 to construct the analytic integration scheme mentioned earlier). Similarly, only a few points need be specified in the initial function to guarantee the uniqueness of the solution. The procedure is illustrated here with a one dimensional map obtained from (1.59). The details of the various derivations can be found in [24]. The idea is to construct a transformation \mathcal{T} mapping a time interval into a point (which completely characterizes the interval), and then to follow the evolution of this point under the action of a diffeomorphism. The sequence of points obtained by iterating the map completely describes the solution of the D.D.E.

To understand the derivation it is useful to realize that most of the information contained in a time interval of length 1 is redundant. To describe completely the solution on such an interval one needs to know the following:

1. When the solution crossed the thresholds θ_1 and θ_2 within the last delay.
2. Which region of phase-space the solution entered at these crossing times (i.e. whether it entered or exited the interval $[\theta_1, \theta_2]$).

Restricting our considerations to situations in which the solution crosses a given threshold at most once within a given delay (excluding the endpoints of the interval), only one variable is necessary to describe the solution on a time interval of length 1.

Let us define a set S of initial functions $\varphi(t)$, defined for $t \in [-1, 0]$, on which the transformation \mathcal{T} will act:

Definition 1.5 $\varphi \in S$ if and only if there exists a w such that for all $t \in [-1, -1+w)$, $\varphi(t) > \theta_1$, for all $t \in [-1+w, 0)$, $\varphi(t) < \theta_1$ and $\varphi(0) = \theta_1$. The solution is completely determined by w on $(0, 1]$. We label it $x_w(t)$.

It is noted here without proof that there exists a unique $w_1 \in (0, 1)$ such that for all $w < w_1$ the solution will tend to the lower asymptote without ever crossing θ_1 and a unique w_2 such that if $w > w_2$ the solution will tend to the upper asymptote and cross θ_2 before crossing θ_1 . The proof can be found in an der Heiden and Mackey [24]

Definition 1.6 Let c_i label the i^{th} solution of $x_w(t) = 1$ for $t > 0$ (i.e. the instant at which $x_w(t)$ crosses the bottom threshold for the i^{th} time). Also let e_i denote the i^{th} extremum of $x_w(t)$.

Without loss of generality we scale F (see Appendix A for details) such that

$$F(\zeta) = \begin{cases} c & \text{if } \zeta \in [1, b], \\ 0 & \text{if } \zeta \notin [1, b]. \end{cases} \quad (1.61)$$

Suppose that the parameters satisfy

$$\gamma - (\gamma - 1)e^{-\alpha} \leq me^\alpha < \gamma \quad \text{and} \quad \gamma(\gamma - 1 + e^{-\alpha})^{-1} \leq me^\alpha, \quad (1.62)$$

where m is the positive root of the quadratic

$$m^2 - (\gamma - (\gamma - 1)e^{-\alpha} - \gamma^2)m - \gamma(\gamma - 1)e^{-\alpha} = 0. \quad (1.63)$$

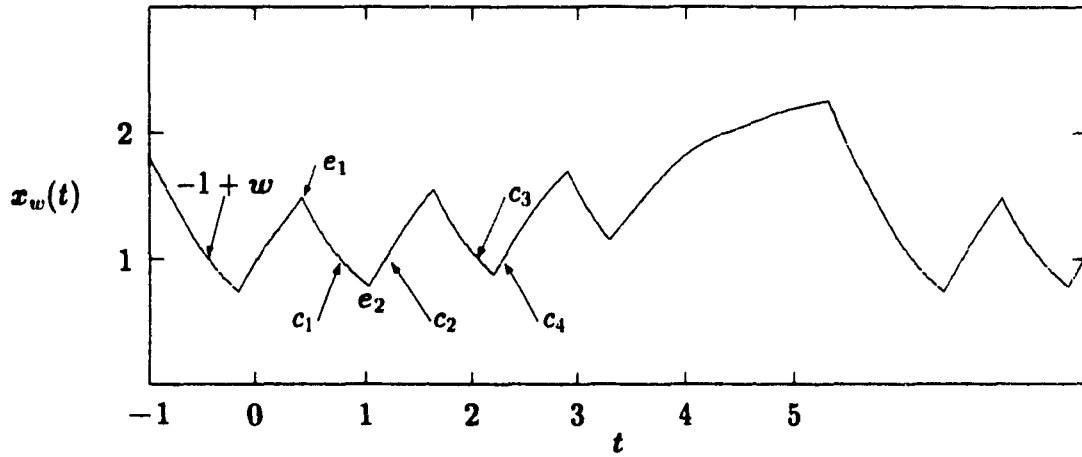


Figure 1.3: A typical solution of equation (1.59) with $\alpha = 2$, $c = 5$, $\theta_1 = 1$, $\theta_2 = 2$. Note that the initial function belongs to the set S introduced in Definition 1.4.

Both of these conditions are necessary to ensure that $x_w(t)$ does not cross 1 more than once within a delay, and that $e_1 < b$. Since $x_w(t)$ is piecewise exponential, it is straightforward to calculate e_1 , c_1 , e_2 , c_2 . If $\varphi \in S$, then e_i is a maximum if i is odd, and it is a minimum if i is even:

$$e_1 = x_w(w) = \gamma + (1 - \gamma)e^{-\alpha w}, \quad (1.64)$$

$$c_1 = -\frac{1}{\alpha} \ln \left[\frac{1}{e_1} \right] + 1, \quad (1.65)$$

$$e_2 = x_w(1) = e_1 e^{-\alpha(1-w)}, \quad (1.66)$$

$$c_2 = -\frac{1}{\alpha} \ln \left[\frac{1 - \gamma}{e_2 - \gamma} \right] + 1. \quad (1.67)$$

From Figure 1.3 it is clear that the solution on the interval $\Delta_2 = [c_2 - 1, c_2]$ belongs to S . If we now go back to the original interval Δ_1 in which $t \in [-1, 0]$ the time spent above the first threshold $\theta_1 = 1$ is w . In Δ_2 , the time spent above the same threshold is now $c_1 - c_2 + 1$. Formally,

$$\begin{aligned} T(\Delta_1) &= w \\ T(\Delta_2) &= c_1 - c_2 + 1 \end{aligned} \quad (1.68)$$

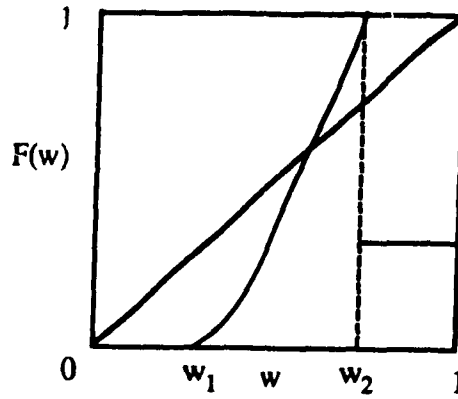


Figure 1.4: The one dimensional map \mathcal{F} when the parameters in equation (1.59) are such that its solution is the one displayed in Figure 1.3.

and this information is enough to describe the evolution of the solution $x_w(t)$ for all $t > 0$. In the mathematics literature, \mathcal{T} is known as a *shift operator*. It is a functional operator, but in our example (equation (1.59)), \mathcal{T} can be written as a one dimensional map because the functions on which it operates are described by the single parameter w .

This one-dimensional map \mathcal{F} of the unit interval onto itself,

$$\mathcal{F}(w) = c_1 - c_2 + 1 = w + \frac{1}{\alpha} \left\{ \ln[x_w(w)] + \ln \left[\frac{1 - \gamma}{x_w(1) - \gamma} \right] \right\} \quad (1.69)$$

is a discrete-time system which describes the evolution of $x_w(t)$ for all $t > 0$. Note that $x_w(w)$ and $x_w(1)$ are given by equations (1.64) and (1.66) respectively.

If $\mathcal{F}(w) > 1$, the solution escapes to θ_2 . In the simplest case (illustrated in Figure 1.3) it spends more than one delay above θ_2 and is then "reinjected" towards $\theta_1 = 1$. Because the solution remains above θ_2 longer than one delay, it *loses memory* of its behaviour in the neighborhood of θ_1 . As a result, on $\Delta_3 = [c_6 - 1, c_6]$ the time spent above θ_1 is independent of the way the solution reached θ_2 . In other words, with this choice of parameters, the transformation \mathcal{F} is constant on the interval $(w_2, 1]$. Figure 1.4 shows an example of a transformation \mathcal{F} derived with a set of parameters for which the solution looks like the one displayed in Figure (1.3).

The dynamics of the map are directly related to the behaviour of the original D.D.E. For example, a fixed point of the map corresponds to a periodic solution of the equation, and the linear stability analysis around the fixed point determines the local stability of the corresponding limit cycle. The presence of chaotic orbits in the map would imply the existence

of chaotic solutions of the continuous time system. Similarly, the basins of attraction of the map characterize some of the basins of attraction in the infinite dimensional phase space of the delay differential equation.

In regions of parameter space where the solutions cross a given threshold more than once within a delay, the reduction to a discrete time system is in principle possible. However, the dimension of the map increases with the number of variables necessary to describe the solution on an interval of length τ . In practice, this approach seems to not be efficient for the characterization of the more complex solutions of equation (1.59). Indeed, in some regions of parameter space, the complexity of the dynamics makes a deterministic investigation not only arduous but perhaps meaningless.

1.6 Summary.

In this introductory chapter, we presented a formulation of history dependent models in terms of functional differential equations. Some important ideas of non-linear dynamics and their relevance to the study of non-linear delay differential equations were then explored in Section 1.2. They include the concept of deterministic chaos and the sensitive dependence displayed by many non-linear equations on changes of their initial conditions.

In Sections 1.3 and 1.4 the important connection between hereditary systems and partial differential equations was then highlighted. It is shown that for a large class of systems, results existing concerning one formulation can be applied to the study of the other.

Finally, in Section 1.5, the approximation of D.D.E's by "simpler" dynamical systems, difference equations and finite dimensional maps was introduced for a class of non-linear D.D.E's with discrete delays modeling production-destruction processes.

In the following chapter, we describe an electronic circuit accurately modeled by such an equation in order to get an insight into the dynamics of a paradigm system for delayed mixed feedback mechanisms.

Chapter 2

Analog simulation of a D.D.E.

This chapter examines the dynamics of an electronic analog computer constructed to simulate a large class of systems described by the production destruction models introduced in Section 1.5. The details of the design are specific to the D.D.E under consideration. Circuit performance will be evaluated here for the simulation of an integrable delay differential equation introduced in Section 2.1.

Analog simulation might appear an archaic way to investigate the behavior of delay differential equations. As we have seen, several methods to study these equations analytically and numerically already exist. However, only simple equations (absence of noise, constant initial functions, simple non-linearities) have been studied so far.

The rationale for using an analog computer lies in the fact that we are no longer working with a model, but with a physical system described accurately by a chosen delay differential equation. There are several advantages to the use of analog simulations for the study of hereditary systems.

- 1) The real time integration allows rapid explorations of parameter space: changing a parameter is obtained by changing the value of a potentiometer.
- 2) Once the circuit is oscillating it is straightforward to investigate the influence of continuous parameter changes on solution behavior.
- 3) In addition, the presence of continuous electrical signals in the circuit avoids some of problems associated with specifying non constant initial functions since at equilibrium, the signal is an initial condition to itself, whether the parameters are fixed or in the process of

being varied continuously.

In this chapter, the circuit design is first presented in Section 2.1 along with a stage by stage description of its components. The attention is restricted to the simulation of the production-destruction models presented in Section 1.5. A detailed derivation of the equation simulated by the electronic analog computer is given in Section 2.2 and it is shown that this equation is equivalent to equation (2.3). In Section 2.3 the performance of the analog computer is evaluated from comparison with some digital simulations of equation (2.3). Finally, Section 2.4 explores the dependence of solution behavior on changes in the initial function.

2.1 Design of the analog computer.

We restrict our attention to equations introduced in Section 1.5 of the form

$$\frac{dx}{dt} = -\alpha x(t) + F(x(t - \tau)). \quad (2.1)$$

The computer designed to study (2.1) is a closed electronic loop. The voltage $x(t)$ is monitored at a given point in the loop. The idea behind the design is the following. If an electrical signal is to exist in the loop, it has to satisfy the constraints imposed by the different stages of the circuit. These constraints can be chosen so that the only signal possibly remaining is such that the voltage $x(t)$ satisfies the delay differential equation (2.1).

To simulate equation (2.1), the signal present in the circuit must be differentiated by one of the components. This is undesirable for two reasons.

1) Electronic differentiators are inherently unstable. They have a tendency to drift in time, due to charge build-ups on one of the capacitors present at a differentiating stage.

2) In addition, if a signal varies rapidly, its time derivative will be large. This means that there will be a voltage surge past the differentiator in the loop. Most electronic components are vulnerable to these surges.

To improve performance it is desirable to avoid differentiators in the analog computer. This can be done by rewriting equation (2.1) as an integral equation,

$$x(t) = \int_{t_0}^t [-\alpha x(s) + F(x(s - \tau))] ds + x(t_0) \quad \text{where} \quad \begin{cases} t & \geq t_0, \\ s & \geq -\tau. \end{cases} \quad (2.2)$$

The circuit is then built to simulate this equation. It must be able to amplify the present signal $x(t)$ by a factor of α , delay it and then transform it according to the desired F , sum the resulting signals, integrate the sum and then equate the result of the integration with the initial signal. These operations are represented schematically in Figure 2.1.

At this point, we need to know what the exact production rate F is in order to describe the design in detail. Thus we focus attention on a simple system given by

$$\frac{dx}{dt} = -\alpha x(t) + F(x(t - \tau)), \quad \text{where } F(x_\tau) = \begin{cases} c & \text{if } x_\tau \in [\theta_1, \theta_2] \\ 0 & \text{otherwise} \end{cases} \quad (2.3)$$

with $\alpha > 0$. The production rate F is piecewise constant and the destruction rate is proportional to the present signal $x(t)$ so that the solution is a sequence of piecewise exponential segments, alternatively increasing and decreasing (see equation (1.60) for an analytic expression of the solutions of (2.3) when $\tau = 1$).

The analog computer is built to simulate equation (2.3) for several reasons.

1) The availability of analytic results for this system make it an ideal candidate because the performance of the analog computer can be calibrated with analytic results rather than with numerical ones.

2) In addition, it is hoped that the analytic investigation of new types of behaviors observed with the electronic circuit will be facilitated by the integrability of equation (2.1). It seems that there is little point in simulating electronically a D.D.E which has been integrated numerically and for which analytic results appear to be out of reach.

The proper calibration of the various components and the precise delimitation of their range of applicability is necessary for a proper interpretation of the data. To understand the behavior of the analog electronic oscillator, it is crucial to know what the effect of each stage is on its input signal.

2.1.1 Stage by stage description of the circuit.

Most components of the oscillator are simple applications of operational amplifier technology. We begin with the description of these elements.

a) Op-amp based components.

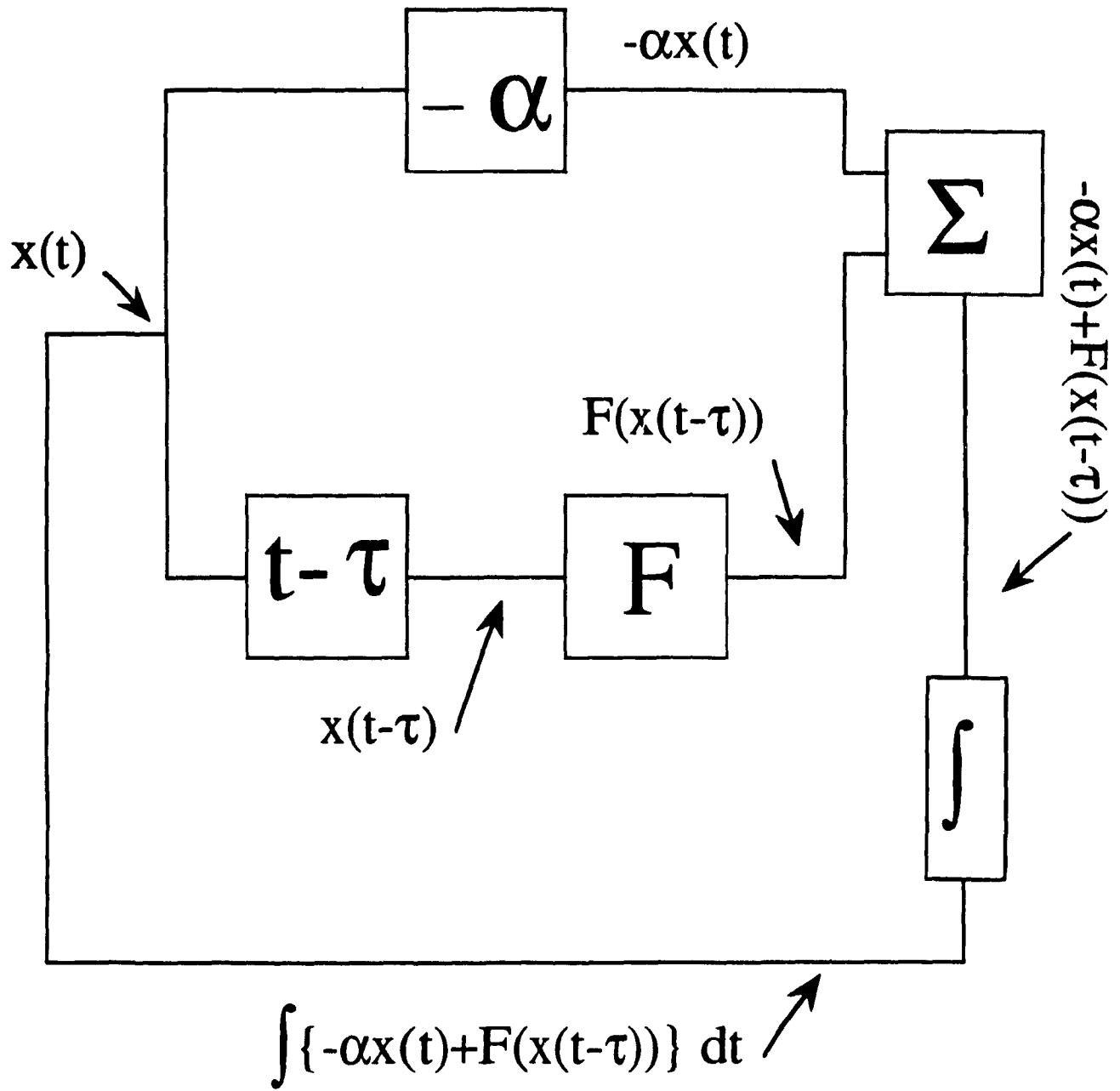


Figure 2.1: Block diagram of the electronic analog computer.

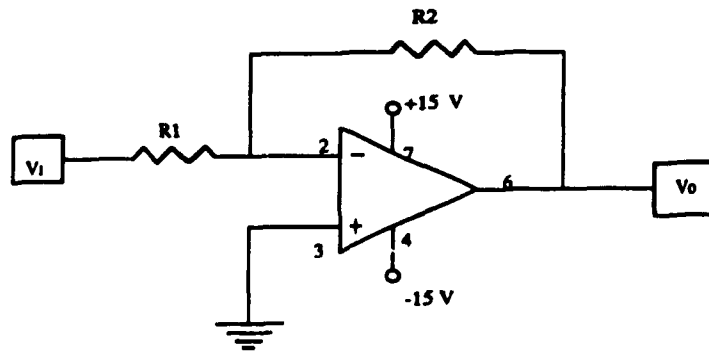


Figure 2.2: The finite gain inverting amplifier, used in the computer to simulate the destruction rate in equation (2.3).

The finite gain inverting amplifier. (Figure 2.2) As a function of the input voltage $V_i(t)$, the output voltage $V_o(t)$ is given by the relation:

$$V_o(t) = -\frac{R_2}{R_1} V_i(t).$$

Throughout the circuit, the finite gain operational amplifiers were built using a standard amplifier, the uA741TC [31].

The main limitation of this component is an attenuation of the output for high input frequencies. This effect is absent for signals varying at less than 10KHz. Since the Bessel filter (see below, Section 2.1.1b) is adjusted to have a corner frequency at 1 KHz, we need not consider this problem further.

The summing amplifier. (Figure 2.3) The role of a summing amplifier is to add two signals present at its inverting input. The relation between input voltages $V_1(t)$ and $V_2(t)$ and output voltage $V_o(t)$ is

$$V_o(t) = -\frac{R_3}{R_1} V_1(t) - \frac{R_3}{R_2} V_2(t)$$

This component is built with a CA3140E, an op-amp with low input current and high input impedance, necessary qualities to improve the stability.

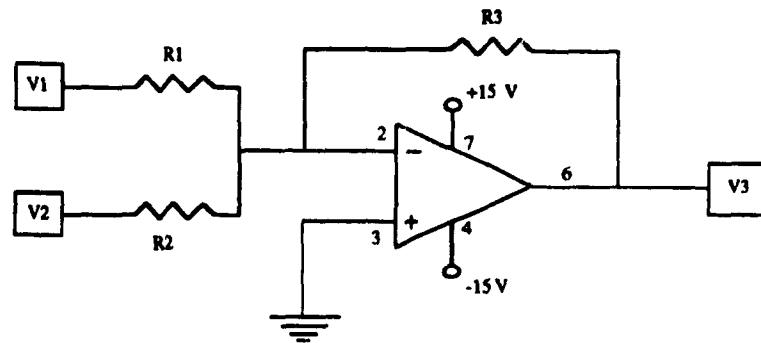


Figure 2.3: *Summing amplifier stage. It is used in the computer to add the production and destruction rates before integrating the sum. The op-amp used here is a CA3140E.*

As in the previous stage, the main limitation is an attenuation of the output for frequencies higher than 10KHz but again this effect will not be considered further.

The integrator. (Figure 2.4) This part of the circuit is straightforward. The output voltage V_0 of the integrator is given as a function of the input V_i by,

$$V_0(t) = -\frac{1}{RC} \int_{t_0}^t V_i(s) ds + V_0(t_0).$$

However, some care has to be taken to choose the proper chip because integrators have a tendency to saturate, primarily due to charge build-up on the capacitor C_1 . The offset voltages and offset currents are responsible for this effect [see [28] for concise definitions of the terms employed here]. The rate at which the integrator saturates increases as the frequency of the input signal decreases. For reasons detailed in Section 2.1.1b, the frequency of the expected solutions should vary between 1Hz and 100Hz. The op-amp chosen for this component is an OP-07E, specifically designed for this type of application. Its main characteristics are a very low drift current and small temperature coefficient.

The values of R and C are chosen to minimize leakage current, saturation rate and other problems frequently encountered with integrators [For a detailed discussion of electronic analog integration, see [31]]. The frequency response is flat at frequencies below 2KHz.

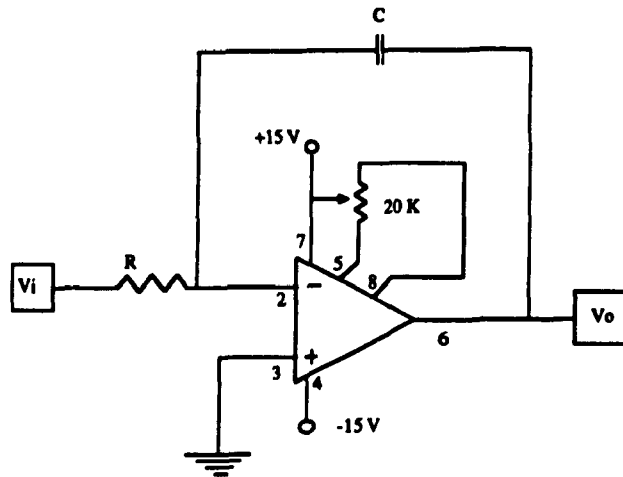


Figure 2.4: Schematic diagram of the integrating stage. The $20\text{ K}\Omega$ resistor between pins 1 and 8 is part of a recommended trimming circuit needed to improve the integrator's stability.

Bias adjusting stages. (Figure 2.5) These elements add or subtract a controllable DC level to the input signal. They are necessary since the circuit component which delays the signal (the Bucket Brigade Device (see below)) only works properly when the AC input has an 8 volt DC offset. Bias adjusting circuits are needed to raise the signal before the delay chip, and then lower it back to its initial value after it has been delayed.

As for the other simple op-amp based stages, there is no attenuation at low frequencies. The gain of these components is unity, and the attainable offsets range from -10V to $+10\text{V}$.

b) The delay circuit. (Figure 2.6)

The time delay in the system is totally responsible for the wealth of dynamics displayed by equation (2.3). Electronically, this delay is obtained with an analog delay line, a CMOS sampling device sometimes called a bucket brigade device (hereafter referred to as a B.B.D). It samples and delays a signal by storing it in a series of capacitor circuits. Each of these capacitor circuits is referred to as a "bucket" and the B.B.D transfers the contents of one bucket into the next at every other logic high of the clock pulse. The time delay is inversely proportional to the clock pulse frequency F_{clock} and proportional to the number N of buckets in the chip. Given the sampling frequency F_s ,

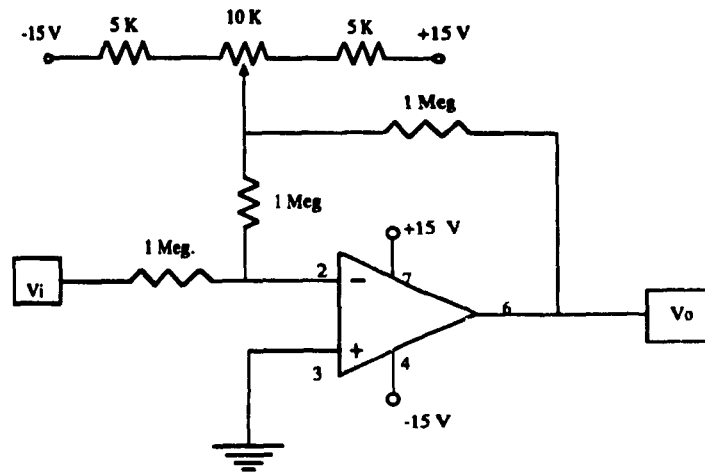


Figure 2.5: Diagram of the bias adjusting circuits, needed to operate the delaying elements in the analog computer.

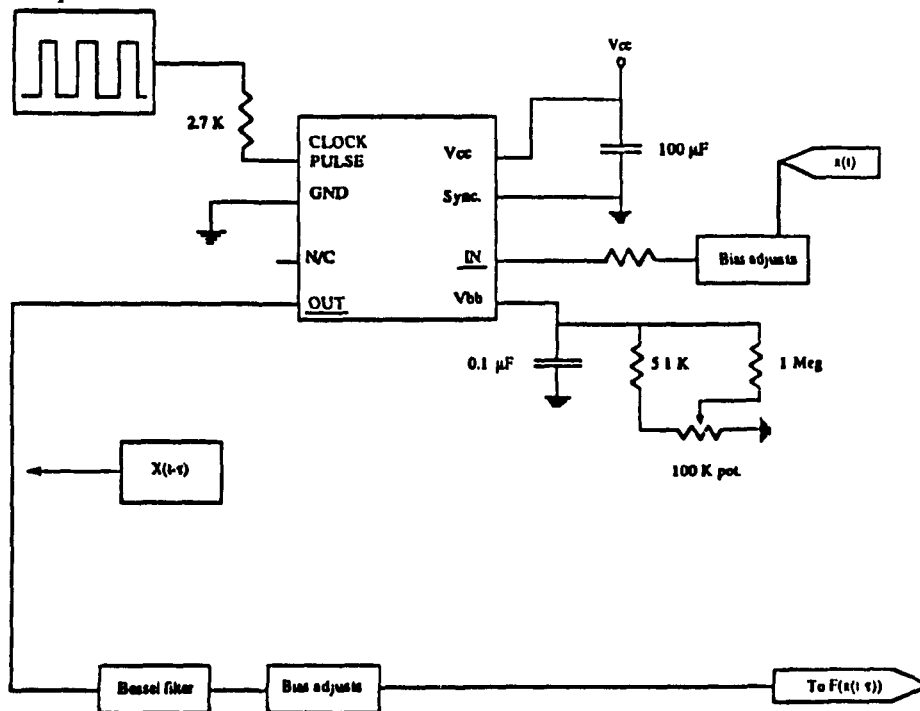


Figure 2.6: The delay circuit is made of four components: an analog delay line (B.B.D), two bias adjustment circuits and a bessel filter. A pulse generator provides the sampling pulse. The sampling pulse frequency determines the length of the delay.

$$F_s = \frac{F_{clock}}{2},$$

the delay τ is

$$\tau = \frac{N}{F_s}. \quad (2.4)$$

The B.B.D used here was a RD5108 analog delay line for which $N = 1024$.

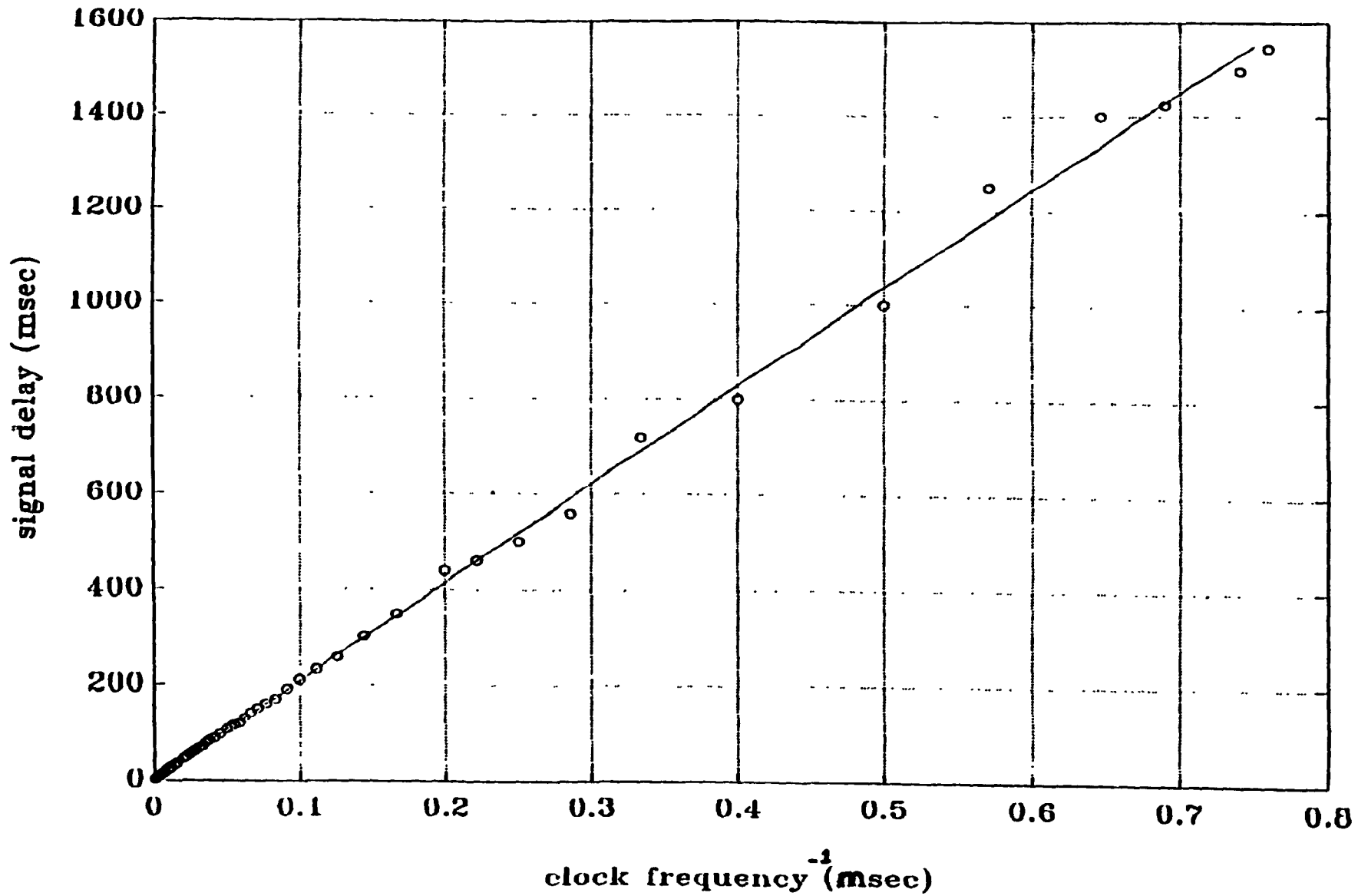
Figure 2.7 shows the dependence of the delay on the sampling frequency. Observations agree with equation (2.4) for sampling frequencies below 500KHz with an error of less than 1%. We are interested in having sampling frequencies of about 10KHz for reasons that will be clear shortly, and in this case equation (2.4) is a reliable determinant of τ . However to increase the reliability of our observations, the delay was determined from the calibration curve displayed in Figure 2.7.

B.B.D calibration was performed by observing the relative phases of the input signal and the filtered output with a digital oscilloscope. The filtering was performed by a Bessel filter, an active filter with a controllable corner frequency (cut-off frequency). The use of such a filter is necessary to smooth the B.B.D's output since this chip samples its input and restores it as a sequence of steps.

The sampling frequency, which determines the delay, is chosen to minimize the various destabilizing factors in the computer. The frequency of the simplest limit cycle (indicative of the frequency of most other limit cycles observed) increases with τ . However, the amplitude decreases with τ [24]. A signal oscillating too slowly is difficult to integrate because the charge accumulated on the integrator's capacitor causes saturation unless the chip can be finely trimmed (i.e. the sources of error present in the chip, like the offset current the offset voltage are reduced to an absolute minimum). In this case, temporal drifts due to small temperature changes will decrease the accuracy of the integrator. On the other hand, we do not want to work with signals of too small amplitude since the signal to noise ratio should be as high as possible.

A sampling frequency of about 10KHz gives a signal amplitude of about one volt, keeping the signal to noise ratio (see Section 2.1.2 below) in the circuit above 100 while maintaining the frequency of the simplest limit cycle between 2 and 3Hz. With these parameters fixed the integrator works as intended.

Figure 2.7: Calibration curve for the analog delay line. This data was used to determine the delay in the circuit, the sampling frequency being given by a digital frequency meter.



Independently of the calibration of the B.B.D, which only gives us information about the length of the delay, we want to study the frequency response of the combined elements of the circuits lying between points (11) and (6) (see Figure 2.10). This set of components will hereafter be referred to as the delay box.

• Frequency response of the delay box (see Figure 2.8). Since the gain of the delay box is observed to depend on the offset of the input signal, the frequency response was examined at four values of the offset: 0.25, 0.45, 1.00, 1.5 volts. These offsets were chosen because all the measured offsets for the observed limit cycles lie within this interval. The signals used for the frequency analysis are triangle waves of 1 volt amplitude. The triangle wave is chosen because of its resemblance to the simple limit cycle. The results, shown in Figure 2.8 show a constant unity gain for a given offset at low frequencies ($\leq 100\text{Hz}$). These results are in good agreement with the measured gain when the circuit is spontaneously oscillating.

The initial preparation of the analog computer (corresponding to the initial function for the D.D.E) is the turn-on state of the B.B.D *i.e.* the various voltages present in the 1024 buckets when the circuit starts oscillating.

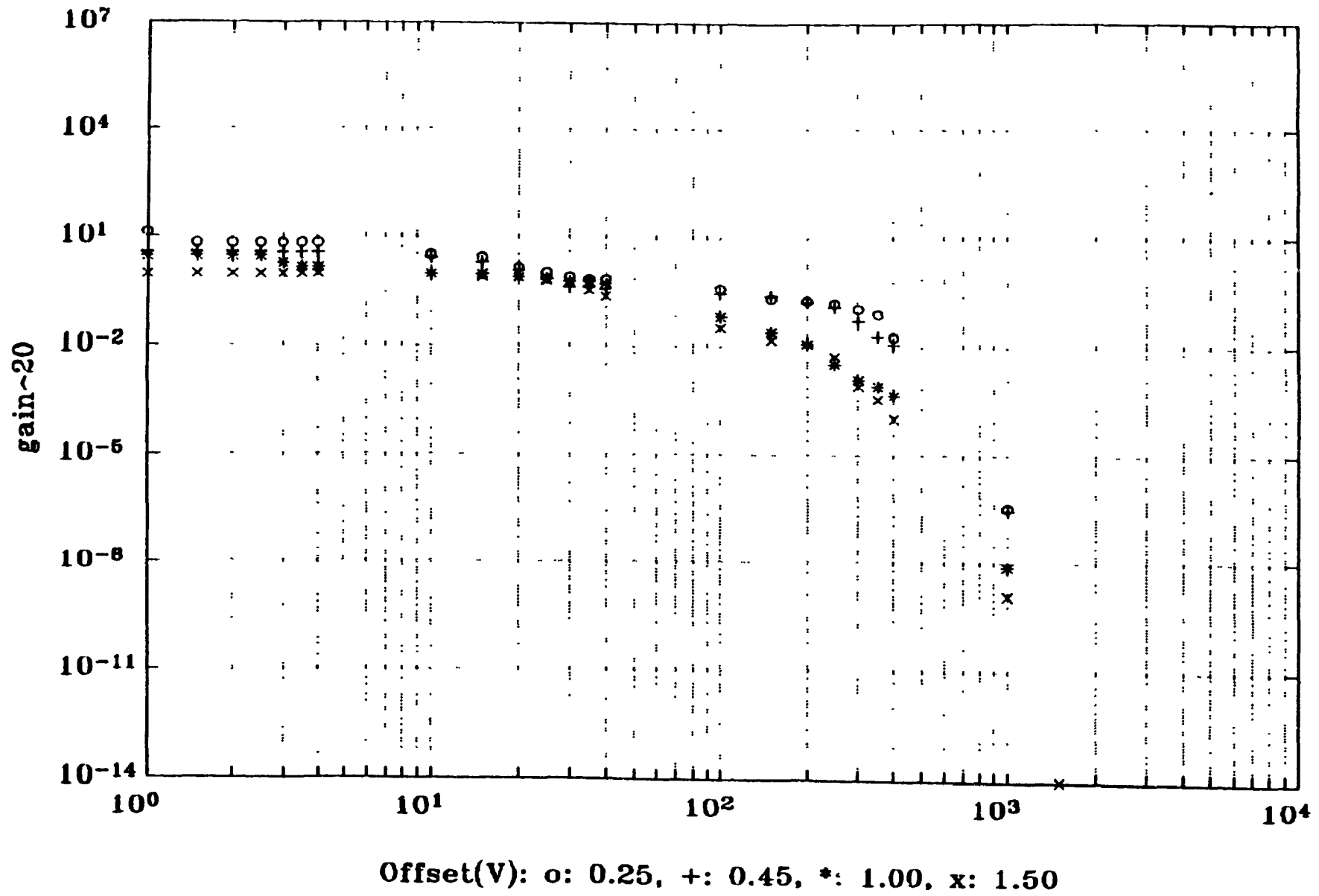
c) The feedback function. (Figure 2.9)

The feedback function F used here is the PCNL idealization of a smooth function describing a mixed feedback situation. It is defined by,

$$F(q) = \begin{cases} c & \text{if } q \in [\theta_1, \theta_2], \\ 0 & \text{otherwise.} \end{cases} \quad (2.5)$$

This function is simulated electronically with two comparator circuits. This stage is most easily understood by looking at the behavior of each comparator circuit separately, and then at how their outputs are combined by logic gates. For the detailed description of a comparator see [28]. The comparator output is either saturated at V_{cc} or at ground depending on whether the non-inverting input is above or below the inverting one. Standard op-amps are not comparators and should not be used as comparators even though their electronic symbols are the same. Dual packages designed for this type of application are standard. The one used here is an LM393.

Figure 2.8: Frequency response of the delay box.



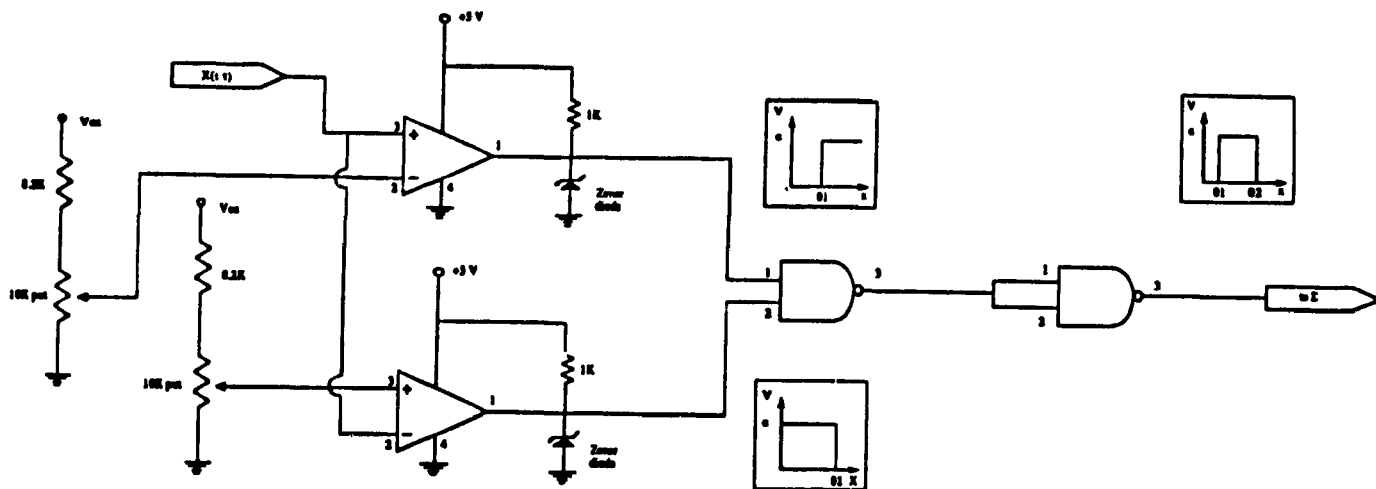


Figure 2.9: Diagram of the components simulating the piecewise constant function defined in (2.5).

The voltage dividers are used to set the values on one of the inputs on each comparator. The output of comparator 1 is V_{cc} when the voltage $x(t)$ at the noninverting input is *higher* than the one set by the divider at the inverting input corresponding to θ_1 . The output of comparator 2 is V_{cc} when the voltage $x(t)$ at the inverting input is *lower* than the voltage set by the divider at the non-inverting input corresponding to θ_2 . These two outputs are combined by a 74LS00P NAND gate, the output of which is V_{cc} when $x(t)$ is between θ_1 and θ_2 , and zero otherwise. The resulting signal is sent to a logic inverter which produces the desired feedback function.

• Limitations.

The only limitations that need be considered regarding this stage are the threshold sensitivities. The feedback function was found to toggle between its low and high values for input voltages differing by less than 2 mv. The time derivative of the signal is sufficiently large [typically of the order of 1 (v/s)], so this limitation does not affect the analysis.

2.1.2 Noise level in the circuit.

As in all electronic systems, noise is present. Aperiodic fluctuations are observed even when the power is turned off. During the simulations, the noise shows up as small, rapid oscillations riding the main cycle. However, the signal we are interested in is clearly distinguishable from this noise since its fundamental frequency lies below 10Hz and amplitude (of order 1 volt) is about two orders of magnitude larger than the fine structure fluctuations.

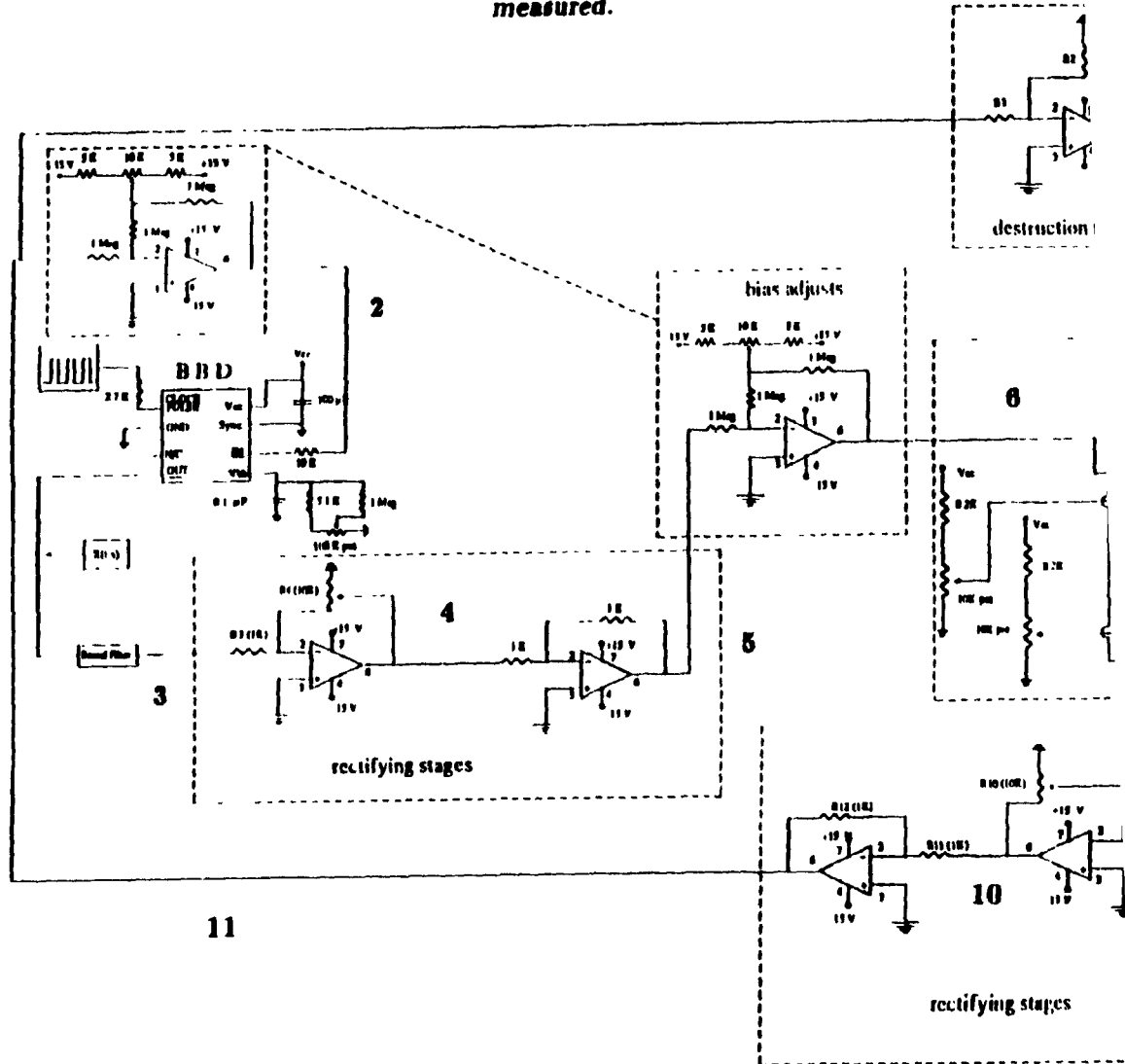
The exact influence of this noise on the system dynamics are not known. It is known that dynamical systems can be very sensitive to stochastic perturbations even when the (amplitude) scale of the perturbations is much smaller than the scale of the process under consideration. For example, the presence of noise in a deterministic system might result in a shift in parameter space of the point at which a bifurcation occurs in the unperturbed case (the bifurcation could either be *advanced* or *postponed*). These phenomena are known as *noise-induced transitions* and have been the subject of intense scrutiny for some time [29] [47]. Noise can also induce chaotic behavior or, conversely, highlight the coherence underlying chaotic dynamics.

Figures 2.20 – 2.21 give some information concerning the power spectra of analytic solutions and analog simulations of equation (2.3). They indicate that for slowly varying cycles, the influence of stochastic perturbations on solution behavior is negligible. On the other hand, the systematic shifts in parameter space observed in Figures 2.11 – 2.19, and discussed in Section 2.3.1a, may be due to the subtle (and unexplained) action of noise on the delay differential equation. These two observations are not contradictory, but reflect the natural complexity arising from the interactions between purely deterministic and purely probabilistic contributions.

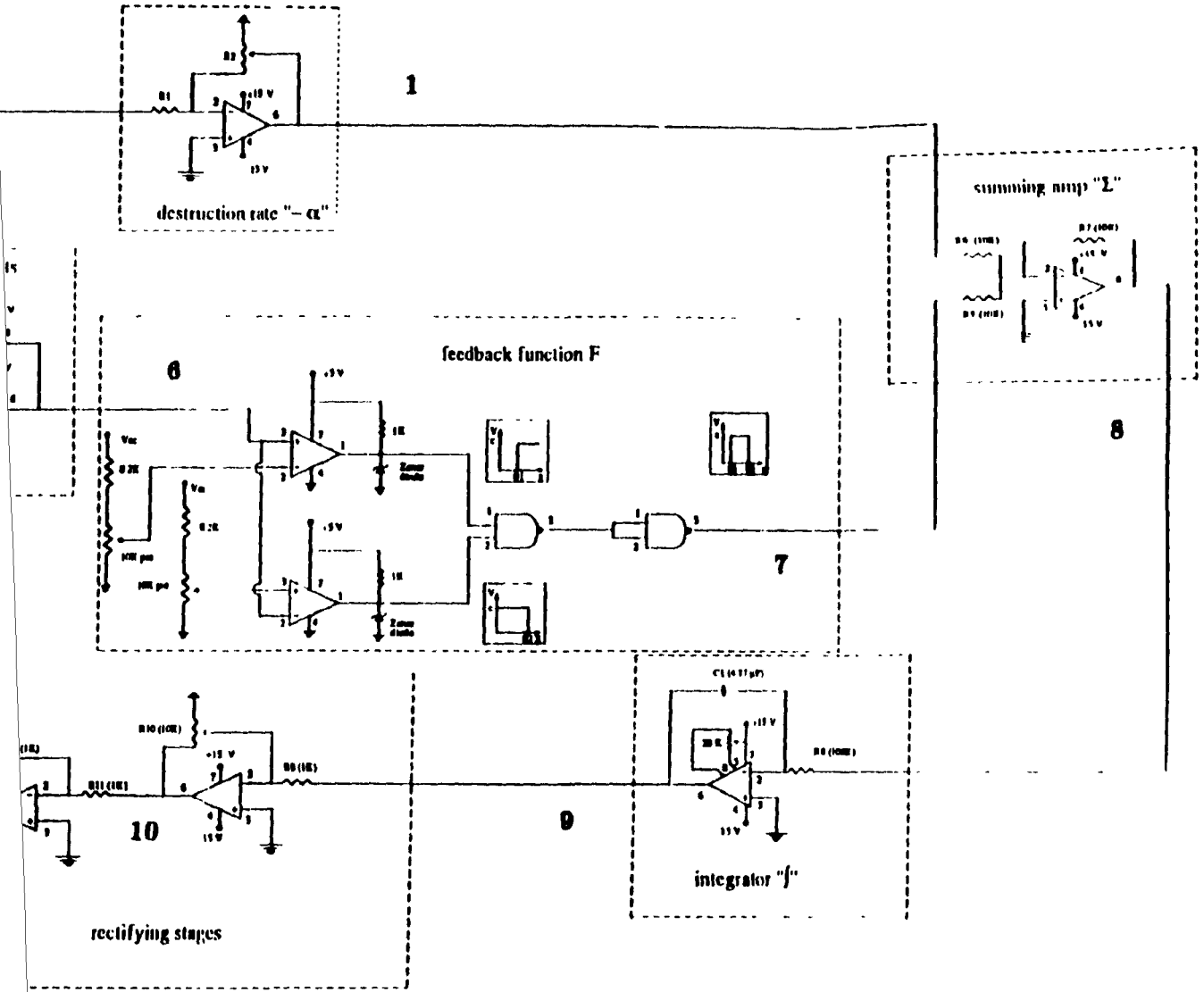
2.2 Derivation of the circuit equation.

After calibration of the different stages, the closed loop oscillates spontaneously and the computer integrates a D.D.E. Unambiguously identifying the equation being simulated requires additional analysis, but is crucial if the electronic loop is to be a reliable tool. It is possible that the different stages influence one another in a way such that the integrated system is no

Figure 2.10: Detailed diagram of the analog co indicate the points in the circuit at which the measured.



gram of the analog computer. The bold numbers from 1 to 11
 circuit at which the voltages $x_i(t)$ defined in Section 2.2.3 are



longer described by equation (2.3). Therefore, before any attempts to electronically match the results with the theory are made, it is important to verify that some basic characteristic properties of equation (2.3) are present in the circuit. Similarly, it is crucial to study the stability of the closed loop. This will tell us if the parameters set in the oscillator are time dependent or not.

These observations are necessary to justify some assumptions that are made when a quantitative analysis of the results is undertaken in an attempt to establish the exact correspondence between the D.D.E and the analog computer.

2.2.1 Stability of the closed loop.

The identification of offset drifts due to temperature changes is relevant whenever one deals with analog computers. It is equivalent to asking whether or not there exists a state of thermal equilibrium for the circuit. Charge accumulation on the various capacitors could have a similar effect, potentially causing saturation of the whole system.

The warm-up time for the circuit is approximately one hour. During this time, the offset of the waveform decreases by 0.1 ± 0.03 volts. Once equilibrium is reached, the offsets are constant to within the measurement uncertainty (10^{-3} volts) for periods of up to ten hours (this is the longest time for which the oscillator was observed continuously, and is therefore a lower bound on the temporal stability of the offsets in the loop). The shape and amplitude of the waveform are also constant indicating that the parameters are indeed time-independent.

2.2.2 Qualitative observations.

Analytically, the upper asymptotic value $\gamma = c/\alpha$ of the solution $x(t)$ is obtained by simultaneously taking the limits $\theta_1 \rightarrow 0$ and $\theta_2 \rightarrow \infty$. The lower asymptotic value is obtained by setting $\theta_1 = \theta_2$. Electronically, if the measured second threshold is set at values higher than 3 volts while the lower threshold is taken to zero, the observed waveform reaches a constant value interpreted as the upper asymptote. Similarly, if the two voltages simulating the thresholds θ_1 and θ_2 are set equal to each other the solution goes to zero.

Bifurcations closely resembling those predicted theoretically are observed. According to the theory [24], in certain regions of parameter space the solutions periodically approach an

unstable homoclinic cycle. This tendency is also observed in the electronic loop, the unstable limit cycle being, as in the theoretical case, a periodic oscillation around the lower threshold with period $P \in [\tau, 2\tau]$.

It is important to keep in mind the nature of the observations in the preceding paragraph. They are qualitative in the sense that we do not know exactly which equation is simulated by the analog computer. To be more precise, the circuit was designed to simulate a particular delay differential equation (i.e. (2.3)) and the circuit's behavior indicates that, indeed, its dynamics can be described by an equation which possesses certain properties of equation (2.3). On the other hand, further analysis is required to establish the formal 1 between the circuit and the equation it is supposed to simulate. The reason for the care being taken here to distinguish between the electronic solutions (the voltage observed at a chosen point in the circuit) and the analytic solutions of (2.3) (the solutions obtained on a digital computer with the algorithm of integration described in Chapter 3) is threefold.

- 1) The analog computer is a physical system and it is designed to be modeled by a chosen D.D.E ((2.3) in our case). The imprecisions in the design may add up to make the loop behave quite differently from (2.3), even though some of the properties of (2.3), discussed above in this section, seem to be present in the electronic analog computer.

- 2) Ideally, except for the amplifier simulating the destruction rate in equation (2.3), the gain of all stages in the electronic loop should be identically unity. In addition, there should be no offsets anywhere in the circuit. This cannot be the case because there are technical constraints in the construction of the circuit which imply the addition compensating circuits which cannot always have unity gain and zero offsets. Similarly, an integrator's gain is closely linked to its cutoff frequency, and the frequency of the signal to be integrated is the main factor influencing the designer in the choice of the values of the various resistors and capacitors present at an integrating stage, regardless of its total gain. As a consequence, the destruction rate in the circuit (i.e. amplifier 1 in Figure 2.10) is not the only component which participates in the effective simulation of a destruction rate, and it is necessary to derive the "circuit equation" before proceeding to a quantitative interpretation of the data (i.e. one in which the electronic and the analytic solutions are compared quantitatively for equal parameter values).

3) Finally, although it appears that equation (2.3) possesses five independent control parameters α , θ_1 , θ_2 , τ , and c , it is shown in Appendix A that the equation can be scaled such that only three independent parameters remain. In other words, (2.3) is equivalent to

$$\frac{dx}{dt} = \delta[G(x(t-1)) - \epsilon x(t)],$$

with

$$G(\xi) = \begin{cases} 1 & \text{if } \xi \in [1, \rho] \\ 0 & \text{otherwise,} \end{cases}$$

and

$$\begin{aligned} \delta &= \frac{\tau c}{\alpha} \\ \epsilon &= \frac{\alpha \theta_1}{c} \\ \rho &= \frac{\theta_2}{\theta_1}. \end{aligned}$$

2.2.3 Quantitative interpretation of the data.

It is possible to formulate the equation simulated by the analog computer by simply tracing the signal as it passes through all the individual stages. The underlying assumption, justified by the discussion of Section 2.2.2, is that when the loop is closed each stage continues to behave as it did in an open loop configuration.

It is useful to define $x_i(t)$ as the voltage present at time t at point i of Figure 2.10. Expressed in terms of one another, these voltages are:

$$\begin{aligned} x_1(t) &= -(R_2/R_1)x(t), \\ x_2(t) &= -x(t) + k_1, \\ x_3(t) &= \alpha_3 x_2(t - \tau) + k_B, \\ x_4(t) &= -(R_1/R_3)x_3(t) + k_1, \\ x_5(t) &= -x_4(t) + k_5, \\ x_6(t) &= -x_5(t) + k_2, \end{aligned} \tag{2.6}$$

$$\begin{aligned}
x_7(t) &= F(x_6), \\
x_8(t) &= -(R_7/R_5)x_7(t) - (R_7/R_6)x_1(t), \\
x_9(t) &= \frac{-1}{(R_8C_1)} \int_{t_0}^t x_8(t') dt' + x_9(t_0), \\
x_{10}(t) &= (R_{10}/R_9)x_9(t), \\
x_{11}(t) &\equiv x(t) = -(R_{12}/R_{11})x_{10}(t),
\end{aligned}$$

where

$$\begin{aligned}
k_1 &\equiv \text{offset due to bias adjust 1,} \\
k_2 &\equiv \text{offset used to recover the DC level before amplifier 2,} \\
k_B &\equiv \text{offset due to B.B.D + Bessel filter,} \\
k_4 &\equiv \text{offset due to amplifier 4,} \\
k_5 &\equiv \text{offset due to amplifier 5,} \\
\alpha_3 &\equiv \text{gain of B.B.D + Bessel filter.}
\end{aligned}$$

Using these definitions, we obtain the following relation between $x(t)$ and $x_6(t)$,

$$x(t) = \frac{R_{12}R_{10}R_7}{R_{11}R_9R_8R_5C_1} \int_{t_0}^t F(x_6(s)) ds - \frac{R_{12}R_{10}R_7R_2}{R_{11}R_9R_8R_6R_1C_1} \int_{t_0}^t x(s) ds + x(t_0). \quad (2.7)$$

Differentiating (2.7) and rewriting x_6 using (2.6) yields,

$$\begin{aligned}
\frac{dx}{dt} &= \frac{R_{12}R_{10}R_7}{R_{11}R_9R_8R_5C_1} F \left(\frac{R_4\alpha_3}{R_3} x(t - \tau) - \frac{R_4\alpha_3}{R_3} k_1 - \left(\frac{R_4}{R_3} \right) k_B + k_2 + k_4 - k_5 \right) \\
&\quad - \frac{R_{12}R_{10}R_7R_2}{R_{11}R_9R_8R_6R_1C_1} x(t). \quad (2.8)
\end{aligned}$$

This equation is the one simulated by the analog computer and it is equivalent to the original D.D.E (2.3). The only difference is that the parameters specified in the original equation (2.3) are functions of the parameters in equation (2.8). To avoid any ambiguity in the designation of the system variables, the parameters set electronically through control of the circuit components will be referred to as the measured parameters. The corresponding values obtained with the following analysis will be referred to as effective parameters.

Measured and effective parameters: Establishing the correspondence.

From equation (2.8), the definition of the feedback function in the circuit is:

$$F(a_1 x(t - \tau) + o_1) = \begin{cases} c & \text{if } (a_1 x(t - \tau) + o_1) \in [\theta_1, \theta_2], \\ 0 & \text{otherwise,} \end{cases} \quad (2.9)$$

where

$$a_1 = \alpha_3 \left(\frac{R_4}{R_3} \right),$$

and

$$o_1 = -a_1 k_1 + k_2 - k_B \left(\frac{R_4}{R_3} \right) + k_4 - k_5.$$

These relations follow from the equations in (2.6). The problem we are faced with is that the circuit was designed so that the argument of the feedback function be the delayed variable $x(t)$, not a linear function of it: $a_1 x(t - \tau) + o_1$. The same is true for the signal amplified by R_2/R_1 : it was supposed to be $x(t)$, but it turns out to be $x_{11}(t)$ from equation (2.6). The purpose of the following analysis is to transform, or scale, the various terms of (2.3), so that it can be compared with the circuit equation (2.7). To make these ideas clear, consider equation (2.9). It can be written as

$$F(x(t - \tau)) = \begin{cases} c & \text{if } x(t - \tau) \in [\theta_1^e, \theta_2^e], \\ 0 & \text{otherwise,} \end{cases} \quad (2.10)$$

with

$$\theta_1^e = \frac{(\theta_1 - o_1)}{a_1}, \quad \theta_2^e = \frac{(\theta_2 - o_1)}{a_1}. \quad (2.11)$$

In other words, a change in the argument of F is equivalent to a change in the thresholds. The circuit was initially designed so that the argument of F would be $x(t - \tau)$. In practice, it is $x_6(t)$. The dynamically relevant parameters are no longer θ_1 and θ_2 but θ_1^e and θ_2^e .

As the thresholds change, so do the gain and the height of the feedback function. From equation (2.7), the constant multiplying $x(t)$ is:

$$\alpha^e = \frac{R_{12} R_{10} R_7 R_2}{R_{11} R_9 R_8 R_6 R_1 C_1},$$

or, since $\alpha = (R_2/R_1)$,

$$\alpha^e = \frac{R_{12} R_{10} R_7}{R_{11} R_9 R_8 R_6 C_1} \alpha. \quad (2.12)$$

Again from equation (2.7), the effective height of the feedback function is proportional to its measured value:

$$c^e = \frac{R_{12}R_{10}R_7}{R_{11}R_9R_8R_5C_1}c. \quad (2.13)$$

It is observed that the off state of the function F is not 0 (ground) but a finite, positive voltage d . This must be taken into account when performing the numerical integration. In the same way as c^e was obtained, we obtain

$$d^e = \frac{R_{12}R_{10}R_7}{R_{11}R_9R_8R_5C_1}d, \quad (2.14)$$

where d is a measured value, and d^e an effective one.

The delay measured in the circuit is not affected by this analysis since $\tau^e = \tau$. The values of the measured parameters suffer from the experimental error which can be determined accurately. This experimental error propagates to the value of the effective parameters. The error analysis for measured and effective parameters is explained in appendix A.

2.3 Comparing electronic and numerical solutions.

It is now possible to compare electronic solutions of equation (2.3) with some numerical simulations. The algorithm used to solve the D.D.E is not a standard numerical integration scheme but it is more accurate and efficient than Runge-Kutta or Adams routines, which are schemes used commonly to perform D.D.E integration (when the delays are discrete). It specifically makes use of the fact that the information on an initial interval is redundant for this equation. It is presented in Appendix D. Figures 2.11 – 2.19 display electronic and numerical solutions obtained with constant initial functions. It was noted in Section 2.1.1b that the voltages present in the 1024 “buckets” of the B.B.D correspond to the initial function for the D.D.E. For the following results, the delay line was preprogrammed with a constant voltage belonging to the interval $[\theta_1^e, \theta_2^e]$ and the numerical simulations were also carried out with a constant initial function.

2.3.1 Variation of a single measured parameter.

In this section, some solutions obtained with the analog computer are compared to digital simulations of equation (2.3). The electronic and digital simulations are compared for various

values of the control parameters.

The delay is held constant throughout (*cf.* Section 2.1.1b). Similarly, for all the data presented in this section, the initial function is a constant. This constant is such that the forcing term is high (*i.e.* it is a constant voltage belonging to $[\theta_1^c, \theta_2^c]$ for the electronic simulations and it is a number in $[\theta_1, \theta_2]$ for the digital simulations).

In parts a) and b) below, the protocol we used to obtain the electronic solutions was the following. While the loop was oscillating, the measured parameters were set so that the effective parameters took on the desired value. The loop was then opened, the B.B.D was filled with the desired constant initial voltage and the loop was subsequently closed and set into oscillation. The oscillations were recorded with a microcomputer (AT/386) through an A/D board (Dagitek 2800). During a given recording session, no parameters were changed in the oscillator (the dependence of solution behavior on changes of parameters while the loop was oscillating is discussed in Section 2.4.1).

In part a), we discuss the behavior of the circuit as the thresholds θ_1 and θ_2 are varied, and the solutions are compared to digital simulations. In part b), the gain α is changed, and the resulting variations in solution are compared to the changes observed in the digital simulations of equation (2.3).

a) Variations of θ_1 and θ_2 .

When θ_1 and θ_2 are sufficiently far apart, the dynamics of the equation are effectively controlled by a negative feedback control loop. In this case the electronic and the numerical simulations agree in the following way: Both the shape and the offset of the waveforms are the same though the values of amplitude and period differ slightly (see Figure 2.11). The differences are caused by the experimental errors in the determination of the measured parameters.

As the first threshold is raised towards the second one, approximately the same sequence of bifurcations is observed in both the analog computer and the digital computer simulation. However, some cycles observed numerically did not appear electronically. This is due to the fact that the region of parameter space in which these cycles are observed are smaller than the error on the values of the measured parameters (see Figures 2.17 and 2.18). The

bifurcation observed in Figure 2.12a is not present in Figure 2.12b. Given the fact that this type of discrepancy also occurs in Figures 2.13a and b, and in 2.17 – 2.19a and b, it is possible that there is a systematic shift in our estimation of the effective parameters in spite of the attempts made to correct for such possible displacements. Another explanation for this difference between electronic and numerical bifurcations is the presence of noise in the circuit. Unfortunately, the exact influence of noise on delayed dynamics is difficult to study, but Longtin [47] showed that certain stochastically perturbed non-linear D.D.E's displayed a postponement of the point at which a Hopf bifurcation occurred. The bifurcations showed in Figures 2.11 to 2.19 are not Hopf bifurcations because they involve the bifurcation from one limit cycle to another whereas the Hopf bifurcation is characterized by the emergence of a limit cycle where steady state behavior was previously observed. For a detailed description of standard bifurcations of vector fields (including the Hopf bifurcation) the reader is referred to [20].

b) Variations of α .

The most interesting feature displayed by the solutions is a recurrent "flirt" with an unstable homoclinic cycle, shown in Figures 2.16a-2.19a. This phenomenon is described by the diffeomorphism presented in Section 1.5.2 (i.e. solutions like the ones presented in Figure 1.3). As α is raised, the duration of the residence of the solution around θ_1 increases (this is clear in Figures 2.16a to 2.19a). There is again a systematic shift in the values of α describing the same numerical and electronic solutions. This is interesting because it gives a physical example of a system periodically approaching an unstable manifold.

c) Power spectra.

One other possible means of comparison between theory and experiment is the study of the distribution of peaks in the power spectra of electronic and numerical solutions. For example, consider Figures 2.20 and 2.21. The experimental sampling frequency was 500Hz for all the experimental solutions. The power spectrum analysis was performed with analytic solutions obtained with our algorithm (described in Appendix D). The integration step in

the algorithm corresponds to an effective sampling frequency of 500Hz.

The solutions typically oscillate between 1 and 5Hz, and it seems unlikely that the solution possess significant components beyond 50Hz. Aliasing is therefore not a problem. The data was treated with a Hanning window $w_j = 1/2(1 - \cos(2\pi j/(N - 1)))$, where j is the channel number [62]. The DC peak in channel 0 is removed. There are no observable components of the signals above 20Hz, and it therefore appears that the transmission line noise does not affect the electronic solutions. The distribution of peaks for experimental and theoretical signals is remarkably similar. The consistent shift of 2 to 3Hz observed is due to the discrepancy between the periods of the two types of solution. The first peaks correspond in both spectra to the observed periods of oscillation of 1.2 to 1.6Hz.

2.4 Multistability in the oscillator.

The initial preparation of the system is the initial state of the B.B.D, and it corresponds to the initial function for the D.D.E. All the properties of the analog oscillator discussed to this point have been obtained with constant initial voltages. When the parameters are varied continuously without restarting the system, the initial functions are no longer constant because they are oscillatory solutions of equation (2.3).

2.4.1 Hysteresis in the bifurcation diagram:

In (2.3.1a), the parameters in the analog computer were set and then the loop was closed. Parameters were not changed as the loop was oscillating. This protocol was followed to allow a comparison between experimental observations and existing numerical and analytic predictions. The parameters can also be changed as the computer is oscillating: this is called a *smooth* change of the parameters.

As the threshold θ_1 is slowly increased towards θ_2 , the solutions undergo a series of period-increasing bifurcations (see Figures 2.11 – 2.15). When θ_1 gets too close to the second threshold (above 2 volts for $\theta_2 = 3.2$ volts), the solution decays to the lower asymptote. As θ_1 is subsequently decreased, the first oscillatory solution observed in the system is the slowest limit cycle in the system corresponding to the ideal negative feedback situation. Thus, different solutions of equation (2.3) are found at the same parameter values depending on whether θ_1 is being raised or lowered! This *hysteresis* in the bifurcation diagram indicates the possible existence of multistability in the system. The only difference in behavior between the rise and the fall of θ_1 is the initial condition for the system, because in the closed loop the continuous electrical signal is an initial function for itself.

Bistability has been observed in physical systems described by delayed feedback mechanisms and it has been shown to exist in equation (2.3) with uncontrolled (i.e. with the parameters being varied continuously, the dynamical variable being an initial condition to itself) initial functions [14]. It has not yet been observed with controlled nonconstant I.F's. To examine the sensitivity of solution behavior on changing initial functions, we first present a modification of the analog computer which allows any initial function to be entered into

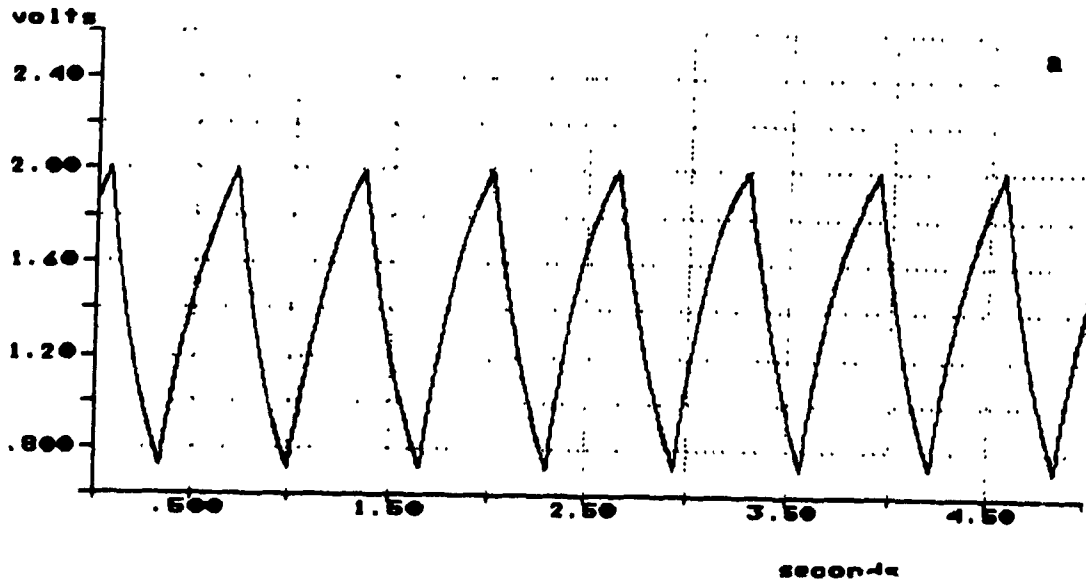
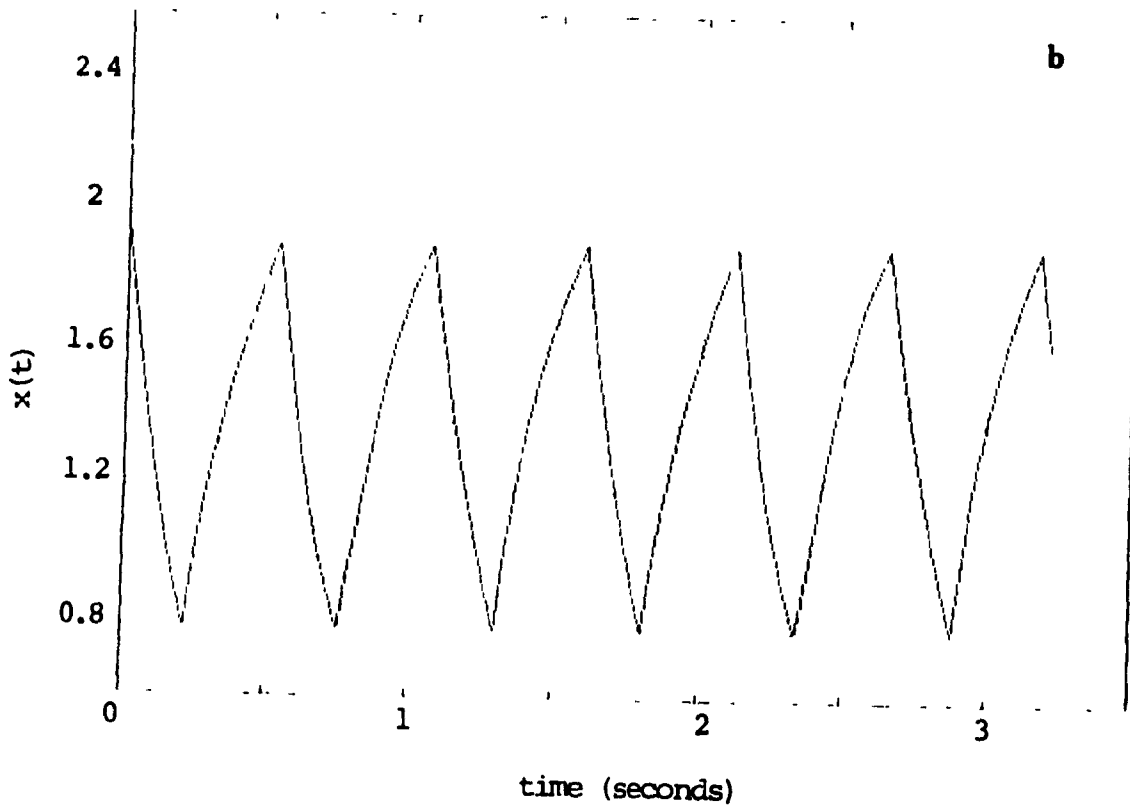


Figure 2.11: a) Electronic solution. b) Numerical solution. The parameters in both cases are effective parameters and equal to: $\tau = 0.161 \pm 0.001s$, $\theta_1 = 0.5 \pm 0.0005$, $\theta_2 = 1.604 \pm 0.0005$, $\alpha = 1.48 \pm 0.04$, $c = 3.49 \pm 0.0005$.



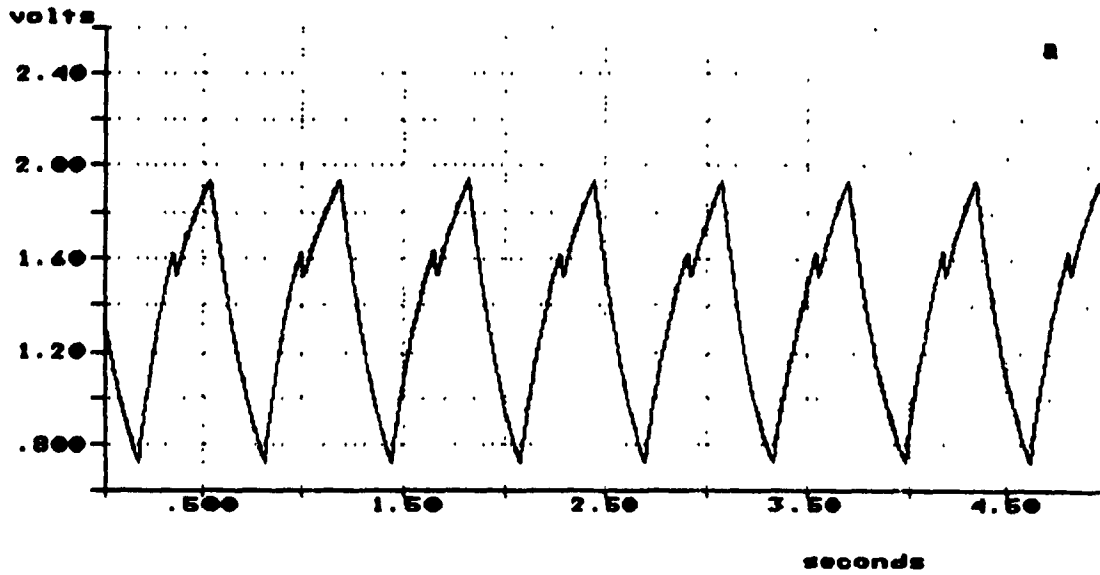
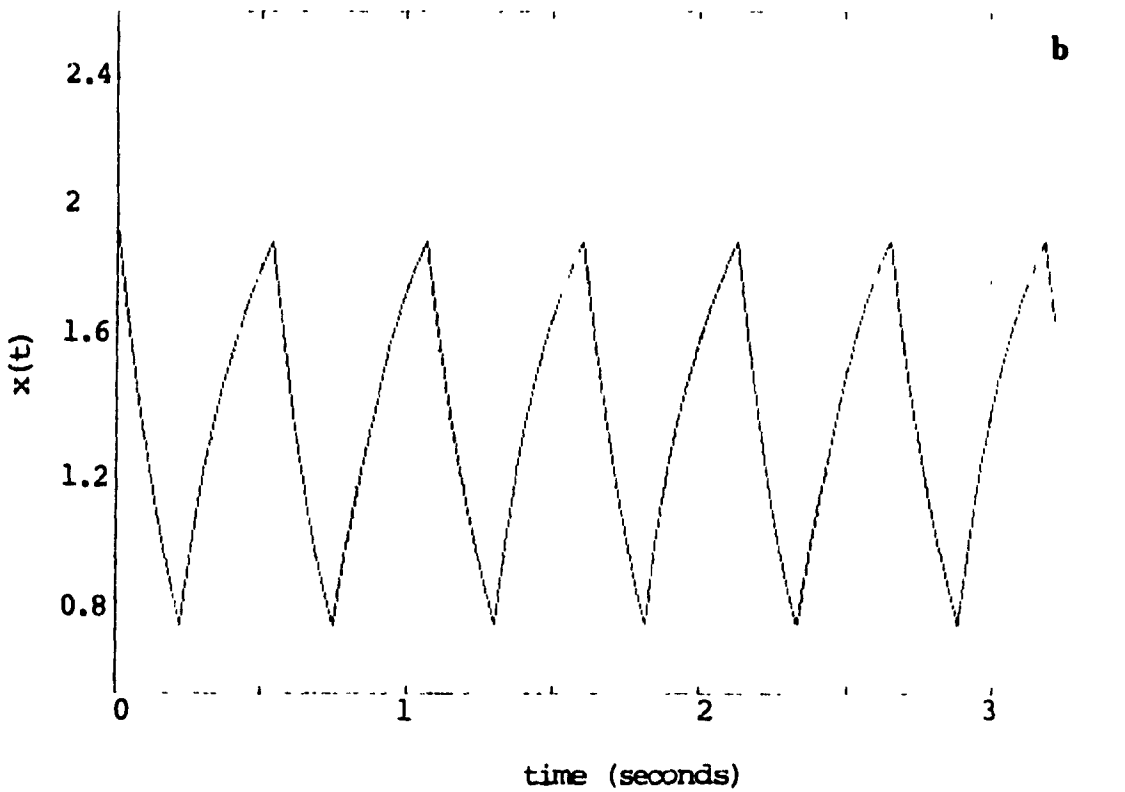


Figure 2.12: a) *Electronic solution.* b) *Numerical solution.* The parameters in both cases are effective parameters and equal to: $\tau = 0.161 \pm 0.001s.$, $\theta_1 = 0.802 \pm 0.0005$, $\theta_2 = 1.604 \pm 0.0005$, $\alpha = 1.48 \pm 0.04$, $c = 3.49 \pm 0.0005$.



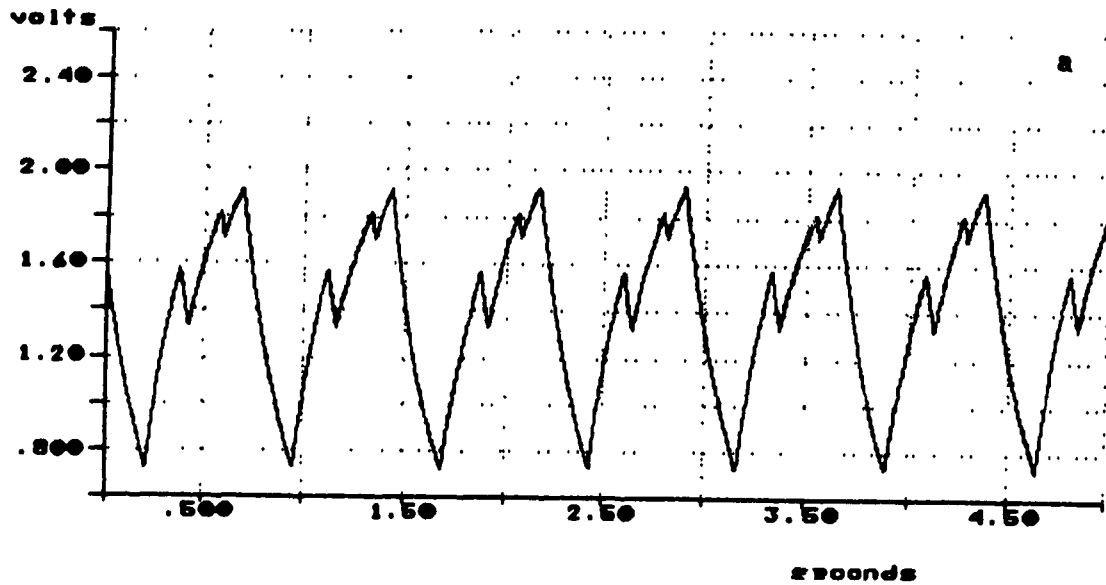
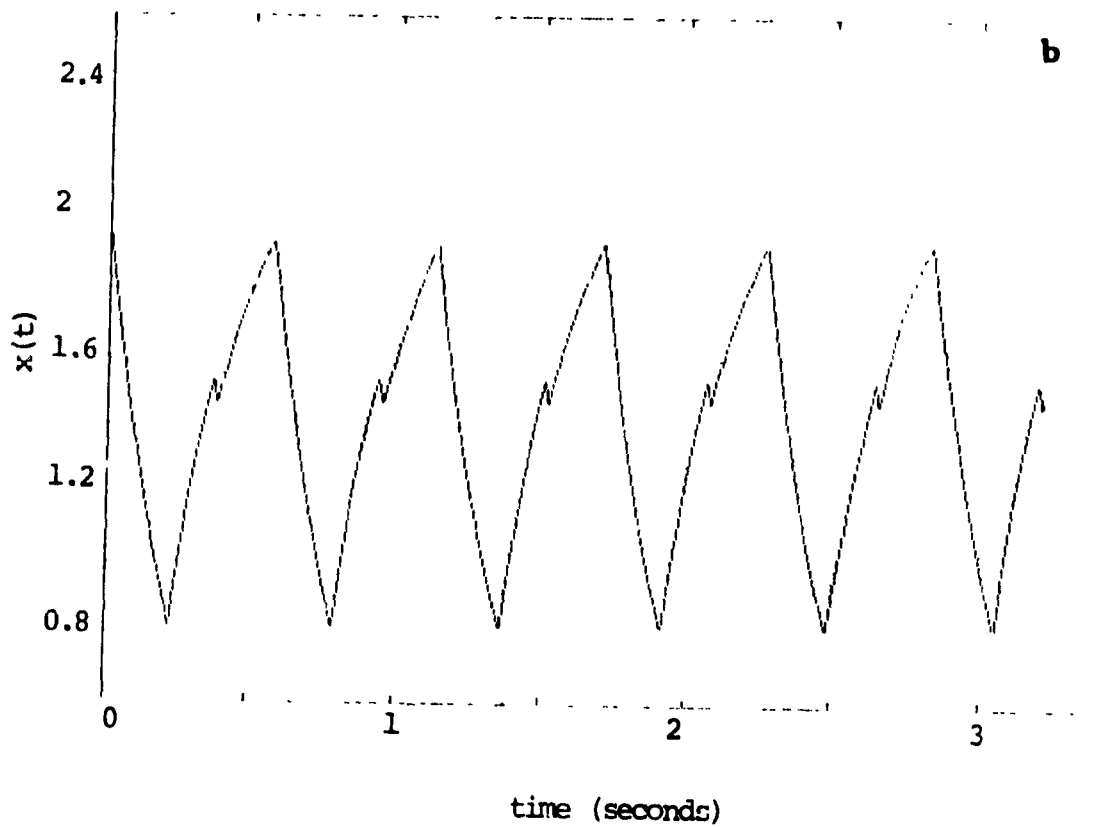


Figure 2.13: a) *Electronic solution.* b) *Numerical solution.* The parameters in both cases are effective parameters and equal to: $\tau = 0.161 \pm 0.001s.$, $\theta_1 = 0.877 \pm 0.0005$, $\theta_2 = 1.604 \pm 0.0005$, $\alpha = 1.49 \pm 0.04$, $c = 3.49 \pm 0.0005$.



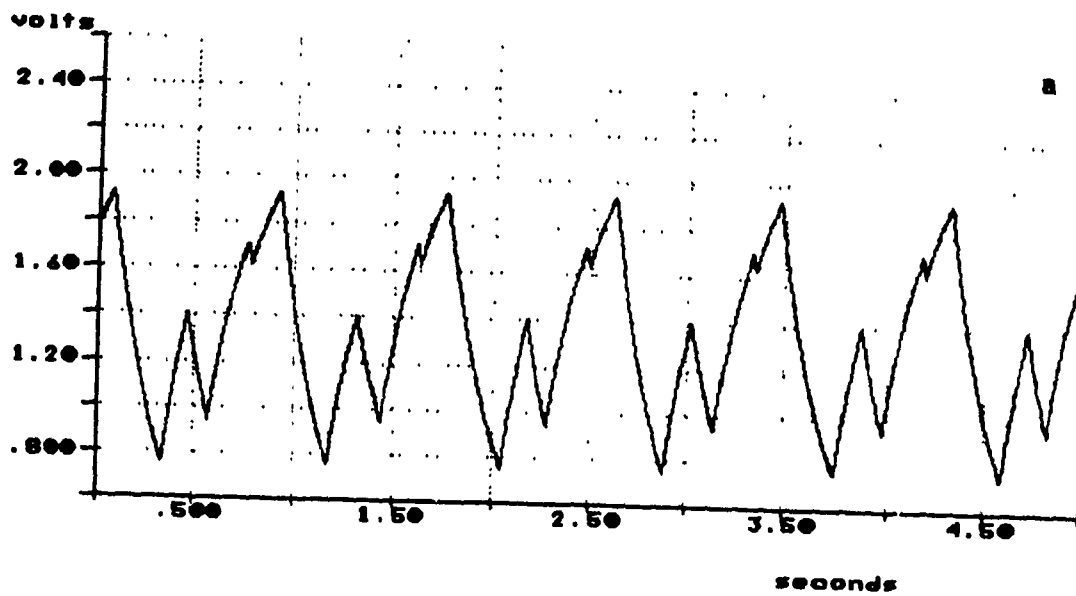
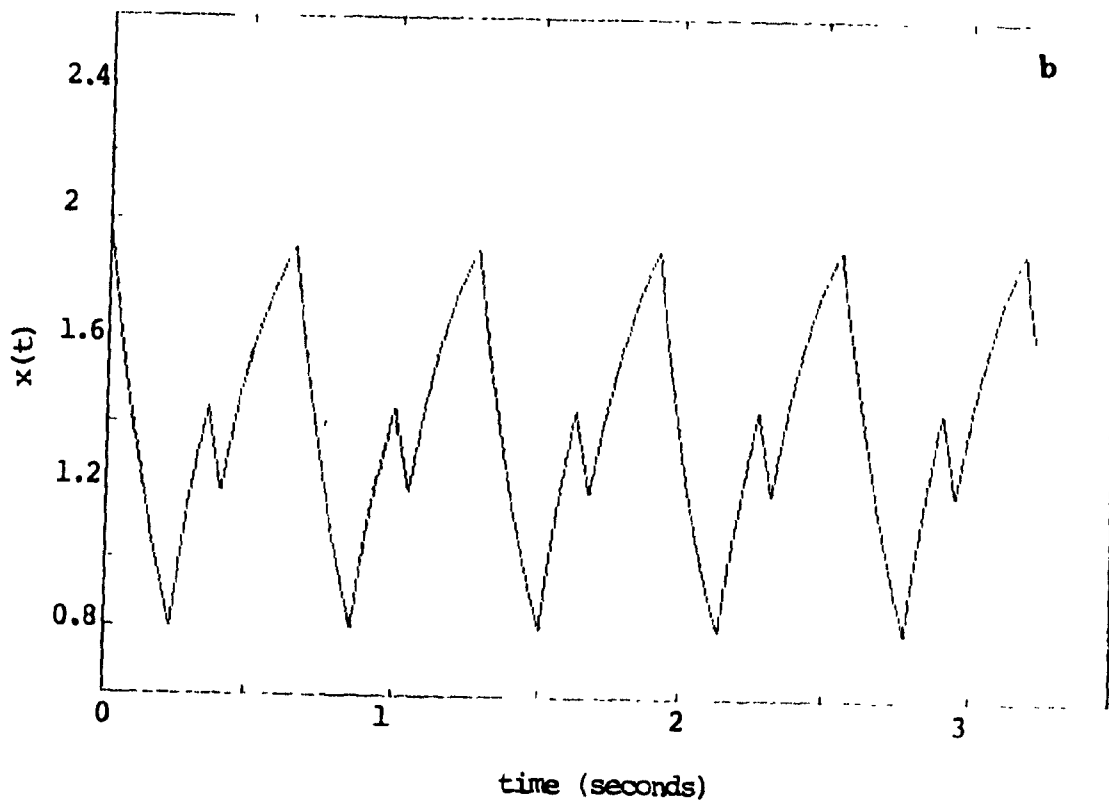


Figure 2.14: a) *Electronic solution.* b) *Numerical solution.* The parameters in both cases are effective parameters and equal to: $\tau = 0.161 \pm 0.001s.$, $\theta_1 = 0.947 \pm 0.0005$, $\theta_2 = 1.604 \pm 0.0005$, $\alpha = 1.41 \pm 0.04$, $c = 3.49 \pm 0.0005$.



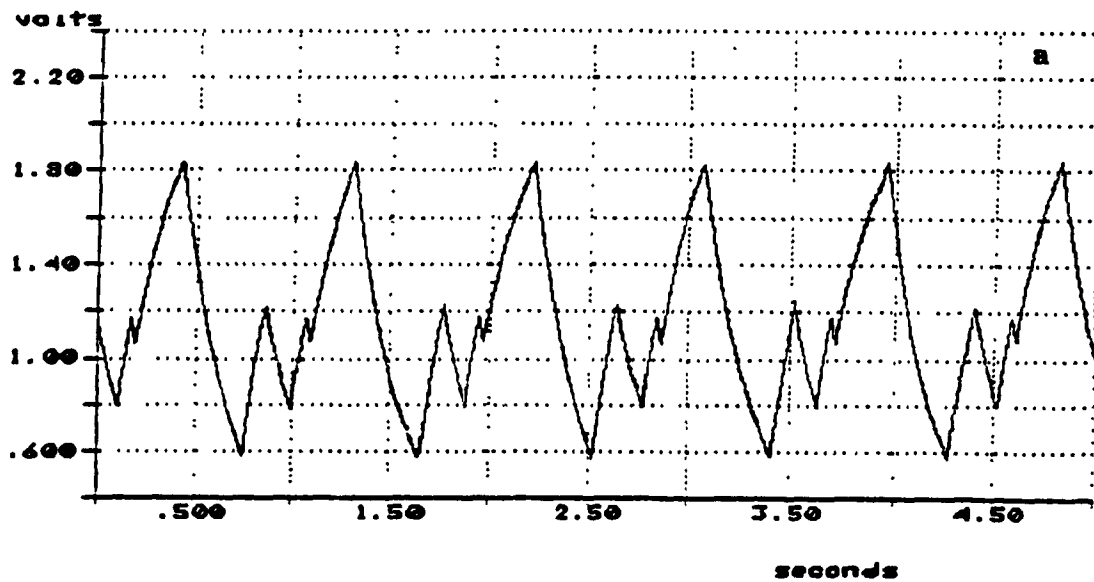
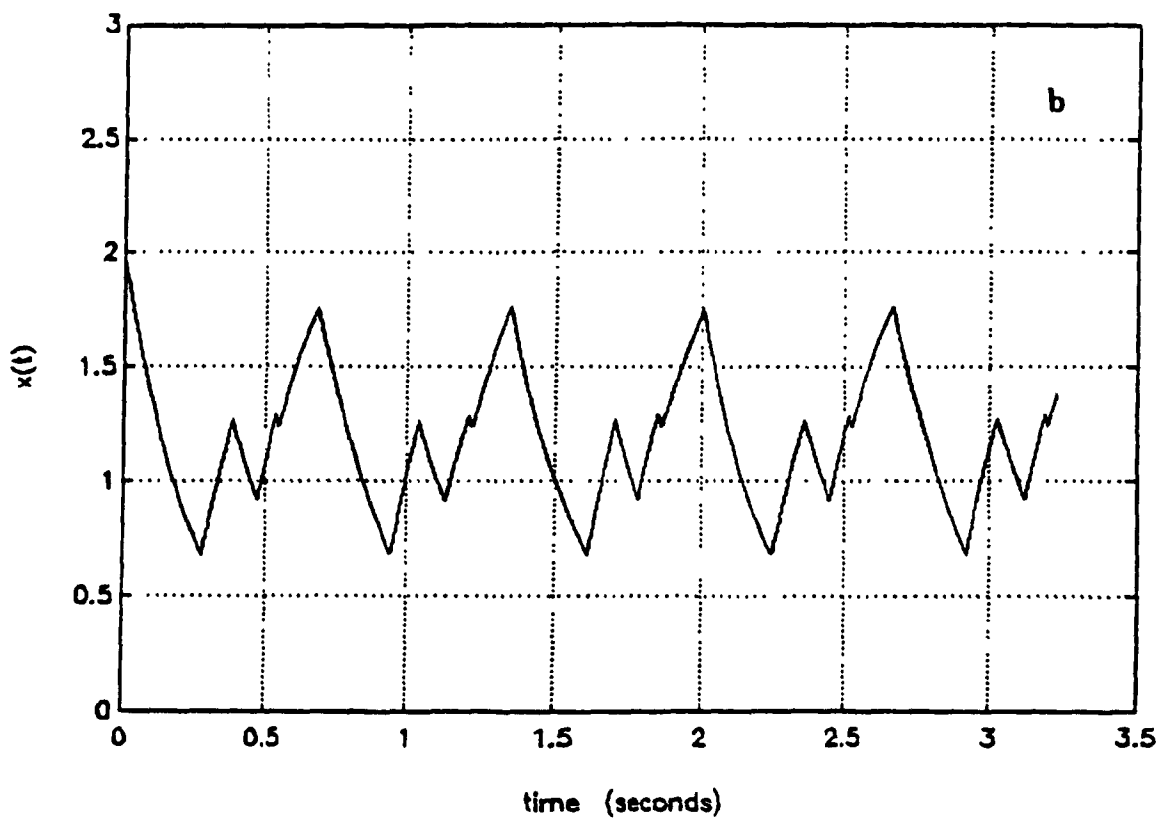


Figure 2.15: a) *Electronic solution.* b) *Numerical solution.* The parameters in both cases are effective parameters and equal to: $\tau = 0.161 \pm 0.001s.$, $\theta_1 = 1.042 \pm 0.0005$, $\theta_2 = 1.604 \pm 0.0005$, $\alpha = 1.49 \pm 0.04$, $c = 3.49 \pm 0.0005$.



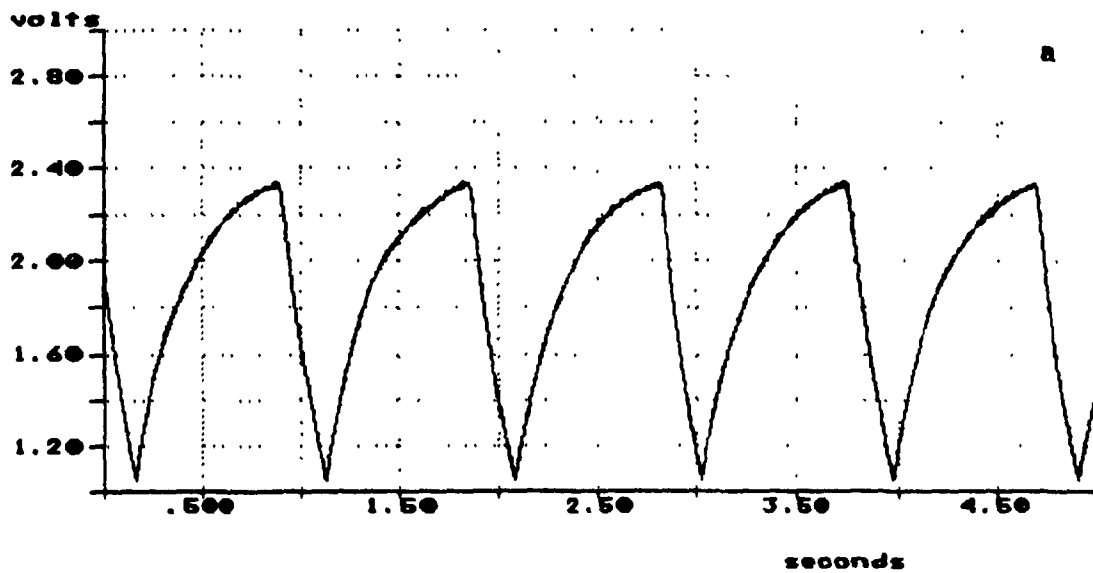
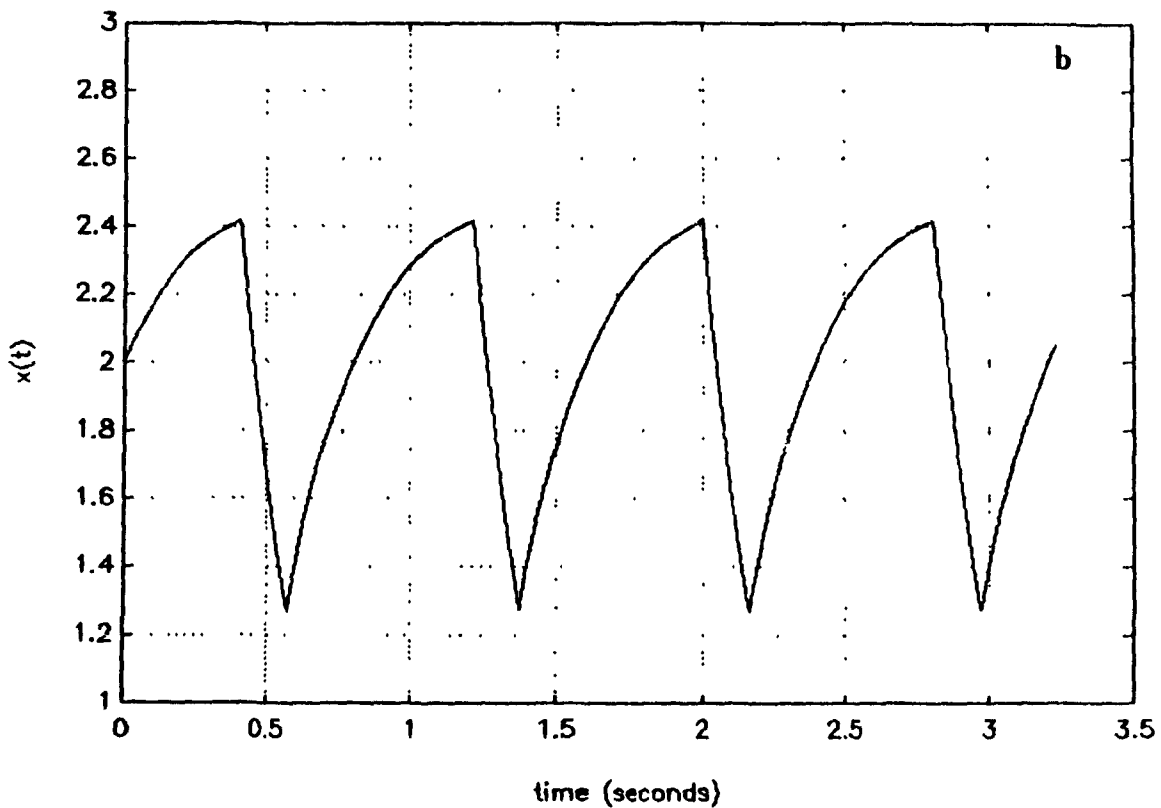


Figure 2.16: a) *Electronic solution.* b) *Numerical solution.* The parameters in both cases are effective parameters and equal to: $\tau = 0.161 \pm 0.001s.$, $\theta_1 = 0.896 \pm 0.0005$, $\theta_2 = 1.604 \pm 0.0005$, $\alpha = 1.00 \pm 0.03$, $c = 3.49 \pm 0.0005$.



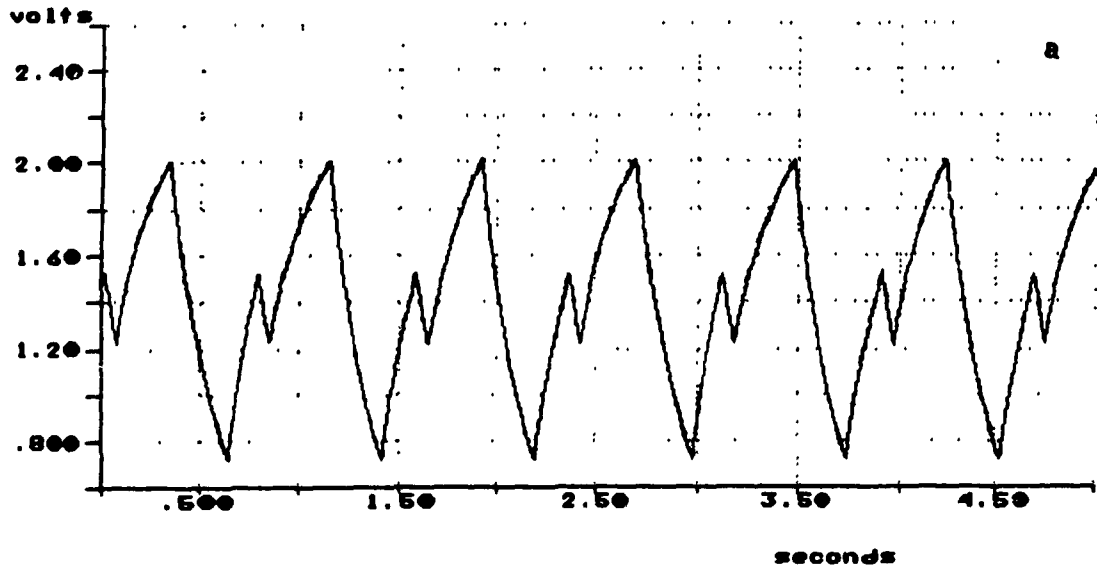
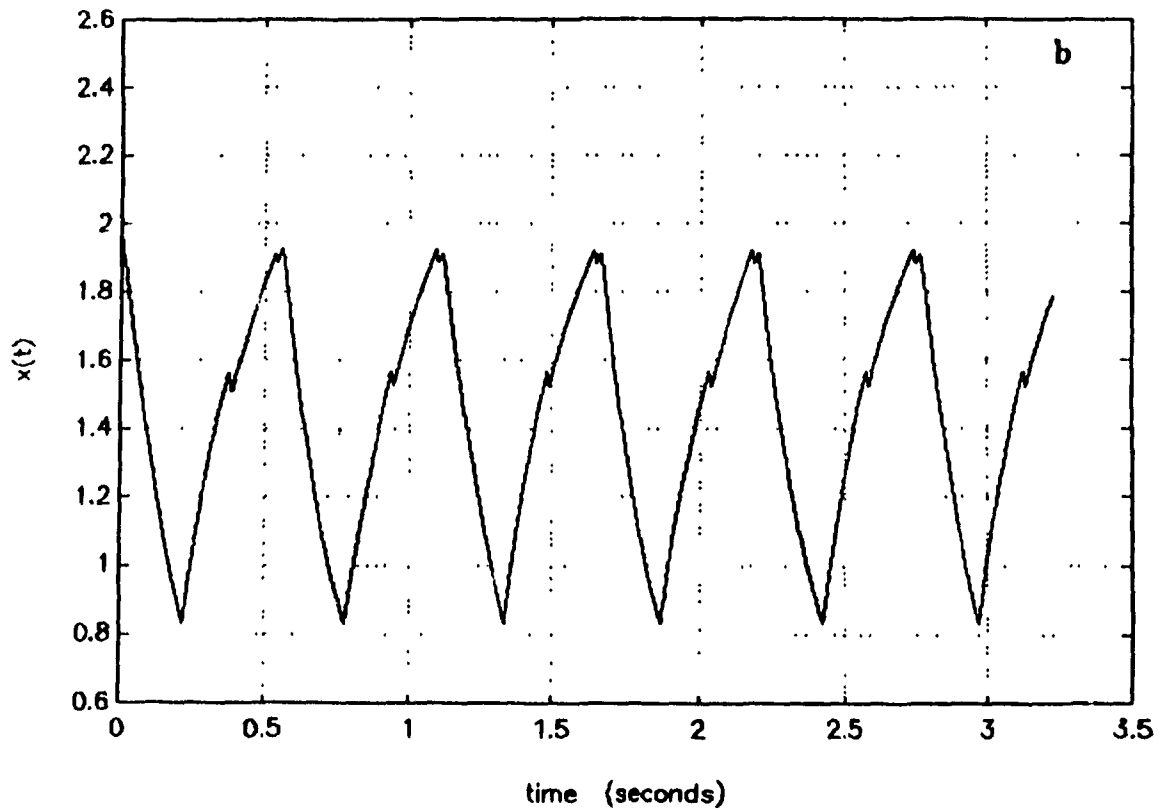


Figure 2.17: a) *Electronic solution.* b) *Numerical solution.* The parameters in both cases are effective parameters and equal to: $\tau = 0.161 \pm 0.001s.$, $\theta_1 = 0.896 \pm 0.0005$, $\theta_2 = 1.604 \pm 0.0005$, $\alpha = 1.26 \pm 0.03$, $c = 3.49 \pm 0.0005$.



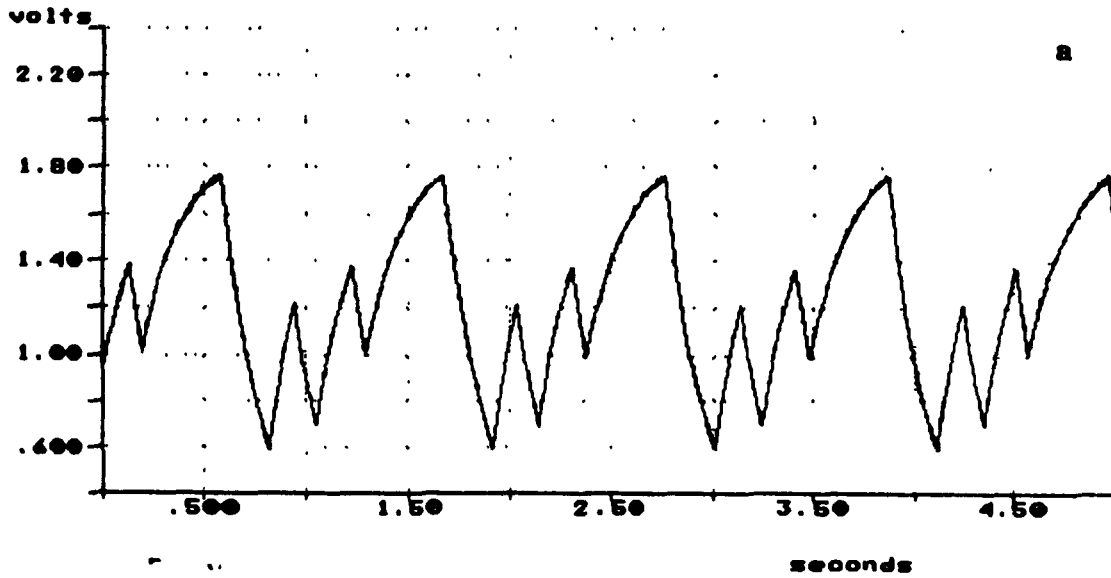
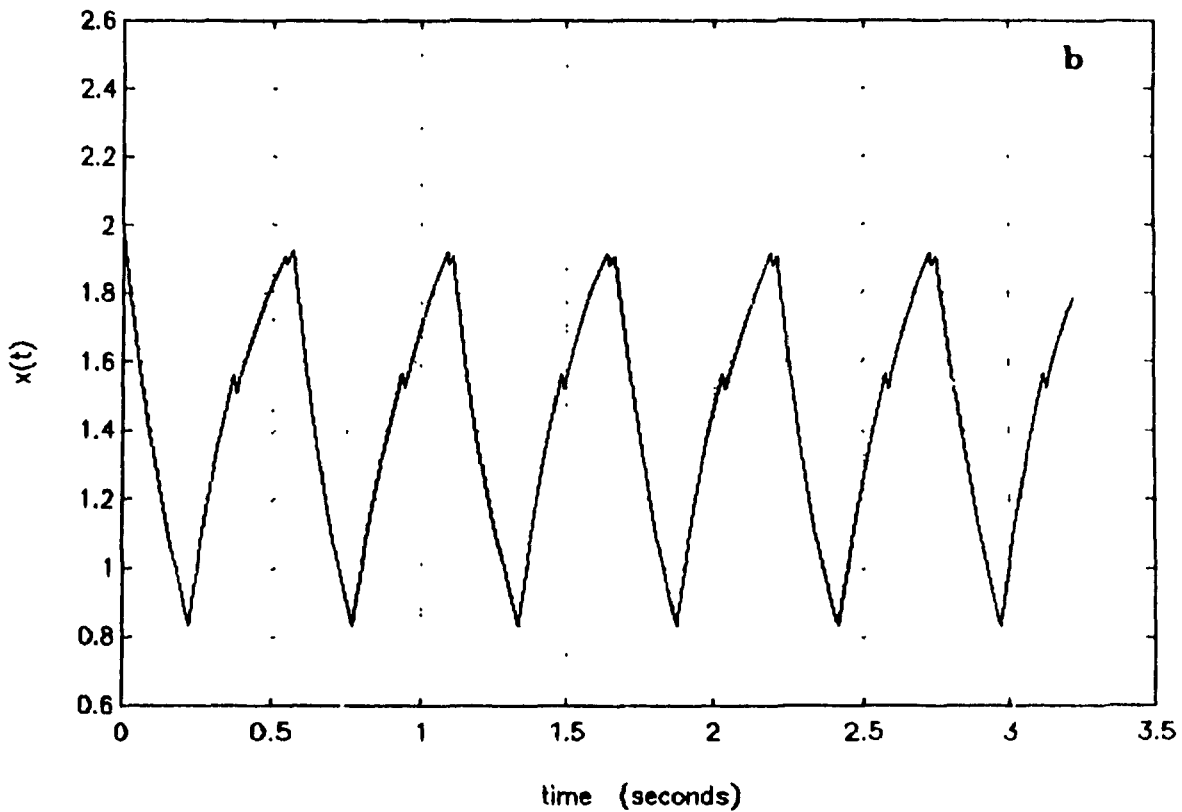


Figure 2.18: a) *Electronic solution.* b) *Numerical solution.* The parameters in both cases are effective parameters and equal to: $\tau = 0.161 \pm 0.001s.$, $\theta_1 = 0.896 \pm 0.0005$, $\theta_2 = 1.604 \pm 0.0005$, $\alpha = 1.83 \pm 0.03$, $c = 3.49 \pm 0.0005$.



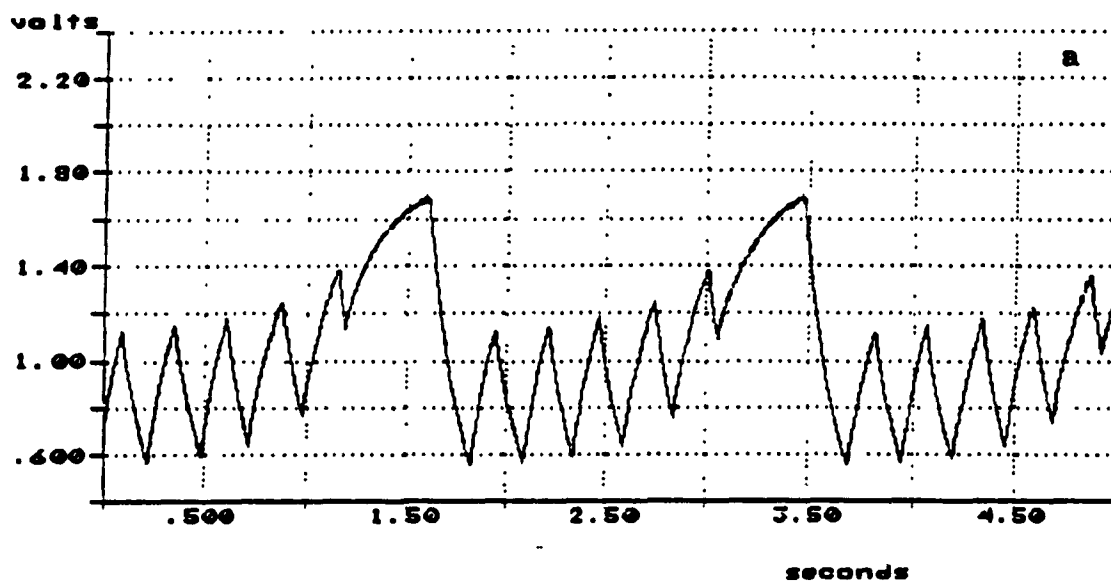
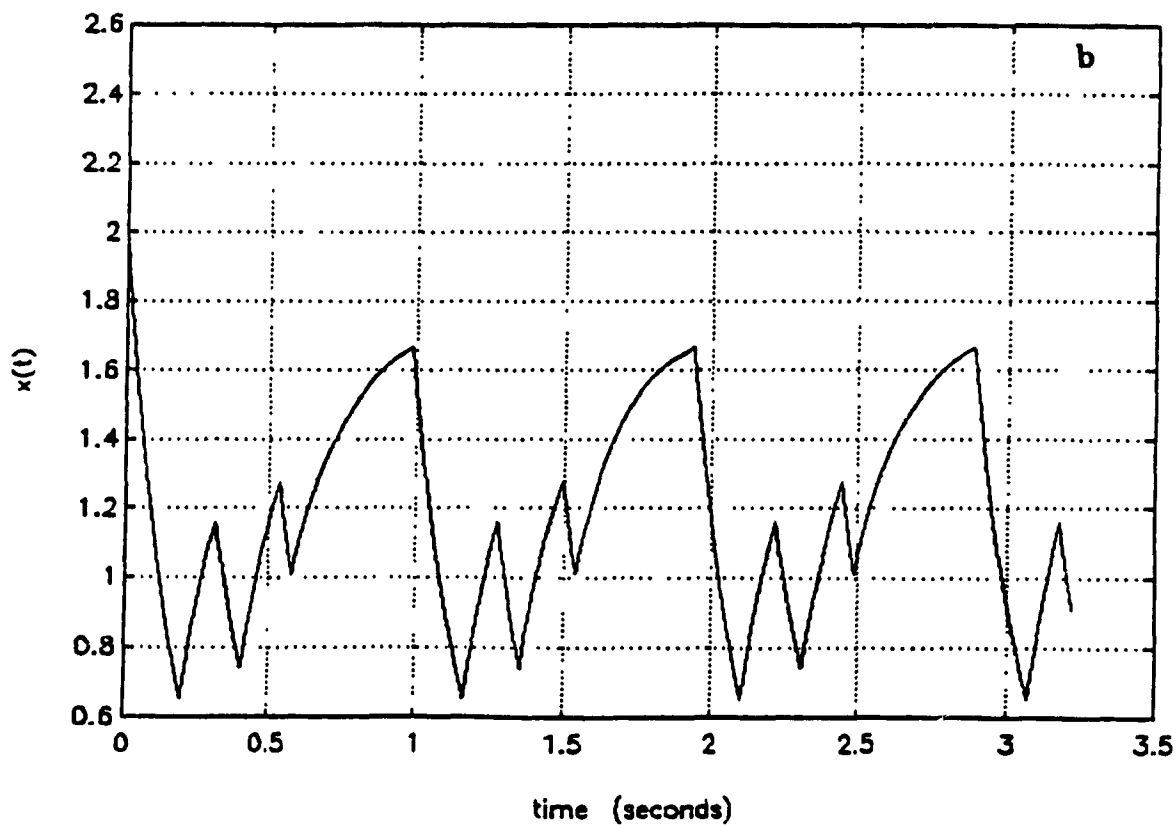


Figure 2.19: a) *Electronic solution.* b) *Numerical solution.* The parameters in both cases are effective parameters and equal to: $\tau = 0.161 \pm 0.001s.$, $\theta_1 = 0.896 \pm 0.0005$, $\theta_2 = 1.604 \pm 0.0005$, $\alpha = 2.0 \pm 0.03$, $c = 3.49 \pm 0.0005$.



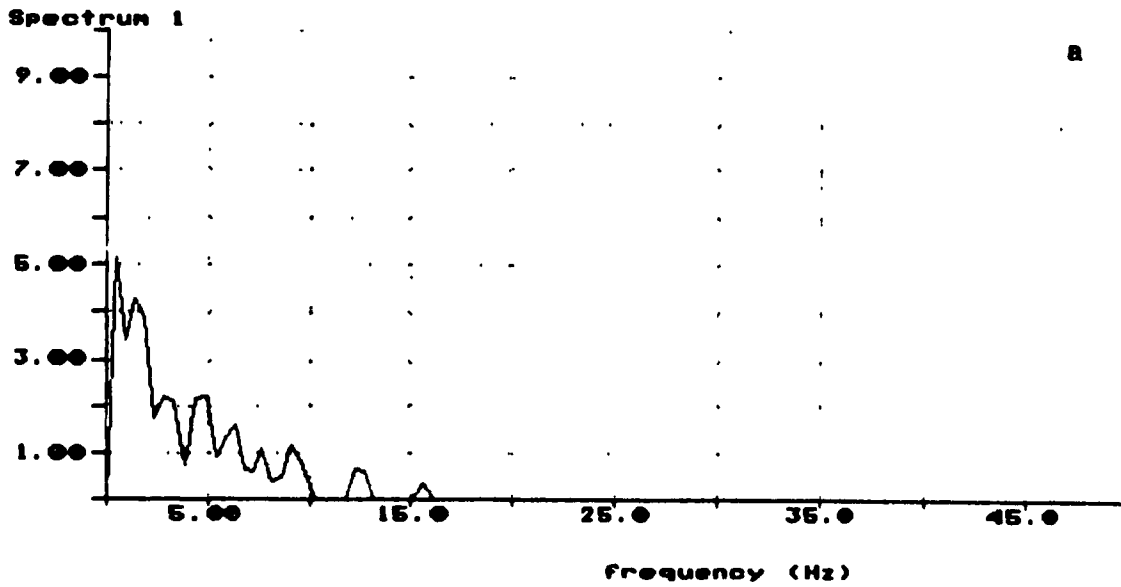
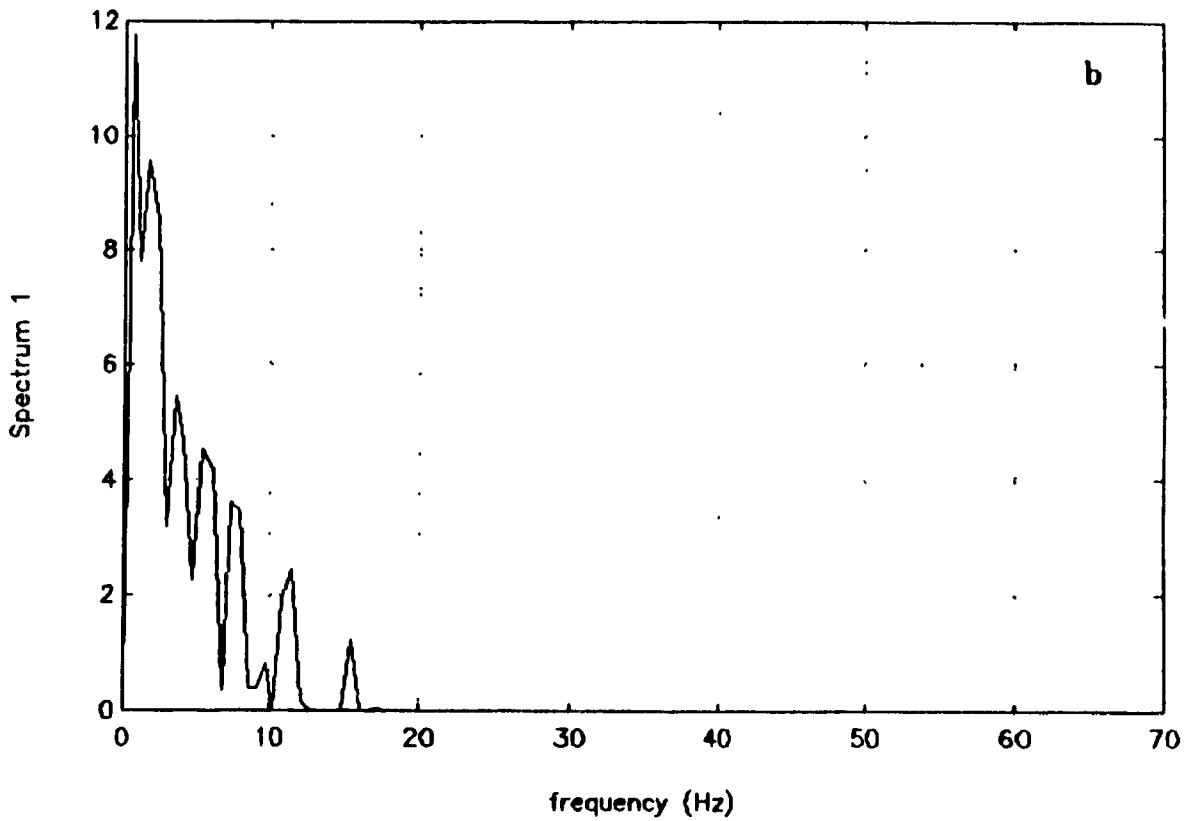


Figure 2.20: a) *Power spectrum of the electronic solution displayed in Figure 2.11a.* b) *Power spectrum of the numerical solution presented in Figure 2.11b.*



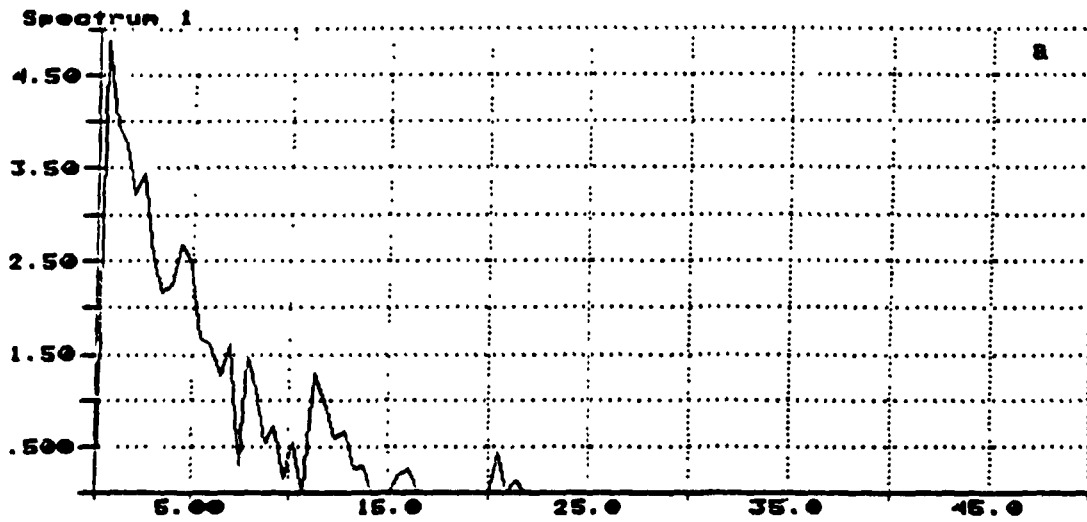
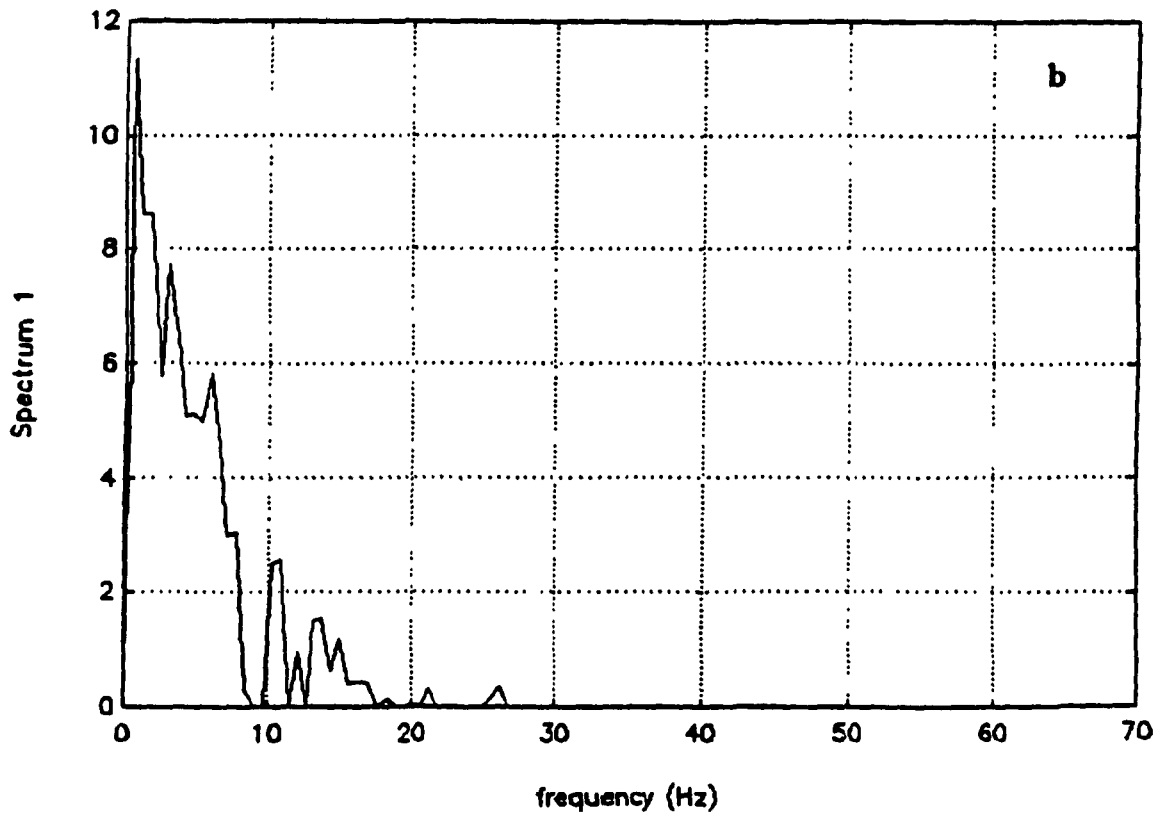


Figure 2.21: a) Power spectrum of the electronic solution presented in Figure 2.15a. b) Power spectrum of the numerical solution presented in Figure 2.15b.



the B.B.D.

2.4.2 Controlling non-constant I.F's.

The initial voltages present in the 1024 buckets of the B.B.D just prior to the closing of the loop constitute the initial function for the D.D.E. It is possible to control these voltages accurately by interfacing the B.B.D with a digital computer.

Remember that the B.B.D is sampling device: it stores in one of its 1024 capacitor circuits a given voltage at every other logic high of a control sampling square wave. The trick is to store the desired initial function into the digital computer. Then, using a D/A converter, it is sent to the B.B.D. Therefore, the B.B.D receives two synchronized signals from the digital computer: the initial function itself and the sampling pulse. A switching circuit closes the loop on itself once the initial function is sent and the computer once again oscillates on its own.

The idea is simple but the design is not. The synchronization between the initial function and the sampling signal has to be very precise. In fact, the only way to achieve the required accuracy is to send a single signal from the digital computer, which contains both the sampling pulse and the initial function. This single signal is programmed so that it can be split by the switching circuit into a control component (the sampling pulse) and a controlled component (the I.F.) which is directed by the switches to the input of the B.B.D.

Additional difficulties arise because the D/A's output settling time is longer than the maximum rise or fall time allowed at the B.B.D's clock input. To circumvent this problem, the digital pulse is sent to trigger a waveform generator's TTL output which is the actual sampling pulse in the analog computer.

The circuit presented in Figure 2.22 is more complex than it should be because we only had access to one D/A port, so that in addition to the the preceding two signals, the single waveform sent to the switching circuit had to contain information about the control signals of the switches themselves.

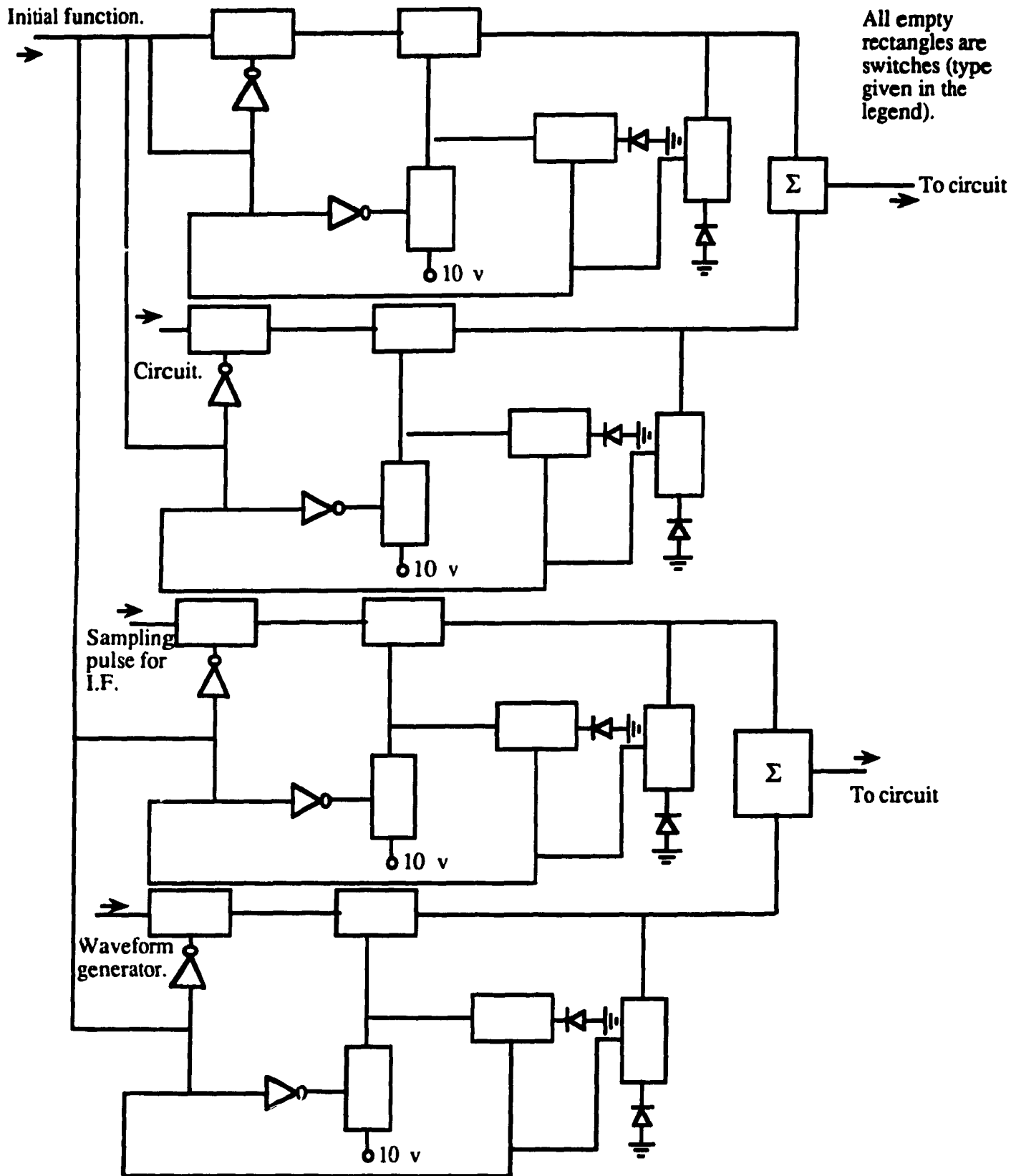


Figure 2.22: Diagram of the switching circuit discussed in Section 2.4.2. The switches used for this circuit were HEF4069UBP while the op-amps were standard uA741TC

2.4.3 Discussion.

Equation (2.3) serves as paradigm for the production-destruction models presented in Section 1.5. The initial function corresponds to the initial preparation of the system. It is very important to understand how changes in the initial function affect the behavior of the solution because experimenters can rarely control the initial state of their system accurately. Understanding the dependence of system dynamics on the initial preparation is essential for a good interpretation of experimental data. Once again, the analog oscillator is not a tool designed for the systematic and quantitative investigation of the problem, but it does provide us with a reliable physical system with which to investigate multistable behavior in delayed mixed feedback control loops.

The behavior of solutions when the I.F.'s are varied is investigated with initial functions which cross both θ_1 and θ_2 only once each (see Figure 2.23a). It is hoped that experimental results concerning this type of initial function can be analytically understood and then generalized to more complicated I.F.'s. The simplicity of the chosen I.F.'s reflects the total absence of results concerning this problem.

Figure 2.23b shows a typical type of behavior observed when non-constant initial functions are varied slightly. In this case, the parameter t_2 describing the initial function was changed by 1.8 %. As t_2 is varied between t_1 and 0, the interval seems to be separated in two sets. One attracts the short period solution and the other attracts the long period solution. This separation of the interval $[t_1, 0]$ in several sets, each attracting a different limit cycle is an illustration of multistability. This multistability is observed in the oscillator for large ranges of parameters when the initial functions are of the type described above. The structure of these sets is very complicated and cannot be determined with the electronic loop. In fact, it is shown in Chapter 3 that the solutions display a pathological dependence on initial functions for many classes of initial functions and for wide ranges of parameters.

2.5 Summary

In this chapter we discussed the design and performance of an electronic analog computer used to investigate the dynamics of a delay differential equation proposed as a paradigm for production-destruction processes with mixed delayed feedback. Section 2.1 is a stage by stage description of the circuit. In Section 2.2, the unambiguous correspondence between the analog computer and the D.D.E it simulates is established and the stability of the system is assessed. The electronically obtained solutions are compared to digital simulations (with constant initial functions) in Section 2.3. Finally, the influence of changing non-constant initial functions on solution behavior is discussed, and the existence of multistability in the system is demonstrated in Section 2.4.

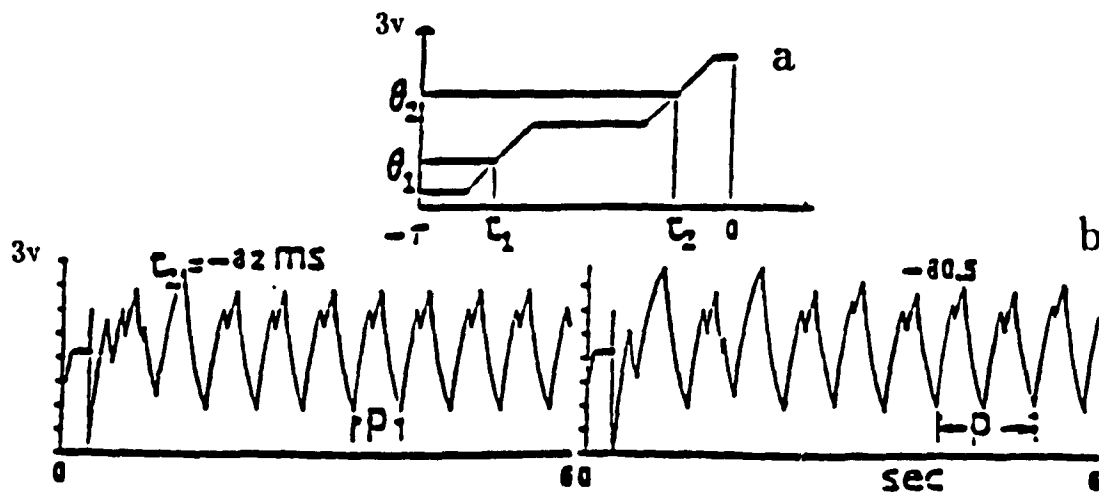


Figure 2.23: a) The initial function used for the experiments on bistable behavior in the analog computer. b) Two bistable electronic solutions. The difference between the two cases is a change of the parameter t_2 of about 1.8 %. The period of the solution on the right is about twice that of the solution on the left.

Chapter 3

Multistability in delay differential equations.

In this chapter, we explore multistable behavior in a class of delay differential equations presented in Section 1.5 as models for production-destruction processes. Multistability is defined as the coexistence of different asymptotic solutions at the same point in parameter space: the type of solution is determined by the exact initial preparation (initial function) of the system.

The dependence of system behavior on initial preparation is a concept familiar to nonlinear dynamicists, since one of the definitions of chaos states that the difference between trajectories generated by close initial conditions diverges exponentially. However, when the system is not chaotic, the dependence of the dynamics on initial preparation is often discarded as a non-issue even though multistability in no way requires chaoticity.

Ignoring the presence of multistability in a dynamical system can greatly hamper the process of matching theoretical predictions and experimental observations because it is impossible to perform an experiment twice with the exact same initial conditions. We illustrate in Section 3.3 that the dependence of system behavior on initial preparation can be pathological in the sense that minute variations in the initial function can generate important qualitative differences in observed behavior. Thus, multistability is an interesting paradigm with which to explore the variability of experimental data obtained from different performances of the same experiment.

A dynamical (or semi-dynamical) system displays multistability when it possesses several

locally stable attractors. The evolution of the system to a given attractor is determined by the initial conditions. When there is multistability, the space of system initial conditions is partitioned into basins of attraction. All initial conditions belonging to a given basin of attraction will generate a unique asymptotic solution, but the phase of the solution depends on the particular initial condition. Initial conditions belonging to different basins of attractions will generate different types of solutions. The boundary separating two basins of attraction is called a separatrix (or a basin boundary) and its structure may be quite complex. In particular, it is known [8] that separatrices in certain two dimensional maps of the complex plane into itself possess self similar (or fractal) properties.

In Section 3.1, we recall some of the concepts of nonlinear dynamics relevant to the investigation of multistable finite dimensional dynamical systems.

Multistability in delay differential systems has been investigated in the context of nonlinear optics. Optical bistability was first predicted theoretically by Ikeda [32, 33], and demonstrated experimentally by Gibbs *et al.* [21, 27]. These experiments, along with experimental and numerical work on bistable delay differential equations used in nonlinear optics are presented in Section 3.2.

In Section 3.3 we discuss the dependence of solution behavior on changes of the initial function in equation (2.3), and illustrate the existence of multistable periodic solutions.

In Section 3.4, we investigate the structure of the basin boundaries in the space of initial functions of equation (2.3). This appears to be the first attempt to characterize the structure of basin boundaries for delay differential equations.

3.1 Multistability and nonlinear dynamics.

The idea that qualitatively different behaviors can coexist in a given system at the same point in parameter space is not novel. Mathematicians have always been concerned with the existence and uniqueness properties of solutions of dynamical and semidynamical systems. The omnipresence of existence and uniqueness proofs in the mathematics literature, though sometimes motivated by the difficulty to obtain more stringent analytic results, attests to that concern. The recent burgeoning of nonlinear dynamics has stimulated interest in the

modeling community for systems whose solutions are not necessarily unique.

To illustrate the following introductory definitions, in this section we consider multistability in electrophysiological cardiac models formulated as ordinary and partial differential equations.

3.1.1 Introductory definitions.

We consider a generic n -dimensional set of ordinary differential equations

$$\frac{d\mathbf{x}(t)}{dt} = F(\mathbf{x}(t)), \quad \mathbf{x}(t=0) = \mathbf{x}_0 \quad (3.1)$$

with

$$\mathbf{x}(t) = (x_1(t), \dots, x_n(t)),$$

and

$$F(\mathbf{x}) = (f_1(\mathbf{x}), \dots, f_n(\mathbf{x})) \text{ for all } \mathbf{x} \in R^n.$$

The vector field F generates a flow $\phi_t : R^n \rightarrow R^n$, where $\phi_t(\mathbf{x}) = \phi(\mathbf{x}, t)$ is a smooth function defined for all \mathbf{x} in R^n and $t \in R$, and ϕ_t satisfies (3.1) because

$$\left. \frac{d}{dt}(\phi(\mathbf{x}, t)) \right|_{t=i} = F(\phi(\mathbf{x}, i)) \quad (3.2)$$

for all $\mathbf{x} \in R^n$ and $t \in R$. Therefore, the flow generated by (3.1) is the continuum of trajectories generated by (3.1) originating from a continuum of initial conditions in R^n [note that if $\phi_t : S \rightarrow R^n$, then the flow is the continuum of trajectories generated by the continuum of initial conditions in S].

Now we suppose that the system (3.1) possesses k locally stable fixed points: $\mathbf{x}_j^* = (x_{1j}^*, \dots, x_{nj}^*)$ satisfying

$$F(\mathbf{x}_j^*) = 0 \quad \text{for } j = 1, \dots, k. \quad (3.3)$$

Assume the existence of k mutually disjoint sets B_j such that

$$\mathbf{x}_0 \in B_j \iff \lim_{t \rightarrow \infty} \mathbf{x}(t) = \mathbf{x}_j^*. \quad (3.4)$$

The k sets B_j are the k basins of attraction for the k fixed points of (3.1). The boundary separating any two disjoint basins of attraction is called the separatrix [20].

Consider the evolution of a continuum of trajectories of system (3.1) generated by a continuum of initial conditions defined on a set S such that

$$B_i \subset S \text{ for } i = 1, \dots, k \text{ and } B_i \cap B_j = \emptyset \text{ if } i \neq j.$$

It is clear that the flow $\phi_t : S \rightarrow R^n$ will “separate” into (at least) k different branches, each branch being attracted to a specific locally stable fixed point of system (3.1).

In general, multistable behavior is of interest when the system possesses k locally stable attractors, rather than the k locally stable fixed points discussed above. When this the case, then the continuum of initial conditions on a set (like S) encompassing k basins of attraction will evolve into k different oscillatory solutions. The exact nature of the solutions (i.e. whether they are periodic, quasiperiodic or chaotic) depends on the nature of the k attractors.

This is the dynamical picture of multistable behavior. It is precisely this picture which is difficult to study in the case of flows generated by delay differential systems, for then the flows discussed above are flows of functions generated by continua of initial functions. There are attempts to formalize the study of flows in Banach spaces [22] but they exceed the scope of this thesis. We defer to Chapter 5 the introduction of a formalism to start investigating the statistical evolution of functionals.

Before proceeding to study bistable behavior in systems with delayed feedback, it is instructive to illustrate some of the concepts presented in this section with examples taken from cardiac electrophysiology.

3.1.2 Bistability in electrophysiological cardiac models.

The mathematical modeling of cardiac activity (and, more generally, the study of excitable media) with the tools of nonlinear dynamics is an active field of investigation [83] [9]. In this section, we focus attention on the presence of multistable behavior in models for the electrical activity of cardiac tissue formulated as ordinary and partial differential equations. First, consider the Van Capelle-Durrer (VCD) [79] model for the electrical activity of a single cardiac cell. The model is a two dimensional set of ordinary equations:

$$\frac{dV}{dt} = -C^{-1}[g(V) + (1 - Y)f(V)] \quad (3.5)$$

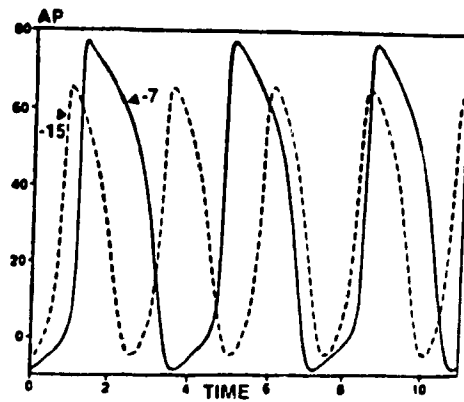


Figure 3.1: *Bistable solutions of system (3.5)-(3.6).*

$$\frac{dY}{dt} = T^{-1}[h(V) - Y] \quad (3.6)$$

where V is the transmembrane potential in the cell, and Y is a variable which indicates the level of excitability of the cell (i.e. its ability to respond to an electric stimulus). C is the membrane capacitance and T denotes the time constant of the activation/inactivation process. The functions f, g are related to the current-voltage relations of maximally excitable and completely unexcitable cells while h carries information concerning the ability of a stimulated cell to recover after excitation. Figure 3.1 displays a typical solution $V(t)$ of system (3.5)-(3.6) (i.e. a simulated action potential), taken from Landau *et al.* [39] where the model is discussed in detail. The interesting observation is that the model possesses two Hopf bifurcation points around which there coexist bistable solutions. In one case, the two solutions are periodic, while in the other one solution is periodic and the second is a steady state. These numerical observations on a simple model may have great importance in the correct interpretation and understanding of cardiac pathologies involving an abrupt change in rhythmicity.

These observations might seem somewhat ambitious given that we have only talked about the multistability in a very simple model of the electrical activity of a single cardiac cell, but they are analogous to similar observations in other models for the propagation of electric stimuli in excitable media. For example, Lewis and Guevara [44] have studied the effect of periodic electrical stimulations on the behavior of a strand of ventricular muscle. The model they used to investigate the dynamics of the transmembrane potential V was the parabolic partial differential cable equation

$$\frac{a}{2R_i} \frac{\partial^2 V}{\partial x^2} = C \frac{\partial V}{\partial t} + I_m, \quad (3.7)$$

where x is the distance along the cable, a the cell radius, C the membrane capacitance and

I_m is the net ionic current as described in a standard model of the ventricular muscle [44].

The numerical investigation of equation (3.7) indicates that there are regions of bistability of the solutions in parameter space. Lewis and Guevara observed different synchronization rhythms for the same stimulation frequency. In other words, a shift of the solutions of equation (3.7) in phase space (generated by the addition of a bias potential) resulted in a qualitative change in the period of this solution, indicating the presence of bistable attractors.

The clinical implications of these numerical observations are important. For example, ventricular fibrillation is a fatal cardiac arrhythmia characterized by rapid, apparently random contractions of the myocardium. The heart stops beating in an organized fashion depriving muscles of oxygenated blood, and the lungs with oxygen depleted blood. Fibrillation is dealt with clinically by administering to the heart a series of electroshocks. If the treatment is successful, the heart beat returns to normal. In light of the results on bistability, it has been claimed that the phenomenon underlying the abrupt change of cardiac rhythm due to electroshocks might be interpreted as an abrupt shift in the phase space of the fibrillating tissues. More precisely, it is supposed that the shocks transport the cardiac dynamics from one basin of attraction (fibrillation) into another (normal rhythm).

Another cardiac arrhythmia known as tachycardia has been studied within the context of the theory of multistable dynamical systems. Tachycardia is characterized by a rapid periodic oscillation of the myocardium, usually not fatal, and sometimes preceding fibrillation. There are two types of tachycardia: ventricular tachycardia and re-entrant tachycardia. Ventricular tachycardia is the variant often observed to precede fibrillation. The two tachycardias result from different pathologies, but they are both thought to be bistable in the sense that a normal heart rhythm can be shifted to tachycardia and *vice versa* through the application of an electric shock. Moreover, ventricular tachycardias and normal rhythms are quite frequently observed alternatively (without any external perturbation) in healthy patients.

There are models describing this switching behavior [39] which make use of the concept of multistability to account for the odd tachycardiac segment of an otherwise normal electrocardiogram. However, this approach is hampered by the paucity of results concerning multistability in infinite dimensional dynamical systems like P.D.E's, even though these equations are frequently used in models of cardiac dynamics to account for the switching

between metastable basins of attraction. It is therefore important to undertake a systematic study of this behavior to facilitate the process of modeling complex biological entities, in which multistability might be used as a paradigm to study system variability. More specifically, a better understanding of the multistability in partial differential equations may help clinicians improve their treatment of frequently encountered cardiac arrhythmias.

We touch here on another motivation for the study of multistability in high dimensional dynamical systems. As mentioned below, the investigation of optical bistable devices was historically motivated by their potential applications as high speed switching mechanisms. We discussed above how multistable systems were capable of this switching behavior. In fact, preliminary results [37] indicate that multistable optical devices are potentially more efficient for storing and processing information than conventional semiconductor based circuitry.

We now discuss some results on optical bistability, because during the past decade the study of nonlinear optical cavities has greatly motivated the investigation of D.D.E dynamics.

3.2 Multistability in physics.

In this section, we review experimental observations of multistability in physical systems that have been modeled by delay differential equations.

3.2.1 Optical bistability.

The motivation for studying optically bistable devices is twofold:

- 1) Intrinsic optically bistable devices (i.e. devices which exhibit two distinct states of optical transmission) can serve as extremely fast optical switches, and be used as short pulse generators when their behavior is periodic [45];

- 2) Optical bistability has received a substantial amount of attention as a "toy problem" in nonequilibrium statistical mechanics because of the relative simplicity of experimental manipulations. When compared to turbulence in fluid flows, the problem of optical turbulence (or chaos) is simple to study both experimentally and theoretically, and it is hoped that it might yield some insight into the problem of understanding and characterizing fully developed fluid turbulence [75, 76, 77].

The pioneering work on the dynamics of multistable nonlinear optical cavities is due to Ikeda [32, 33] and Gibbs [21, 27]. Ikeda showed that the Maxwell-Bloch equations for a ring cavity filled with a nonlinear medium were reducible to a differential delay equation in the limit of fast transverse atomic relaxation. The experimental realization of Ikeda's model was provided by Gibbs using a hybrid optical device, providing the first evidence of optical chaos. In this section, we describe the experiments in some detail because there are still relatively few studies discussing the experimental observations of multistability as a phenomenon worthy of investigation.

a) Experimental observations.

The observations discussed here are summarized from Gibbs *et al.* [21] who designed the experiment to investigate the instabilities predicted by Ikeda in intrinsically bistable optical ring cavities. The experiments consist in measuring the light intensity emanating from a nonlinear optical cavity driven by a laser source of constant intensity. The optical cavity is a conventional potassium dihydrogen phosphate modulator, illuminated with a constant intensity He-Ne laser. The input and output of the modulator are polarized with linear polarizers. The modulator's output light intensity is converted into a voltage with a photodiode, and this voltage is in turn fed back, after a controlled delay, to the modulator. This artificially induced delay plays the role of the cavity round trip time in an intrinsically bistable device.

The equation used to model the dynamics of the modulator's output intensity is

$$\epsilon \frac{dx}{dt} + x(t) = \pi \mu \{1 - \xi \cos[x(t - \tau) + x_b]\}, \quad (3.8)$$

and when the optical cavity is a liquid crystal, the delay equation describing the dynamics of the output is

$$\epsilon \frac{dx}{dt} + x(t) = \mu \sin^2(x(t - \tau) - x_b), \quad (3.9)$$

where, in both equations x is proportional to the voltage fed to the modulator, ϵ is the response time of the electronic circuit, ξ measures the modulator's ability to achieve extinction between the cross linear polarizers and τ plays the role of the cavity round trip time. x_b is a controlled D.C. bias applied to the modulator.

The bifurcation parameter μ is proportional to the gains of two amplifiers required for the proper functioning of the delay circuit. The first amplifier is located between the photodiode and the delay circuit, and the second is located on the feedback loop between the delay circuit and the modulator. μ is the only parameter varied in the experiment.

Oscillations in output intensity have been the subject of intense scrutiny for the past decade, and the presence of metastable solutions has been confirmed experimentally. The main results relevant to bistable behavior can be summarized as follows.

1) When μ is varied continuously from 0 to values greater than 1, the output intensity of the modulator undergoes two period doubling bifurcations before entering a chaotic regime.

2) As μ is lowered back to zero, the solution undergoes a series of period halving bifurcations, and does not follow the same path in phase space as it did when μ was increased.

This type of behavior was discussed in Chapter 2 for an electronic analog oscillator simulating a delay differential equation. It is strongly indicative of multistability in the system since hysteresis in the bifurcation pattern can be explained by a sensitive dependence of the solution behavior on changes in the initial functions. To confirm the presence of multistability experimentally, it would be necessary to artificially control the initial function in the hybrid optical device, vary it and observe the subsequent variations in observed solutions. This type of experiment has not been performed with optical devices, but numerical investigations of the model D.D.E's did highlight the presence of metastable attractors of periodic solutions [14, 45]. For this reason, we turn to analytic and numerical techniques used to get some insight into the stability properties of the phase space of equation (3.9).

b) Analytic and numerical results.

In general, the delay differential equation for a hybrid optical device is

$$\epsilon \frac{dx}{dt} = -x(t) + F(\mu, x(t - \tau)), \quad (3.10)$$

where $x(t)$ is the dimensionless output of the system at time t (related to the intensity of the light transmitted by the optical cavity at time t), τ is the time delay of the feedback loop and ϵ is the response time of the nonlinear medium. The control parameter μ is proportional to the intensity of the incident light (the laser). The function F characterizes the system

with nonlinearities. We consider equation (3.10) with a nonlinearity F given by

$$F(\mu; x) = \mu \sin^2(x(t - \tau) - x_b). \quad (3.11)$$

[This function was introduced by Zhang *et al.* when considering a liquid crystal hybrid optical bistable device [84]]. For illustrative purposes, we follow the linear stability analysis given by Li *et al.* [45] as an example of the preliminary analysis usually performed on nonlinear delay differential systems. We then extend their numerical investigation to the paradigm system with piecewise constant nonlinearities presented in Section 1.5 and investigate the attractor basin boundaries for this system.

Equation (3.10) with (3.11) can be linearized about a fixed point x^* such that if $y(t) = x(t) - x^*$, we have

$$\hat{\epsilon} \frac{dy}{dt} = -y(t) + z y(t - 1) + W(\mu, y(t - 1)) \quad (3.12)$$

where

$$\hat{\epsilon} = \frac{\epsilon}{\tau}, \quad z \equiv \left. \frac{\partial F(\mu, x)}{\partial x} \right|_{x=x^*},$$

and W is of order $\mathcal{O}(y^2(t - 1))$ (for a scaling of equations like (3.10) we refer the reader to Appendix A). The initial condition for the linearized equation (3.12) is

$$y(t') = \varphi(t') \text{ for } t' \in [-1, 0].$$

As long as y remains small enough, we can neglect terms of higher order in y , and consider the linear equation

$$\hat{\epsilon} \frac{dy}{dt} = -y(t) + z y(t - 1). \quad (3.13)$$

The Laplace transform of $y(t)$ is, by definition,

$$L(y) \equiv \int_0^\infty e^{-\lambda t} y(t) dt = \tilde{y}(\lambda). \quad (3.14)$$

A closed form solution of equation (3.13) can be written and its Laplace transform is

$$\tilde{y}(\lambda) = \left\{ \hat{\epsilon} \varphi(0) + z e^{-\lambda} \int_{-1}^0 \varphi(u) e^{-\lambda u} du \right\} \times \tilde{G}_0(\lambda), \quad (3.15)$$

where

$$\tilde{G}_0(\lambda) = (\hat{\epsilon} \lambda + 1 - z e^{-\lambda})^{-1}. \quad (3.16)$$

$\tilde{G}_0(\lambda)$ is a meromorphic function because it possesses an infinite number of conjugate pairs of isolated poles. Using the Mittag-Leffler theorem [70], $\tilde{G}_0(\lambda)$ can be expanded to give

$$\tilde{G}_0(\lambda) = \sum_{k=-\infty}^{\infty} \frac{c_k}{\lambda - \lambda_k} \quad (3.17)$$

where c_k , the residue of the left hand side at λ_k , is obtained using l'Hôpital's rule.

Taking the inverse Laplace transform of equation (3.15) yields

$$y(t) = \lim_{l \rightarrow \infty} \int_{C-l}^{C+l} d\lambda \frac{e^{\lambda t}}{\tilde{G}_0(\lambda)} \varphi(0) + z e^{\lambda} \int_{-1}^0 e^{-\lambda u} \varphi(u) du \quad (3.18)$$

$$= \hat{\epsilon} \varphi(0) G_0(t) + z \int_{-1}^0 G_0(t-u-1) \varphi(u) du \quad (3.19)$$

where

$$G_0(t) = \lim_{l \rightarrow \infty} \int_{C-l}^{C+l} \frac{e^{\lambda t}}{\tilde{G}_0(\lambda)} d\lambda. \quad (3.20)$$

We can write the solution $y(t)$ in an alternate way using the Mittag-Leffler expansion,

$$y(t) = \sum_{k=-\infty}^{\infty} \rho_k e^{\lambda_k t} \quad (3.21)$$

where

$$\rho_k \equiv c_k \varphi(0) + z c_k e^{\lambda_k} \int_{-1}^0 \varphi(u) e^{\lambda_k u} du.$$

Therefore, computing the solution involves computing an infinite number of integrals over the initial interval. Note that if different initial functions are such that the integrals corresponding to the different λ_k 's have the same value, then they will yield the same asymptotic solutions of equation (3.13). Every residue c_k determines a possible mode of time evolution of equation (3.13). The sign of the real parts of the c_k 's determine the stability of the fixed point x^* . In particular, at the boundaries between the stable and unstable regions, the real parts of all the c_k 's must vanish. Therefore, the critical conditions separating stable and unstable regions of the $(z, \hat{\epsilon})$ plane are given by

$$\tilde{G}_0^{-1}(c_k) = 0 \quad (3.22)$$

$$Re(c_k) = 0. \quad (3.23)$$

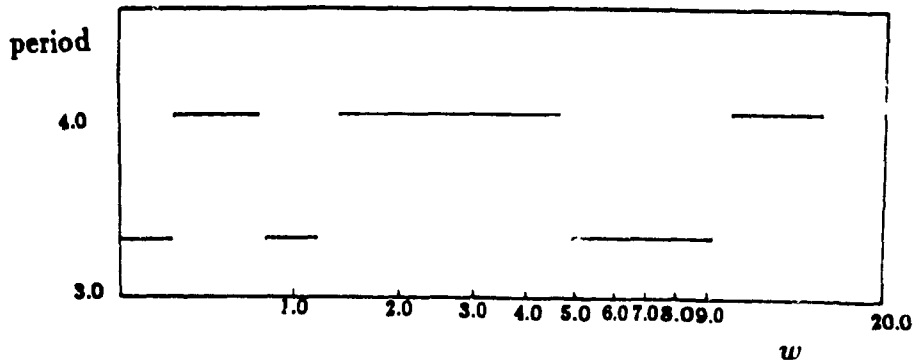


Figure 3.2: Period of the solution of (3.10) with nonlinearity (3.11) as the frequency of the initial function $\varphi(t) = A \sin(\omega t)$ varies. The figure is a first glimpse at the structure of the boundary separating two basins of attraction of the solutions.

Letting $\text{Im}(c_k) = \omega_k$, if $\omega_k \neq 0$, the solutions to this system are given by

$$s_k = \frac{1}{\cos(\omega_k)} \quad (3.24)$$

along with

$$\hat{\epsilon} = -\frac{\tan(\omega_k)}{\omega_k}. \quad (3.25)$$

When $\omega = 0$, then

$$s_0 = 1, \quad \hat{\epsilon} \in [0, \infty),$$

and therefore, if $s_k > 1$ then x^* is unstable. Since we are interested in stable fixed points, we only discuss the case $s_k < 0$.

Suppose that $\hat{\epsilon}$ has been determined from equation (3.25). We then have, from (3.22) (with (3.23))

$$\text{Re}(c_k) = -\ln \left| \frac{\hat{\epsilon} \omega}{s \sin(\omega)} \right| = \ln \left| \frac{s}{s_k} \right| - \ln \left| \frac{\hat{\epsilon} \omega}{s_k \sin(\omega_k)} \right|. \quad (3.26)$$

Now, if ω satisfies (3.24), that is $\omega = \omega_n$, $n = 1, 3, 5, \dots$, then $\text{Re}(c_n) = \ln |s/s_n|$. The mode ω_n is excitable (or unstable to a small perturbation) when $|s| > |s_n|$. On the other hand, the steady state x^* is stable when $|s| < |s_n|$. If $|s| < |s_1|$, the steady state is always stable. Therefore, s_1 is the instability threshold for system (3.13), and the stability conditions for a steady state become

$$\begin{aligned} |s(x^*)| &< |s_1| \\ s(x) &< 1 \end{aligned} \quad (3.27)$$

It is possible to find similar criteria for the bistable states using the integral averaging method

and the theory of retarded functional differential equations. Such an analysis is explicitly given by Li and Hao. [45] for the D.D.E considered in this section. The formalism is involved, and makes use of the theory of retarded functional differential equations [45, 22, 59] so we only give a brief summary of their main results. They are representative of the types of investigation presently under way concerning the dynamics of real systems modeled by delay differential equations.

1) Li and Hao showed that the point $s = s_1$ is a bifurcation point for the nonlinear system even though it was determined from the linearized equation. However, the other s_i 's with $i > 1$ do not have such a clear meaning because in the nonlinear system one expects different modes to couple and influence the critical values for the s_i 's obtained from the linear stability analysis. When ϵ is not too small, it is acceptable to neglect the mode-mode coupling for higher modes.

2) There exist bistable periodic solutions. The period of these solutions is denoted by T_1 and T_2 . The initial function is of the form $\varphi(t) = A \sin(\omega t)$, and Figure 3.2 displays the dependence of the period of the solution on the frequency of the initial function. In some sense, Figure 3.2 is our first glimpse at the structure of basin boundaries in the Banach space of initial functions for equation (3.10) with (3.11). In Section 3.3 we will try to systematize this type of approach for the integrable equation (2.3).

In the next section we will see how our own numerical results on delay differential systems complement those of Li and Hao [45].

3.3 Multistable behavior of an integrable delay differential equation.

We now focus our attention on the integrable D.D.E with piecewise constant forcing presented in Section 1.5 as a paradigm for production-destruction processes involving a mixed delayed feedback control loop. The simulations presented here were obtained with an algorithm designed to emulate an analytic integration of

$$\frac{dx}{dt} = -\alpha x(t) + F(x(t - \tau)) \text{ where } F(x) = \begin{cases} c & \text{if } x \in [\theta_1, \theta_2] \\ 0 & \text{otherwise.} \end{cases} \quad (2.3)$$

The algorithm is described in detail in Appendix D (a listing of its Fortran implementation is given in that appendix, along with other program listings).

3.3.1 Higher order multistability.

It is clear from the observations of Section 2.4 (concerning the analog computer simulating (2.3)) and Section 3.2, that changing initial functions of D.D.E's may have dramatic repercussions on solution behavior. At this point there is good evidence that control loops involving time delays can be multistable, but there is no systematic investigation of this property other than the occasional figure published to illustrate the phenomenon. We want to explore this behavior for (2.3) numerically in the hope that the results stimulate further analytic work. We begin by investigating the existence of cycles that are tristable, quadristable *etc.*, because bistability is the only kind of multistability discussed in the literature.

a) Parametrizing the initial functions.

It was mentioned in Section 1.5.2 that the information content of the initial functions for equation (2.3) was redundant. This observation is at the basis of a simple parametrization of the initial functions for equation (2.3). Since the feedback function is piecewise constant, the solution $x_\varphi(t)$ of equation (2.3) with initial function $\varphi(t)$, $t \in [-\tau, 0]$, is completely described by the times in $[-\tau, 0]$ at which φ crosses either θ_1 or θ_2 . If we label these crossing times t_i , then the solution $x_\varphi(t)$ can be written $x_{\{t_i\}}(t)$. To clarify our discussion, we focus attention on the solutions $x_{\{t_i\}}(t)$ generated by initial functions $\varphi(t)$ belonging to a set Φ defined as follows

$$\Phi(t) = \{\Phi_1(t), \Phi_2(t), \Phi_3(t)\} \quad (3.28)$$

where

$$\begin{aligned} \Phi_1(t) &= \{\phi(t) : \phi(-\tau) < \theta_1, \phi(t_1) = \theta_1, \forall t \in [-\tau, t_1]\} \\ \Phi_2(t) &= \{\phi(t) : \phi(t) \in (\theta_1, \theta_2) \forall t \in (t_1, t_2)\} \\ \Phi_3(t) &= \{\phi(t) : \phi(t_2) = \theta_2, \phi(t) > \theta_2 \forall t \in [t_2, 0), \phi(0) = \theta_2\}. \end{aligned} \quad (3.29)$$

The rationale for restricting the initial functions under consideration to the elements of Φ is to try and simplify the eventual analytic work suggested by the numerics.

We can now investigate the effect of changing t_1 and t_2 on solution behavior.

b) Digital simulations.

The results presented here appear to be the first reports of higher order multistability in a delay differential equation. Figures 3.3 and 3.4 display typical examples of the type of bistability observed in large areas of the space of control parameters [N.B. The control parameters in the system do not include t_1 and t_2 ; these two quantities characterize the initial function and thus cannot be considered as bifurcation or control parameters]. The difference between the two initial functions generating the solutions presented in Figures 3.3(a,b), 3.4(a,b) is the value of the time t_2 at which it crosses θ_2 on the initial interval.

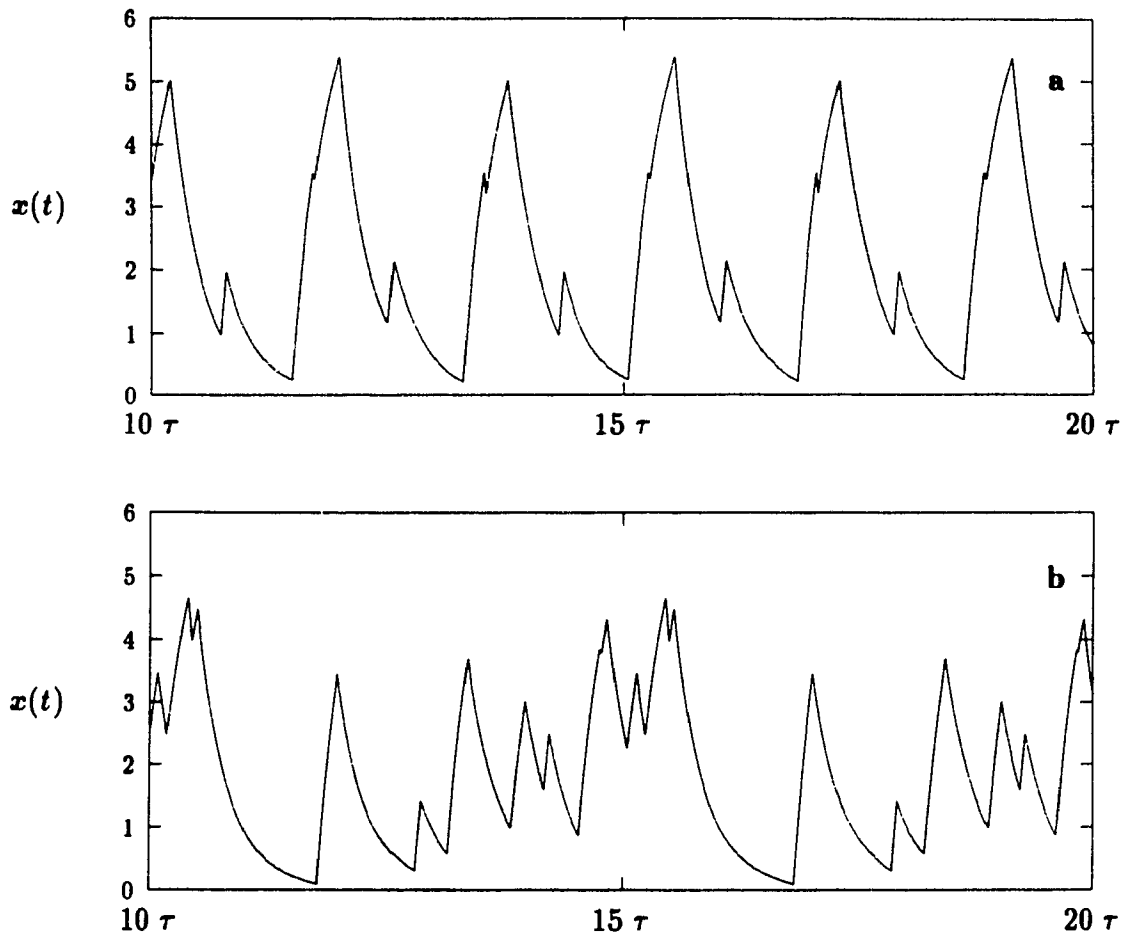


Figure 3.3: Typical bistable solutions of equation (2.3). The parameters are: $\alpha = 3.25$, $c = 20.5$, $\tau = 1$, $\theta_1 = 1$, $\theta_2 = 2$. **a)** $t_1 = -0.9925$, $t_2 = -0.6$ and the period is $P = 3.66$. **b)** $P = 5.19$, $t_1 = -0.995$, $t_2 = -0.27$.

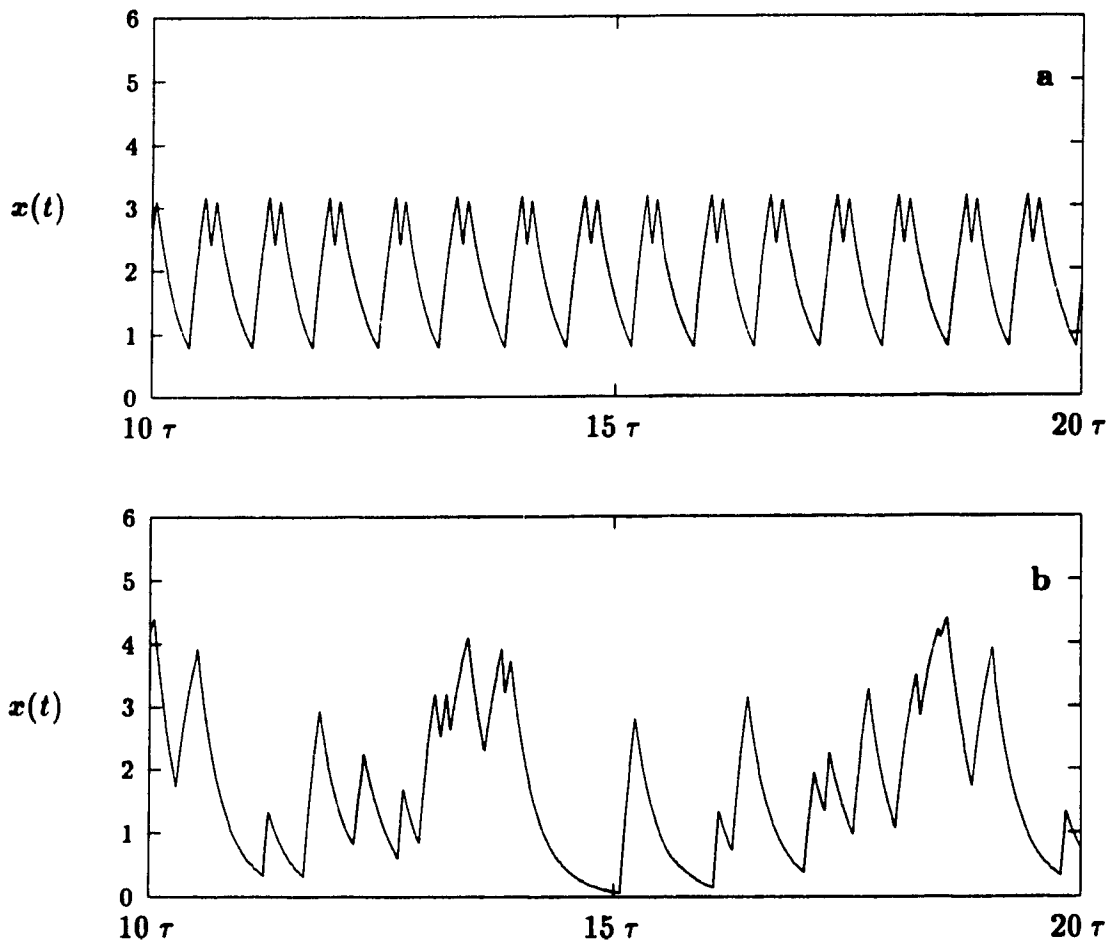


Figure 3.4: Another example of bistability in (2.3). The parameters are the same as in Figure (3.3) except: $\alpha = 3.5$, $c = 19.5$. a) $t_1 = -0.985$, $t_2 = -0.834$ and the period is $P = 0.75$. b) $t_1 = -0.9925$, $t_2 = -0.4$ and $P = 8.96$.

Figure 3.5 displays a typical example of tristability. It is important at this point to note that the multistability is *robust* in the sense that it is observed in large regions of parameter space. Figure 3.6 illustrates this robustness. It is a plot of the periods of the solutions of equation (2.3) as a function of the parameter α , when all the other control parameters are held constant. The initial functions used here are of the type described in 3.3.1a. Figure 3.6 illustrates the relative prevalence of short limit cycles (containing at most 12 extrema per period), an example of which is displayed in Figure 3.3a. It appears that the long limit cycles (containing more than 12 extrema per period) are less frequent than the short limit cycles when controlled parameters are varied. On the other hand, for a given set of fixed control parameters, the long limit cycles appear to be more abundant than the short ones as the initial functions are varied. In other words, the locii at which short limit cycles are observed in (t_1, t_2) space, (displayed in figures 3.7 – 3.9) are less numerous than those at which long limit cycles are observed.

These apparently contradictory observations are illustrated by comparing Figures 3.6 and 3.7. They highlight one aspect of the complexity of multistable behavior in simple D.D.E's. Before proceeding, note that there appears to be no limit to the order of multistability displayed by equation (2.3). The more finely one looks at the structure of (t_1, t_2) space, the more limit cycles one is likely to find. This observation is based on numerical observations and should be taken at best as an educated conjecture.

1.1.1 Basin boundaries in the space of initial functions.

With respect to multistability an important question to address, directly related to the structure of basin boundaries in the space of initial functions, is :“Given a fixed set of parameters, what is the relative distribution of long and short period limit cycles?” This question is perhaps more crucial than the simple determination of the existence of multistable behavior. When performing an experiment, little attention is usually given to the initial preparation of the system. Being aware of the presence of multistability in the system under consideration is useful, but it is more interesting to qualitatively know to what extent perturbations to the initial functions will affect the asymptotic solution. The fact that

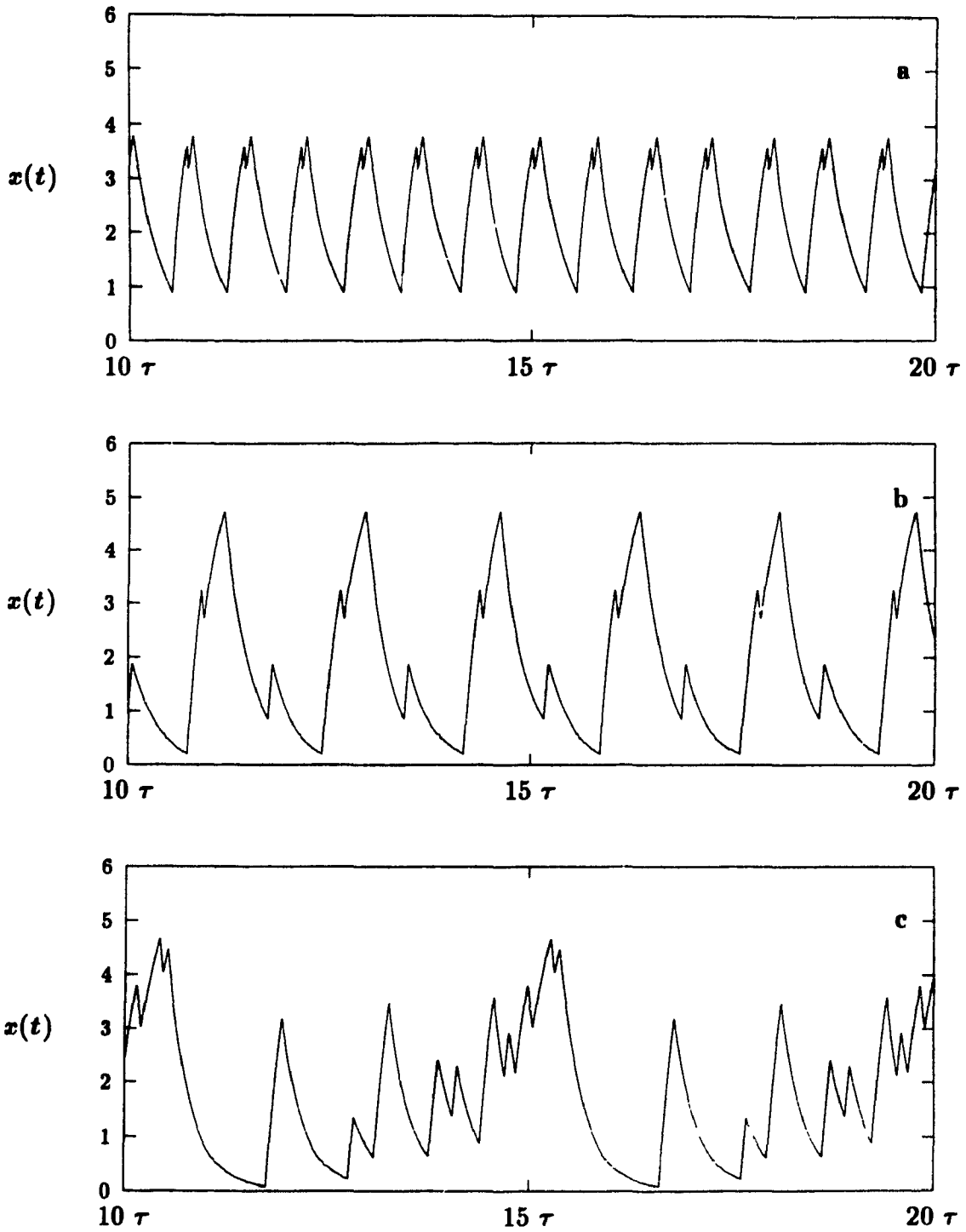


Figure 3.5: *Tristability in equation (2.3). The parameters are the same as in Figure 3.3 except $\alpha = 3.25$. a) $t_1 = -0.925$, $t_2 = -0.711$, and the period is $P = 0.75$. b) $t_1 = -0.9$, $t_2 = -0.386$, and $P = 1.78$. c) $t_1 = -0.9925$, $t_2 = -0.4$ and $P = 5.05$.*

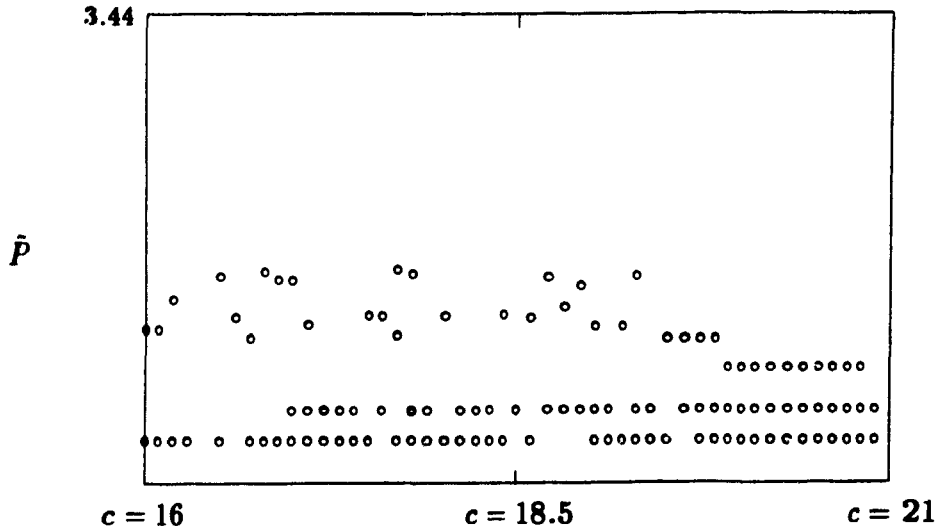


Figure 3.6: The quantity $\tilde{P} = \log(1 + \log(1 + P))$ as the parameter c is varied for $\tau = 1$, $\alpha = 3.25$, $\theta_1 = 1$ and $\theta_2 = 2$. \tilde{P} was plotted here rather than P for the clarity of the figure.

minute changes in the initial preparation of an experiment can have a dramatic influence on observed behavior is not widely recognized. We illustrate this in the next section.

a) Digital simulations.

Consider equation (2.3) with the parameters of Figure 3.3. As the parameters t_1 and t_2 are varied, we expect to generate both types of solutions presented in Figure 3.3. Figure 3.7 represents 10^6 solutions of equation (2.3) obtained with 10^6 different initial functions belonging to Φ . More specifically, for each t_1 , the graph represents 1000 values of t_2 , distributed uniformly between t_1 and 0, and the procedure was repeated for 1000 values of t_1 . The plotted points represent the loci in (t_1, t_2) space which generated the short limit cycle solution of Figure 3.3a.

A noticeable feature of Figure 3.7 is unfortunately not clear without the original data: The figure was obtained by discarding the points in (t_1, t_2) space which did not generate the solution of Figure 3.3a, and the relative importance (or size in some sense) of the basin of attraction of this short period solution compared with the size of the basin of attraction of the long period solution (Figure 3.3b) does not appear unambiguously. This size difference was unambiguous in the original data, but the information is lost on Figure 3.7 because of the impossibility to estimate the relative dominance of the "white spots" embedding the black ones. Though it is impossible for the eye to determine roughly the ratio of the number of dots on Figure 3.7 to 10^6 , this ratio is of order 0.1. Thus, if an initial function belonging to Φ is picked at random, it is ten times more likely to generate the solution of Figure 3.3b than that of Figure 3.3a.

Figures 3.8 and 3.9 are similar to 3.7 for different values of the parameters. It should be kept in mind that these figures give only an indication of the complexity of the separatrix. A black and white two dimensional picture cannot carry enough information to describe the boundary separating more than two distinct basins of attraction. To illustrate the distribution of (t_1, t_2) pairs generating the three solutions shown in Figure 3.5 one might use a three color graph, each color representing a given solution.

Figure 3.7: The boundary of the basins of attraction of two bistable solutions of (2.3) displayed in Figure 3.3. The black dots represent values of (t_1, t_2) for which the asymptotic solution is the one shown in 3.3a.

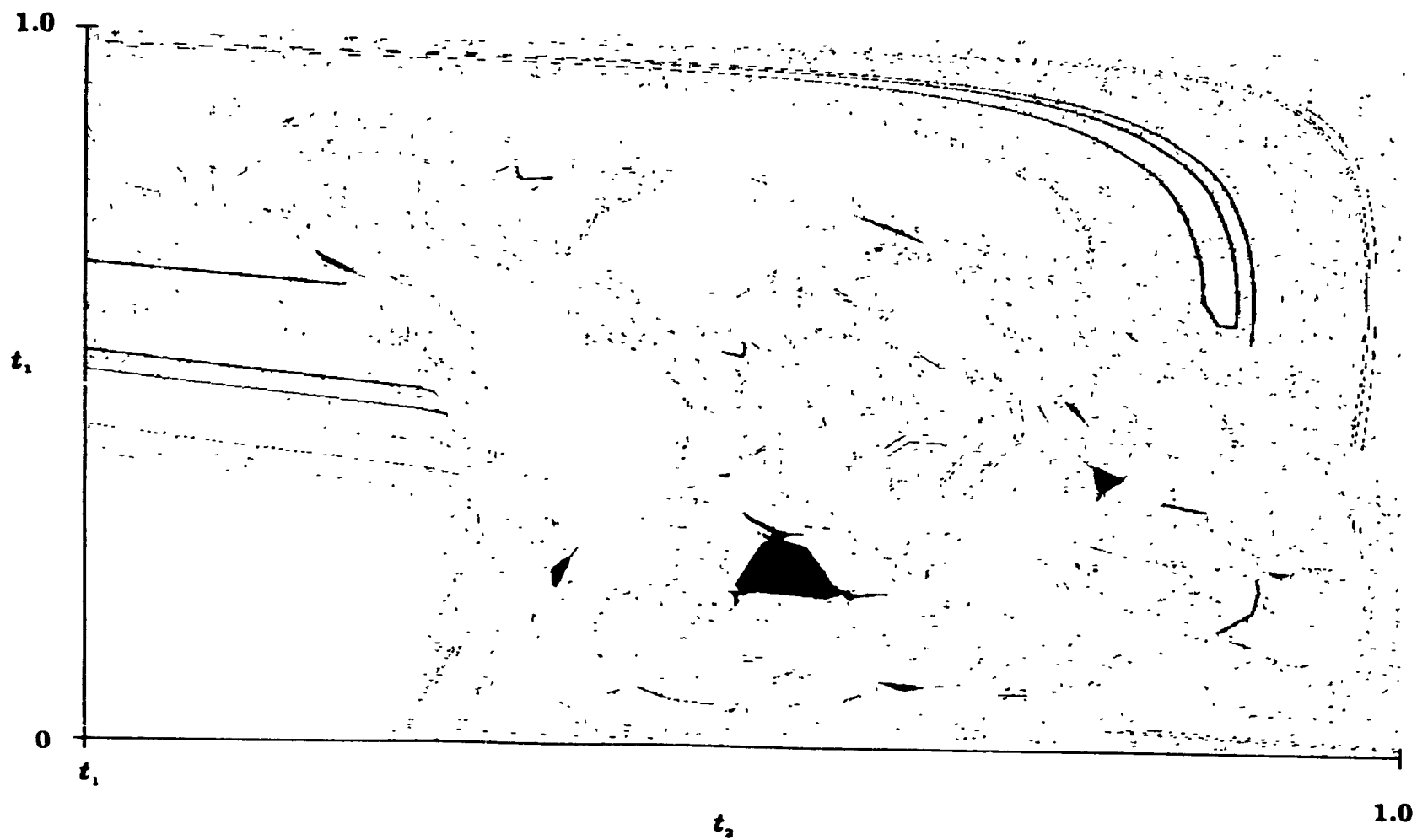


Figure 3.8: The black dots on this picture represent values of (t_1, t_2) for which the asymptotic solution of (2.3) is the one displayed in Figure 3.5b

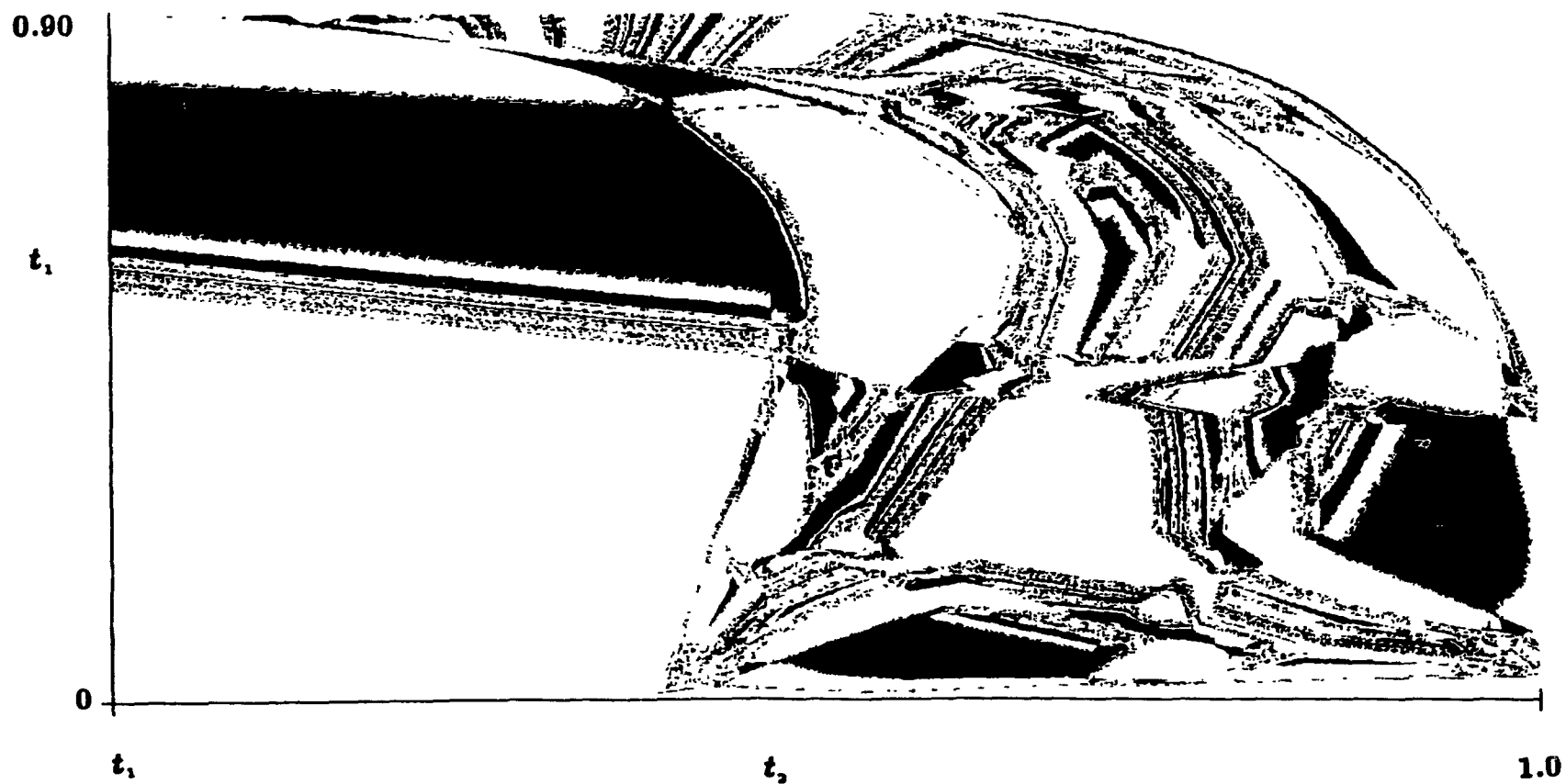
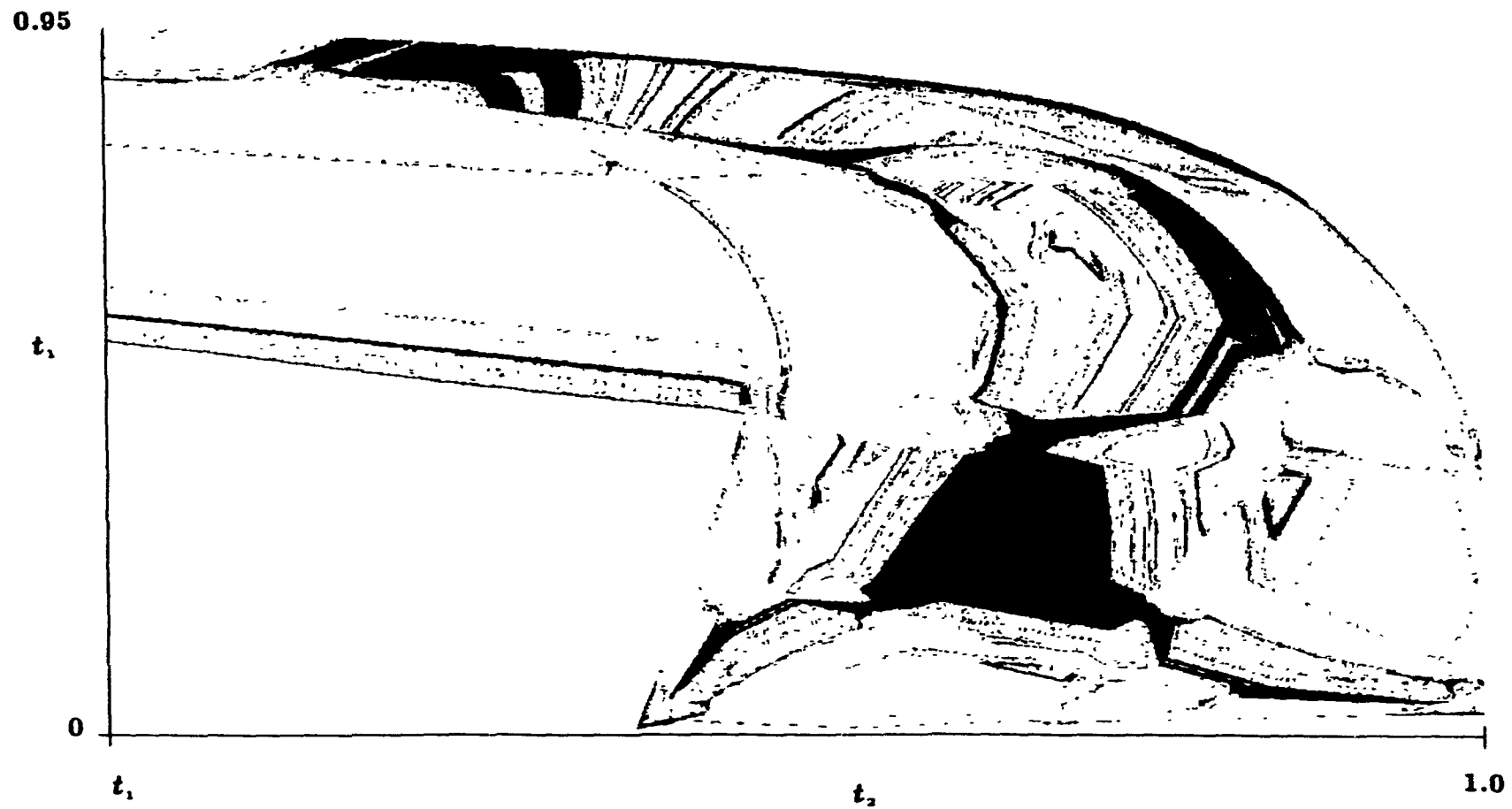


Figure 3.9: The black dots on this picture represent values of (t_1, t_2) for which the asymptotic solution is the one displayed in Figure 3.5a



When the initial conditions are more complex, for instance when they possess n crossings of the thresholds θ_1 and θ_2 , the structure of the basin boundaries are difficult to comprehend, for then the parameters characterizing an initial function span a surface embedded in an n -dimensional space. Whatever the class of initial functions under consideration, it is probably a good idea to limit the number of parameters specifying them to at most two. For example, Figure 3.2 is similar to 3.7 but the initial functions used to draw this figure belong to a set Φ' such that

$$\Phi' : \{\varphi(t) \mid \varphi(t) = A \sin(\omega t) \text{ for } t \in [-\tau, 0].\} \quad (3.30)$$

In this case, the frequency content of the initial function is allowed to vary much more than when $\varphi(t) \in \Phi$ even though the number of parameters specifying $\varphi(t)$ remains manageable.

3.4 Summary.

In this chapter, we have presented some results concerning multistability in delay differential equations. In Section 3.1, the motivations to understand this behavior are given from a biological perspective. We discuss how multistability may explain certain cardiac arrhythmias and the potential clinical applications of a better understanding of the structure of basin boundaries in infinite dimensional dynamical systems.

In Section 3.2, we present earlier results concerning multistability in nonlinear optics. We also review the basic analytic techniques used to determine the stability of solutions.

Section 3.3 is a systematic investigation of multistable behavior in delay differential equations. The numerical results illustrate both the robustness of the property and its complexity.

The structure of basin boundaries for parametrized initial functions is discussed in Section 3.4, where we demonstrate the possibility of extremely sensitive dependence of solution dynamics on small perturbations of the initial function.

Chapter 4

Dynamics of ensembles of D.D.E's.

To now, attention has been focused on the examination of single trajectory behavior, *i.e.* the study of the behavior of single solutions of delay differential equations, their complexity and their bifurcations. In this chapter, we examine the behavior of ensembles of solutions as the first step in the development of techniques to yield useful information about the statistics of systems with delayed dynamics.

Why investigate purely deterministic systems from a statistical perspective? The motivation for doing so lies in the observation that determinism does not imply predictability. For example classical statistical mechanics was developed as a theoretical framework for the investigation of large numbers (of order 10^{23}) of particles whose individual evolution equations were deterministic (Hamilton's equations). Furthermore, if the evolution of a system is chaotic, then it is also reasonable to characterize its motion statistically. If system evolution cannot be predicted exactly, then the way to carry out this statistical investigation is to consider the evolution of phase space density functions so a statistical description of the system can be given by its phase space density function. This density function weights the phase space according to where the system is most likely to be found and can be used to describe the nonequilibrium properties of the system and its measurable quantities [30].

In Section 4.1 we summarize some of the existing results on the evolution of phase space densities evolving under the action of finite dimensional dynamical systems. In particular, we introduce the Frobenius-Perron operator, and the Liouville equation, and introduce a type of density behavior for discrete time maps known as asymptotic periodicity.

The difficulties inherent with the description of phase space densities for delay differential systems are discussed in Section 4.2. We compare numerical observations concerning the hat map with those concerning the corresponding singularly perturbed delay differential equation.

In Section 4.3 we present some techniques to derive analytic expressions for densities along the trajectories of an integrable delay differential equation. We then show how these techniques are applicable to the study of certain neural nets.

4.1 Densities and dynamical systems.

4.1.1 Densities *versus* single trajectories.

The need to study a deterministic system statistically arises when the dynamics of this system become “unpredictable”, when one is studying a large number of simple systems (as in classical statistical mechanics), and when the deterministic system is perturbed stochastically.

To elaborate on these points, note that:

1) It is well known that simple deterministic systems can display complicated unpredictable behavior or “deterministic chaos”. When the dynamics of a system are chaotic, exact long term predictions become impossible from a practical point of view and the search for an underlying order is necessarily probabilistic in nature. The density behavior can often be easily characterized when the single trajectory behavior is chaotic. For example, the study of chaotic discrete time maps of the unit interval onto itself has greatly benefited from this approach. When the maps are one dimensional, the density of initial conditions is a function defined on a subinterval (or a collection of subintervals) of the unit interval. The evolution of this function is then given by a *linear* integral operator, the Frobenius-Perron operator. A precise definition of the Frobenius-Perron operator (FPO) and a review of its applications to the study of interval maps is given in [40]. The FPO can also be defined for continuous time systems, and it is a powerful tool for the investigation of the entropy behavior of deterministic dynamical systems [51].

2) At the end of the nineteenth century a few physicists (including Boltzmann and Gibbs)

realized that a meaningful investigation of macroscopic behavior could only be carried out statistically. This idea led to the formulation of classical statistical mechanics and the elaboration of techniques with which to study the evolution of systems composed of large numbers of units (atoms for example) each governed by simple equations of motion (e.g. Newton's laws). In the spirit of statistical mechanics and ergodic theory it is reasonable to develop techniques to deal with large collections of "particles" whose dynamical evolution depends on their history. One potential area of application is the mathematical modeling of neural organization, and neural information processing. Since time delays (due to finite conduction times) in the brain are ubiquitous, modeling neural dynamics is an area in which the use of D.D.E's may prove to be most promising [47]. Because of the large numbers of individual neurons (some chosen property of which is governed by a D.D.E) involved in a given task it will be interesting to see to what extent the ideas of statistical mechanics can be applied to large collections of D.D.E's.

3) Finally, a statistical investigation is required when dealing with stochastically perturbed systems. When this is the case, the specifications of the noisy component in the system are probabilistic in nature and, therefore, the only meaningful observations can be made within a statistical framework [71].

4.1.2 Temporal evolution of phase space densities.

In this section, we present some techniques developed to investigate the evolution of phase space densities of ordinary differential equations and discrete time maps. If an ensemble of initial conditions is specified (rather than a single initial condition) then this ensemble is described by a phase space density. The time evolution of this density under the action of the ODE or the map is associated with the evolution of the system's thermodynamic state. Before proceeding, we define a *density*.

Definition 4.1. A nonnegative L^1 function defined on a space X and satisfying

$$\int_X f(x) dx = 1 \quad (4.1)$$

is called a density. The space X is the phase space on which the dynamical system operates. For the one dimensional maps of the unit interval onto itself considered below, X is the

segment of the real line $[0, 1]$.

a) Discrete time systems.

The generic form of an l -dimensional discrete time system is

$$\mathbf{x}_{t+1} = \mathbf{F}(\mathbf{x}_t) \quad (4.2)$$

where $\mathbf{x}_t = (x_t^1, \dots, x_t^l)$, and \mathbf{F} is a function of l variables. For the introductory definitions presented in this section, we restrict ourselves to the one dimensional system

$$x_{t+1} = F(x_t) \quad \text{and } x_t \in [0, 1]. \quad (4.3)$$

Suppose we are given a density of initial conditions $f_0(x)$. The time evolution of f as x evolves under the action of system (4.3) is given by an integral operator \mathcal{P} such that

$$f_{t+1}(x) = \mathcal{P} f_t(x), \quad (4.4)$$

or, alternately

$$f_t(x) = \mathcal{P}^t f_0(x). \quad (4.5)$$

For the dynamical systems discussed here, the integral operator \mathcal{P} is a **Markov operator**.

Definition 4.2. Any linear operator $\mathcal{P} : L^1 \rightarrow L^1$ satisfying

$$\mathcal{P}^t f \geq 0$$

and

$$\int_X \mathcal{P}^t f(x) dx = \int_X f(x) dx$$

for all $t \in \mathbb{R}$, $f \geq 0$, $f \in L^1$ is called a **Markov operator**. This general Markov operator describes the evolution of densities under the action of stochastically perturbed dynamical systems. When the systems are completely deterministic, the Markov operator governing the evolution of densities is called a **Frobenius-Perron operator**.

The sequence of densities $\{f_t\}$ evolving under the action of a Markov operator \mathcal{P} is denoted $\{\mathcal{P}^t f_0\}$.

In Section 4.3 we discuss the connection between some statistical properties of a given one dimensional map and numerical simulations of the corresponding delay differential equation obtained *via* a singular perturbation procedure. It therefore useful to explain the derivation of the Frobenius-Perron operator for a one dimensional map F acting on the phase space X . Thus, we consider the dynamical system (4.3).

Let f_0 again denote the density of initial points (the initial ensemble). After one application of F to this ensemble, the points are distributed in X according to $\mathcal{P}f_0$. The fraction of this ensemble contained in the interval $[0, x]$ is

$$\int_0^x \mathcal{P}f_0(y) dy.$$

The points which are contained in the interval $[0, x]$ originated in its counterimage under the action of F . Let $F^{-1}([0, x])$ denote this counterimage, *i.e.*

$$F^{-1}([0, x]) = \{y \in X \mid F(y) \in [0, x]\}.$$

Therefore, we can write,

$$\int_0^x \mathcal{P}f_0(y) dy = \int_{F^{-1}([0, x])} f_0(y) dy. \quad (4.6)$$

Differentiating both sides of (4.6) yields

$$\mathcal{P}f_0(x) = \frac{d}{dx} \int_{F^{-1}([0, x])} f_0(y) dy. \quad (4.7)$$

This relation gives the prescription for obtaining the Frobenius-Perron operator when a specific F is considered.

Example 4.1. The generalized hat map is defined by $x_{t+1} = F(x_t)$, where

$$F(x) = \begin{cases} ax & \text{when } x \in [0, \frac{1}{2}] \\ a(1-x) & \text{when } x \in (\frac{1}{2}, 1], \end{cases} \quad (4.8)$$

for $a \in (1, 2]$.

The counterimage of a set $[0, x]$ under the action of the hat map is

$$F^{-1}([0, x]) = \left[0, \frac{1}{a}x\right] \cup \left[1 - \frac{1}{a}x, 1\right].$$

Therefore, using (4.7), the Frobenius-Perron operator for this transformation is defined by

$$\mathcal{P}f(x) = \frac{1}{a} \left[f\left(\frac{1}{a}x\right) + f\left(1 - \frac{1}{a}x\right) \right] \bullet \quad (4.9)$$

o) Continuous time systems.

Since most physical laws are framed as differential equations, it is natural to consider the evolution of densities in the phase space of these continuous time systems. The equations of Hamilton are

$$\begin{aligned}\frac{dp_i}{dx} &= -\frac{\partial H}{\partial q_i} \\ \frac{dq_i}{dx} &= \frac{\partial H}{\partial p_i}\end{aligned}$$

for $i = 1, \dots, N$, p_i and q_i are $6N$ conjugate generalized variables and H is the Hamiltonian function for the system. The evolution of an ensemble of initial points distributed according to the density f in (p_i, q_i) space is given by Liouville's equation [18],

$$\frac{\partial f}{\partial t} = -\sum_{i=1}^{3N} \left[\frac{\partial f}{\partial q_i} \frac{\partial H}{\partial p_i} - \frac{\partial f}{\partial p_i} \frac{\partial H}{\partial q_i} \right]. \quad (4.10)$$

The Liouville equation can be reduced to the Boltzmann equation with (many!) simplifying assumptions when the system under consideration is a dilute gas [25]. The equilibrium density of the Boltzmann equation (i.e. the density f_* for which $\partial f_*/\partial t = 0$) is known in physics as the Maxwell-Boltzmann distribution.

More generally, the evolution of densities in phase space when the dynamics are given by the n dimensional system of O.D.E's

$$\frac{dx_i}{dt} = F_i(x_1, \dots, x_n), \quad i = 1, \dots, n, \quad (4.11)$$

is given by the *generalized Liouville equation*

$$\frac{\partial f}{\partial t} = -\sum_{i=1}^n \frac{\partial(f F_i)}{\partial x_i}. \quad (4.12)$$

If the solution of (4.12) is written $f(x, t) = \mathcal{P}^t f_0(x)$, then \mathcal{P}^t is the continuous time version of the Frobenius-Perron operator presented here. When one considers a system of O.D.E's perturbed by a white noise term, then the equation giving the evolution of phase space densities is called the *Fokker-Planck equation* [68].

4.1.3 Asymptotically periodic Markov operators.

To now nothing has been said about the asymptotic properties of the sequence of densities evolving under the action of the Frobenius-Perron operator. This is an important problem since the phase space densities are associated with thermodynamic states. Therefore, if there exists a unique stationary distribution f_* to which the sequence (continuous or discrete) $\{f_t\}$ converges, the system evolves to a unique state of thermodynamic equilibrium. The converse is true. For a detailed discussion of the possible types of density behavior and the connection with the corresponding entropy behavior of the dynamical laws, the reader is referred to Lasota and Mackey [51]. We focus attention on one possible type of density evolution known as asymptotic periodicity.

To now asymptotic periodicity has only been investigated in discrete time systems [38, 40, 63, 64]. In Section 4.3, we discuss some results concerning strikingly similar behavior in a continuous time system, and their implications. To explain asymptotic periodicity, we need to introduce a property of certain Markov operators known as *smoothing*.

Definition 4.3. A Markov operator \mathcal{P} , acting in a space $X = [0, 1]$ is said to be *smoothing* if there exists a set $A \subset X$ of finite Lebesgue measure, and two constants δ and $\varepsilon < 1$ such that for every set $E \subset X$ whose Lebesgue measure satisfies $\mu_L(E) > \delta$, and for every initial density f_0 there is some integer $t_0(f_0, E)$ for which

$$\int_{E \cup (X \setminus A)} \mathcal{P}^t f_0(x) dx \leq \varepsilon, \quad \text{for } t \geq t_0.$$

In other words, regardless of how small the support of the initial density, it will spread out under the action of a smoothing Markov operator.

Smoothing operators possess a remarkable property explained in the following theorem proved by Komornik and Lasota [38].

Theorem 4.1.1 (Komornik and Lasota) *Let \mathcal{P} be a smoothing Markov operator. Then there is an integer $r > 0$, two sequences of functions $g_i \in D$ and $K_i \in L^\infty$, $i = 1, \dots, r$, and a bounded linear operator $Q : L^1 \rightarrow L^1$ such that for all $f \in L^1$, $\mathcal{P}f$ takes the form*

$$\mathcal{P}f(x) = \sum_{i=1}^r \lambda_i(f) g_i(x) + Qf(x), \quad (4.13)$$

where

$$\lambda_i(f) = \int_X K_i(x) f(x) dx. \quad (4.14)$$

The densities $g_i(x)$ and the operator Q satisfy the following:

- (1) The $g_i(x)$ have disjoint support so $g_i(x)g_j(x) = 0$ for all $i \neq j$.
- (2) For each integer i there is a unique integer $\alpha(i)$ such that $\mathcal{P}g_i = g_{\alpha(i)}$ and where $\alpha(i) \neq \alpha(j)$ for $i \neq j$. Thus, the action of the operator \mathcal{P} is to permute the densities $g_i(x)$.
- (3) $\|\mathcal{P}^t Q f(x)\| \rightarrow 0$ as $t \rightarrow \infty$. •

From property (2), the operator equation (4.13) can be written

$$\mathcal{P}^{t+1} f(x) = \sum_{i=1}^r \lambda_i(f) g_{\alpha^t(i)}(x) + \mathcal{P}^t Q f(x), \quad (4.15)$$

where the subscript $\alpha^t(i)$ is just the t^{th} application of the permutation $\alpha(i)$.

In simpler terms, the evolution of phase space densities for an asymptotically periodic system is characterized by a periodic cycling of the functions λ_i ($i = 1, \dots, r$) which weight the various components g_i ($i = 1, \dots, r$) of the density $f(x)$. The period of this cycle is at most $r!$ since the supports of the g_i 's are mutually disjoint.

This type of statistical cycling of the system in the asymptotic regime has profound implications. For instance, asymptotically periodic systems never evolve to a unique state of thermodynamic equilibrium, but endlessly visit a finite number of metastable states. The exact cycle depends on the initial preparation of the system (the initial density f_0). We note that this cycling of densities does not imply a cycling in the entropy behavior of the system. In fact, asymptotically periodic transformations evolve to a local entropy maximum [63]. The maximum depends, like the density cycle, on the initial preparation of the system (the initial density).

In Figure 4.1, we display the cycling of densities under the action of the Frobenius-Perron operator for the hat map which is asymptotically periodic in certain parameter ranges.

The most intriguing property of asymptotically periodic systems is illustrated by the following *Gedanken* experiment. Suppose the initial preparation of a given system is described by a uniform distribution over the entire phase space. As the density evolves in time, its support splits into r disjoint sets. Asymptotically, the system is to be found in one of r

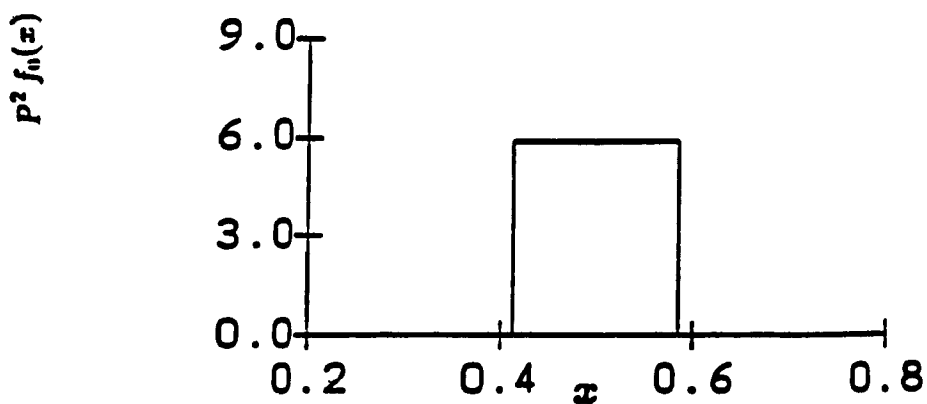
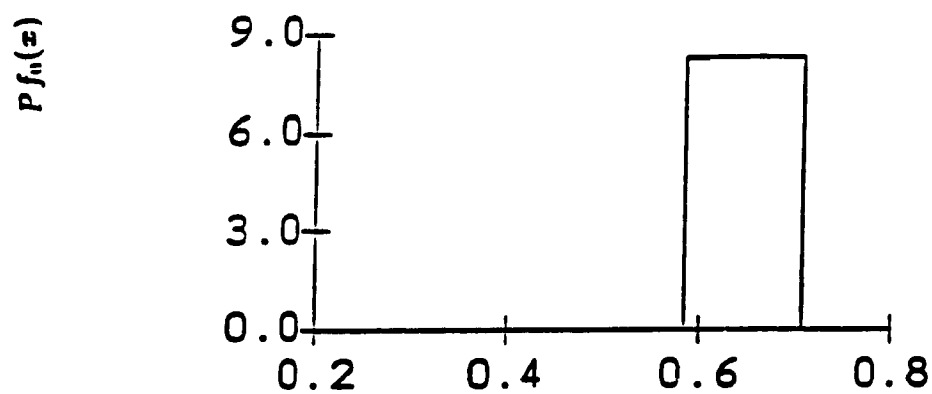
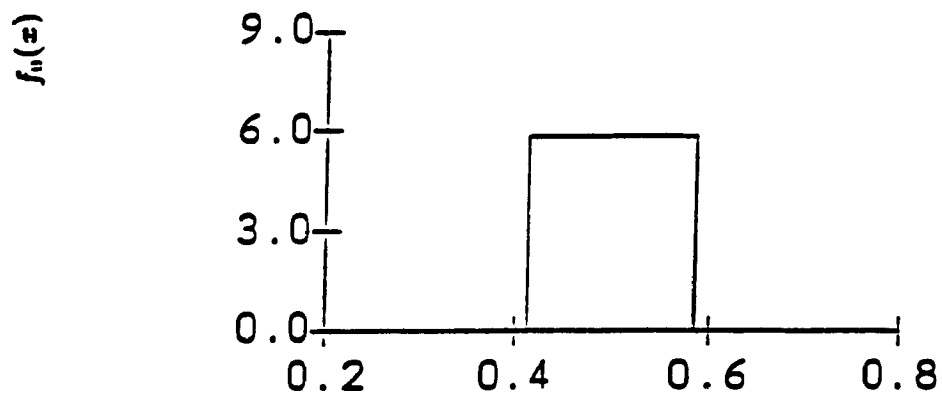


Figure 4.1: The evolution of densities under the action of the asymptotically periodic Frobenius-Perron operator P for the hat map when $a = 2^{1/2}$. The initial density $f_0(x)$ is plotted on the top graph. There are no transients in this case. The cycle shown here is of period 2

distinct states, or in a linear combination of these states, each weighted by the function g_i . Thus, asymptotic periodicity offers one possible framework within which to investigate spontaneous quantization in discrete time systems.

There is no formal analog of asymptotic periodicity for continuous time systems so the applications to physical models, usually framed as differential equations, cannot be discussed at this point. However, the combination of results from ergodic theory and insights from dynamical systems theory has been instrumental in the classification of nonequilibrium thermodynamic behavior [51], and it can be expected that the tools of nonlinear dynamics will prove useful in the discovery of dynamical principles underlying quantum mechanical behavior (if such principles exist).

4.2 Ensembles of D.D.E's: Numerical insight.

It is clear from the considerations of the preceding section that a coherent analytic treatment of ensembles of delay differential equations should make use of the tools of probability theory in function spaces, since the distributions to be associated with the thermodynamic states of D.D.E's should be distributions of functions. In Chapter 5, we introduce some techniques to proceed with such an analysis. In this section we focus attention on the numerical investigation of the dynamics of large collections of delay equations.

We restrict ourselves to a particular D.D.E, which is the singular perturbation limit of the hat map (4.8) presented in Section 4.1.1

$$\epsilon \frac{dx}{dt} = -x(t) + \begin{cases} ax_\tau & \text{if } x_\tau \in [0, \frac{1}{2}] \\ a(1-x_\tau) & \text{if } x_\tau \in (\frac{1}{2}, 1], \end{cases} \quad x_\tau = x(t-\tau). \quad (4.16)$$

The rationale for studying this (nonintegrable) D.D.E, rather than the paradigm system (2.3) considered in the previous chapters, is that there is a formal connection between this system and a well understood discrete time system: the hat map. We noted in the previous section that a particularly interesting type of density evolution consisted in an asymptotic cycling of the densities in phase space under the action of the Frobenius-Perron operator (see Section 4.2, equation (4.8)). If the limit $\epsilon \rightarrow 0$ is taken in (4.16), then we obtain the

difference equation

$$x(t) = \begin{cases} ax(t - \tau) & \text{if } x(t - \tau) \in [0, \frac{1}{2}] \\ a(1 - x(t - \tau)) & \text{if } x(t - \tau) \in (\frac{1}{2}, 1]. \end{cases} \quad (4.17)$$

The results of Ivanov and Sharkovskii (Section 1.5.1) demonstrate that the dynamics of the difference equation are accurately described by the dynamics of the corresponding one dimensional map

$$x_{n+1} = \begin{cases} ax_n & \text{if } x_n \in [0, \frac{1}{2}] \\ a(1 - x_n) & \text{if } x_n \in (\frac{1}{2}, 1]. \end{cases} \quad (4.18)$$

The hat map was studied extensively by Provatas [63, 65] who proved several interesting results concerning its statistical behavior. We summarize these results in the following section.

4.2.1 The hat map.

Consider the generalized map (4.8), and its Frobenius-Perron operator (4.9). From Lasota and Mackey [40], we know that the Frobenius-Perron operator for a map $F: [0, 1] \rightarrow [0, 1]$ is asymptotically periodic if $F(x)$ satisfies the following (sufficient) conditions:

(1) There exists a partition $0 = b_0 < b_1 < \dots < b_m = 1$ of $[0, 1]$ such that for each integer $i = 1, \dots, m$ the restriction of F to $[b_{i-1}, b_i]$ is a C^2 function.

(2) $|F'(x)| \geq \vartheta > 1$, $x \neq b_i$, $i = 0, \dots, m$ where ϑ denotes the right derivative of $F(x)$ at $x = 0$.

(3) There exists a real, finite constant c such that

$$\frac{|F''(x)|}{|F'(x)|^2} \leq c, \quad x \neq b_i, i = 0, 1, \dots, m.$$

For $a \in (1, 2]$, and for the partition $b_0 = 0 < b_1 = 1/2 < b_2 = 1$ the hat map satisfies these conditions. Thus the hat map is asymptotically periodic and the Frobenius-Perron operator can be represented with the spectral decomposition of Theorem 4.1.

One remarkable result relates the value of the parameter a to the period of the density cycle. Specifically, if $a \in (a_{n+1}, a_n]$, where $a_n = 2^{2^n}$, then the period of the density cycle is 2^n . In other words, in these parameter ranges, $\mathcal{P}^t f(x) = \mathcal{P}^{t+2^n} f(x)$. It is also straight forward to show that the hat map is ergodic.

In the next section, we make use of ergodicity in the hat map to construct densities along trajectories. We would like to determine to what extent the properties of the map carry over to the delay differential equation.

4.2.2 Densities and D.D.E's.

The phase space of (4.16) is the normed function space $C([0, \tau])$ [see the notation above Definition 1.2 for a precise definition. Here the functions are not bounded so that $B = (-\infty, +\infty)$ is omitted]. Thus, the phase space density functions associated with the thermodynamic state of a D.D.E. are really *phase space density functionals*. Techniques to analytically investigate the behavior of these functionals are presented in Chapter 5. In this section, we focus attention on possible ways to obtain numerical insight into the dynamics of these functionals. Several of the constructions presented in the next sections are motivated by the observation that the hat map is ergodic.

Roughly speaking, a transformation is said to be ergodic if its invariant sets are trivial. This implies that a trajectory will visit all points in the phase space, and that space averages can be replaced with time averages. An exact definition of ergodicity is given in [40]. For this reason, we begin our investigation of densities for delay differential equations by the construction of time averages to approximate space averages.

a) Densities along trajectories.

The first natural construction of densities in delay differential equations is to project the solution $x(t)$ onto the x -axis. Figures 4.2-4.4 display such projections for numerical solutions of equation (4.16) with constant initial functions. The only parameter being changed is a and $\varepsilon = 0.1$ throughout. Recall that there are windows in the interval $a \in (1, 2]$ such that the density cycles for the hat map have period 2^n when a belongs to the n^{th} window $w_n = [2^{\frac{1}{2^{n+1}}}, 2^{\frac{1}{2^n}}]$. The number of peaks in the densities for the D.D.E equals the period of the cycle for the map at the same parameter values, up to a shift depending on ε . Qualitatively, the effect of the singular perturbation procedure is to alter the w_n windows. As ε is increased, the behavior of the D.D.E deviates from that of the map.

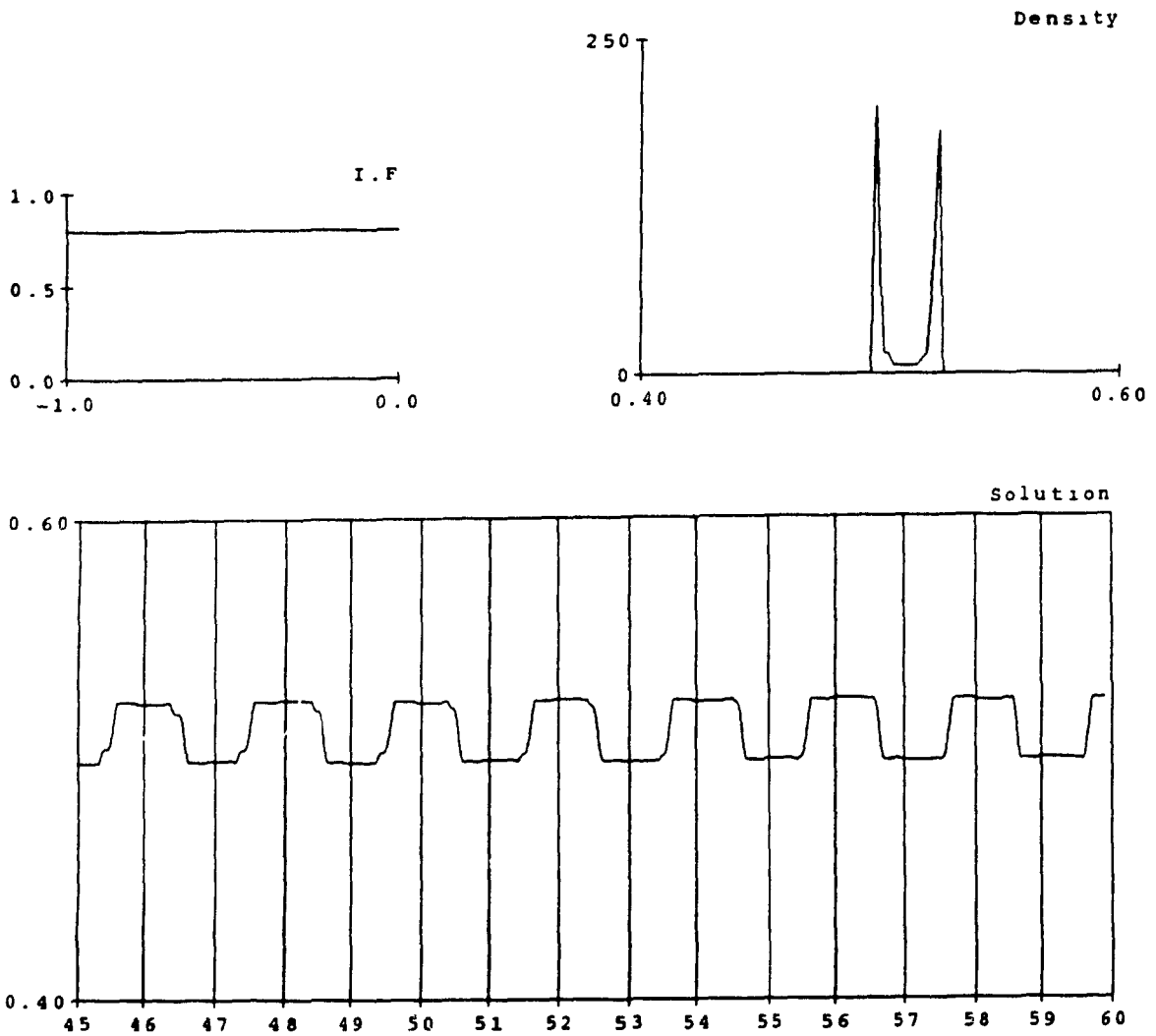


Figure 4.2: Solution of equation (4.16) when $\tau = 3$, $\varepsilon = 0.1$, $a = 1.28$. For the same value of a , the cycle of densities in the hat map is 2. The top right graph is the projection of the solution along the x axis.

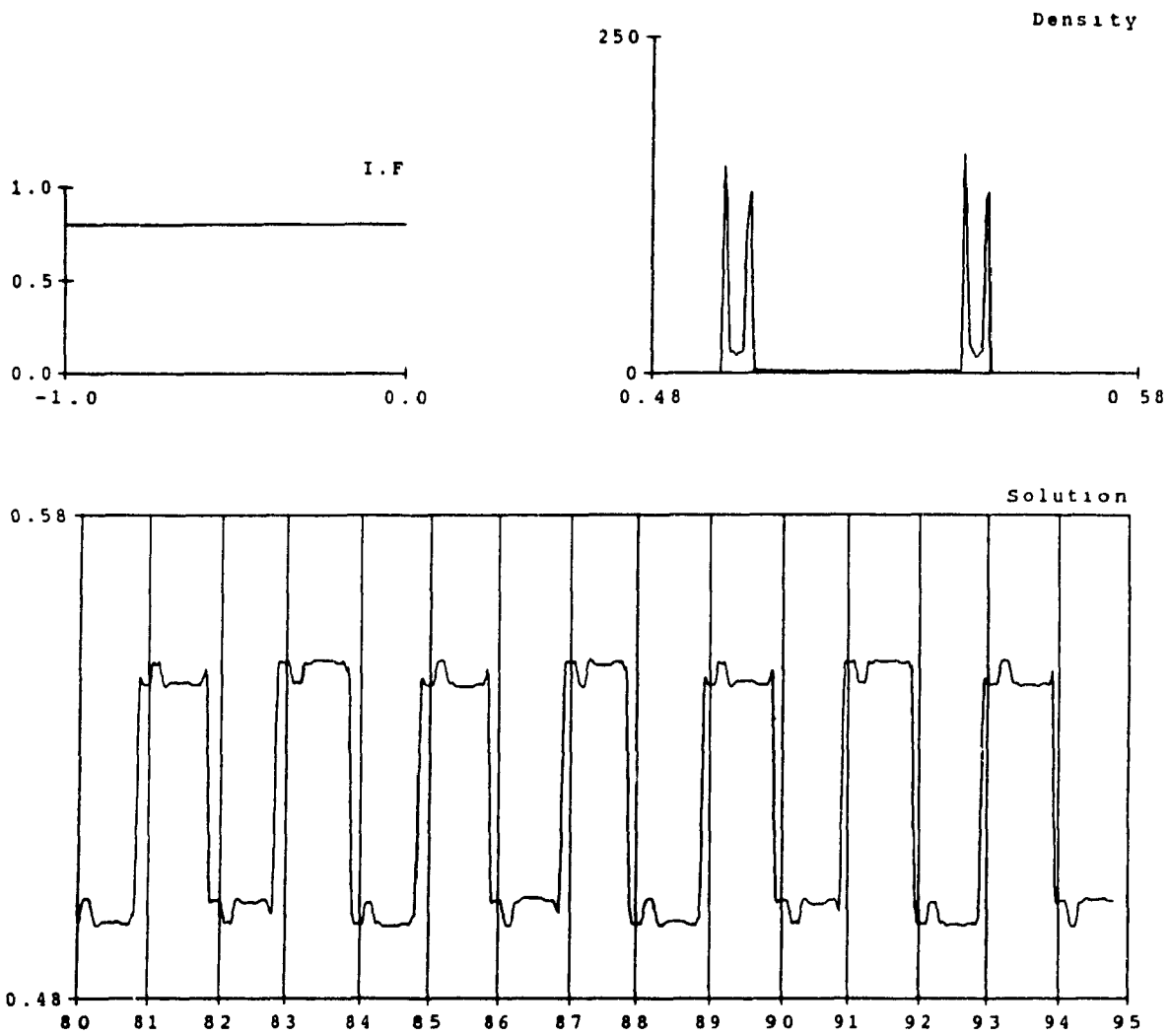


Figure 4.3: Solution of equation (4.16) when $\tau = 3$, $\varepsilon = 0.1$, $a = 1.10$. For the same value of a , the cycle of densities in the hat map is 4.

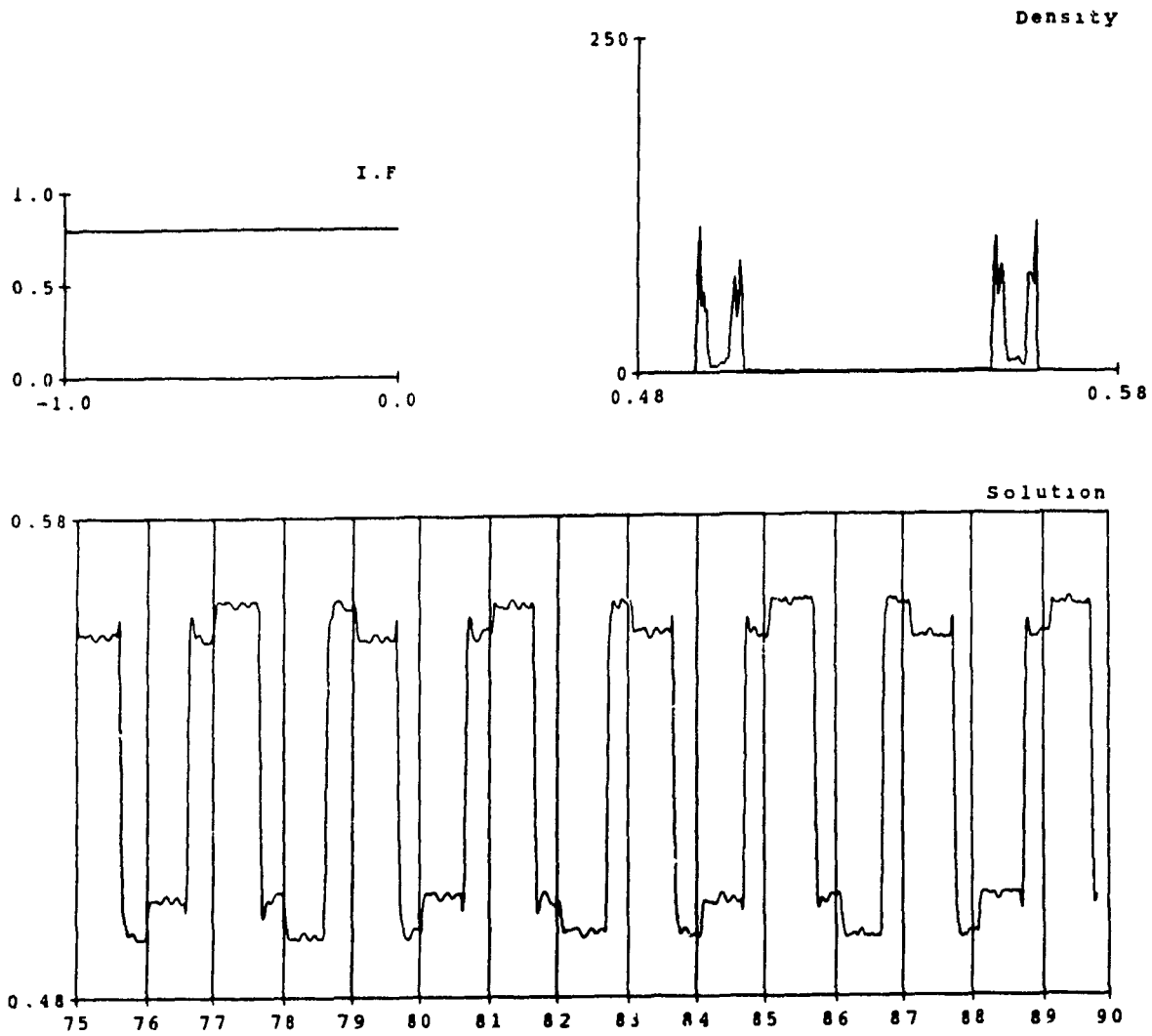


Figure 4.4: Solution of equation (4.16) when $\tau = 1$, $\epsilon = 0.1$, $a = 1.003$. For the same value of a , the cycle of densities in the hat map is 8.

b) Densities for a "sliding" segment of solution.

The densities obtained by projecting the solution onto the x axis are time independent and there is no hope to reproduce any cycling of the densities in the D.D.E. Therefore, the next logical construction of D.D.E densities comes from the observation that the dynamical system S_t corresponding to equation (4.16) acts on the elements of the normed function space $C([0, \tau])$, and transforms a function defined on $[-\tau, 0]$ into a function defined on $[t - \tau, t]$. In other words it is relevant to look at the evolution of a density defined as *the projection on the x axis of a segment of the solution $x(t)$ defined on the time interval $t \in [t^* - \tau, t^*]$ as t^* increases*. [An element of C -i.e. a segment of $x(t)$ of length τ - will be referred to as a *buffer* from now on]. Figures 4.5-4.6 display such projections. Cycling is observed, and the number of different supports of the densities is related to the period of the density cycle for the map. Again, the value of ϵ determines the degree of similarity between the map and the differential equation.

c) Average of an ensemble of buffers.

A generalization of the approach discussed in the previous section consists in following the evolution of n buffers generated by n initial functions. More specifically, we look at the evolution of a function defined as the average of the n buffers. The results of such a construction are somewhat puzzling. They are displayed in Figures 4.7 obtained with a given value of a corresponding to a period 2 cycling in the hat map. The number of peaks in the densities again corresponds to the period of the density cycle in the map, but it is not yet understood how to establish a clear connection between this evolution of averages and the evolution of densities in the discrete time case. A detailed investigation is extremely time consuming since it involves the numerical integration of large numbers (at least 10^5) of D.D.E's, and it could not be carried out for this thesis. The results presented in this and the following section merely indicate the direction for further numerical investigation, and they highlight the need for a theoretical framework to investigate D.D.E's from statistical point of view. This framework is presented in Chapter 5.

d) Sampling ensembles of D.D.E's

Suppose that one is interested in studying the evolution of a collection of n noninteracting particles, some property of which is governed by a D.D.E. If this property is a measurable quantity (like velocity, electric charge *etc.*) monitored experimentally, it is sampled throughout the system at discrete times. We label the quantity we are monitoring by $Q_i(t)$ for the i^{th} particle. In the limit of infinitely many particles (the thermodynamic limit, in which the index i becomes continuous), the result of a measurement on our "gas" of D.D.E's at time t^* will be a function $Q^{t^*}(i)$. In Figures 4.8 – 4.9, we display such functions as t^* varies. Here, again a cycling is observed. This cycling indicates that the initial functions did not belong to one single basin of attraction. If they did, then all the initial functions would have generated the same asymptotic solution up to a phase shift. In that case, regardless of the instant t^* at which the sampling is done, the function $Q^{t^*}(i)$ is a projection on the x axis of all the possible phases of $x(t)$ and therefore $Q^{t^*}(i)$ would be invariant in time. However, the information content of the Q -cycles concerning the basins of attraction has not been studied, again for lack of computing time, and our observations should be taken as conjectures rather than affirmations.

Figure 4.5: *Densities of a buffer of length τ as it slides along a solution of (4.16). The parameters are the same as those in Figure 4.2. The 20 densities are obtained between $t = 15\tau$ and $t = 17\tau$ at equally spaced intervals. Observe the smooth cycling as the densities visit the two supports of the projection of Figure 4.2. The difference in the appearance of the density is due to the change in the number of bins used to produce the two graphs. The same remark holds for the discrepancy between Figures 4.6 and 4.3*

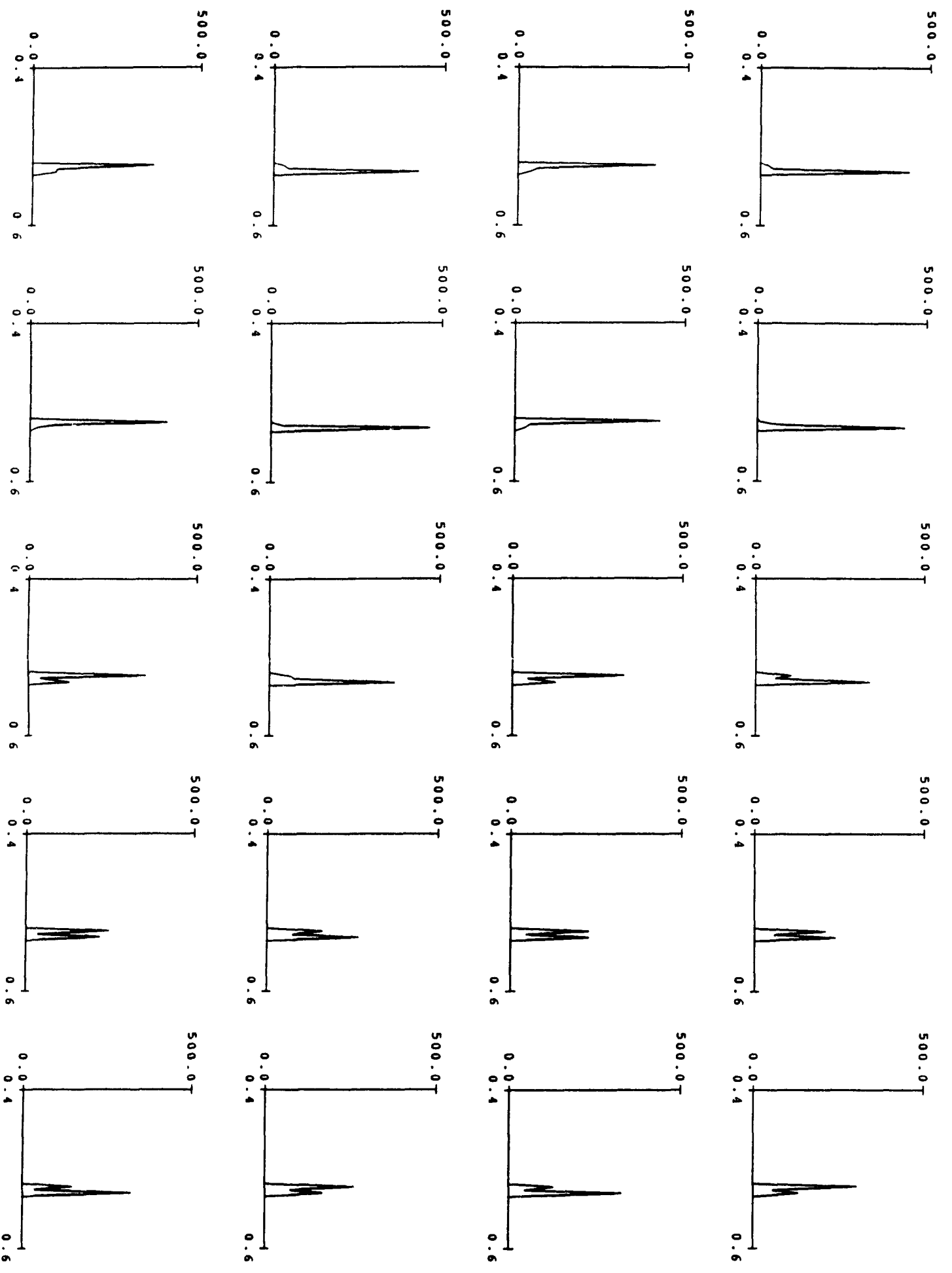


Figure 5

Figure 4.6: *Densities of a buffer of length τ as it slides along a solution of (4.16). The parameters are the same as those in Figure 4.3. The 20 densities are obtained between $t = 15\tau$ and $t = 17\tau$ at equally spaced intervals. Observe the smooth cycling as the densities visit the four supports of the projection of Figure 4.3.*

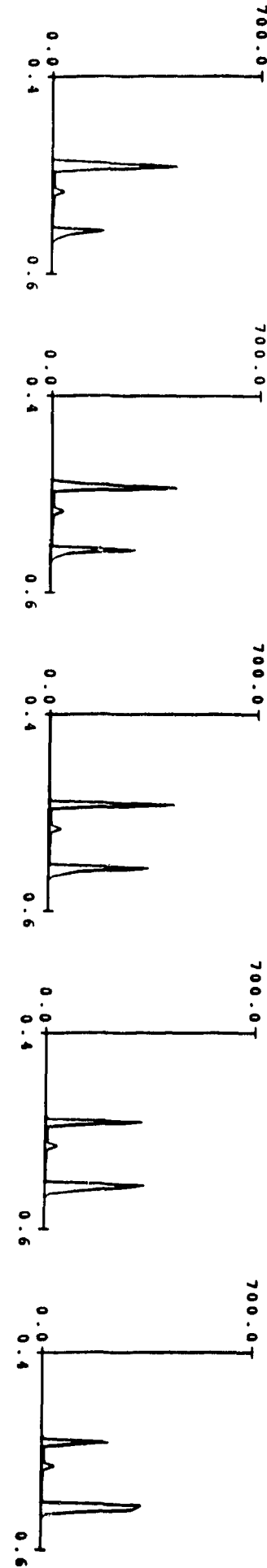
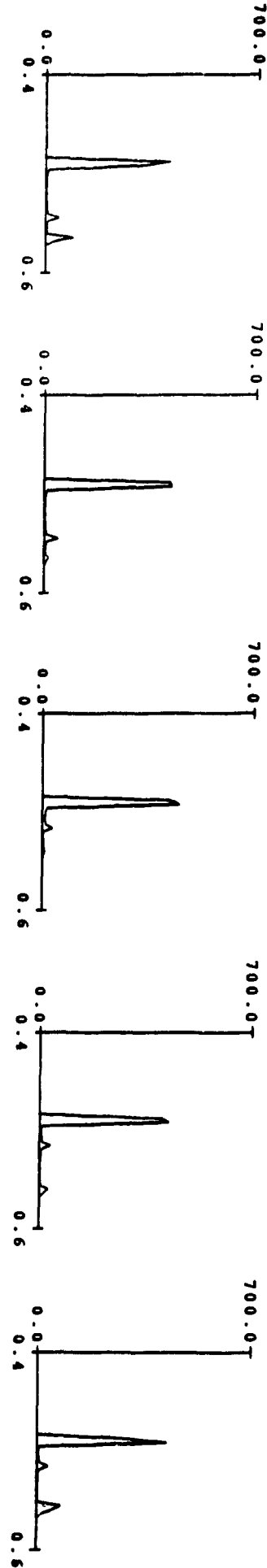
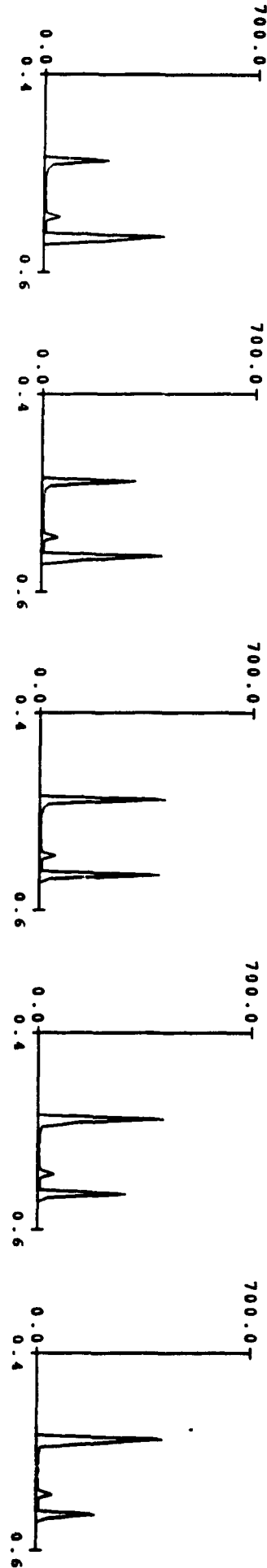
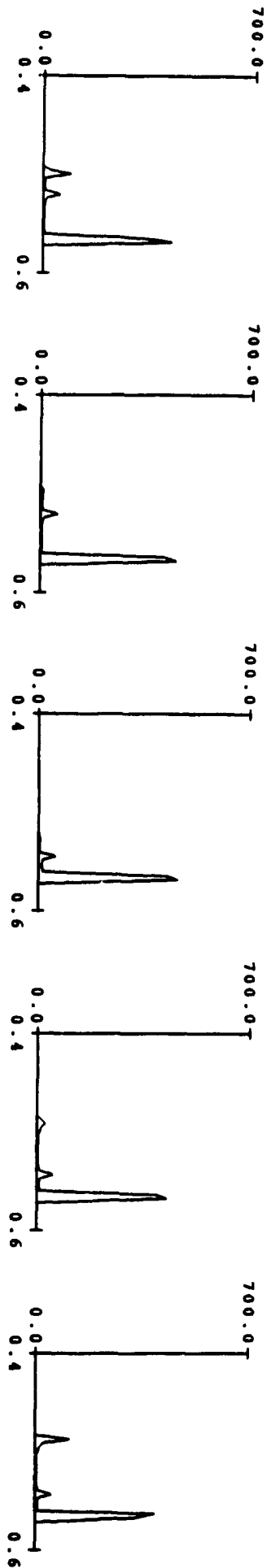


Figure 4.7: Time evolution of the average of an ensemble of buffers sliding along 10^3 solutions of (4.16) generated by 10^3 constant initial functions distributed uniformly over the interval $(0, 1)$. The parameters are those of Figure 4.2.

Figure 4.8: Temporal evolution of the distribution of points $x(t^*)$ generated by 10^3 constant initial functions distributed uniformly over the interval $(0,1)$, for 20 values of t^* at equally spaced intervals between $t = 15\tau$ and $t = 20\tau$. The parameters are the same as in Figure 4.2. This figure illustrates the sampling procedure discussed in Section 4.2.2d. Observe the cycle of period approximately τ .

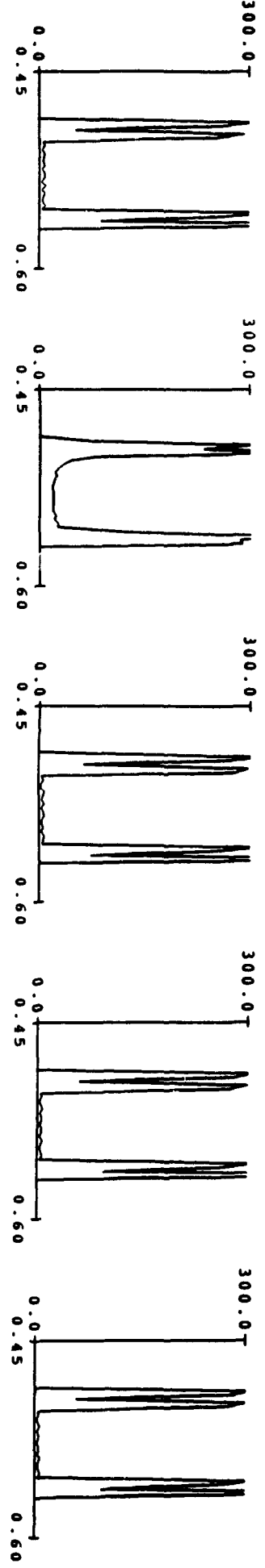
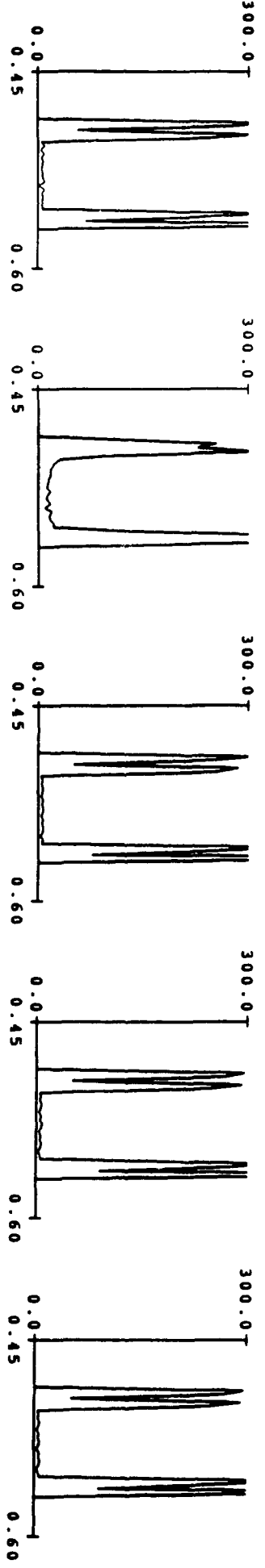
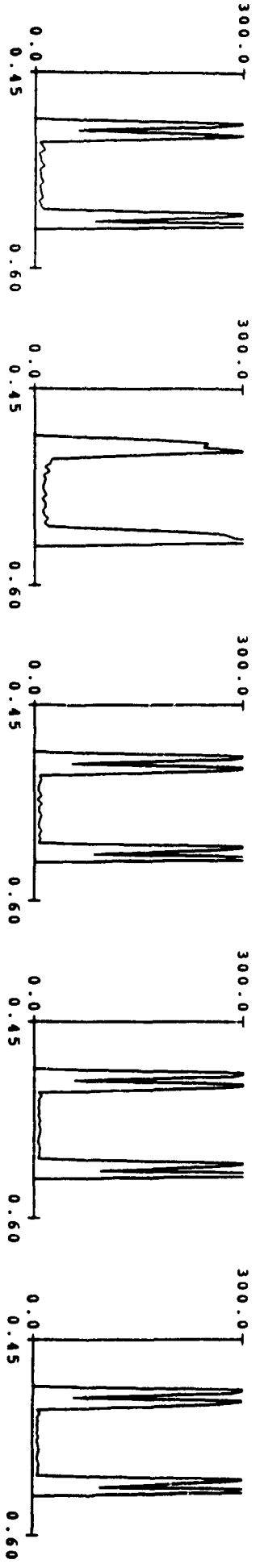
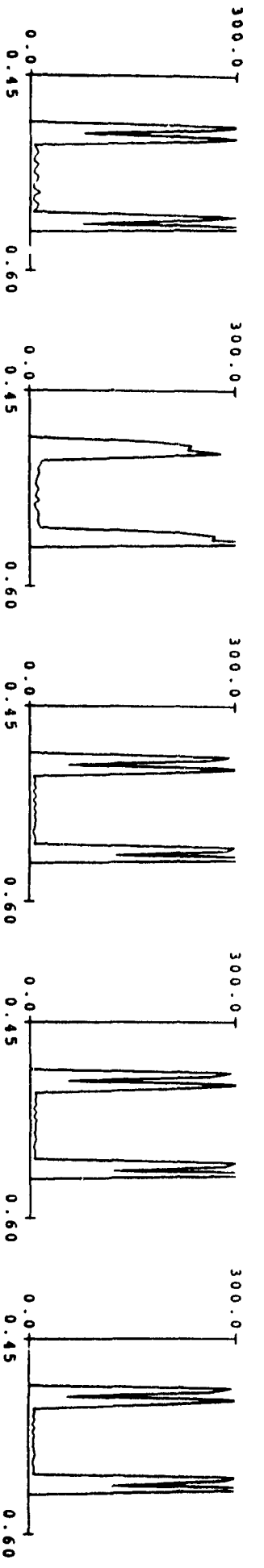
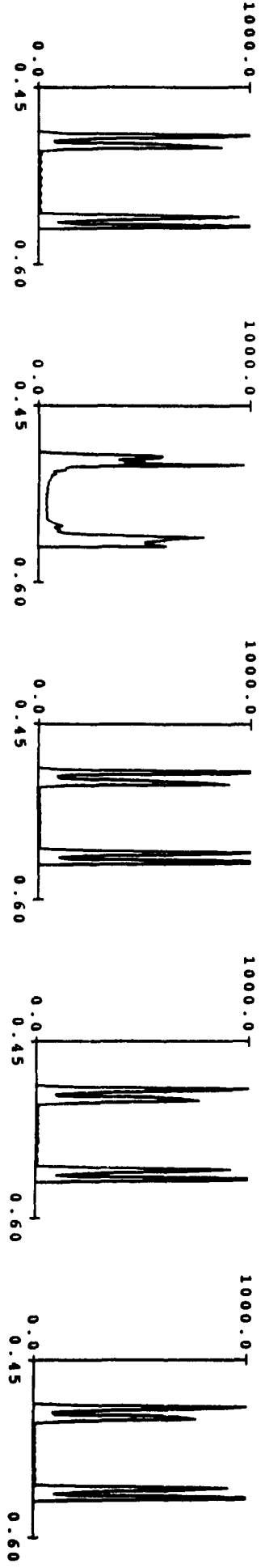
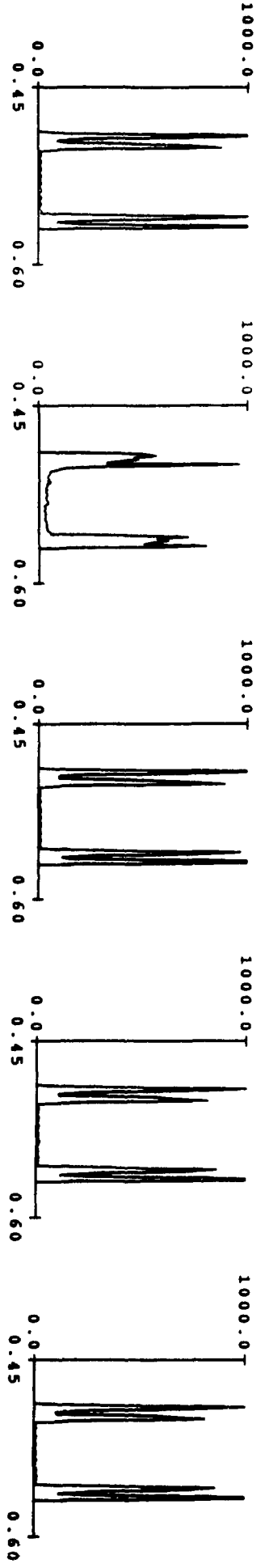
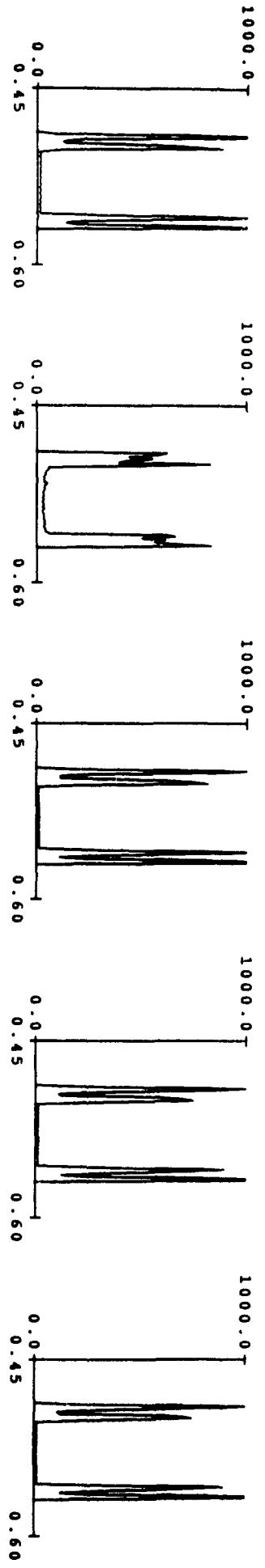
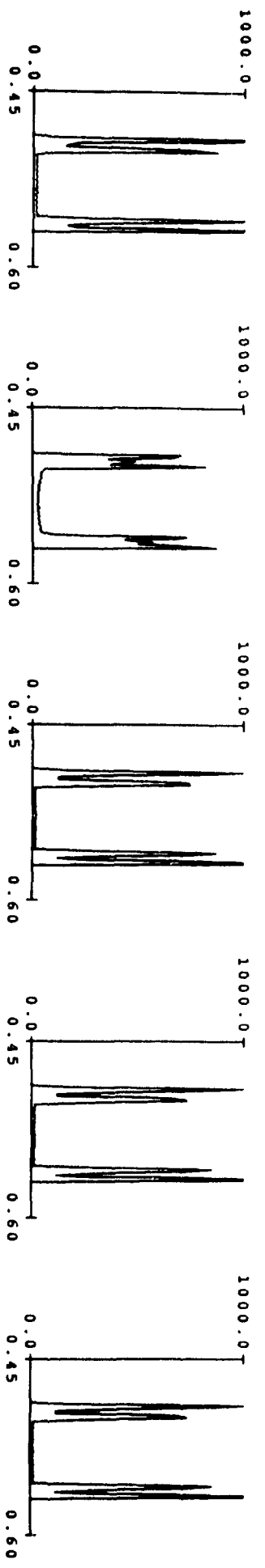


Figure 4.9: *Temporal evolution of the distribution of points $x(t^*)$ generated by 10^4 initial functions distributed uniformly over the interval $(0,1)$, for 20 values of t^* equally spaced between $t = 15\tau$ and $t = 20\tau$. Again, the parameters are those of Figure 4.2. This Figure illustrates the sampling procedure discussed in Section 4.2.2.d.*



4.3 Analytic expression of the density for an integrable D.D.E.

In this section we present a technique to derive the analytic expression for the density constructed along the trajectory of a piecewise integrable dynamical system. We illustrate the procedure for the paradigm D.D.E of Section 1.5.2 and with a set of coupled O.D.E's giving the rule of evolution of a simple neural network studied by Lewis *et al.* [42].

The equation we consider is

$$\frac{dx}{dt} = -\alpha x(t) + F(x(t - \tau)) \quad (4.19)$$

where

$$F(\xi) = \begin{cases} c & \text{if } \xi \in [1, b] \\ 0 & \text{otherwise.} \end{cases} \quad (4.20)$$

The solution $x(t)$ of equation (4.19) with nonlinearity (4.20) is:

$$x(t - t_0) = \begin{cases} (x(t_0) - \gamma)e^{-\alpha(t-t_0)+\gamma} & \text{if } x(t - t_0) \in [1, b] \\ x(t - t_0)e^{-\alpha(t-t_0)} & \text{otherwise.} \end{cases} \quad (4.21)$$

where $\gamma = c/\alpha$ is the upper asymptote. As mentioned in Section 1.5.2 the solution is composed of a sequence of piecewise exponential segments evolving towards an asymptote which is either γ or 0 depending on the value of the delayed variable $x(t - \tau)$. To simplify the following analysis it is useful to classify all solutions $x(t)$ according to the sign of the slope of the first piecewise exponential segment of the solution:

If the first extremum of $x(t)$, $t > 0$ is a maximum (*i.e.* the slope of the first segment is positive), then we say that $x(t)$ is an S^+ solution.

If the first extremum of $x(t)$, $t > 0$ is a minimum, then we say that $x(t)$ is an S^- solution.

Unless otherwise specified it is assumed from now on that $x(t)$ is an S^+ solution. The analysis presented holds for S^- solutions, but the notation is greatly simplified by introducing this classification of solutions. We explain at the end of the section how the results should be modified in case $x(t)$ is S^- .

Definitions

* T_k is the time at which $x(t)$ crosses either one of the thresholds 1 or b for the k^{th} time.

* E_k is the k^{th} extremum of $x(t)$. The time at which the k^{th} extremum occurs is $T_k + \tau$.

* We label each piecewise exponential segment of $x(t)$, $x_k(t_k)$, with k being the index of the extremum ending the segment. For all k $x_k(t_k)$ is defined on $[T_{k-1}, T_k]$.

With the above definitions we can now rewrite the solution (4.21) in a more compact form for all $t \in [T_{k-1}, T_k]$,

$$x_k(t_k) = E_{k-1} e^{-\alpha(t_k - (T_{k-1} + \tau))} + \gamma(k \bmod 2)(1 - e^{-\alpha(t_k - (T_{k-1} + \tau))}). \quad (4.22)$$

Hence the solution $x(t)$ defined for all $t > 0$ can be written as the sum of the successive $x^k(t)$'s each defined on a finite time interval. Their supports (in time) are disjoint. We write

$$x(t) = \sum_{k=1}^{\infty} x_k(t_k). \quad (4.23)$$

Differentiate equation (4.23):

$$\frac{dx}{dt} = \sum_{k=1}^{\infty} \frac{dx_k}{dt_k}. \quad (4.24)$$

Remember that at any point in time, only one $x_k(t_k)$ is defined, and therefore it will be the only contributor to the sum. Hence we can write

$$\left(\frac{dx}{dt}\right)^{-1} = \sum_{k=1}^{\infty} \left(\frac{dx_k}{dt_k}\right)^{-1}. \quad (4.25)$$

Inverting relation (4.22) to obtain $t_k \in [T_{k-1} + \tau, t_k + \tau]$ explicitly, we get

$$t_k = -\frac{1}{\alpha} \log \left(\frac{x_k - \gamma(k \bmod 2)}{E_{k-1} - \gamma(k \bmod 2)} \right) + T_{k-1} + \tau. \quad (4.26)$$

Differentiating equation (4.22) with respect to t_k yields

$$\frac{dx_k(t_k)}{dt_k} = -\alpha E_{k-1} \left(e^{-\alpha(t_k - (T_{k-1} + \tau))} + \alpha \gamma(k \bmod 2) e^{-\alpha(t_k - (T_{k-1} + \tau))} \right). \quad (4.27)$$

Substituting (4.26) into (4.27) we finally get

$$\frac{dx_k(t_k)}{dt_k} = -\alpha(x_k(t_k) - \gamma(k \bmod 2)). \quad (4.28)$$

Therefore, we can write (4.25)

$$\left(\frac{dx(t)}{dt}\right)^{-1} = -\sum_{k=1}^{\infty} \frac{1}{\alpha(x_k(t_k) - \gamma(k \bmod 2))}. \quad (4.29)$$

In order to eliminate the cumbersome labeling of the segments of solutions $x_k(t_k)$ in (4.29), we have to multiply the equation by a term such that the time domain $\{TD_k\} = [T_{k-1} + \tau, T_k + \tau]$ on which each t_k is defined is mapped properly into a corresponding x -domain of definition $\{XD_k\}$. This can be done by noting that the time interval $[T_{k-1} + \tau, T_k + \tau]$ corresponds to the x -interval $[\min(E_{k-1}, E_k), \max(E_{k-1}, E_k)]$ if $x(t)$ satisfies (4.19) with (4.20). [Remember that $E_k > E_{k-1}$ only if the k^{th} segment of solution is decreasing.]

Let us now define the set counting function

$$1_{[a,b]}(x) = \begin{cases} 1 & \text{if } x \in [a,b] \\ 0 & \text{otherwise.} \end{cases} \quad (4.30)$$

Using (4.30), we can rewrite (4.29) for any S^+ solution $x(t)$:

$$\left(\frac{dx(t)}{dt}\right)^{-1} = \sum_{k=1}^{\infty} \frac{1}{\alpha(x(t) - \gamma(k \bmod 2))} \times \left[1_{[E_{k-1}, E_k]}(x)(k \bmod 2) + 1_{[E_k, E_{k-1}]}(x)(1 - k \bmod 2) \right]. \quad (4.31)$$

We can now compute the density $f(x)$ along the trajectory $x(t)$. To do so, note that

$$\int_A f(x) dx = \int_B dt, \quad (4.32)$$

where A is the x -interval visited by $x(t)$ when t belongs to B . Then, we have the following expression for the density:

$$f(x) \propto \left(\frac{dx}{dt}\right)^{-1}, \quad (4.33)$$

along with the normalization condition

$$\int_A f(x) dx = 1. \quad (4.34)$$

As a result, using (4.33) and (4.31), we obtain the analytic expression for the density along a trajectory of the delay differential equation (4.19) with (4.20), from E_k to E_{k+N}

$$f(x) = \sum_{k=1}^N -\alpha(x - \gamma(k \bmod 2))^{-1} I_k \left[1_{[E_{k-1}, E_k]}(x) k \bmod 2 + (1 - k \bmod 2) 1_{[E_k, E_{k-1}]}(x) \right] \quad (4.35)$$

where $T_{k+N} - T_k = P$ and I_k is the normalization factor

$$I_k = \left(\frac{T_k - T_{k-1}}{P} \right).$$

Note that (4.35) is valid whether the segment of solution is the period or not. If the solution is not periodic, and the segment chosen for the analysis contains N extrema, the normalization condition (4.34) will not be satisfied but (4.35) will nevertheless give a qualitative idea of the form of the density.

Were the initial condition chosen so that $x(t)$ were S^- (i.e. the slope of the first segment being negative) the above expression would still be valid providing $k \bmod 2$ were replaced by $(1 - k \bmod 2)$.

Numerically $f(x)$ can be computed in a straightforward way if one knows the sequence of crossing times, because the modulo operator can be replaced by conditional if statements.

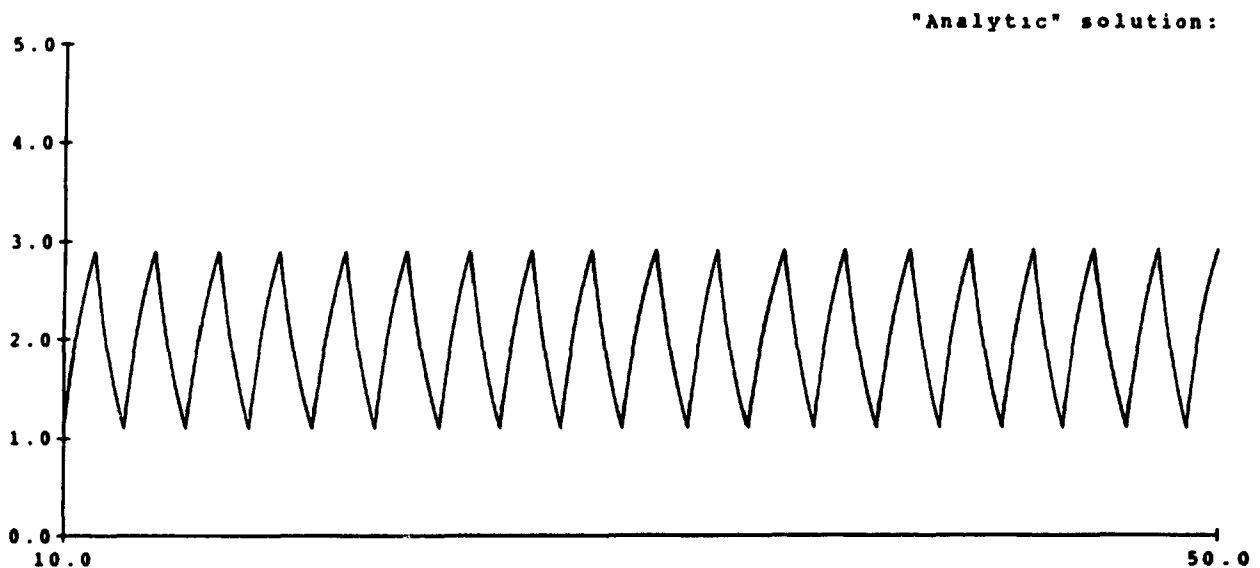
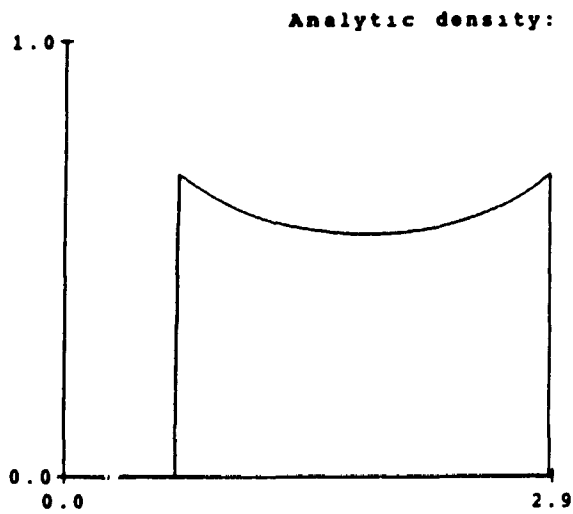


Figure 4.10: Analytic solution of equation (2.3) for $\tau = 1$, $\theta_1 = 1$, $\theta_2 = 2$, $\alpha = 0.6$, and $c = 2.4$. The density was obtained from equation (4.35).

4.3.1 Application to a neural network.

It should be clear that equation (4.35) is a valid expression for the density along a trajectory no matter what the dynamical system generating $x(t)$. We explain here how formula (4.35) can be generalized for an N -dimensional set of O.D.E's describing the dynamics of a simple neural network consisting of N interacting particles, examined by Lewis and Glass as a paradigm for a class of complex biological networks [42].

The set of O.D.E's is

$$\frac{dx_i}{dt} = -x_i + \sum_{j=1}^N w_{ij} G_j(x_j) - \rho_i, \quad i = 1, \dots, N, \quad (4.36)$$

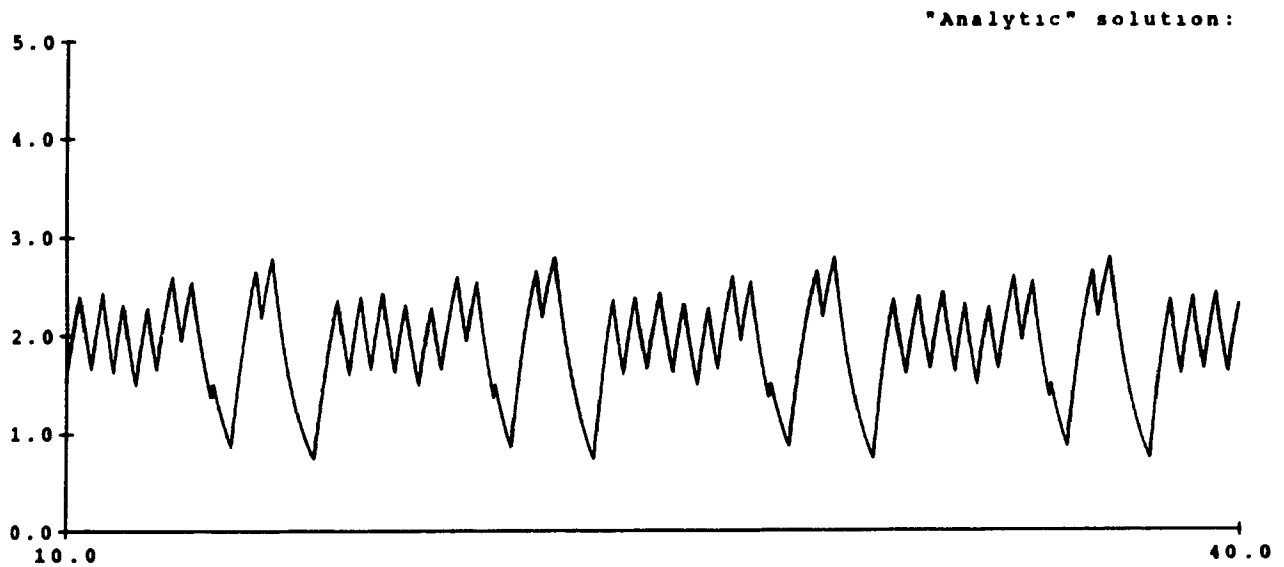
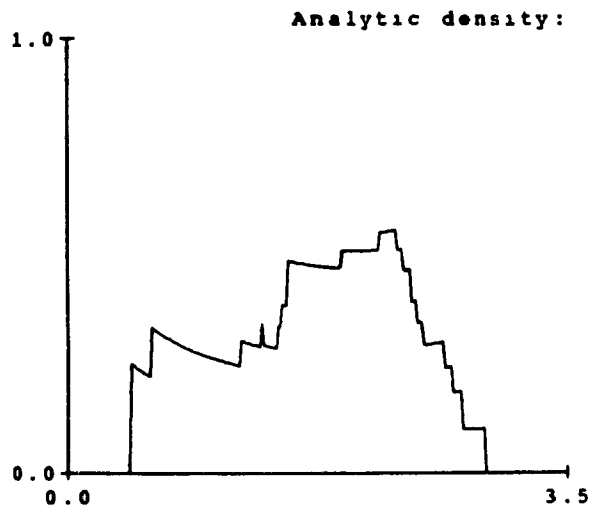


Figure 4.11: Analytic solution of equation (2.3) for $\tau = 1$, $\theta_1 = 1$, $\theta_2 = 2$, $\alpha = 1$, and $c = 4$. The density was obtained from equation (4.35).

where G is a function describing the response of each element to an input, ρ_i is a parameter interpreted as the response threshold, and w_{ij} gives the weight of the input of element j to element i . Lewis and Glass [42] assumed that there is no self input (*i.e.* $w_{ii} \equiv 0$). Usually, G is defined as a nonlinear monotonically increasing function. Lewis and Glass considered G to be the limit of infinite slope of the sigmoidal function, in which the functions G_j are piecewise constant with a single discontinuity at $x = 0$, so that

$$G_j(x_j) = \begin{cases} a_j & \text{if } x_j < 0 \\ b_j & \text{if } x_j \geq 0 \end{cases} \quad (4.37)$$

with the condition

$$\sum_{j=1}^N w_{ij} G_j(x_j) \neq \rho_i \quad i = 1, \dots, N. \quad (4.38)$$

System (4.36) can be integrated analytically, and the solution is piecewise exponential:

$$x_i(t) = \gamma' + (x_i(0) - \gamma')e^{-t} \quad (4.39)$$

where the constant γ' (the asymptote) is given by

$$\gamma' = \begin{cases} \sum_{j=p}^q w_{ij} a_j - \rho_i & \text{if } x_j < 0 \\ \sum_{j=p}^q w_{ij} b_j - \rho_i & \text{if } x_j \geq 0, \end{cases} \quad j = p, \dots, q, \quad 1 \leq p < q \leq N. \quad (4.40)$$

Labeling the times at which each x_i crosses 0 carefully, it is straightforward to construct the analytic density along an N dimensional trajectory for this system [42]. The use of such a density facilitates a simple classification of the network's dynamics.

4.4 Summary.

The purpose of this chapter is to illustrate the insight that can be gained by studying the statistical evolution of D.D.E's rather than by simply investigating single solution behavior.

In Section 4.1 we review some of the techniques used to characterize the probabilistic properties of finite dimensional dynamical systems.

Section 4.2 is a numerical investigation of the dynamics of densities constructed along the trajectories of a delay differential equation which is the singular perturbation of a well studied one dimensional map known as the "hat map". The behavior of solutions generated

by ensembles of initial functions is discussed along with the effect of sampling a "gas" of delay equations.

In Section 4.3, we present a technique to obtain the analytic expression for the density along the trajectory of an integrable D.D.E. The technique is also applied to a simple neural network framed as an N -dimensional set of O.D.E's.

Chapter 5

PROBABILISTIC DESCRIPTION OF DELAYED FEEDBACK SYSTEMS.

As we pointed out in the previous chapter, from a modeling perspective it may be crucial to understand the statistical behavior of deterministic systems. Modern statistical mechanics is based on this apparently contradictory observation. This chapter is motivated by the absence of a theoretical framework with which to treat delayed dynamics statistically.

We present a way to statistically investigate the dynamics of delay differential equations extending techniques introduced by E. Hopf [26] to study the statistics of turbulent flows generated by the Navier-Stokes equation. The approach is illustrated with a class of delay differential equations (with discrete delay) introduced in Section 1.5.

The central idea is based on the observation that these equations can be viewed as functional operators acting the elements of the function space $\mathcal{C}([0, 1])$ (defined in Chapter 1) since at time $t > 0$, the D.D.E has transformed an initial function defined everywhere on $[-1, 0]$ into a function defined everywhere on $[t - 1, t]$.

As the formalism used throughout this chapter is that of probability theory in function spaces, there is a strong analogy between the presentation here, the quantum theory of fields (QFT), and the functional description of fluid mechanics. In particular perturbation theory, and the graphical methods used in QFT and in the study of stochastic wave propagation are applicable to the study of delay differential equations.

In this chapter, the generating functional \mathcal{Z} for n -point correlation functions is first introduced in Section 5.1. The quantity \mathcal{Z} allows one to directly obtain all the n -point correlation functions via functional differentiation.

The application of this probabilistic concept to the statistical study of D.D.E's is then developed in Section 5.2. A functional differential equation for \mathcal{Z} is obtained from the original delay equation.

The hierarchy equations for the first and second order moments are obtained explicitly in Section 5.3 and the problem of obtaining a moment of order k is reduced to solving successive hyperbolic partial differential equations and ordinary differential equations. This simplification of the problem is possible when the generating functional can be expanded in a power series, each term of which can then be represented by a Feynman graph.

In Section 5.4 the connection with the quantum theory of fields is established. The transition amplitudes calculated with the Feynman rules used in particle physics are obtained from a functional, which is a special case of \mathcal{Z} when the dynamics are given by the field equations obtained from the principle of least action.

5.1 Introductory definitions.

The core of this chapter is the presentation of a formalism with which to study the behavior of a D.D.E from a statistical point of view. The spirit of this approach is that of classical statistical mechanics in which, since the work of Gibbs and Boltzmann, physicists have grown accustomed to dealing with densities describing the thermodynamic states of a given system. We are interested here in examining the evolution of a density of functions.

This evolution is described by a family of probability measures defined on a function space, and it is shown how this family of measures can be described by a functional differential equation. We start by introducing some concepts from measure theory and probability theory.

5.1.1 σ -algebras, measures and measure-spaces.

An important idea used in the following sections is that a density of functions can be described by a measure defined on a function space. We start with the definition of a σ -algebra.

Definition 5.1.1: A collection \mathcal{A} of subsets of a set X is called a σ -algebra if:

- (a) When $A \in \mathcal{A}$ then $X \setminus A \in \mathcal{A}$;
- (b) Given a sequence (finite or not) $\{A_k\}$ of subsets of X , $A_k \in \mathcal{A}$, then $\bigcup_k A_k \in \mathcal{A}$,
- (c) $X \in \mathcal{A}$.

With this, we now define a measure defined on a σ -algebra.

Definition 5.1.2: A real valued function μ defined on a σ -algebra is called a measure if:

- (a) $\mu(\emptyset) = 0$
- (b) $\mu(A) \geq 0$ for all $A \in \mathcal{A}$; and
- (c) $\mu(\bigcup_k A_k) = \sum_k \mu(A_k)$ if $\{A_k\}$ is a finite or infinite sequence of pairwise disjoint subsets of \mathcal{A} , that is, $A_i \cap A_j = \emptyset$ for $i \neq j$.

Finally, we have the concept of a measure space.

Definition 5.1.3: If \mathcal{A} is a σ -algebra of subsets of X and if μ is a measure on \mathcal{A} then, the triple (X, \mathcal{A}, μ) is called a measure space. The sets belonging to \mathcal{A} are called measurable sets because, for them, the measure is defined.

A simple example of a measure space is the real line $X = R$ in which the σ -algebra is a partition of mutually disjoint subsets of X . If the measure μ is defined by ascribing a non-negative number to each element of \mathcal{A} , then the measure describes a piecewise constant distribution of points on the real line, each constant segment corresponding to an element of \mathcal{A} . This example illustrates the fact that a measure describes a density. The same is true when the measure space is infinite dimensional. The *Wiener measure* is an example of such a measure. It has been discussed in detail in the context of stochastic wave propagation [74, 43], and used to study a class of partial differential equations encountered in some cell population dynamics problems [40].

5.1.2 Generating functions and the functional \mathcal{Z} .

In this section, we introduce the basic tool used to derive the P.D.E's for the moments of the distribution of initial functions: the generating functional. The origin of the generating functional is most easily understood by realizing that it is the infinite dimensional analogue of the generating function.

In probability theory, the moments of all order of a given probability distribution P_ξ can be obtained from a so-called *generating function*. If we have a random vector (ξ_1, \dots, ξ_n) and a vector (v_1, \dots, v_n) , the characteristic function is (with $i^2 = -1$)

$$\begin{aligned} E \left(e^{i(v_1 \xi_1 + \dots + v_n \xi_n)} \right) &= \int_X e^{i(v_1 \xi_1 + \dots + v_n \xi_n)} P_\xi(dw), \\ &= \int_X e^{i(v, \xi)} dP_\xi, \\ &= \phi(v). \end{aligned} \tag{5.1}$$

Differentiation of $\phi(v)$ yields

$$\left. \frac{\partial \phi}{\partial v} \right|_{v=0} = i E(\xi), \tag{5.2}$$

and, in general,

$$\left. \frac{\partial^n \phi}{\partial v^n} \right|_{v=0} = i^n E(v^n). \tag{5.3}$$

In other words, differentiation of the generating function ϕ yields all the moments of the distribution P_ξ , when the vectors ξ are finite dimensional.

We now consider the case when ξ is a function f defined on an interval Δ (finite or not). Let \mathcal{C} be a function space with the topology given by the supremum norm defined in Definition 1.4. (i.e. the distance between two functions is the L^1 norm of their difference). μ is a probability measure (i.e. it is properly normalized) defined on this space and $f(r)$ is an element of \mathcal{C} . If f is defined for all $r \in \Delta$, the *characteristic functional* \mathcal{Z} of the measure μ [or the *generating functional* for the correlation functions associated with the distribution of functions $f(r)$] is defined by

$$\begin{aligned} \mathcal{Z}[J] &= \int_{\mathcal{C}} \exp \left[i \int_{\Delta} J(r) f(r) dr \right] d\mu(f) \\ &\equiv \left\langle \exp \left[i \int_{\Delta} J(r) f(r) dr \right] \right\rangle. \end{aligned} \tag{5.4}$$

$J(r)$ is called the *source* of the function $f(r)$. [This terminology will become transparent when the formalism is applied to the theory of quantum fields in Section 5.3].

The set of all possible functions f is known as a *random field of functions*. The situation here is that a first realization of the process will yield a function f_1 , a second realization will yield a another function f_2 , etc... Throughout this chapter, the term *field* will be used, unless otherwise specified, to denote a set of functions. It is not a field in the physical sense, which is just a single function.

Functionally differentiating \mathcal{Z} with respect to the source $J(r)$ gives:

$$\begin{aligned}\frac{\delta \mathcal{Z}[J]}{\delta J(\xi)} &= \left\langle \frac{\delta}{\delta J(\xi)} \exp \left[i \int_{\Delta} J(r) f(r) dr \right] \right\rangle \\ &= i \left\langle f(\xi) \exp \left[i \int_{\Delta} J(r) f(r) dr \right] \right\rangle.\end{aligned}\quad (5.5)$$

[For a precise definition of the functional (or *variational*) derivative see Appendix C.] In general, we have

$$\begin{aligned}\left(\frac{1}{i} \frac{\delta}{\delta J(\xi_1)} \right) \cdots \left(\frac{1}{i} \frac{\delta}{\delta J(\xi_n)} \right) \mathcal{Z}[J] &= \\ \left\langle f(\xi_1) \cdots f(\xi_n) \exp \left[i \int_{\Delta} J(r) f(r) dr \right] \right\rangle.\end{aligned}\quad (5.6)$$

Thus, we have the following important result:

$$\langle f(\xi_1) \cdots f(\xi_n) \rangle = \frac{1}{i^n} \frac{\delta^n \mathcal{Z}[J]}{\delta J(\xi_1) \cdots \delta J(\xi_n)} \Big|_{J(\xi) \equiv 0}.\quad (5.7)$$

In other words, functional differentiation of \mathcal{Z} with respect to the sources yields the n-point correlation functions

$$\langle f(\xi_1) \cdots f(\xi_n) \rangle,$$

giving the complete statistical description of the distribution of functions in the space \mathcal{C} of which f is a fixed but arbitrary element. Remember that this distribution of functions is also described by the probability measure μ defined on \mathcal{C} . Hence, \mathcal{Z} is sometimes called the **characteristic functional of the measure μ** .

We can generalize these ideas to the case where $\mathcal{Z} = \mathcal{Z}_t$ is time varying, describing a family of measures μ_t . In particular, \mathcal{Z}_t can describe the evolution of a density of functions

changing under the action of a prescribed dynamical system. For example, a D.D.E will transform a density of initial functions with measure μ_0 into another density of functions with measure μ_{t_1} for $t_1 > 0$. The functional differential equation derived in the following section will be an evolution equation for the characteristic functional of the family of measures generated by the action of a D.D.E on an initial density of functions.

In conclusion, we define the characteristic functional of a two variable density. The associated measure is defined on a "two-dimensional" function space Ξ , the elements of which are pairs of functions $(f_1(r_1), f_2(r_2))$. If these functions are defined for $(r_1, r_2) \in \Delta_1 \times \Delta_2$ the characteristic functional is defined by

$$\mathcal{Z}[J_1, J_2] = \left\langle \exp \left[i \int_{\Delta_1} J_1(r_1) f_1(r_1) dr_1 + \int_{\Delta_2} J_2(r_2) f_2(r_2) dr_2 \right] \right\rangle \quad (5.8)$$

where the brackets indicate integration with respect to the probability measure of the random field $(f_1(r_1), f_2(r_2))$. This measure is called a *joint probability measure* [43]. We can now apply the above definitions to the study of delay differential equations.

5.2 Characteristic Functionals and D.D.E's.

Here, we restrict our attention to equations of the form

$$\frac{dx}{dt} = -\alpha x(t) + F(x(t-1)), \quad (5.9)$$

with the initial function

$$x(t) = \varphi(t) \text{ if } t \in [-1, 0].$$

Some care should be taken to choose a proper notation because the formalism gets somewhat involved! From now on we consider equation (5.9) rewritten as

$$\begin{cases} u(s) = v(s) & \text{for } s \in [0, 1], \\ \frac{du(s)}{ds} = -\alpha u(s) + F(v(s-1)) & \text{for } s \in (1, 2]. \end{cases} \quad (5.10)$$

By \mathcal{S}_t , we denote the corresponding semidynamical system

$$\mathcal{S}_t : \mathcal{C}([0, 1]) \longmapsto \mathcal{C}([0, 1])$$

given by

$$\mathcal{S}_t v(x) = u_v(x+t), \quad (5.11)$$

where $u_v(s)$ denotes the solution of equation (5.10) corresponding to the initial function v . We make use of the term *semidynamical system*, because a D.D.E is **noninvertible**, i.e. it cannot be run unambiguously forward and backwards in time. We note here that all the dynamical laws of physics are invertible. (These laws do not include Schrödinger's equation which is analogous to a Fokker-Planck equation, and therefore is not a dynamical equation *per se* [68]).

From (5.10) and (5.11), we have the following relations

$$\frac{\partial}{\partial t} \mathcal{S}_t v(x) = \begin{cases} v(x+t) & \text{for } x \in [0, 1-t], \\ -\alpha u_v(x+t) + F(u_v(x+t-1)) & \text{for } x \in (1-t, 1]. \end{cases} \quad (5.12)$$

Thus, we consider a function $f(x)$ [which is a segment of a solution of 5.10] defined on an interval $I_t = [t, t+1]$, as t increases (continuously). The above definition states that this f is the initial condition v when the argument $(x+t)$ is less than 1, and the solution u_v of the equation otherwise.

We next introduce the characteristic functional \mathcal{Z}_t of a Borel probability measure μ_0 defined on the space of initial functions. This space is the Banach space $\mathcal{C}([0,1])$, again with the topology given by the supremum norm (see the notation above Definition 1.2 for details). We define

$$\mathcal{Z}_t[J_1, J_2] = \int_{\mathcal{C}} \exp \left[i \int_0^1 J_1(x) \mathcal{S}_t v(x) dx + i \int_0^1 J_2(x) v(x) dx \right] d\mu_0(v). \quad (5.13)$$

The source functions J_1 and J_2 are elements of $\mathcal{C}([0,1])$.

Before deriving the functional differential equation satisfied by \mathcal{Z}_t it is useful to define the family of measures μ_t referred to earlier. If μ_0 is the probability measure on the space of initial functions, and A is a subspace of $\mathcal{C}([0,1])$, then

$$\mu_t(A) \equiv \mu_0(\mathcal{S}_t^{-1}(A)). \quad (5.14)$$

In other words, the probability that a randomly chosen function belongs to A at time t equals the probability that the counterimage of that function (under the action of \mathcal{S}_t) belonged to

the counterimage of the set A . This conservation of probability equation defines the family of measures characterized by the solutions \mathcal{Z}_t of the Hopf functional differential equation. As mentioned, this type of equation has been used in the quantum theory of fields and in the study of stochastic partial differential equation [69, 74, 78]. Work by Capiński [7] seems to be the first attempt to use this technique to investigate the dynamics of delay differential equation.

5.2.1 A functional differential equation for \mathcal{Z} .

If $f(x)$ and $g(x)$ are two functions defined on an interval I , we define

$$\{f, g\} \equiv \int_I f(x)g(x) dx.$$

To simplify the notation we write

$$\Upsilon[J_1, J_2; v] = e^{i\{J_1(x), S_t v(x)\} + \{J_2(x), v(x)\}}. \quad (5.15)$$

Υ is used from now on to denote the function of J_1, J_2 and v defined in (5.15) We begin with the following relations

$$\begin{aligned} \frac{\delta \mathcal{Z}_t}{\delta J_1(\xi)} &= i \left\langle \Upsilon \int_0^1 J_1(\xi) S_t v(\xi) d\xi \right\rangle \\ &= i \left\langle \Upsilon \int_0^{1-t} J_1(\xi) v(\xi) d\xi \right\rangle \\ &\quad + i \left\langle \Upsilon \int_{1-t}^1 J_1(\xi) [-\alpha u_v(\xi) + F(u_v(\xi - 1))] d\xi \right\rangle \end{aligned} \quad (5.16)$$

$$\frac{\delta \mathcal{Z}_t}{\delta J_2(\xi)} = i \left\langle \Upsilon \int_0^1 J_2(\xi) v(\xi) d\xi \right\rangle, \quad (5.17)$$

$$\frac{\delta^n \mathcal{Z}_t}{\delta J_1^n(\xi)} = i^n \left\langle \Upsilon \int_0^1 J_1^n(\xi) S_t v(\xi) d\xi \right\rangle, \quad (5.18)$$

where it is understood that

$$\left\langle \left(\begin{array}{c} \vdots \\ \vdots \end{array} \right) \right\rangle = \int \left(\begin{array}{c} \vdots \\ \vdots \end{array} \right) d\mu_0(v).$$

Time differentiation of the characteristic functional \mathcal{Z}_t yields

$$\frac{\partial \mathcal{Z}_t}{\partial t} = \left\langle \Upsilon \int_0^1 J_1(x) \frac{\partial S_t v(x)}{\partial x} dx \right\rangle$$

$$\begin{aligned}
&= i \left\langle \Upsilon \int_0^{1-t} J_1(x) v(x+t) dx + \Upsilon \int_{1-t}^1 J_1(x) u_v(x+t) dx \right\rangle \\
&\quad + \left\langle \Upsilon \int_{1-t}^1 J_1(x) F(u_v(x+t-1)) dx \right\rangle
\end{aligned} \tag{5.19}$$

Therefore, from (5.16) – (5.18), we obtain a functional differential equation for the characteristic functional

$$\begin{aligned}
\frac{\partial \mathcal{Z}_t}{\partial t} &= \int_0^{1-t} J_1(x) \frac{\partial}{\partial x} \left(\frac{\delta \mathcal{Z}_t}{\delta J_1(x+t)} \right) dx - \alpha \int_{1-t}^1 J_1(x) \frac{\delta \mathcal{Z}_t}{\delta J_1(x+t)} dx \\
&\quad + \left\langle \Upsilon \int_{1-t}^0 J_1(x) F(u_v(x+t-1)) dx \right\rangle.
\end{aligned} \tag{5.20}$$

Equation (5.20) contains all the statistical information describing the evolution of a density of initial functions under the action of the delay differential equation (5.12). It is not possible to go any further without restricting F .

For illustrative purposes, assume that the feedback F function in the D.D.E is a polynomial expression in the delayed variable

$$F(x(t-\tau)) = \sum_{k=1}^n a_k x(t-\tau)^k. \tag{5.21}$$

Using (5.21), equation (5.20) becomes

$$\begin{aligned}
\frac{\partial \mathcal{Z}_t}{\partial t} &= \int_0^{1-t} J_1(x) \frac{\partial}{\partial x} \left(\frac{\delta \mathcal{Z}_t}{\delta J_1(x+t)} \right) dx - \alpha \int_{1-t}^1 J_1(x) \frac{\delta \mathcal{Z}_t}{\delta J_1(x+t)} dx \\
&\quad + \sum_{k=1}^n i^{(1-k)} a_k \int_{1-t}^1 J_1(x) \frac{\delta^k \mathcal{Z}_t}{\delta J_2^k(x+t-1)} dx.
\end{aligned} \tag{5.22}$$

We illustrate this analysis with a linear delay differential equation.

Example 5.1. Consider the linear D.D.E,

$$\frac{du}{ds} = -\alpha u(s) + \beta u(s-1), \quad \text{for } s \in (1, 2] \tag{5.23}$$

with initial condition v as in (5.10). The corresponding semidynamical system is defined by (5.11). For this equation, the definition (5.13) for the characteristic functional holds and the relations (5.16) to (5.18) are valid. The Hopf differential equation becomes

$$\begin{aligned}
\frac{\partial \mathcal{Z}_t}{\partial t} &= \int_0^{1-t} J_1(x) \frac{\partial}{\partial x} \left(\frac{\delta \mathcal{Z}_t}{\delta J_1(x+t)} \right) dx - \alpha \int_{1-t}^1 J_1(x) \frac{\delta \mathcal{Z}_t}{\delta J_1(x+t)} dx \\
&\quad + \int_{1-t}^1 J_1(x) \frac{\delta \mathcal{Z}_t}{\delta J_2(x+t-1)} dx. \quad \bullet
\end{aligned} \tag{5.24}$$

Example 5.2. A continuous analogue of the quadratic map

$$x_{n+1} = rx_n(1 - x_n) \quad (5.25)$$

is the difference equation

$$\varepsilon \frac{du}{ds} = -\alpha u(s) + ru(s-1)(1 - u(s-1)), \quad (5.26)$$

where again the initial conditions, and the corresponding semidynamical system are defined as in (5.11). Note that (5.26) is the *singular perturbation* of the quadratic map (5.25) as defined in Section 1.5.1. The characteristic functional is defined by (5.13), and the preceding analysis holds. The functional differential equation corresponding to (5.26) is

$$\begin{aligned} \frac{\partial \mathcal{Z}_t}{\partial t} = & \int_0^{1-t} J_1(x) \frac{\partial}{\partial x} \left(\frac{\delta \mathcal{Z}_t}{\delta J_1(x+t)} \right) dx - \alpha \int_{1-t}^1 J_1(x) \frac{\delta \mathcal{Z}_t}{\delta J_1(x+t)} dx \\ & + r \int_{1-t}^1 J_1(x) \frac{\delta \mathcal{Z}_t}{\delta J_2(x+t-1)} dx - r \int_{1-t}^1 i J_1(x) \frac{\delta^2 \mathcal{Z}_t}{\delta J_2^2(x+t-1)} dx. \quad \bullet \quad (5.27) \end{aligned}$$

Finding a general solution for these equations is not possible at present. A correct method of solution should make use of integration with respect to measures defined on function spaces. At present, the theory of such integrals does not allow their consistent utilization in solving functional differential equations. These observations presently limit the role to be played by Hopf functional equations in the study of infinite dimensional dynamical systems. Nevertheless, relatively mild assumptions about their solutions allow one to gain significant insight into their dynamics.

5.2.2 Moment functions of μ_t :

The statistical properties of the random field of functions v and u_v are described by the infinity of moments of the measure μ_t . It is possible to write the moment evolution equations (and, in some cases, to solve them) in the spirit of the preceding analysis. For fixed t , the average value of the function defined on $I_t = [t, t+1]$ (i.e. v on $[t, 1]$ and u_v on $(1, 1+t]$), which is just the first order moment of the measure μ_t , is

$$M_v^1(t, x) \equiv \int v(x+t) d\mu_0(v) \quad \text{for } x \in [0, 1-t], \quad (5.28)$$

$$M_u^1(t, x) \equiv \int u_v(x+t) d\mu_0(v) \quad \text{for } x \in (1-t, 1]. \quad (5.29)$$

These two equations can be written as one relation:

$$M_u^1(t, x) \equiv \int u(x+t) d\mu_t(u) \quad \text{for } x \in [0, 1]. \quad (5.30)$$

The definition of the second order moment (or covariance function) $M^2(t, x, y)$ is, with the same notation,

$$M^2(t, x, y) = \int v(x+t)v(y+t) d\mu_0(v) \equiv M_{vv}^2(t, x, y) \quad \text{for } x, y \in [0, 1-t] \times [0, 1-t],$$

$$M^2(t, x, y) = \int u_v(x+t)v(y+t) d\mu_0(v) \equiv M_{uv}^2(t, x, y) \quad \text{for } x, y \in (1-t, 1] \times [0, 1-t],$$

$$M^2(t, x, y) = \int v(x+t)u_v(y+t) d\mu_0(v) \equiv M_{vu}^2(t, x, y) \quad \text{for } x, y \in [0, 1-t] \times (1-t, 1],$$

$$M^2(t, x, y) = \int u_v(x+t)u_v(y+t) d\mu_0(v) \equiv M_{uu}^2(t, x, y) \quad \text{for } x, y \in (1-t, 1] \times (1-t, 1].$$

The subscripts of the various components of M^2 refer to the segments of the solution whose correlation is given by the particular component. For example, M_{uv}^2 describes the correlation between u and v segments of the solution. This notation is made clearer by Figure 5.1. Remember that the initial function is defined on an interval $[0, 1]$ so that to complete the description of the statistical dependence of the solution u on the initial function, it is necessary to introduce the functions M_{ou}^2 . Of course, M_o^1 is the first order moment of measure μ_0 , M_{oo}^2 is the second order moment of μ_0 etc. The relatively mild condition imposed on the solution of equation (5.22) is that it be an analytic functional with respect to J_1 and J_2 . [In other words, we require that \mathcal{Z}_t can be expanded in a "power series about the functions J_1, J_2 ".]

The expression for the series expansion of a functional can be understood with the following argument. Let

$$F(y_1, \dots, y_k) = F(\mathbf{y})$$

be a function of k variables. The power series expansion of this function is

$$F(\mathbf{y}) = \sum_{n=0}^{\infty} \sum_{i_1=0}^k \dots \sum_{i_n=0}^k \frac{1}{n!} \mathcal{E}_n(i_1, \dots, i_n)(y_1, \dots, y_n), \quad (5.31)$$

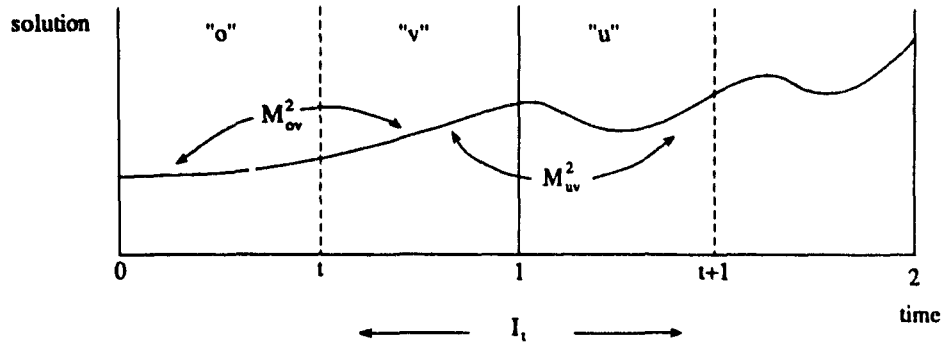


Figure 5.1: A discrete delay D.D.E transforms a function defined on $[0, 1]$ into a function defined on I_t . Illustration of the "o", "v" and "u" segments of the solution.

where

$$\mathcal{E}_n = \frac{\partial^n F(y)}{\partial y_1 \cdots \partial y_n} \Big|_{y=0}.$$

Going over to the case of infinitely many variables,

$$\begin{aligned} i &\rightarrow x_i, \\ y_i (i = 1, \dots, k) &\rightarrow y(x), \\ -\infty < x < \infty \\ \sum_i &\rightarrow \int dx \end{aligned} \quad (5.32)$$

we obtain the corresponding series expansion of a functional

$$F[y] = \sum_{n=0}^{\infty} \int dx_1 \cdots dx_n \frac{1}{n!} \mathcal{E}_n(x_1, \dots, x_n) y(x_1) \cdots y(x_n), \quad (5.33)$$

where

$$\mathcal{E}_n = \frac{\delta^n F[y]}{\delta y(x_1) \cdots \delta y(x_n)} \Big|_{y=0}. \quad (5.34)$$

$F[y]$ is called the *generating functional* of the functions \mathcal{E}_n . Therefore, the expansion of the characteristic functional is

$$\mathcal{Z}_t[J_1, J_2] = \sum_{p=0}^{\infty} \sum_{q=0}^p \int \cdots \int \mathcal{E}_{pq}(t, x_1, \dots, x_p) \left(\prod_{j=1}^q J_1(x_j) dx_j \right) \left(\prod_{j=q+1}^p J_2(x_j) dx_j \right) \quad (5.35)$$

The kernels \mathcal{E}_{pq} in the expansion are proportional to the moment functions of the measure μ_t . From equations (5.17), (5.18) and (5.34) they are given by

$$\mathcal{E}_{pq} = \frac{1}{p!} \frac{\delta^p \mathcal{Z}_t}{\delta J_1^q \delta J_2^{p-q}} = \frac{i^p}{p!} \langle u(x_1) \cdots u(x_q) v(x_{q+1}) \cdots v(x_p) \rangle \quad (5.36)$$

$$= \frac{i^p}{p!} M_{u^q v^{p-q}}^p(x_1, \dots, x_p) \quad (5.37)$$

Therefore, the Hopf equation (5.22) is equivalent to an infinite number of partial differential equations for the moments. [This observation is the infinite dimensional generalization of the well known expansion of a distribution function in terms of the corresponding probability moments (or their Legendre transforms, the cumulants)].

Consider the first and second order moments of the measure μ_t . If we substitute the definitions (5.36)-(5.37) along with the expansion (5.35) into equation (5.22), we obtain a P.D.E for the moment $M_v^1(t, x)$:

$$\begin{aligned} \frac{\partial}{\partial t} M_v^1(t, x) &= \frac{\partial}{\partial x} M_v^1(t, x) \text{ for } x \in [0, 1-t], \\ \frac{\partial}{\partial t} M_u^1(t, x) &= -\alpha M_u^1(t, x) + \sum_{k=1}^n a_k M_{\sigma^k}^k(x+t-1, \dots, x+t-1) \\ &\text{for } x \in (1-t, 1], \end{aligned} \quad (5.38)$$

the n arguments of $M_{\sigma^k}^k$ indicating that this quantity is the k -point autocorrelation function of the initial function distribution described by μ_0 . What we have done in (5.38) is simply rewrite the Hopf equation (5.22) for the first order moments. It is important to realize that the Hopf equation is equivalent to an infinity of moment equations. The equation of evolution of the k^{th} moment is given by substituting the definition of the moment under consideration into (5.22) and then use formulae (5.35) and (5.37) to the appropriate order. N.B. To illustrate the notation,

$$\begin{aligned} M_{\sigma^3 v}^1(t, w, x, y, z) &= M_{\sigma\sigma\sigma v}^1 \int v(w)v(x)v(y)v(z+t) d\mu_0. \\ &\text{for } w, x, y \in [0, 1-t] \text{ and } z \in (1-t, 1]. \quad \bullet \end{aligned}$$

To continue the example, the second order moment function $M^2(t, x)$ are given by the four

equations

$$\frac{\partial}{\partial t} M_{vv}^2(t, x, y) = \frac{\partial}{\partial x} M_{vv}^2(t, x, y) + \frac{\partial}{\partial y} M_{vv}^2(t, x, y) \quad \text{for } (x, y) \in [0, 1-t] \times [0, 1-t], \quad (5.39)$$

$$\begin{aligned} \frac{\partial}{\partial t} M_{uv}^2(t, x, y) &= \frac{\partial}{\partial y} M_{uv}^2(t, x, y) - \alpha M_{uv}^2(t, x, y) + \\ &+ \sum_{k=2}^n a_k M_{o^{(k-1)}v}^k(t, x+t-1, {}^{(k-1)}x+t-1, y) \end{aligned} \quad \text{for } (x, y) \in (1-t] \times [0, 1-t], \quad (5.40)$$

$$\begin{aligned} \frac{\partial}{\partial t} M_{vu}^2(t, x, y) &= \frac{\partial}{\partial x} M_{vu}^2(t, x, y) - \alpha M_{vu}^2(t, x, y) + \\ &+ \sum_{k=2}^n a_k M_{vo^{(k-1)}}^k(t, x, y+t-1, {}^{(k-1)}y+t-1) \end{aligned} \quad \text{for } (x, y) \in [0, 1-t] \times (1-t, 1], \quad (5.41)$$

$$\begin{aligned} \frac{\partial}{\partial t} M_{uu}^2(t, x, y) &= -2\alpha M_{uu}^2(t, x, y) + \\ &+ \sum_{k=1}^n a_k \{ M_{o^{(k-1)}u}^k(t, x+t-1, {}^{(k-1)}x+t-1, y) + \\ &+ M_{uo^{(k-1)}}^k(t, x, y+t-1, {}^{(k-1)}y+t-1) \}, \end{aligned} \quad \text{for } (x, y) \in (1-t, 1] \times (1-t, 1]. \quad (5.42)$$

The functions M_{ou}^2 and M_{oou}^2 are given by

$$\begin{aligned} \frac{\partial}{\partial t} M_{ou}^2(t, x, y) &= -\alpha M_{ou}^2 + \\ &+ \sum_{k=2}^n a_k M_{o^k}^k(x, y+t-1, {}^{(k-1)}y+t-1), \end{aligned} \quad (5.43)$$

$$\begin{aligned} \frac{\partial}{\partial t} M_{oou}^3(t, x, y, z) &= -\alpha M_{oou}^3(t, x, y, z) + \\ &+ \sum_{k=3}^n a_k M_{o^k}^k(x, y, z+t-1, {}^{(k-1)}z+t-1). \end{aligned} \quad (5.44)$$

The functions whose label does not contain u are given moments of the initial measure. Therefore the solution of each equation gives us the initial condition for the next one.

A pattern clearly emerges from the preceding analysis: The moment $M^p(t, x_1, \dots, x_p) = M^p(t, \mathbf{x})$ is given by 2^p partial differential equations of the same form as the ones given above because it is a function of p variables each of which can belong to one of two possible intervals

([0, 1 - t] or (1 - t, 1]). The first of these equations (when all the x_k 's belong to [0, 1 - t]) is

$$\frac{\partial}{\partial t} M_{v^p}^p(t, \mathbf{x}) = \sum_{j=1}^p \frac{\partial}{\partial x_j} M_{v^p}^p(t, \mathbf{x}). \quad (5.45)$$

We call the equations which give the moments of the form $M_{v^l u^{(p-l)}}^p$ mixed equations because they yield functions which correlate mixed u and v segments of the solution. For the moment of order p , there are $(2^p - 2)$ mixed equations and 2 pure equations. The pure equations give $M_{v^p}^p$ and $M_{u^p}^p$, the p -point correlation functions of the v and u segments of the solution.

If $x_j \in [0, 1 - t]$ for $j = 1, \dots, l$ and $x_j \in (1 - t, 1]$ for $j = l + 1, \dots, p$, then when the forcing term F of equation (5.10) is the polynomial (5.21), the generic form of the mixed equation for $M_{v^l u^{(p-l)}}^p$ is

$$\begin{aligned} \frac{\partial}{\partial t} M_{v^l u^{(p-l)}}^p &= \sum_{i=1}^l \frac{\partial}{\partial x_i} M_{v^l u^{(p-l)}}^p(t, \mathbf{x}) - \alpha(p-l) M_{v^l u^{(p-l)}}^p(t, \mathbf{x}) + \\ &\sum_{j=0}^{n-1} a_j \left\{ M_{v^l u^{(p-l)}}^{(p+j)}(t, \mathbf{x}) + M_{v^l u^{(p-l)}}^{(p+j)}(t, \mathbf{x}) \right\}. \end{aligned} \quad (5.46)$$

Once again, this equation is one representative of the $(2^p - 2)$ mixed equations to be solved to obtain the moment of order p . Deriving these equations is tedious, but the task is greatly simplified by the "similarity" existing between the systems of equations for moments of different orders. In fact, it is possible to derive the equation for the p^{th} moment *graphically*, with the introduction of Feynman diagrams used to represent each term in a moment of given order. Before proceeding, we derive the partial differential equations analogous to (5.38) and (5.39)-(5.42) in the case of the linear D.D.E considered in Example 5.1.

Example 4.3: When the D.D.E is

$$\frac{dx}{dt} = -\alpha x(t) + \beta x(t-1), \quad (5.47)$$

the first order moment equations are given by

$$\frac{\partial M_v^1(t, x)}{\partial t} = \frac{\partial M_v^1(t, x)}{\partial x}, \quad (5.48)$$

$$\frac{\partial M_u^1(t, x)}{\partial t} = -\alpha M_u^1(t, x) + \beta M_u^1(t, x). \quad (5.49)$$

The four equations of evolution of the second order moments are

$$\frac{\partial M_{vv}^2(t, x, y)}{\partial t} = \frac{\partial M_{vv}^2(t, x, y)}{\partial x} + \frac{\partial M_{vv}^2(t, x, y)}{\partial y}, \quad (5.50)$$

$$\frac{\partial M_{vu}^2(t, x, y)}{\partial t} = \frac{\partial M_{vu}^2(t, x, y)}{\partial x} - \alpha M_{vu}^2(t, x, y) + \beta M_{vo}^2(t, x, y), \quad (5.51)$$

$$\frac{\partial M_{uv}^2(t, x, y)}{\partial t} = \frac{\partial M_{uv}^2(t, x, y)}{\partial y} - \alpha M_{uv}^2(t, x, y) + \beta M_{ov}^2(t, x, y), \quad (5.52)$$

$$\frac{\partial M_{uu}^2(t, x, y)}{\partial t} = -2\alpha M_{uu}^2(t, x, y) + \beta [M_{ou}^2(t, x, y) + M_{uo}^2(t, x, y)]. \quad (5.53)$$

To solve these equations, one needs to solve first for the moments M_{ou}^2 and M_{uo}^2 , which satisfy

$$\frac{\partial M_{uo}^2(t, x, y)}{\partial t} = -\alpha M_{uo}^2(t, x, y) + \beta M_{oo}^2(t, x, y), \quad (5.54)$$

$$\frac{\partial M_{ou}^2(t, x, y)}{\partial t} = -\alpha M_{ou}^2(t, x, y) + \beta M_{oo}^2(t, x, y). \quad (5.55)$$

Remember that M_{ov}^2 and M_{vo}^2 are given, hence the moments can be obtained by solving successive ordinary or hyperbolic partial differential equations. •

Before we proceed, it is interesting to note that these equations can be obtained from a graphical analysis.

5.3 Perturbation theory and the diagram technique.

In this section, a technique to graphically represent a functional expansion is explained and used to simplify the derivation of moment equations. Recall that the generating functional can be represented by a series expansion. Each term in the series is proportional to a probability moment (the exact proportionality factor is given by equation (5.37)). Each one of these moments is a *correlation function*, as is illustrated by the definitions of the second order moment, and each moment can in turn be represented by a unique Feynman-like graph. The exact form of the equation for this moment is then determined by the number of vertices and loops in the diagram. This graphical method of investigation has many features in common with the methods of quantum field theory. In Section 5.4, the connection between the formalism presented here and quantum field theory is explained. We first investigate the application of diagrams to the study of wave propagation in strongly fluctuating continuous media.

5.3.1 Diagrams in stochastic wave analysis.

The diagram technique is presented here in the context of wave analysis in a continuous medium [74]. More precisely, we consider the propagation of a harmonic scalar wave in an unbounded medium characterized for illustrative purposes by a Gaussian random field. The function characterizing this field (the *stochastic Green's function*) satisfies

$$\nabla^2 G(\mathbf{r}, \mathbf{r}_0) + k^2 [1 + \xi(\mathbf{r}, \mu)] G(\mathbf{r}, \mathbf{r}_0) = \delta(\mathbf{r}, \mathbf{r}_0), \quad (5.56)$$

where ξ is called the *stochastic forcing term* and μ is some control parameter. The Laplacian operates on the variable \mathbf{r} , and the field is therefore generated by a function at point \mathbf{r}_0 . Writing equation (5.56) as an integral equation and applying the method of successive approximations, we obtain,

$$\begin{aligned} G(\mathbf{r}, \mathbf{r}_0; \mu) = & G_0(\mathbf{r}, \mathbf{r}_0) - k^2 \int G_0(\mathbf{r}, \mathbf{r}_1) \xi(\mathbf{r}_1) G_0(\mathbf{r}_1, \mathbf{r}_0) d\mathbf{r}_1 \\ & + (-k^2)^2 \int G_0(\mathbf{r}, \mathbf{r}_1) \xi(\mathbf{r}_1) G_0(\mathbf{r}_1, \mathbf{r}_2) \xi(\mathbf{r}_2) G_0(\mathbf{r}_2, \mathbf{r}_0) d\mathbf{r}_1 d\mathbf{r}_2 \\ & + (k^2)^3 \int G_0(\mathbf{r}, \mathbf{r}_1) \xi(\mathbf{r}_1) G_0(\mathbf{r}_1, \mathbf{r}_2) \xi(\mathbf{r}_2) G_0(\mathbf{r}_2, \mathbf{r}_3) \\ & \xi(\mathbf{r}_3) G_0(\mathbf{r}_3, \mathbf{r}_0) d\mathbf{r} d\mathbf{r}_2 d\mathbf{r}_3 + \dots, \end{aligned} \quad (5.57)$$

where $G_0(\mathbf{r}, \mathbf{r}_0)$ satisfies the Helmholtz equation with a point source

$$\nabla^2 G_0(\mathbf{r}, \mathbf{r}_0) + k_0^2 G_0(\mathbf{r}, \mathbf{r}_0) = \delta(\mathbf{r}, \mathbf{r}_0) \quad (5.58)$$

(i.e. it is a Green's function for the free field problem). As is well known, the solution of this equation is

$$G_0(\mathbf{r}, \mathbf{r}_0) = \frac{e^{ik_0|\mathbf{r}-\mathbf{r}_0|}}{4\pi |\mathbf{r}-\mathbf{r}_0|}. \quad (5.59)$$

In order to determine the stochastic Green's function $G_0(\mathbf{r}, \mathbf{r}_0; \mu)$ we must take the average of the integral equation (5.57). The first term in relation (5.57) (i.e. the Green's function for the free field problem) is not affected by the averaging procedure because it is by definition unrelated to any stochastic perturbations (the interest of this function is precisely that it represents the response of the system when the source is point-like in the purely deterministic case; the problem is then solved as a perturbation around this known solution). Since the

function $\xi(\mathbf{r}, \mu)$ is Gaussian we have the identities

$$\begin{aligned} \langle \xi(\mathbf{r}_1) \cdots \xi(\mathbf{r}_{2n-1}) \rangle &= 0 \\ \langle \xi(\mathbf{r}_1) \cdots \xi(\mathbf{r}_{2n}) \rangle &= \sum K_\xi(\mathbf{r}_i, \mathbf{r}_j) \cdots K_\xi(\mathbf{r}_p, \mathbf{r}_q), \end{aligned} \quad (5.60)$$

and the sum is taken over all possible partitions of $2n$ points into couples. We use these identities to rewrite the average of equation (5.57). Using the above identities we obtain the following expression

$$\begin{aligned} \langle G(\mathbf{r}, \mathbf{r}_0; \mu) \rangle &= G_0(\mathbf{r}, \mathbf{r}_0) + \\ &+ k_0^4 \int G_0(\mathbf{r}, \mathbf{r}_1) G_0(\mathbf{r}_1, \mathbf{r}_2) G_0(\mathbf{r}_2, \mathbf{r}_0) K_\xi(\mathbf{r}_1, \mathbf{r}_2) + \\ &+ k_0^8 \int G_0(\mathbf{r}, \mathbf{r}_1) G_0(\mathbf{r}_1, \mathbf{r}_2) G_0(\mathbf{r}_2, \mathbf{r}_3) G_0(\mathbf{r}_3, \mathbf{r}_4) G_0(\mathbf{r}_4, \mathbf{r}_0) \times \\ &\times [K_\xi(\mathbf{r}_1, \mathbf{r}_2) K_\xi(\mathbf{r}_3, \mathbf{r}_4) + K_\xi(\mathbf{r}_1, \mathbf{r}_3) K_\xi(\mathbf{r}_2, \mathbf{r}_4) + \\ &+ K_\xi(\mathbf{r}_1, \mathbf{r}_4) K_\xi(\mathbf{r}_2, \mathbf{r}_3)] d\mathbf{r}_1 \cdots d\mathbf{r}_4 + \cdots, \end{aligned} \quad (5.61)$$

The second term of (5.61) is the average of the third term in (5.57). The first term of (5.57) does not appear in (5.61); it vanishes according to the two identities given before (5.61).

The structure of relation (5.61) can be easily understood with the introduction of Feynman Diagrams. They were first introduced in quantum electrodynamics, but have proven useful in many other fields over the past 30 years. To represent the series (5.61) we express the functions G_0 by a graph:

$$G_0(\mathbf{r}_i, \mathbf{r}_j) : \begin{array}{ccc} \times & \text{-----} & \times \\ & & \begin{array}{cc} \mathbf{r}_i & \mathbf{r}_j \end{array} \end{array}$$

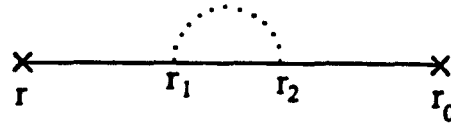
Furthermore, the coefficients k_0^2 are represented by dots (.) placed at those points of the graphs to which correspond the coefficients $\mu(\mathbf{r})$. These dots are the vertices of the graph. The points for which the functions $\xi(\mathbf{r}_i)$ and $\xi(\mathbf{r}_j)$ are contained under a common averaging symbol are connected with a dotted line:

$$k_0^4 K_\xi(\mathbf{r}_j, \mathbf{r}_l) : \begin{array}{ccc} \times & \text{-----} & \times \\ & & \begin{array}{cc} \mathbf{r}_j & \mathbf{r}_l \end{array} \end{array}$$

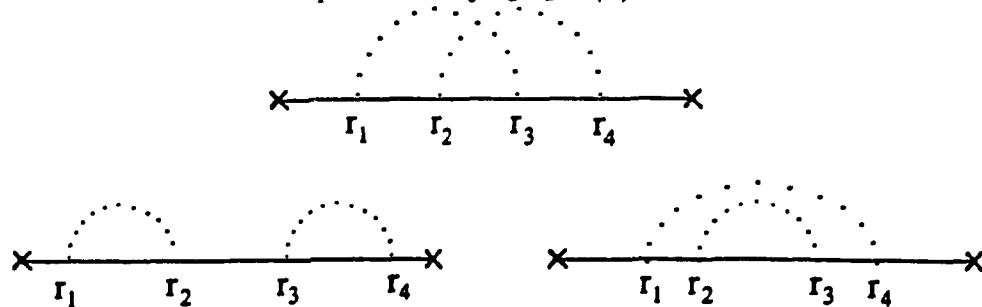
In addition, integration is performed with respect to the coordinates of intrinsic vertices of the graph. The number of all such vertices in a graph is called the order of the graph. To illustrate these definitions, the first term of series 4 is represented by graph (1)



and the second term is expressed in graph (2)



The third term in the series is represented by graph (3)



The advantage of representing the mean field $\langle G(r, r_0; \mu) \rangle$ in the form of a sum of graphs lies not only in the clarity of the presentation, but also in the observation that it is possible to transform the series using the topological features of the different graphs. In addition, introducing an appropriate classification of the graphs it is possible to express the sum of the perturbation series (5.61) as the sum of a certain subseries.

These ideas are far reaching and their applications to fluid dynamical problems lies beyond the scope of this work. Nevertheless, they are applicable to the derivation of the moment equations presented above, and a graphical description of expansion (5.35) reduces the algebraic work and helps clarify the structure underlying the form of the moment equations.

5.3.2 Feynman graphs and the moment equations.

The kernels in the functional expansion (5.35) are now expressed as Feynman-like graphs, and some topological properties of these graphs are used to write down the equation for the corresponding moment.

Consider the moment $M_{v^k-t_v}^k$. The diagram to represent it is made up of semicircles (loops) and lines. Loops can both be plain or dotted. The dotted part of the diagram represents the v contribution to the moment. The plain part of the diagram represents the u contribution to the moment. Diagrams corresponding to moments which are pure in the sense of the previous sections (*i.e.* moments of the form M_u^k or M_v^k) contain plain loops

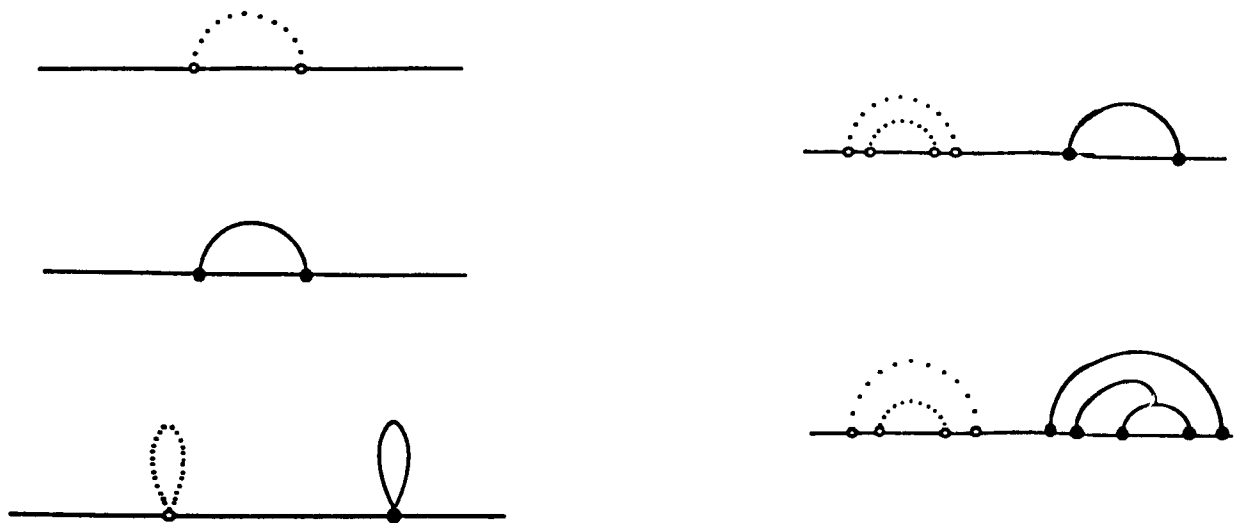


Figure 5.2: From top to bottom, and left to right, the graphs for the moments $M_{v^2}^2$, $M_{u^2}^2$, M_{vu}^2 , $M_{v^4 u^2}^6$ and $M_{v^4 u^3}^9$.

only, or dotted loops only. Every diagram is made up of loops connected to a plain horizontal line (the base line). The points at which loops intersect this plain line are called the vertices of the graph. The number of vertices in a graph equals the order of the moment it represents. When the order of the moment is odd, the topology of the graphs is modified in order to accommodate an odd number of intersections between a number of semicircular loops and a straight line, which is an impossible constraint. The point of intersection of a plain (dotted) loop with the base line is called a plain (dotted) apex. The number of plain (dotted) vertices in a graph equals the exponent of u (v) in the subscript of the moment corresponding to the graph. These definitions are illustrated in Figure 5.2.

Deriving the moment equations.

Suppose the delay equation under consideration has a polynomial forcing term given by (5.21). We enumerate the following rules, to write down the equations for a moment represented as a diagram.

1. The number $k - l$ of dotted vertices in the diagrams equals the number of partial differential terms on the right hand side of the moment equations (*i.e.* the first sum on the right hand side of (5.46)).

2. The number (l) of plain vertices equals the coefficient of terms of the form

$$-\alpha M_{v^{(k-l)}_i u^l}^k(t, \mathbf{x},$$

(*i.e.* the second term on the right hand side of (5.46)).

3. When k and l are determined in a graph, the third term in the equation of evolution of the corresponding moment is

$$\sum_{j=0}^{n-1} a_j \left\{ M_{v^{(k-l)}_i u^l}^{(k+j)}(t, \mathbf{x}) + M_{v^{(k-l)}_i u^l}^{(k+j)}(t, \mathbf{x}) \right\}$$

Therefore, to write down the partial differential evolution equation for a given moment, the first step is to draw the Feynman diagram. The second step is to analyze the diagram with the three rules enumerated above. It is clear that the diagrams presented here do not possess the topological properties allowing a significant simplification of (5.35) *via* straightforward graphical manipulation. The purpose of introducing diagrams to study delayed dynamics is to illustrate the potential relevance of this powerful technique in dynamical systems theory. They have proven to be extremely useful for the statistical investigation of P.D.E's in physics and it can be expected that their use to investigate delayed dynamics will be just as rewarding.

5.4 Connection with the quantum theory of fields.

There is a strong analogy between the formalism presented here and the theory of quantum fields. We now explore this connection. The starting point is the observation that the characteristic, or generating, functional plays a fundamental role in the formulation of quantum field theory. More precisely, *the path integrals used to quantize field theory are generating functionals.*

Before proceeding, it is necessary to clarify the nomenclature. In this section, unlike in the preceding ones, a field is understood in the physical sense, *i.e.* it is just a function (or

alternately, a path or a trajectory). In the statistical study of D.D.E's, $\mathcal{Z}[j]$ is the generating functional for the n -point correlation functions of a distribution in a Banach space. The evolution of this distribution of functions (the "random field" in the mathematics sense) is prescribed by the Hopf equation. Analogously, in quantum field theory, the concept of a generating functional is used to study the statistics of a distribution of functions (a physicist would say a "distribution of fields").

The problems of interest in quantum field theory are mainly scattering processes. The generic situation is the following. A particle is observed at (q_i, t_i) . To calculate a scattering cross section, it is necessary to know with what probability it will be observed at (q_f, t_f) . In other words it is important to calculate the *transition probability amplitude* from (q_i, t_i) to (q_f, t_f) . We now show how transition amplitudes are related to generating functionals. The presentation follows closely that given in Ryder [69].

5.4.1 Path integral formulation of quantum mechanics.

The concept of a propagator $\mathcal{K}(q_f, t_f; q_i, t_i)$ is of central importance here. Given a wave function $\Psi(q_i, t_i)$ at time t_i , the propagator \mathcal{K} gives the corresponding wave function at time t_f :

$$\Psi(q_f, t_f) = \int \mathcal{K}(q_f, t_f; q_i, t_i) \Psi(q_i, t_i) dq_i, \quad (5.62)$$

where for simplicity, only the spatial dimension is considered. $\mathcal{K}(q_f, t_f; q_i, t_i)$ is the probability amplitude for a *transition* from (q_i, t_i) to (q_f, t_f) . Given that the particle is observed at (q_i, t_i) , the probability that it is at q_f at time t_f is

$$P(q_f, t_f; q_i, t_i) = |\mathcal{K}(q_f, t_f; q_i, t_i)|^2. \quad (5.63)$$

In reality, the propagator is just $\langle q_f, t_f | q_i, t_i \rangle$. To see this, note that the state vector $|\Psi, t\rangle_S$ in the Schrödinger picture is related to that in the Heisenberg picture ($|\Psi\rangle_H$) by

$$|\Psi, t\rangle_S = e^{-iHt/\hbar} |\Psi\rangle_H. \quad (5.64)$$

Define the vector

$$|qt\rangle = e^{iHt/\hbar} |q\rangle. \quad (5.65)$$

We then have

$$\Psi(q, t) = \langle q | \Psi \rangle_H. \quad (5.66)$$

Completeness of states enables us to write

$$\langle q_f t_f | \Psi \rangle = \int \langle q_f t_f | q_i t_i \rangle dq_i \quad (5.67)$$

which using (5.66) is

$$\Psi(q_f, t_f) = \int \langle q_f t_f | q_i t_i \rangle \Psi(q_i, t_i) dq_i. \quad (5.68)$$

Therefore, on comparison with (5.62) we see that

$$\langle q_f t_f | q_i t_i \rangle = \mathcal{K}(q_f, t_f; q_i, t_i). \quad (5.69)$$

If the interval $[t_i, t_f]$ is split into $(n + 1)$ equal pieces of length τ , then

$$\begin{aligned} \langle q_f t_f | q_i t_i \rangle = \\ \int \cdots \int dq_1 \cdots dq_n \langle q_f t_f | q_n t_n \rangle \langle q_n t_n | q_{n-1} t_{n-1} \rangle \cdots \langle q_1 t_1 | q_i t_i \rangle. \end{aligned} \quad (5.70)$$

Note that the integral is taken over all possible "trajectories" (they are not trajectories in the normal sense since each segment $(q_j t_j; q_{j-1} t_{j-1})$ can be subdivided into smaller intervals and so there are no derivatives: they are Markov chains). Now, over a segment of one possible path, it is possible to calculate the propagator

$$\begin{aligned} \langle q_{j+1} t_{j+1} | q_j t_j \rangle &= \langle q_{j+1} | e^{iH\tau/\hbar} | q_j \rangle \\ &= \frac{1}{2\pi\hbar} \int dp \exp \left[\frac{i}{\hbar} p(q_{j+1} - q_j) \right] - i \frac{\tau}{\hbar} \langle q_{j+1} | H | q_j \rangle. \end{aligned} \quad (5.71)$$

Here, p , is the momentum between q_j and q_{j+1} or, equivalently between t_j and t_{j+1} .

As an example, if the Hamiltonian is of the form

$$H(p, q) = H_1(p) + H_2(q) \quad (5.72)$$

where p and q are the generalized conjugate variables, then the propagator, [or alternately, the path integral expression for the transition amplitude from (q_i, t_i) to (q_f, t_f)] is, when the

number of divisions of $(q, t_i, q_f t_f)$ goes to infinity,

$$\begin{aligned} \langle q_f t_f | q, t_i \rangle &= \lim_{n \rightarrow \infty} \int \prod_{j=1}^n dq_j \prod_{j=0}^n \frac{dp_j}{h} \times \\ &\times \exp \left\{ \frac{i}{\hbar} \sum_{j=0}^n [p_j (q_{j+1} - q_j) - \tau H(p_j, \bar{q}_j)] \right\}, \end{aligned} \quad (5.73)$$

with $q_0 = q_i$ and $q_{n+1} = q_f$. This can be written symbolically as

$$\langle q_f t_f | q, t_i \rangle = \int \frac{\mathcal{D}q \mathcal{D}p}{h} \exp \frac{i}{\hbar} \left[\int_{t_i}^{t_f} dt [p\dot{q} - H(p, q)] \right]. \quad (5.74)$$

In the above, each function $q(t)$ and $p(t)$ defines a path in phase space and (5.74) is an integral over all possible paths. Thus it is a path integral. The integral is infinite dimensional in the sense that the integration is performed over a function. If the Hamiltonian (5.72) has the form

$$H(p, q) = \frac{p^2}{2m} + V(q),$$

the p -integration in (5.73) can be performed and we arrive at the famous result

$$\langle q_f t_f | q, t_i \rangle = N \int \mathcal{D}q \exp \left[\frac{i}{\hbar} \int_{t_i}^{t_f} L(q, \dot{q}) dt \right], \quad (5.75)$$

and proper initial/boundary conditions are given by $q(t_f) = q_f$ and $q(t_i) = q_i$. $L = T - V$ is the classical Lagrangian. The integral

$$S = \int L dt$$

is called the action.

For simplicity we focus attention on systems for which (5.74) holds. The boundary conditions given above are appropriate when studying the motion of classical particles, but they are not useful to study the evolution of fields where the condition analogous to $[q(t_f) = q_f$ and $q(t_i) = q_i]$ would be $\psi(t_i) = \psi_i$ and $\psi(t_f) = \psi_f$. This is because actual particles are created, they interact and they are then destroyed. In other words, the simple boundary conditions at t_i and t_f are no longer satisfactory physically, because they "bypass" the creation-annihilation processes taking place at intermediate times. For example, in determining the differential cross section of πN scattering, the pion is created by an NN collision

and it is destroyed when it is detected [73]. The "object" responsible for the creation and annihilation of particles is called a *source* (for creation) or a *sink* (for annihilation). The source $J(t)$ is added as a "perturbation" to the Lagrangian L :

$$L \longrightarrow L + \hbar J(t)q(t).$$

When $|0, t >^J$ is the ground state (the vacuum) in the presence of source J , the transition amplitude is related to a functional of J , $\mathcal{Z}[J]$ by

$$\begin{aligned} \mathcal{Z}[J] &= \int \mathcal{D}q \exp \left[\frac{i}{\hbar} \int_{-\infty}^{+\infty} L + \hbar Jq + \frac{1}{2} i \epsilon q^2 dt \right] \\ &\propto \langle 0, +\infty | 0, -\infty \rangle^J. \end{aligned} \quad (5.76)$$

The actual derivation of the functional $\mathcal{Z}[J]$ is lengthy, and the complex perturbative term $\frac{1}{2} i \epsilon q^2$ is added to the Lagrangian because a small imaginary part is added to the Hamiltonian to isolate the ground state's contribution when performing the complex integrals involved in deriving formula (5.75). It is now straightforward to obtain the vacuum expectation value of the time-ordered product $\langle 0, +\infty | q(t_1) \cdots q(t_n) | 0, -\infty \rangle$, with $t_i > t_j$ if $i > j$ which is sometimes called the n -point function of the theory. To obtain an expression for this n -point function, one functionally differentiates the functional \mathcal{Z} ,

$$\left. \frac{\delta^n \mathcal{Z}[J]}{\delta J_1(t_1) \cdots \delta J_n(t_n)} \right|_{J=0} \propto i^n \langle 0, +\infty | q(t_1) \cdots q(t_n) | 0, -\infty \rangle. \quad (5.77)$$

This relation is interesting because it illustrates the fact that the n^{th} order functional differentiation of \mathcal{Z} with respect to the source function yields the expectation value of the time ordered product of operators $(q(t_1) \cdots q(t_n))$, which is proportional to the n^{th} moment of the distribution of paths q . The idea that \mathcal{Z} is the generating functional for the correlation functions will be taken up in the next section in the context of field theory, and the connection with the statistical study of D.D.E's is then made explicit.

5.4.2 Generating functionals for scalar fields.

If the scalar field ϕ has a source in the sense of the previous section, then the vacuum-to-vacuum transition amplitude in the presence of that source is

$$\mathcal{Z}[J] = \int \mathcal{D}\phi \exp \left\{ i \int d^4x \left[L(\phi) + J(x)\phi(x) + \frac{1}{2} \epsilon \phi^2 \right] \right\}$$

$$\alpha < 0, +\infty | 0, -\infty >^J. \quad (5.78)$$

This relation is analogous to (5.75) with the substitution $Dq \rightarrow D\phi(x'')$ and $\hbar = 1$. After coarse-graining Minkowski space *i.e.* breaking it up into four dimensional cubes of volume δ^4 , and assuming that the field ϕ is constant in a unit cell, it is possible to obtain the vacuum-vacuum transition amplitude in the case of a free particle. The fact that the particle is free comes in the definition of the Lagrangian which is, in this case,

$$L = L_0 = \frac{1}{2}(\delta_\mu \phi \delta^\mu \phi - m^2 \phi). \quad (5.79)$$

The derivation is again quite tedious and it can be found in [69]. The resulting expression for the transition amplitude is

$$\mathcal{Z}_0[J] = N \exp \left\{ -\frac{i}{2} \int J(x) \Delta_F(x-y) J(y) dx dy \right\}, \quad (5.80)$$

where $\Delta_F(x-y)$ is the Feynman propagator which satisfies

$$(\square + m^2 - i\epsilon) \Delta_F(x) = \delta^4(x), \quad (5.81)$$

and the right hand side of the equation is the Dirac delta function. Expanding this functional yields

$$\begin{aligned} \mathcal{Z}_0[J] = N \left\{ 1 - \frac{i}{2} \int J(x) \Delta_F(x-y) J(y) dx dy \right. \\ \left. + \frac{1}{2!} \left(\frac{i}{2} \right)^2 \left[\int J(x) \Delta_F(x-y) J(y) dx dy \right]^2 \right. \\ \left. + \frac{1}{3!} \left(\frac{-i}{2!} \right)^3 \left[\int J(x) \Delta_F(x-y) J(y) dx dy \right]^3 + \dots \right\}. \end{aligned} \quad (5.82)$$

This equation is analogous to (5.35) in Section 5.2.2. The k^{th} order term in the above expression is the k -point function of the theory or, to use the language of quantum field theory, it is the Green's function for the k free particles problem.

To make the connection with the previous sections more obvious, functionally differentiate \mathcal{Z}_0 with respect to the source term,

$$\frac{1}{i^n} \frac{\delta^n \mathcal{Z}_0[J]}{\delta J(x_1) \cdots \delta J(x_n)} \Big|_{J=0} = \langle 0 | \phi(x_1) \cdots \phi(x_n) | 0 \rangle. \quad (5.83)$$

The right hand side of this equation is the n^{th} moments of the "distribution of fields".

Therefore, \mathcal{Z}_0 is the generating functional for the n -point correlation functions describing the evolution of a distribution of functions. Following the evolution of these correlation functions tells us how the transition amplitudes evolve in time. Since these transition amplitudes are necessary to calculate the scattering cross sections, we have the tools to follow the evolution of the scattering cross sections.

Remark 5.2. The correlation functions, as in stochastic wave analysis, are the quantities represented with Feynman diagrams, and a diagrammatic study of the functional expansion greatly simplifies the problem at hand.

Remark 5.3. The above presentation only holds for free fields. When the fields are interacting, the Lagrangian takes the form

$$L = L_0 + L_{\text{int}}.$$

One can then derive an evolution equation for the generating functional (analogous to the Hopf equation) and solve it approximately by treating the interaction as a perturbative term. Having the generating functional for the Green's functions of the free field problem is then essential to approximate an exact solution of the more interesting interacting field problem.

5.5 Summary

This chapter is an attempt to construct a theoretical framework with which to deal with delay differential equation in the spirit of classical statistical mechanics.

Introductory definitions from measure theory and probability theory are given in Section 5.1. The concepts presented in Section 5.1 are applied in Section 5.2 to the statistical investigation of D.D.E's. In particular, we derive a functional differential equation describing the evolution of a density of functions under the action of a delay differential equation. Partial differential equations describing the evolution of the statistical moments of these functionals are also presented.

In Section 5.3 we illustrate how the Feynman diagram technique can be applied to derive the moment equations from the functional differential equation presented in Section 5.2.

In Section 5.4 we illustrate the analogy between the statistical study of D.D.E's and the quantum theory of fields.

Chapter 6

Conclusion

This thesis studies the dynamics of nonlinear delay differential equations (D.D.E's) used as models for control loops with delayed feedback.

In Chapter 1, we first recall the formal equivalence between models formulated as initial/boundary value problems for hyperbolic partial differential equations and models formulated as delay differential equations. It is demonstrated that systems with memory can be interpreted as being nonlocal, and that this nonlocality is the basis for the equivalence between some partial differential equations and delay differential equations. In fact, in Chapter 5, the tools used by physicists to statistically study the dynamics of P.D.E's are extended to the statistical investigation of D.D.E's. Finally, the singular perturbation limit procedure, and the reduction of a class of D.D.E's to shift operators is discussed and applied to a nonlinear integrable D.D.E with piecewise constant nonlinearities (PCNL).

In Chapter 2, we present the design of an electronic analog computer, built to simulate the dynamics of a class of D.D.E's discussed in Chapter 1. Multistable solutions are observed when the system's control parameters are changed continuously, and when the initial preparation of the circuit varies.

Chapter 3 is a numerical investigation of multistability in the delay differential equation simulated electronically in Chapter 2. The results of these numerical simulations demonstrate the presence of higher order multistability in the system (*i.e.* tristability, quadristability *etc.*). While bistability in delay differential equations has been the subject of intense scrutiny during the past decade, this is the first evidence of higher order multistability. In addition,

we present the first systematic attempt at characterizing the boundary of basins of attraction in the space of initial functions. Pathological dependence of solution behavior on changes in the initial functions is demonstrated for bistable and tristable limit cycles.

In Chapter 4, we numerically explore the behavior of densities for a delay differential equation which is the singular perturbation of the well known "hat map". Densities along the trajectories are first constructed. It is seen that the number of peaks in the density equals the period of the density cycles in the map. Because the phase space of D.D.E's is a normed function space, we then follow the evolution of a density which is the projection of a segment (of length 1: a "buffer") of the solution $x(t)$ on the x axis as this segment slides along the trajectory. A cycling of the densities constructed in this fashion is observed and appears to offer one possible way to extend the concept of asymptotic periodicity to continuous time systems. Cycling is also observed when the density is the average of ensembles of buffers generated by ensembles of D.D.E's. Finally, we look at the evolution of the distribution of points obtained by sampling a large collection of solutions, each generated by a specific initial function, at discrete times. This last construction is of particular interest from an experimental point of view, for it simulates the measurement of a gas of noninteracting D.D.E's with a sampling device.

In Chapter 5, we present a theoretical framework with which to investigate D.D.E's statistically. We extend some techniques applied to the study of turbulent fluid flows to the statistical study of delayed dynamics. Because the phase spaces of D.D.E's are function spaces, phase space densities for these systems are density functionals. We derive a functional differential equation specifying the evolution of density functionals (i.e. it is an infinite dimensional analogue of the Liouville equation). This equation is then reduced to an infinite number of linear partial differential equations using perturbation theory. The connection between Feynman graphs and the statistical study of D.D.E's is demonstrated and used to obtain some rules concerning the derivation of the partial differential equations. Finally, because the Fourier transform of the density functional for a D.D.E can be interpreted as a path integral, we illustrate the analogy between the statistics of D.D.E's and the methods of quantum field theory.

Appendix A

Regrouping the parameters in equation (2.3).

First of all, equation (2.3) can be written

$$\frac{dx(t)}{dt} = c H(x(t - \tau)) - \alpha x(t) \quad \text{where} \quad H(x_\tau) = \begin{cases} 1 & \text{if } x_\tau \in [\theta_1, \theta_2], \\ 0 & \text{otherwise.} \end{cases} \quad (\text{A.1})$$

In addition, time can be scaled by the delay τ :

$$s(t) = \frac{t}{\tau}, \quad y(s) = x(t).$$

This gives

$$\frac{dy(s)}{ds} = \tau [c H(y(s - 1)) - \alpha y(s)]. \quad (\text{A.2})$$

Note that the delay is still present in the equation, and its parametric influence on solution behavior can be studied in the new equation (A.2): it is completely equivalent to the original one (A.1). Further, it is possible to eliminate one of the thresholds by setting:

$$x(t) = \frac{y(t)}{\theta_1} \quad \text{and} \quad G(\xi) = h\left(\frac{\xi}{\theta_1}\right) \quad \forall \xi \in R^+.$$

Therefore,

$$G(\xi) = \begin{cases} 1 & \text{if } \xi \in [1, \theta_2/\theta_1], \\ 0 & \text{otherwise.} \end{cases}$$

Defining

$$\begin{cases} \delta & = \tau c / \alpha, \\ \epsilon & = \alpha \theta_1 / c, \\ \varrho & = \theta_2 / \theta_1, \end{cases}$$

studying the original system (A.1) is completely equivalent to studying

$$\frac{dx}{dt} = \delta[G(x(t-1)) - \epsilon x(t)], \quad (\text{A.3})$$

with

$$G(\xi) = \begin{cases} 1 & \text{if } \xi \in [1, \varrho], \\ 0 & \text{otherwise.} \end{cases}$$

These new parameters are the three independent parameters of equation (A.1). Being aware of this reduction of the number of apparent parameters is important because varying one of the original parameters (θ_1 , α , etc.) is equivalent to varying several intrinsic parameters.

Appendix B

Error analysis.

B.1 Error on measured quantities.

The systematic error on the values of the measured parameters is due to the uncertainty of the measurements. We can estimate this error from the known accuracy of the various pieces of equipment.

• **Error on the measured thresholds:** They were measured with a digital voltmeter, therefore the error is the meter resolution:

$$\sigma_{th} = \pm 0.5 \times 10^{-3} \text{ volts.} \quad (\text{B.1})$$

• **Error on the measured gain α :** The gain was obtained from a digital oscilloscope reading. The finest division reading 0.1 volts, the error associated with the measurement is of order $0.1/\pi$. Let $(V_i \pm \sigma_i)$ be the signal at the input of the amplifier and $(V_o \pm \sigma_o)$ be the measured output of an amplifier stage, so the gain α is given by

$$\alpha = \frac{V_o}{V_i}.$$

Therefore, the error on the gain is

$$\sigma_\alpha = \left[\left(\frac{\partial \alpha}{\partial V_o} \right)^2 \sigma_o^2 + \left(\frac{\partial \alpha}{\partial V_i} \right)^2 \sigma_i^2 \right]^{(1/2)} \quad (\text{B.2})$$

where, $\sigma_o = \sigma_i \simeq 0.03$ volts. Differentiating α ,

$$\sigma_\alpha = \frac{0.03}{V_i} \left[\left(\frac{V_o}{V_i} \right)^2 + 1 \right]^{(1/2)}. \quad (\text{B.3})$$

• **Errors on the gain and offset of the delay box:** The error on the measured gain of the delay box is the same as the error on α of amplifier 2. The error on the measured gain is the same as that on the threshold because offsets are obtained by comparing input and output stages on an oscilloscope screen. Therefore $\sigma_{off} \simeq 0.03$ volts.

• **Error on the values of the passive components:** The resistors were measured using a digital Ohmmeter. The error on their value is equal to its resolution. $\sigma_R = 0.5$ (Ω) for all resistances smaller than or equal to 10 K Ω . For R_8 , the error is $\sigma_{R_8} = 50$ (Ω).

The value of the capacitor C_1 was determined with a Wheatstone bridge. The error on this measurement is

$$\sigma_{C_1} \simeq 0.15 \times 10^{-6} \text{ Fd.}$$

• **Error on the height of the Feedback function:** Once again, this parameter was obtained with a digital voltmeter and the error in its measurement is $\sigma_c \simeq 0.005$ volts.

• **Error on the delay:**

The clock frequency was determined with a frequency counter accurate to within 1Hz. The delay calibration curve (see Figure 2.7) was fitted with the equation

$$\tau = \frac{1}{f_{clock}} (2073 \pm 10) \text{ s.} \quad (\text{B.4})$$

so for all practical purposes, $\sigma_{f_{clock}} = 0$ and $\sigma_\tau = 10/f_{clock}$. In all measurements, $f_{clock} = 10315\text{Hz}$, therefore

$$\sigma_\tau \simeq 0.001 \text{ s.} \quad (\text{B.5})$$

B.2 Errors on effective parameters:

• **Error on the effective gain α^e :**

Remember,

$$\alpha^e = \left(\frac{R_{12} R_{10} R_7}{R_{11} R_9 R_8 R_6 C_1} \right) \alpha,$$

so

$$\begin{aligned} \sigma_{\alpha^e}^2 = & \left(\frac{\alpha R_{10} R_7}{R_{11} R_9 R_8 R_6 C_1} \right)^2 (\sigma_{R_{12}})^2 + \left(\frac{\alpha R_{12} R_7}{R_{11} R_9 R_8 R_6 C_1} \right)^2 (\sigma_{R_{10}})^2 + \left(\frac{\alpha R_{10} R_{12}}{R_{11} R_9 R_8 R_6 C_1} \right)^2 (\sigma_{R_7})^2 \\ & \left(\frac{R_{12} R_{10} R_7}{R_{11} R_9 R_8 R_6 C_1} \right)^2 (\sigma_\alpha)^2 + \left(\frac{R_{12} R_{10} R_7 \alpha}{R_{11}^2 R_9 R_8 R_6 C_1} \right)^2 (\sigma_{R_{11}})^2 + \left(\frac{R_{12} R_{10} R_7 \alpha}{R_{11} R_9^2 R_8 R_6 C_1} \right)^2 (\sigma_{R_9})^2 \\ & \left(\frac{R_{12} R_{10} R_7 \alpha}{R_{11} R_9 R_8^2 R_6 C_1} \right)^2 (\sigma_{R_8})^2 + \left(\frac{R_{12} R_{10} R_7 \alpha}{R_{11} R_9 R_8 R_6^2 C_1} \right)^2 (\sigma_{R_6})^2 + \left(\frac{R_{12} R_{10} R_7 \alpha}{R_{11} R_9 R_8 R_6 C_1^2} \right)^2 (\sigma_{C_1})^2. \end{aligned} \quad (\text{B.6})$$

• **Error on the effective height of the feedback function c^e :**

We had

$$c^e = \left(\frac{R_{12}R_{10}R_7}{R_{11}R_9R_8R_5C_1} \right) c.$$

Thus

$$\begin{aligned} \sigma_{c^e}^2 = & \left(\frac{cR_{10}R_7}{R_{11}R_9R_8R_5C_1} \right)^2 (\sigma_{R_{12}})^2 + \left(\frac{cR_{12}R_7}{R_{11}R_9R_8R_5C_1} \right)^2 (\sigma_{R_{10}})^2 + \left(\frac{cR_{10}R_{12}}{R_{11}R_9R_8R_5C_1} \right)^2 (\sigma_{R_7})^2 \\ & \left(\frac{R_{12}R_{10}R_7}{R_{11}R_9R_8R_5C_1} \right)^2 (\sigma_c)^2 + \left(\frac{R_{12}R_{10}R_7c}{R_{11}^2R_9R_8R_5C_1} \right)^2 (\sigma_{R_{11}})^2 + \left(\frac{R_{12}R_{10}R_7c}{R_{11}R_9^2R_8R_5C_1} \right)^2 (\sigma_{R_9})^2 \\ & \left(\frac{R_{12}R_{10}R_7c}{R_{11}R_9R_8^2R_5C_1} \right)^2 (\sigma_{R_8})^2 + \left(\frac{R_{12}R_{10}R_7c}{R_{11}R_9R_8R_6^2C_1} \right)^2 (\sigma_{R_6})^2 + \left(\frac{R_{12}R_{10}R_7c}{R_{11}R_9R_8R_6C_1^2} \right)^2 (\sigma_{C_1})^2. \end{aligned} \quad (\text{B.7})$$

• **Error on the value of the effective threshold:**

The two effective thresholds θ_1^e and θ_2^e are given in terms θ_1 and θ_2 by relation (2.11). The errors on θ_1 and θ_2 are equal and we therefore have

$$\sigma_{\theta_i^e} = \left[\left(\frac{-o_1}{a_1} \right)^2 \sigma_{\theta_i}^2 + \left(\frac{\theta_i}{a_1} \right)^2 \sigma_{o_1}^2 + \left(\frac{\theta_i - o_1}{a_1} \right)^2 \sigma_{a_1}^2 \right]^{(1/2)} \quad (\text{B.8})$$

where $i = 1, 2$.

The errors on the effective parameters, derived above, are used to minimize the discrepancies between the electronic and numerical solutions presented in Figures 2.11-2.19.

Appendix C

Functional derivatives.

The concept of a functional is well known; a functional is a mapping whose arguments are functions and whose values are real numbers. Usually functionals are defined by integrals:

$$\Phi[\lambda] = \int_a^b F[\lambda(\tau)] d\tau \quad (\text{C.1})$$

where F is a given function. A variation $\delta\Phi[\lambda]$ of the functional $\Phi[\lambda]$ is defined by:

$$\delta\Phi[\lambda] = \{\Phi[\lambda + \delta\lambda] - \Phi[\lambda]\}$$

where the brackets indicate that we only consider the part of the difference which is linear in $\delta\lambda$, and $\delta\lambda(\tau)$ is zero everywhere except in a neighbourhood $\Delta(x)$ of some point x lying in the interval $[a, b]$. The functional derivative (or variational derivative) of the functional $\Phi[\lambda]$ at the point x is defined by

$$\frac{\delta\Phi[\lambda]}{\delta\lambda(x)} = \lim_{\Delta(x) \rightarrow 0} \frac{\{\Phi[\lambda + \delta\lambda] - \Phi[\lambda]\}}{\int_{\Delta(x)} \delta\lambda(\tau) d\tau}. \quad (\text{C.2})$$

As an example consider the linear functional

$$\Phi[\lambda] = \int_a^b \lambda(\tau)g(\tau) d\tau. \quad (\text{C.3})$$

Its derivative is calculated according to the definition as follows:

$$\Phi[\lambda + \delta\lambda] = \int_a^b \lambda(\tau)g(\tau) d\tau + \int_a^b \delta\lambda(\tau)g(\tau) d\tau,$$

hence

$$\Phi[\lambda + \delta\lambda] - \Phi[\lambda] = \int_{\Delta(x)} \delta\lambda(\tau)g(\tau) d\tau,$$

and we can calculate the functional derivative

$$\frac{\delta\Phi[\lambda]}{\delta\lambda(x)} = \lim_{\Delta \rightarrow 0} \frac{\int_{\Delta(x)} \delta\lambda(\tau)g(\tau) d\tau}{\int_{\Delta(x)} \delta\lambda(\tau) d\tau}. \quad (\text{C.4})$$

If $g(\tau)$ is continuous, then by virtue of the mean value theorem,

$$\int_{\Delta(x)} \delta\lambda(\tau)g(\tau) d\tau = x' \int_{\Delta(x)} \delta\lambda(\tau) d\tau, \quad x' \in \Delta(x).$$

Because $x' \rightarrow x$ as $\Delta(x) \rightarrow 0$, one finally gets, for the functional derivative of (C.3),

$$\frac{\delta}{\delta\lambda(x)} \left[\int_a^b \lambda(\tau)g(\tau) d\tau \right] = g(x). \quad (\text{C.5})$$

It is possible to define functional derivatives of higher order, in analogy to the finite dimensional situation. In fact, many well known results concerning the differential calculus of finite dimensional objects have analogues in the infinite dimensional case. For a summary of the main results of functional calculus we refer the reader to Sobczyk (1988) [74].

Remark. The concept of a functional derivative presented here is a special case of the differentiation of a mapping of a topological space into another. If this space is the Banach function space, then the derivatives can be Fréchet or Gâteaux derivatives. Furthermore, if the mapping under study is a functional whose arguments are elements of the Banach space C , then its Fréchet derivative is the functional derivative defined in this section.

Appendix D

Program listings

Due to space constraints all the programs used in the calculations in this thesis could not be presented. The programs given here are:

- 1) The program used to compute Figures 3.3-3.6 illustrating the multistability in equation (2.3). This analytic integration algorithm was used to obtain the other simulations labelled "Analytic solutions" in Chapter 4 and the Figures related to equation (2.3) in Chapter 3.
- 2) The numerical integration of equation (4.16).
- 3) The program used to produce Figures (4.5) and (4.6).

A complete listing of all programs used is available on request.

```

c      program gadapcmf
c      This program integrates the MCM-ADH equation using an
c      algorithm which solves the equation analytically. The
c      Initial Functions can cross th1 and th2 once at w1-tau
c      and w2-tau (fi=1) or remain in [th1,th2] (fi=0). In
c      both cases the I.F is at th2 at t=0. The arrays are
c      first initialized, then the type of initial function
c      is selected. The solution is computed in the loop ending
c      at line 1000 (the counter for the loop being j). On line 1100
c      the period of the signal is computed (using the extrema (E(j)'s)).
c      Every time the slope changes the program goes through the entire
c      j-loop (ending at line 1000). The program checks whether or
c      not it knows the crossing time corresponding to the extremum it
c      wants to compute. It then computes E(j) and checks for
c      new crossings between E(j-1) and E(j), and stores these crossings
c      for later use in computing extrema. Inside the "j-loop", the proper
c      indexing of the new crossing times is done with the
c      counter k which depends on the type of initial function used.
c      The density is then analytically computed until line 1800 and
c      stored in the array ds(1).

c      E(j) contains the extrema corresponding to a given parameters/I.F
c      set. T(j) contains the crossing times with th1 and/or th2. x(j)
c      contains an array of point obtained with the E's and T's representing
c      the solution in a way such that it can be plotted by any exterior
c      graphics package. In this edition of the program the graphics are
c      performed by MGS, a set of FORTRAN routines written by J.S.
c      Outerbridge. The routines are called directly in the program every
c      time plotting of an array is desired. Newd was also written by J.S.O.
c      It is used for input/output.
c      "initst" and the "include" statement are necessary for MGS to work
c      properly.

      real*8 c,alpha,th1,th2,w1,w2,accur,dnext
      real*8 E(1000),T(1000),x(100000),tag(3),ds(251)
      real*8 tau,gamma,Tprim1,Tprim2,fi,btime,inifar(15)
      real*8 k,Elast,i,w,del,inter,dt,time,nl,nt
      real*8 n,flag(8),flags,v,s,nmax,np,fin
      real*8 ntrans,na,npossible,dif1,dif2,period
      real*8 delta1,delta2,delta3,delta4,transplot,length
      real*8 de,Emin,Emax,sstart,ssttoopp
      integer intrans,ina,impossible,m,kounter,label,nextr,mn,in
      integer idif,b,isstart,issttoopp
      include 'st$exe:STDEF.'

      call initst

c      open(45,file='ct.dat',status='new')
c      open(55,file='et.dat',status='new')
c      open(60,file='dens.dat',status='new')
c      open(63,file='per.dat',status='new')
      open(64,file='sol.dat',status='new')
      call newd('non-constant IC', fi, 0., 1.)
      call newd('first crossing time', w1, 0., 1.)
      call newd('second crossing time', w2, 0., 1.)
      call newd('enter the delay', tau, 0., 5000.)
      call newd('enter th1', th1, 0., 5.)
      call newd('enter th2', th2, 0., 5.)
      call newd('enter the gain', alpha, 0., 40.)
      call newd('enter height of the feedback', c, 0., 200.)
      call newd('enter total number of crossings', n, 0., 1000000.)
      call newd('enter length of transient', ntrans, 0., 1000000.)
      call newd('enter transplot', transplot, 0., 1000000.)
      call newd('enter length of plot', length, 0., 1000000.)
      do 5 l=1,3
          tag(l)=0.0d0

```

```

5      continue
      do 10 l=1,1000
          T(l)=0.0d0
10     continue
      do 15 l=1,8
          flag(l)=0.0d0
15     continue
      do 20 l=1,1000
          E(l)=0.0d0
20     continue
      gamma=c/(alpha)
      v=0.0d0
      in=int(n)
      na=n-ntrans
      npossible=n/2.0d0-10.0d0
      inpossible=in/2-10
      intrans=int(ntrans)
      accur=0.0000000000000001
      if(fi.eq.1.0d0) then
          T(1)=w1-tau
          T(2)=w2-tau
          T(3)=0.0d0
          Tpriml=w1
          E(1)=th2*dexp(-alpha*w1)
          if(E(1).lt.th1) then
              T(4)= (1/(alpha))*log(th2/th1)
              k=4.0d0
          else
              k=3.0d0
          endif
      else
          T(1)=0.0d0
          k=1.0d0
          Tpriml=tau
          E(1)=gamma+(th2-gamma)*dexp(-alpha*tau)
      endif

c-----WE NOW COMPUTE THE SOLUTION FOR T>0-----

      do 1000 j=2,n
          v=v+1

          if(((v/2)-idint(v/2)).eq.0.0d0) then
              if(fi.eq.1.0d0) then
                  s=0.0d0
              else
                  s=1.0d0
              endif
c-----the slope leading to extremum E(j) is negative.
          else
              if(fi.eq.1.0d0) then
                  s=1.0d0
              else
                  s=0.0d0
              endif
c-----the slope is positive.

          if((T(j).gt.0.0d0).or.(j.le.3.0d0)) then
              tag(1)=1.0d0
          endif
          if((tag(1).eq.1.0d0).and.(fi.eq.1.0d0)) then
              tag(2)=1.0d0
          endif
          if((T(j).gt.0.0d0).and.(fi.eq.0.0d0)) then

```

```

tag(3)=1.0d0
endif
if((tag(2).eq.1.0d0).or.(tag(3).eq.1.0d0)) then
c----- crossing time is known.
          flags=1.0d0
          Tprim2=T(j)+tau
c----- that's the time of the extremum corresponding to the
c----- jth crossing.
          if(s.eq.0.0d0) then
            E(j)=E(j-1)*dexp((-alpha)*(Tprim2-Tprim1))
          else
            E(j)=(c/(alpha))+(E(j-1)-c/(alpha))*dexp((-alpha)*(Tprim2-Tprim1))
          endif

c----- If  $\bar{E}(j)$  and  $E(j-1)$  are in the same region no crossing occurs
c----- between them. You can then go on to the next j. If this is not
c----- the case, we have to find the new crossings by performing tests
c----- on the extrema. We do this now.

          if((E(j).gt.th2).and.(E(j-1).gt.th2)) then
            flag(1)=1.0d0
          endif
          if((E(j).lt.th2).and.(E(j-1).lt.th2)) then
            flag(2)=1.0d0
          endif
          if((E(j).gt.th1).and.(E(j-1).gt.th1)) then
            flag(3)=1.0d0
          endif
          if((E(j).lt.th1).and.(E(j-1).lt.th1)) then
            flag(4)=1.0d0
          endif
          if((flag(2).eq.1.0d0).and.(flag(3).eq.1.0d0)) then
            flag(5)=1.0d0
          endif
          if((flag(1).eq.1.0d0).or.(flag(4).eq.1.0d0)) then
            flag(6)=1.0d0
          endif
          if((flag(5).eq.1.0d0).or.(flag(6).eq.1.0d0)) then
            fin=1.0d0
          else
            i=k+1
            fin=0.0d0
          endif

c----- we now find the new crossings:
c----- "i" will label properly any newly discovered crossing time
c----- between  $E(j)$  and its predecessor. For simplicity the search
c----- for crossings is split in two depending on whether the
c----- derivative is positive or negative.
          else
            flags=0.0d0
            fin=0.0d0
          endif
          do 70 l=1,8
            flag(l)=0.0d0
70      continue
          do 75 l=1,3
            tag(l)=0.0d0
75      continue

          if(fin.eq.0.0d0) then

            if(s.eq.0.0d0) then
c----- The slope is negative.
              if(E(j-1).gt.th2) then
c
              If there is a crossing it will be on a decreasing exponential

```

c

```

segment with th2:
if((flags.eq.1.0d0).and.(E(j).lt.th2)) then
  T(i)=Tprim1-(1/(alpha))*dlog(th2/E(j-1))
endif
if(flags.eq.0.0d0) then
  T(j)=Tprim1-(1/alpha)*dlog(th2/E(j-1))
  Tprim2=T(j)+tau
  E(j)=th2*dexp(-(alpha)*(tau))
endif

  if((flags.eq.1.0d0).and.(E(j).lt.th1)) then
    T(i+1)=Tprim1-(1/alpha)*dlog(th1/E(j-1))
    k=k+1
  endif
  if((flags.eq.0.0d0).and.(E(j).lt.th1)) then
    T(j+1)=Tprim1-(1/alpha)*dlog(th1/E(j-1))
    Tprim2=T(j)+tau
    k=k+1
  endif
endif

  if((E(j-1).lt.th2).and.(E(j-1).gt.th1)) then
    if((flags.eq.1.0d0).and.(E(j).lt.th1)) then
      T(i)= Tprim1-(1/(alpha))*dlog(th1/E(j-1))
    endif
    if(flags.eq.0.0d0) then
      T(j)=Tprim1-(1/alpha)*dlog(th1/E(j-1))
      Tprim2=T(j)+tau
      E(j)=th1*dexp((-alpha)*(tau))
    endif
  endif
  if(E(j-1).lt.th1) then
    flag(7)=1.0d0
    n=v
  endif
  k=k+1
  Tprim1=Tprim2
else

```

c-----DETERMINE CROSSINGS WHEN THE SLOPE IS POSITIVE:

```

c-----the slope is positive
250   if(E(j-1).lt.th1) then
      if((flags.eq.1.0d0).and.(E(j).gt.th1)) then
        T(i)=Tprim1-(1/alpha)*dlog((th1-c/alpha)/(E(j-1)-c/alpha))
      endif
c----- crossing of a rising exponential segment with th1.

      if(flags.eq.0.0d0) then
        T(j)=Tprim1-(1/alpha)*dlog((th1-c/alpha)/(E(j-1)-c/alpha))
        Tprim2=T(j)+tau
        E(j)=c/(alpha)+(th1-c/(alpha))*dexp((-alpha)*(tau))
      endif
325   if((flags.eq.1.0d0).and.(E(j).gt.th2)) then
        T(i+1)=Tprim1-(1/alpha)*dlog((th2-c/alpha)/(E(j-1)-c/alpha))
        k=k+1
      endif
      if((flags.eq.0.0d0).and.(E(j).gt.th2)) then
        T(j+1)=Tprim1-(1/alpha)*dlog((th2-c/alpha)/(E(j-1)-c/alpha))
        Tprim2=T(j)+tau
        k=k+1
      endif
    elseif((E(j-1).gt.th1).and.(E(j-1).lt.th2)) then
      if((flags.eq.1.0d0).and.(E(j).gt.th2)) then
        T(i)=Tprim1-(1/alpha)*dlog((th2-c/alpha)/(E(j-1)-c/alpha))

```

```

        endif
        if(flag(8).eq.0.0d0) then
          T(j)=Tprim1-(1/alpha)*dlog((th2-c/alpha)/(E(j-1)-c/alpha))
          Tprim2=T(j)+tau
          E(j)= c/(alpha)+(th2-c/(alpha))*dexp(-(alpha)*(tau))
        endif
      else
        flag(8)=1.0d0
        n=v
      endif

      k=k+1.0d0
      Tprim1=Tprim2
    endif

  else
    Tprim1=Tprim2
  endif

1000   continue
1001   w=0.0d0
      i=0.0d0
      do 1050 m=1,n
      c   write(45,*) T(m)
      c1050 continue
      do 1070 m=1,n
      c   write(55,*) E(m)
      c1070 continue
      if(flag(7).eq.1.0d0) then
        do 1005 l=1,n
          w=w+1
          x(w)=0.0d0
1005    continue
        endif
        if(flag(8).eq.1.0d0) then
          do 1010 l=1,n
            w=w+1
            x(w)=4.0d0
1010    continue
          endif
          if((flag(7).eq.0.0d0).and.(flag(8).eq.0.0d0)) then
            do 1080 j=transplot,transplot+length
              if(j.eq.1) then
                if(fi.eq.1.0d0) then
                  np=idint(250*w1)
                  del=w1/np
                  do 1081 l=1,np
                    w=w+1
                    x(w)=th2*dexp(-(alpha)*l*del)
1081    continue
                  else
                    np=idint(250*tau)
                    del=tau/np
                    do 1082 l=1,np
                      w=w+1
                      x(w)=gamma+(th2-gamma)*dexp(-(alpha)*l*del)
1082    continue
                    endif
                  else
                    if(j.eq.transplot) then
                      sstart=w
                    endif
                    if(E(j).lt.E(j-1)) then
                      inter= (1/(alpha))*dlog(abs(E(j-1)/E(j)))
                      np=idint(250.0d0*inter)
                      if(np.eq.0.0d0) then

```

```

        w=w+1
        x(w)=(E(j-1))*dexp(-(alpha)*inter)
    else
        del=inter/np
        do 1085 l=1,np
            w=w+1
            x(w)=(E(j-1))*dexp(-(alpha)*l*del)
1085         continue
        endif
    else
        inter=(-1/(alpha))*dlog((E(j)-gamma)/(E(j-1)-gamma))
        np=idint(250.0d0*inter)
        if(np.eq.0.0d0) then
            w=w+1
            x(w)=gamma+(E(j-1)-gamma)*dexp(-(alpha)*inter)
        else
            del=inter/np
            do 1090 l=1,np
                w=w+1
                x(w)=gamma+(E(j-1)-gamma)*dexp(-(alpha)*l*del)
1090         continue
            endif
        endif
    endif
    if(j.eq.(transplot+length)) then
        ssttoopp=w
    endif
1080 continue
    endif
c       isstart=sstart
c       issttoopp=ssttoopp
    nmax=w
    call mcinit('default',STDOUT)
    call mdwindow(10.0d0,50.0d0,0.0d0,5.0d0)
    call merase
    call mdport(0.0d0,0.85d0,0.0d0,.40d0)
    call mtsize(2)
    call CXYAX("Analytic" solution:',',',1,1,',',5,1,'inside')
    call mdwindow(sstart,ssttoopp,0.0d0,5.0d0)
    call mdmove(0.0d0,2.0d0)
    time=sstart
    do 1095 l=sstart,ssttoopp
        time=time+1.0d0
        call mddraw(time,x(time))
1095    continue
c       call mdwindow(-1.0d0,0.0d0,0.0d0,3.0d0)
c       call mdport(0.8d0,1.3d0,0.7d0,1.0d0)
c       call mtsize(1.0d0)
c       call CXYAX('Initial Function:',',',1,1,',',3,1,'inside')

mn=int(n-1.0d0)
in=int(n)
do 1500 l=2,impossible,2
    delta1=(T(in)-T(in-1))
    delta2=(T(in-1)-T(in-2*1))
    dif1=dabs(delta2-delta1)
    delta3=(T(mn)-T(mn-1))
    delta4=(T(mn-1)-T(mn-2*1))
    dif2=dabs(delta4-delta3)
    if((dif1.lt.accur).and.(dif2.lt.accur)) then
        nextr=1
        goto 1600
    endif
1500 continue

```

```

1600      nextr=inpossible
          T(3)=T(3)

          Emin=th1*dexp(-alpha*tau)
          Emax=gamma+(th2-gamma)*dexp(-alpha*tau)
          de=(Emax-Emin)/250
do 1800 l=1,251

  ds(1)=0.0d0

  do 1900 m=intrans,intrans+nextr-1

    if((int(m/2)-(m/2)).eq.0) then

      if(((Emin+(l-1)*de).gt.E(m-1)).and.((Emin+(l-1)*de).lt.E(m))) then
ds(1)=ds(1)+(-1/alpha)*(1/((Emin+(l-1)*de)-gamma))*(T(m)-T(m-1))/delta1
      endif

    endif

    if((int((m-1)/2)-((m-1)/2)).eq.0) then

      if(((Emin+(l-1)*de).gt.E(m)).and.((Emin+(l-1)*de).lt.E(m-1))) then
ds(1)=ds(1)+(1/alpha)*(1/(Emin+(l-1)*de))*(T(m)-T(m-1))/delta1
      endif

    endif

1900      continue
1800      continue
          call mdwindow(0.0d0,2.9d0,0.0d0,1.0d0)
          call mdport(0.0d0,0.4d0,0.42d0,0.78d0)
          call mtsize(2)
          call CXYAX('Analytic density:',',',',1,1,',',',1,1','inside')
          call mdwindow(0.0d0,253.0d0,0.0d0,1.50d0)
          call mdmove(0.0d0,0.0d0)
          btime=0.0d0
          do 2000 l=1,251
            btime=btime+1.0d0
            call mdraw(btime,ds(btime))
            write(60,*) ds(l)
c
2000      continue
          call mflush
          call endst(OK)
          do 6000 j=sstart,ssttoopp
            write(64,*) x(j)
6000      continue
2100      end

```

```

c      this program integrates the "hat" DDE using a 4th
c      order Runge-Kutta algorithm.
c      the integration step is delt.
c      deldiv is the length of the delay in units of the step.
c      is the real time length of the delay.
      real*8 xdel(501),x,dxdt,xh,delt,tau,xltau,xtinit,condn,ttime
      real*8 realt,a,solution(501000),time,x1,x2,y1,y2,wx1,wx2,wy1,wy2
      real*8 ntau,ntaumax,deldiv,delpr,t1,t2,ltrans,px1,px2,py1,py2
      real*8 pos(250),den(250),kountp,th,kountn,alpha,th1,th2,k,s
      real*8 swx1,swx2,swy1,swy2,spx1,spx2,spy1,spy2,slo1,slo2
      real*8 temps,xmin,xmax,cif,up,down,trans
      include 'st$exe:STDEF.'
      common/eqparam/a,xdel,delt,tau,t1,t2,alpha,th1,th2,s,slo1,slo2,cif
      common/deloop/k
c      open(35,file='den.dat',status='new')
      call initst

      write(STDOUT,*) 'enter world co-ords'
      read(STDIN,*) x1,x2,y1,y2
      write(STDOUT,*) 'enter down,up'
      read(STDIN,*) down,up

      write(STDOUT,*) 'enter port co-ords'
      read(STDIN,*) px1,px2,py1,py2
      write(STDOUT,*) 'do you want the I.F? (1/0)'
      read(STDIN,*) condn
      if(condn.eq.1) then
        write(STDOUT,*) 'enter inset-world co-ords'
        read(STDIN,*) wx1,wx2,wy1,wy2
        write(STDOUT,*) 'enter co-ords of inset port'
        read(STDIN,*) pwx1,pwx2,pwyl,pwy2
      endif
      write(STDOUT,*) 'enter a'
      read(STDIN,*) a
      write(STDOUT,*) 'enter t1'
      read(STDIN,*) t1
      write(STDOUT,*) 'enter t2'
      read(STDIN,*) t2
      write(STDOUT,*) 'enter ntaumax'
      read(STDIN,*) ntaumax
      write(STDOUT,*) 'enter th1'
      read(STDIN,*) th1
      write(STDOUT,*) 'enter th2'
      read(STDIN,*) th2
      write(STDOUT,*) 'enter slo1 (posi)'
      read(STDIN,*) slo1
      write(STDOUT,*) 'enter slo2 (nega)'
      read(STDIN,*) slo2
      write(STDOUT,*) 'enter gain'
      read(STDIN,*) alpha
      write(STDOUT,*) 'enter s-WORLD co-ords'
      read(STDIN,*) swx1,swx2,swy1,swy2
      write(STDOUT,*) 'enter s-port world'
      read(STDIN,*) spx1,spx2,spy1,spy2
      write(STDOUT,*) 'enter xmin'
      read(STDIN,*) xmin
      write(STDOUT,*) 'enter xmax'
      read(STDIN,*) xmax
      write(STDOUT,*) 'enter delay'
      read(STDIN,*) tau
      write(STDOUT,*) 'cif'
      read(STDIN,*) cif
      write(STDOUT,*) 'ENTER TRANS.'
      read(STDIN,*) trans
      write(STDOUT,*) 'ENTER DELT'
      read(STDIN,*) delt

```

```

deldiv=500.0d0
delpr=deldiv+1

c----- FILL-UP THE INITIAL ARRAY
do 104 ttime=1,t1
  xdel(ttime)=a*(ttime/500)+cif
104   continue
do 204 ttime=t1+1, t2
  xdel(ttime)=a*t1/500+((ttime/500)-t1/500)+cif
204   continue
do 304 ttime=t2+1,501
  xdel(ttime)=(a*t1/500+(t2-t1-a*t2)/500)+a*(ttime/500)+cif
304   continue
c     do 104 ttime=1,500
c       xdel(ttime)=cif
c104   continue
call mcinit('default',STDOUT)
call mdwindow(-1.0d0,0.0d0,0.0d0,1.0d0)
call merase

c-----PLOTTING THE I.F
if(condn.eq.1.0d0) then
  call mdport(pwx1,pwx2,pwy1,pwy2)
  call mtsize(2)
  call CXYAX('I.F',' ',1,1,' ',2,1,'inside')
  call mdwindow(wx1,wx2,wy1,wy2)
  call mdmove(0.8d0,0.8d0)
  do 63 ttime=1,501
    call mddraw(ttime,xdel(ttime))
63   continue
endif
time=0
call mdwindow(trans,trans+15.0d0,down,up)
call mdport(px1,px2,py1,py2)
call mtsize(2)
call cxyax('Solution',' ',15,0,' ',1,2,'inside')
call grid(15,1)
call mdwindow(trans*501,trans*501+7515,xmin,xmax)
call mdmove(0.0d0,xdel(501))
do 100 ntau=1,ntaumax
  x=xdel(deldiv+1)
  do 101 k=1,deldiv

    time=time+1
    tnext=(ntau-1+k*delt)*tau
    reat=tnext-delt*tau
    xltau=xdel(k)
    call derivs(reat,x,dxdt,xltau)
    call rk4(x,dxdt,reat,xh)
    xdel(k)=x
    x=xh
    solution(time)=xh
    if((time.ge.(trans*501+1)).and.(time.le.trans*501+7515)) then
      call mddraw(time,solution(time))
    endif
101   continue
  xdel(deldiv+1)=xh
100   continue
c-----GETTING A DENSITY ALONG THE TRAJECTORY: BINNING.
do 173 j=trans*501+1,trans*501+7515
  solution(j)=dint(100*(solution(j)-xmin)/(xmax-xmin))
173   continue
  temps=0.0d0

do 183 k=1,99
  temps=temps+1.0d0
  do 180 l=1,trans*515+7515

```

```

        if(solution(1).eq.temps) then
            den(k)=den(k)+1.0d0
        endif
180         continue
183     continue

    call mdwindow(down,up,swy1,500.0d0)
    call mdport(spx1,spx2,spy1,spy2)

    call mtsize(2)
    call cxyax('Density',' ',1,2,' ',1,0,'inside')
    call mdwindow(swx1,swx2,swy1,swy2)
    call mdmove(0.0d0,den(1))
        time=0.0d0
        do 350 j=1,99
            time=time+1.0d0
            call mddraw(time,den(time))
350         continue

        call mflush
        call endst(OK)
c         do 400 j=1,249
c             write(35,*) DEN(J),solution(j)
c400        CONTINUE

    end

SUBROUTINE DERIVS(realt,x,dxdt,xltau)
    double precision a,xltau,x,dxdt,xdel(501),delt,tau,realt
    double precision t1,t2,alpha,th1,th2,k,s,slo1,slo2
    include 'st$exe:STDEF.'
    common/eqparam/a,xdel,delt,tau,t1,t2,alpha,th1,th2,s,slo1,slo2,cif
    common/deloop/k
        if((xltau.ge.0.0d0).and.(xltau.le.th1)) then
            dxdt=-alpha*x+slo1*xltau
        else if((xltau.gt.th1).and.(xltau.le.th2)) then
            dxdt=-alpha*x+slo1*(1-xltau)
        else
            dxdt=-alpha*x
        endif
    end

SUBROUTINE RK4(x,dxdt,realt,xh)
    double precision a,x,dxdt,xh,xdel(501),realt,delt,tau
    double precision xt,dxt,dxm,hh,h6,th,tprime,xltau
    double precision t1,t2,alpha,th1,th2,k,s,slo1,slo2
    include 'st$exe:STDEF.'
    common/eqparam/a,xdel,delt,tau,t1,t2,alpha,th1,th2,s,slo1,slo2,cif
    common/deloop/k
        hh=delt*tau/2
        h6=hh/3
        th=realt+hh
        xt=x+(hh*dxdt)
        xltau=(xdel(k)+xdel(k+1))/2
        call derivs(th,xt,dxt,xltau)
        xt=x+hh*dxt
        call derivs(th,xt,dxm,xltau)
        xt=x+delt*tau*dxm
        dxm=dxt+dxm
        xltau=xdel(k+1)
        tprime=realt+delt*tau
        call derivs(tprime,xt,dxt,xltau)
        xh=x+h6*(dxdt+dxt+2*dxm)
    end

```

```

c      this program integrates the "hat" DDE using a 4th
c      order Runge-Kutta algorithm.
c      the integration step is delt.
c      deldiv is the length of the delay in units of the step.
c      is the real time length of the delay.
c      Once the equation is simulated, the program bins 20 buffers
c      containing a segment of length 1 of the solution.
c      The points at which the 20 buffers begin are the sb's.
c      There is only 1 Initial Function since this program simulates the
c      procedure explained in section 4.2.2b which consists
c      in following a segment of solution of length tau and
c      binning this "buffer" as it slides along a solution.
c      real*8 xdel(501),x,dxdt,xh,delt,tau,xltau,xtint,t,ttime
      real*8 reat,a,solution(501000),time
      real*8 ntau,ntaumax,deldiv,delpr,t1,t2,ltrans
      real*8 kounter,th,kountn,alpha,th1,th2,k,s
      real*8 slo1,slo2,buf(501),x1(20),x2(20),y1(20),y2(20)
      real*8 xmin,xmax,cif,start,bufden(50),heit,temp,sb(20)
      include 'st$exe:STDEF.'
      common/eqparam/a,xdel,delt,tau,t1,t2,alpha,th1,th2,s,slo1,slo2,cif
      common/deloop/k
      call initst

```

```

      write(STDOUT,*) 'enter a'
      read(STDIN,*) a
      write(STDOUT,*) 'enter t1'
      read(STDIN,*) t1
      write(STDOUT,*) 'enter t2'
      read(STDIN,*) t2
      write(STDOUT,*) 'enter ntaumax'
      read(STDIN,*) ntaumax
      write(STDOUT,*) 'enter th1'
      read(STDIN,*) th1
      write(STDOUT,*) 'enter th2'
      read(STDIN,*) th2
      write(STDOUT,*) 'enter slo1 (posi)'
      read(STDIN,*) slo1
      write(STDOUT,*) 'enter slo2 (nega)'
      read(STDIN,*) slo2
      write(STDOUT,*) 'enter gain'
      read(STDIN,*) alpha
      write(STDOUT,*) 'enter xmin'
      read(STDIN,*) xmin
      write(STDOUT,*) 'enter xmax'
      read(STDIN,*) xmax
      write(STDOUT,*) 'enter delay'
      read(STDIN,*) tau
      write(STDOUT,*) 'cif'
      read(STDIN,*) cif
      write(STDOUT,*) 'ENTER TRANS.'
      read(STDIN,*) start
      write(STDOUT,*) 'ENTER DELT'
      read(STDIN,*) delt
      write(STDOUT,*) 'enter height'
      read(STDIN,*) heit
      do 37 j=1,20
         write(STDOUT,*) 'enter sb'
         read(STDIN,*) sb(j)
      continue

```

37

```

deldiv=500.0d0
delpr=deldiv+1

```

172

```

c----- FILL-UP THE INITIAL ARRAY
do 104 ttime=1,t1
  xdel(ttime)=a*(ttime/500)+cif
104  continue
do 204 ttime=t1+1, t2
  xdel(ttime)=a*t1/500+((ttime/500)-t1/500)+cif
204  continue
do 304 ttime=t2+1,501
  xdel(ttime)=(a*t1/500+(t2-t1-a*t2)/500)+a*(ttime/500)+cif
304  continue
c    do 104 ttime=1,500
c    xdel(ttime)=cif
c104 continue
C----- FILLING-UP THE X AND Y ARRAYS(COORDS OF THE 20 PORTS)
do 250 j=1,5
  x1(j)=(j-1)*0.26d0
  x2(j)=j*0.26d0
  y1(j)=0.75d0
  y2(j)=1.0d0
250  continue
do 251 j=6,10
  x1(j)=x1(j-5)
  x2(j)=x2(j-5)
  y1(j)=0.5d0
  y2(j)=0.75d0
251  continue
do 252 j=11,15
  x1(j)=x1(j-5)
  x2(j)=x2(j-5)
  y1(j)=0.25d0
  y2(j)=0.50d0
252  continue
do 253 j=16,20
  x1(j)=x1(j-5)
  x2(j)=x2(j-5)
  y1(j)=0.0d0
  y2(j)=0.25d0
253  continue

call mcinit('default',STDOUT)
call merase
time=0

do 100 ntau=1,ntaumax
  x=xdel(deldiv+1)
  do 101 k=1,deldiv

    time=time+1
    tnext=(ntau-1+k*delt)*tau
    reat=tnext-delt*tau
    xltau=xdel(k)
    call derivs(reat,x,dxdt,xltau)
    call rk4(x,dxdt,reat,xh)
    xdel(k)=x
    x=xh
    solution(time)=xh
101  continue
  xdel(deldiv+1)=xh
100  continue

do 750 k=1,20
  m=0
  do 102 j=sb(k),sb(k)+500
    m=m+1
    buf(m)=0.0d0

```

```

        buf(m)=solution(j)
        buf(m)=dint(50*(buf(m)-xmin)/(xmax-xmin))
102    continue
        temps=0
        do 103 l=1,50
            bufden(l)=0.0d0
            temps=temps+1
            do 114 j=1,501
                if(buf(j).eq.temps) then
                    bufden(l)=bufden(l)+1
                endif
            continue
114    continue
103    continue

        call mdwindow(xmin,xmax,0.0d0,heit)
        call mdport(x1(k),x2(k),y1(k),y2(k))
        call mtsize(2)
        call cxyax(' ',' ',1,2,' ',1,1,'inside')
        call mdwindow(0.0d0,50.0d0,0.0d0,heit)
        call mdmove(0.0d0,0.0d0)
        kounter=0
        do 105 n=1,50
            kounter=kounter+1
            call mddraw(kounter,bufden(kounter))
105    continue

750    continue

```

```

        call mflush
        call endst(OK)

```

```

        end

```

```

SUBROUTINE DERIVS(realt,x,dxdt,xltau)
double precision a,xltau,x,dxdt,xdel(501),delt,tau,realt
double precision t1,t2,alpha,th1,th2,k,s,slo1,slo2
include 'st$exe:STDEF.'
common/eqparam/a,xdel,delt,tau,t1,t2,alpha,th1,th2,s,slo1,slo2,cif
common/deloop/k
if((xltau.ge.0.0d0).and.(xltau.le.th1)) then
    dxdt=-alpha*x+slo1*xltau
else if((xltau.gt.th1).and.(xltau.le.th2)) then
    dxdt=-alpha*x+slo1*(1-xltau)
else
    dxdt=-alpha*x
endif
end

```

```

SUBROUTINE RK4(x,dxdt,realt,xh)
double precision a,x,dxdt,xh,xdel(501),realt,delt,tau
double precision xt,dxt,dxm,hh,h6,th,tprime,xltau
double precision t1,t2,alpha,th1,th2,k,s,slo1,slo2
include 'st$exe:STDEF.'
common/eqparam/a,xdel,delt,tau,t1,t2,alpha,th1,th2,s,slo1,slo2,cif
common/deloop/k
    hh=delt*tau/2
    h6=hh/3
    th=realt+hh
    xt=x+(hh*dxdt)
    xltau=(xdel(k)+xdel(k+1))/2
    call derivs(th,xt,dxt,xltau)
    xt=x+hh*dxt
    call derivs(th,xt,dxm,xltau)
    xt=x+delt*tau*dxm
    dxm=dxt+dxm

```

```
x1tau=xdel(k+1)
tprime=realt+delt*tau
call derivs(tprime,xt,dxt,x1tau)
xh=x+h6*(dxdt+dxt+2*dxm)
end
```

Bibliography

- [1] D. Babai. Sur une équation différentielle à délai modélisant des processus de contrôles physiologiques. Master's thesis, Université de Montréal, 1990. (French).
- [2] J. Bélair and M. C. Mackey. Consumer memory and price fluctuations in commodity markets: An integro-differential model. *J. Dynam. Diff. Eq.*, 1:299, 1989.
- [3] Bellman and Kalaba. *Mathematical trends in control theory*. Dover, New York, 1964.
- [4] P. Bergé, Y. Pomeau, and C. Vidal. *L'ordre dans le Chaos*. Hermann, Paris, 1984. (French).
- [5] S. P. Blythe, R. M. Nisbet, and W. S. Gurney. The dynamics of population models with distributed maturation period. *Theor. Pop. Biol.*, 25:289, 1984.
- [6] V. Boffi and R. Scozzafava. A first order linear differential-difference equation with n delays. *J. Math. Anal. Appl.*, 17:577, 1967.
- [7] M. Capiński. Hopf equation for some nonlinear differential delay equation and invariant measures for corresponding dynamical system. *Ann. Pol. Acad. Sci.* (In Press).
- [8] Chaos and Fractals. The mathematics behind the computer graphics. In R. L. Devaney and L. Keen, editors, *Proceedings of Symposia in Applied Mathematics*. American Mathematical Society, 1989. Volume 39.
- [9] D. R. Chialvo and J. Jalife. Nonlinear dynamics of cardiac excitation and impulse propagation. *Nature*, 330:749, 1987.

- [10] S. N. Chow. *Some Results on Singular Delay Differential Equations*, volume 98 of *Lecture Notes in Pure and Applied Mathematics*. Springer-Verlag, Berlin, 1985.
- [11] P. Collet and J. P. Eckmann. *Iterated Maps On the Interval as Dynamical Systems*, volume 1 of *Progress in Physics*. Birkhäuser, Boston, 1980.
- [12] K. Cooke and D. W. Krumme. Differential-difference equations and nonlinear initial-boundary value problems for linear hyperbolic partial differential equations. *J. Math. Anal. Appl.*, 24:372, 1968.
- [13] M. W. Derstine, H. M. Gibbs, F. A. Hopf, and D. L. Kaplan. Alternate path to chaos in optical bistability. *Phys. Rev.*, 27A(3):3200, 1983.
- [14] B. Dorizzi, B. Grammaticos, M. Leberre, Y. Pomeau, E. Ressayre, and E. Tallet. Statistics and dimension of chaos in differential delay systems. *Phys. Rev.*, 35A(1):328, 1987.
- [15] W. K. Ergen. Kinetics of the circulating fuel nuclear reactor. *J. Appl. Phys.*, 25:702, 1954.
- [16] D. Fargue. Réducibilité des systèmes héréditaires à des systèmes dynamiques. *Comptes Rendus de l'Académie des Sciences*, 277B:471, 1973. (French).
- [17] D. Fargue. Réducibilité des systèmes héréditaires. *Int. J. Nonlin. Mech.*, 9:331, 1974. (French).
- [18] H. Goldstein. *Classical Mechanics*. Addison-Wesley, Reading, 1950.
- [19] V. D. Gorjačenko. *Methods in the Theory of Stability in Nuclear Reactor Dynamics*. Atomizdat, Moscow, 1971. (Russian).
- [20] J. Guckenheimer and P. Holmes. *Nonlinear Oscillations, Dynamical Systems and Bifurcations of Vector Fields*, volume 42 of *Applied Mathematical Sciences*. Springer-Verlag, Berlin, 1983.
- [21] D. L. Kaplan H. M. Gibbs, F. A. Hopf and R. L. Shoemaker. Observation of chaos in optical bistability. *Phys. Rev. Lett.*, 46:474, 1981.

- [22] J. Hale. *Theory of Functional Differential equations*, volume 3 of *Applied Mathematical Sciences*. Springer-Verlag, Berlin, 1977.
- [23] U. an der Heiden. Periodic, aperiodic and stochastic behavior of differential-difference equation modeling biological and economical processes. In L. Collaty, G. Meinardus, and W. Wetterling, editors, *Differential-Difference Equations: Applications and Numerical Problems Workshop*, Basel, 1983. Birkhäuser Verlag.
- [24] U. an der Heiden and M. C. Mackey. The dynamics of production and destruction: Analytic insight into complex behavior. *J. Math. Biol.*, **16**:75, 1982.
- [25] J. O. Hirschfelder, C. F. Curtiss, and R. B. Bird. *Molecular Theory of Gases and Liquids*. John Wiley and Sons, New York, 1954. p. 449.
- [26] E. Hopf. Statistical hydromechanics and functional calculus. *J. Ratl. Mech. Anal.*, **1**:87, 1952.
- [27] F. A. Hopf, P. Meystre, P. D. Drummond, and D. F. Walls. Anomalous swtching in dispersive optical bistability. *Optics Comm.*, **31**:245, 1982.
- [28] P. Horowitz and W. Hill. *The Art of Electronics*. Cambridge University Press, Cambridge, 1980.
- [29] W. Horsthemke and R. Lefever. *Noise-Induced Transitions*. Springer-Verlag, Berlin, 1984.
- [30] K. Huang. *Statistical Mechanics*. John Wiley ans Sons, New York, 1977.
- [31] J. Hufault. *Op-Amp Network Design*. John Wiley and Sons, New York, 1986.
- [32] K. Ikeda and O. Akimoto. Successive bifurcations and dynamical multistability in a bistable optical system: A detailed study of the transition to chaos. *Appl. Phys.*, **28B**:170, 1979.
- [33] K. Ikeda, H. Daido, and O. Akimoto. Optical turbulence: Chaotic behavior of transmitted light from a ring cavity. *Phys. Rev. Lett.*, **45**:709, 1980.

- [34] K. Ikeda and K. Matsumoto. High dimensional chaotic behavior in systems with time delayed feedback. *Physica*, **29D**:223, 1987.
- [35] A. F. Ivanov and A. N. Sharkovskii. Oscillations in singularly perturbed delay equations. To appear in *Dynamics Reported* (edited by H. O. Walther and U. Kirchgraber).
- [36] M. Kalecki. A macroeconomic theory of business cycles. *Econometrica*, **3**:327, 1935.
- [37] K. Kaneko. Complexity in high dimensional chaos and its impact. In *The impact of chaos on science and complexity*, Tokyo, 1991.
- [38] J. Komornik and A. Lasota. Asymptotic decomposition of Markov operators. *Bull. Polish Acad. Sci.*, **35**:321, 1987.
- [39] M. Landau, D. Michaels, and J. Jaliffe. Bistabilities and annihilation phenomena in electrophysiological cardiac models. *Circ. Res*, **66**:1658, 1990.
- [40] A. Lasota and M. C. Mackey. *Probabilistic Properties of Deterministic Systems*. Cambridge University Press, Cambridge, 1985.
- [41] J. J. Levin and J. A. Nohel. On a system of integro-differential equations occurring in reactor dynamics. *J. Math. Mech.*, **9**:210, 1960.
- [42] J. E. Lewis and L. Glass. Steady states, limit cycles and chaos in models of complex biological network. To appear in *International Journal of Bifurcations and Chaos*.
- [43] R. M. Lewis and R. H. Kraichnan. A space-time functional formalism for turbulence. *Comm. Pure Appl. Math.*, **15**:397, 1962.
- [44] T. Lewis and M. G. Guevarra. Chaotic dynamics in an ionic model for the propagation of cardiac action potentials. *J. Theor. Biol.*, **146**:407, 1990.
- [45] J.-N. Li and B.-L. Hao. Bifurcation spectrum of a delay differential system related to optical bistability. *Commun. Theor. Phys.*, **11**:265, 1989.
- [46] A. J. Lichtenberg and A. M. Leiberman. *Regular and Stochastic Motion*, volume **38** of *Applied Mathematical Sciences*. Springer-Verlag, Berlin, 1983.

- [47] A. Longtin. *Nonlinear Oscillations, Noise and Chaos in Neural Delayed Feedback*. PhD thesis, McGill University, 1989.
- [48] A. Longtin and J. G. Milton. Modeling autonomous oscillations in the human pupil eye reflex using nonlinear delay differential equations. *Bull. Math. Biol.*, **51**:605, 1989.
- [49] N. Macdonald. *Biological delay systems: Linear stability theory*, volume **8** of *Cambridge Studies in Mathematical Biology*. Cambridge University press, Cambridge, 1989.
- [50] M. C. Mackey. Commodity price fluctuations: Price dependent delays and nonlinearities as explanatory factors. *J. Econ. Theory*, **48**(2):497, 1989.
- [51] M. C. Mackey. The dynamic origin of increasing entropy. *Rev. Mod. Phys.*, **61**:981, 1989.
- [52] M. C. Mackey and U. an der Heiden. The dynamics of recurrent inhibition. *J. Math. Biol.*, **19**:211, 1982.
- [53] M. C. Mackey and L. Glass. Oscillation and chaos in physiological control systems. *Science*, **197**:287, 1977.
- [54] M. C. Mackey and J. G. Milton. Dynamical diseases. *Ann. N. Y. Acad. Sci.*, **504**:16, 1987.
- [55] M. C. Mackey and J. G. Milton. Feedback, delays and the origin of blood cell dynamics. *Comm. Theor. Biol.*, **1**(5):299, 1990.
- [56] A. Manitius. Mathematical models of hereditary systems. Technical report, Université de Montréal, 1974. Report CRM-462.
- [57] J. E. Marshall. *Control of Time Delay systems*, volume 10 of *I.E.E.E. Control Engineering Series*. Peregrinus, Stevenage, 1979.
- [58] W. L. Miranker. The wave equation with a nonlinear interface condition. *IBM Journal of Research and Development*, **5**:2, 1961.

- [59] S.-E. A. Mohammed. *Stochastic Functional Differential Equations*. Pitman, London, 1984.
- [60] P. Morse and H. Feshbach. *Methods of Theoretical Physics*, volume 25 of *International Series in Pure and Applied Physics*. McGraw-Hill, New York, 1953.
- [61] G. Placzek. On the theory of the slowing down of neutrons in heavy substances. *Phys. Rev.*, **69C**:423, 1946.
- [62] W. H. Press, B. P. Flannery, S. A. Teukolski, and W. T. Vetterling. *Numerical Recipes*. Cambridge University Press, Cambridge, 1986.
- [63] N. Provatas. Inherent and noise induced asymptotic periodicity. Master's thesis, McGill University, 1990.
- [64] N. Provatas and M. C. Mackey. Asymptotic periodicity and banded chaos. *Physica D*, 1991. In Press.
- [65] N. Provatas and M. C. Mackey. Noise-induced asymptotic periodicity in a piecewise linear map. *J. Stat. Phys.*, **63**:661, 1991.
- [66] *La Recherche. Spécial: La Science du désordre*, may 1991. Volume 22. (French).
- [67] R. P. Richtmeyer. *Principles of Advanced Mathematical Physics*, volume 9 of *Texts and Monographs in Physics*. Springer-Verlag, Berlin, 1978.
- [68] H. Risken. *The Fokker-Planck Equation*, volume 18 of *Springer Series in Synergetics*. Springer-Verlag, Berlin, 1984.
- [69] L. H. Ryder. *Quantum Field Theory*. Cambridge University Press, Cambridge, 1985.
- [70] T. L. Saaty. *Modern Nonlinear Equations*. Dover, New York, 1981.
- [71] D. Schertzer and S. Lovejoy. Nonlinear variability in geophysics: Multifractal simulation and analysis. In Pietronero, editor, *Fractal*. Plenum Press, 1990.
- [72] H. G. Schuster. *Deterministic Chaos, an Introduction*. Physik Verlag, Weinheim, 1984.

- [73] J. Schwinger. *Particles and Sources*. Gordon and Breach, 1969.
- [74] K. Sobczyk. *Stochastic Wave Propagation*. Elsevier, Amsterdam, 1984.
- [75] B. Szafirski. A functional analytic approach to turbulent convection. *Ann. Polon. Math.*, **23**:7, 1970.
- [76] B. Szafirski. Characteristic functionals and turbulent diffusion. *Bull. Acad. Polon. Sci. Série Sci. Math. Astronom.*, **19**:785, 1971.
- [77] B. Szafirski. A method of first integrals in turbulent diffusion. *Bull. Acad. Polon. Sci. Série Sci. Math. Astronom.*, **26**:791, 1978.
- [78] J. P. Terletsky. Sur la statistique des champs nonlinéaires. *Journ. Phys. Rad.*, **21**:771, 1960. (French).
- [79] F. J. Van Capelle and D. Durrer. Computer simulations of arrhythmias in a network of coupled excitable elements. *Circ. Res.*, **47**:454, 1980.
- [80] A. A. Vitt. K teorii skripichnoï struli. *Zhurnal Tekhnicheskoi Fizike*, **6**:1459, 1936. (Russian).
- [81] T. Vogel. *Théorie des Systèmes Evolutifs*. Gauthiers-Villars, Paris, 1965. (French).
- [82] V. Volterra. *Leçons sur la Théorie Mathématique de la Lutte pour la Vie*. Gauthiers-Villars, Paris, 1931. (French).
- [83] A. T. Winfree. *The Geometry of Biological Time*, volume 8 of *Biomathematics*. Springer-Verlag, Berlin, 1980.
- [84] H.-J. Zhang, J.-H. Dai, P.-Y. Wang, F.-L. Zhang, G. Xu, and S.-P. Yang. Chaos in liquid crystal optical bistability. In B.-L. Hao, editor, *Directions in Chaos*, page 46. World Scientific, Singapore, 1988.